

BIVALENT LIGANDS AS PHARMACOLOGICAL PROBES FOR THE
MELANOCORTIN RECEPTORS: THE BIVALENT ADVANTAGE

A DISSERTATION
SUBMITTED TO THE FACULTY OF
UNIVERSITY OF MINNESOTA
BY

Cody James Lensing

IN PARTIAL FULFILLMENT OF THE REQUIREMENTS
FOR THE DEGREE OF
DOCTOR OF PHILOSOPHY

ADVISOR: Dr. Carrie Haskell-Luevano

May, 2017

© Cody J. Lensing, 2017

Acknowledgments

I would like to thank everyone who has contributed directly and indirectly to the completion of this dissertation. First and foremost, I would like to thank Dr. Carrie Haskell-Luevano for her support and guidance throughout the hills and valleys of my graduate training. I would like to thank my committee members, Dr. Rodney Johnson, Dr. Philip Portoghese, and Dr. Alessandro Bartolomucci, for their support preparing and completing this dissertation work. I am also grateful to all the University of Minnesota Medicinal Chemistry faculty and staff who have helped guide me towards the completion of my Ph.D.

I would like to acknowledge all the past and current members of the Haskell-Luevano Laboratory that have aided me during my graduate training including: Danielle Adank, Dr. Skye Doering, Dr. Mark Ericson, Katlyn Fleming, Katie Freeman, Zoe Koerperich, Mary Lunzer, Mike Powers, Sathya Schnell, Katie Schlasner, Dr. Anamika Singh, Branden Smeester, Dr. Srinivasa Tala, and Stacey Wilber. The opportunity to learn from and work with everyone over the years has been an honor. Specifically, I would like to thank Katlyn Fleming for the discussion of ideas and concepts as well as proofreading the entirety of this dissertation. I would also like to thank my fellow graduate students and colleagues at the University of Minnesota. Specifically, I would like to thank Harrison Trent West, Jacob Petersburg, Joseph Buonomo, Kristen Stoltz, Adam Zarth, and Erika Dahl for their intellectually stimulating conversations that flowed over our beverages of choice.

I would like to acknowledge the financial support that I received including the University of Minnesota Doctoral Dissertation Fellowship and the College of Pharmacy Olsteins Graduate Fellowship. This work was also supported by NIH Grants R01DK091906 and R01DK108893.

Last, but certainly not least, I would like to thank all my friends and family who supported me throughout my graduate studies. I would like to thank my girlfriend Amanda Granaas for her support and patience as I finished up my Ph.D. I would like to thank my siblings, Clark Lensing, Pam Doering, and Wendee Foley, for continuously keeping me motivated. Finally, I would like to thank my mother and father, Rosemary and Merl Lensing, for their unwavering love and support and providing me with every opportunity for success throughout all the stages of my life.

Dedication

The dissertation is dedicated to the memory of my father, Merl Lensing, who through his larger than life character and endless energy bestowed on me the foundation to thrive and succeed in this world, no matter the obstacles.

Abstract

Pharmacological probes for the melanocortin receptors have been utilized for studying various disease states including cancer, sexual function disorders, Alzheimer's disease, social disorders, cachexia, and obesity. Of interest to our laboratory is the melanocortin system's role in energy homeostasis that is mediated through the melanocortin 3 receptor (MC3R) and melanocortin 4 receptor (MC4R). Specifically, our laboratory focuses on the development of novel pharmacological probes to better understand the role of the melanocortin receptor system's effects on energy homeostasis.

This thesis provides the field with foundational work addressing the functional effects of melanocortin bivalent ligands both *in vitro* and *in vivo*. In **Chapter 3** and **Chapter 4**, traditional homobivalent approaches are utilized. The synthesis and *in vitro* evaluation of homobivalent ligands are discussed in **Chapter 3**. Lead ligands (**CJL-1-87** and **CJL-1-31**) increased binding affinity by 14- to 25-fold and increased cAMP signaling potency by 3- to 5-fold compared to their monovalent counterparts depending on the specific melanocortin receptor subtype assayed. In **Chapter 4**, the *in vivo* effects of lead ligand **CJL-1-87** is characterized thoroughly. Bivalent ligand **CJL-1-87** had noteworthy advantages as an anti-obesity probe over its monovalent counterpart in a fasting-refeeding *in vivo* paradigm. Treatment with **CJL-1-87** significantly decreased food intake compared to **CJL-1-14** or saline (50% less intake 2 to 8 hours after treatment). Further energy expenditure parameters are explored, and possible mechanisms are discussed.

In **Chapter 5** and **Chapter 6**, uncommon approaches are attempted to exploit melanocortin dimers to elicit undiscovered pharmacological effects. In the **Chapter 5**,

we present melanocortin unmatched bivalent ligands (MUmBLs) as tools for studying asymmetric function of melanocortin receptor homodimers. MUmBLs contain one agonist scaffold and one antagonist scaffold designed to target a melanocortin homodimer pair such that one receptor is occupied by an agonist scaffold and the other receptor by an antagonist scaffold. Utilizing this design strategy to target the MC4R, first in class biased unmatched bivalent ligands (BUmBLs) were discovered. The BUmBLs displayed biased agonism in which they potently stimulated cAMP signaling, but resulted in minimal activation of the β -arrestin recruitment pathway.

In **Chapter 6**, we describe two different approaches that were pursued to further study melanocortin bivalent ligands' structure activity relationship (SAR). Homobivalent ligands were designed with 13, 16, 19, 20, and 22 atom linkers to explore the effects of linker length. Overall, these studies resulted in a "flat" SAR in which the compounds all have similar potencies and efficacies. Bivalent ligands were also designed to include the retro-inverso tetrapeptide scaffold DTrp-DArg-Phe-DHis. Although this scaffold lacked high binding affinity and potency, it was very metabolically stable. The incorporation of this scaffold into bivalent ligands yielded ligands with varying potencies and metabolic stabilities.

The current discoveries may be broadly applicable to other GPCR systems. As the physiological relevancy to GPCR oligomerization is elucidated, the current medicinal chemistry strategies presented in this thesis should aid in the discovery of probes and possible therapeutics for the further understanding of GPCR pharmacology for various systems.

Table of Contents

Abstract.....	iv
Table of Contents.....	vi
List of Tables.....	x
List of Figures.....	xii
List of Schemes.....	xvii
Chapter 1: Introduction: What do GPCR Oligomers, Entropic Cost of Binding, Melanocortin Signaling, and the Obesity Epidemic have in Common?.....	1
1.1 Bivalent Ligands targeting G Protein-Coupled Receptors.....	1
1.2 The Melanocortin Receptor System.....	3
1.3 Multivalent and Bivalent Ligands Targeting the Melanocortin System.....	7
1.3.1 Melanocortin Multivalent Ligands.....	9
1.3.2 Melanocortin Bivalent Ligands.....	13
1.4 Conclusions.....	19
Chapter 2: Materials and Methods.....	23
2.1 Chapter Overview.....	23
2.2 Solid Phase Peptide Synthesis.....	24
2.3 Resin Splitting Approach.....	27
2.4 Cell Culture.....	29
2.5 Competitive Radioligand Binding Affinity Studies.....	29
2.6 AlphaScreen [®] cAMP Functional Bioassay.....	31
2.7 ALPHAScreen Assay Data Normalization.....	33
2.8 PRESTO-Tango (β -arrestin Recruitment) Assay.....	34
2.9 Bioluminescence Resonance Energy Transfer (BRET) Studies.....	36
2.10 Serum Stability Studies-.....	38
2.11 Animals Studies.....	40
2.12 Cannulation Surgery and Placement Validation.....	41
2.13 In Vivo Energy Metabolism Studies.....	42

2.14 Body Composition Studies	44
2.15 Luminex Milliplex Hormone Panel Studies	44
2.16 Data Analysis	45
Chapter 3: The Design, Synthesis, In Vitro, and In Vivo Investigation of Homobivalent Ligands that Display Preferential Binding and Functional Activity for Different Melanocortin Receptor Homodimers.....	52
3.1 Chapter Overview	53
3.2 Introduction.....	53
3.3 Results and Discussion:	57
3.3.1 Design	57
3.3.2 Peptide synthesis.....	60
3.3.3 ¹²⁵ I-NDP-MSH Competitive Binding Affinity Studies.....	63
3.3.4 Functional cAMP Accumulation Studies.....	69
3.3.5 In Vivo ICV Administration Studies	79
3.4 Conclusion:	82
Chapter 4: A Direct In Vivo Comparison of The Melanocortin Monovalent Agonist Ac- His-DPhe-Arg-Trp-NH ₂ versus The Bivalent Agonist Ac-His-DPhe-Arg-Trp-PEDG20- His-DPhe-Arg-Trp-NH ₂ : A Bivalent Advantage.....	105
4.1 Chapter Overview:	105
4.2 Introduction.....	107
4.3 Results and Discussion:	111
4.3.1 In Vitro Mouse Serum Stability Assays.....	111
4.3.2 The Effect of ICV Administration of CJL-1-14 versus CJL-1-87 on Mouse Energy Homeostasis.....	113

4.3.3 The Effect of ICV Administration of CJL-1-14 and CJL-1-87 on Body Composition.....	119
4.3.4 The Effect of ICV Administration of CJL-1-14 and CJL-1-87 on Hormone Levels.....	121
4.3.5 ¹²⁵ I-AGRP Competitive Binding Studies.....	125
4.3.6 Bioluminescence Resonance Energy Transfer (BRET) Supports mMC3R-mMC4R Heterodimerization	128
4.3.7 Coexpression of mMC3R and mMC4R effects on Functional Potency	131
4.3.8 Coexpression of mMC3R and mMC4R Effects on Functional Potency and Discussion of Expression Levels	134
4.4 Conclusions.....	135
Chapter 5: Developing Biased Unmatched Bivalent Ligands (BUmBLs) to Target Asymmetrically Signaling Melanocortin-4 Receptor Homodimers	153
5.1 Chapter Overview	153
5.2 Introduction.....	154
5.3. Results and Discussion	158
5.3.1 Design and Synthesis.....	158
5.3.2 Biased Signaling at the hMC4R.....	161
5.3.3 Characterization of cAMP Signaling at the Mouse Melanocortin Receptors	168
5.3.4 ¹²⁵ I-NDP-MSH Competitive Binding Assays.	173
5.3.5 Ligand Dependent Modulation of BRET Signal	178
5.3.6 MUmBLs Effects on Energy Homeostasis in Mice.....	181

5.4 Conclusions.....	195
Chapter 6: Progressing the Structure Activity Relationship (SAR) of Bivalent Ligands: Evaluating the Effects of the Linker Length and Pursuing a Retro-Inverso Approach ..	242
6.1 Chapter Overview	242
6.2 Introduction.....	243
6.3 Results and Discussion	246
6.3.1 Synthesis	246
6.3.2 In Vitro Biological Characterization.....	246
6.3.3 In Vitro Mouse Serum Stability Assays.....	255
6.4 Conclusions.....	256
Chapter 7: Advancements Made, Lessons Learned, and Future Directions	269
Bibliography	273
Appendix: Summary of Analytical Information and Pharmacology of Compounds	300

List of Tables

Table 2.1. Competitive radioligand binding assays on the BRET receptor constructs.....	51
Table 3.1. Analytical data for peptides synthesized in this Chapter 3.....	97
Table 3.2. Summary of competitive binding experiments for compounds evaluated at the mouse melanocortin receptors	98
Table 3.3 Summary of functional experiments for His-DPhe-Arg-Trp-based compounds evaluated at the mouse melanocortin receptors	101
Table 3.4 Summary of functional experiments for His-DNal(2')-Arg-Trp and the His-DPhe(p-I)-Arg-Trp based compounds evaluated at the mouse melanocortin receptors.	103
Table 3.5 Latin-square (Cross-over) paradigm used for in vivo feeding experiments in Chapter 3.....	104
Table 4.1. Summary of the effects of fasting and melanocortin (MC) receptor agonism on hormone and cytokine levels from the literature (Lit.) and the current study.	149
Table 4.2: The experimental compounds were used to displace either ¹²⁵ I-NDP-MSH or ¹²⁵ I-AGRP in a dose-response manner to calculate the IC ₅₀ values.....	151
Table 4.3: Functional cAMP AlphaScreen® assays were performed to determine in vitro potency of compounds to induce cAMP signaling in five cell categories	152
Table 5.1: Functional data at the hMC4R.....	232
Table 5.2. The analytical data for peptides synthesized	234

Table 5.3: Summary of cAMP functional experiments and competitive binding experiments at the mMC1R, mMC3R, mMC4R, and mMC5R.	235
Table 5.4: Functional data at the mMC1R, mMC3R, mMC4R, and mMC5R with data from Chapter 3 for comparison.....	237
Table 5.5: Summary of competitive binding experiments at the mMC1R, mMC3R, and mMC4R with data from Chapter 3 for comparison.	239
Table 5.6. Table of adverse reactions observed in the current experiments with CJL-5-58 in wild-type mice, MC3RKO mice, and MC4RKO mice.....	241
Table 6.1. The analytical data for peptides synthesized	265
Table 6.2: Functional cAMP signaling data at the mMC1R, mMC3R, mMC4R, and mMC5R.....	266
Table 6.3: Summary of competitive binding experiments at the mMC1R, mMC3R, and mMC4R.....	268
Appendix Table A-1. The analytical data for peptides synthesized in this thesis	304
Appendix Table A-2: Functional data at the mMC1R, mMC3R, mMC4R, and mMC5R.	306
Appendix Table A-3: Summary of competitive binding experiments with ¹²⁵ I-NDP-MSH at the mMC1R, mMC3R, and mMC4R.	308

List of Figures

Figure 1.1: Structures of classic melanocortin ligands.	21
Figure 1.2. Bivalent and multivalent ligand binding modes.	22
Figure 2.1. Representative radioligand binding curves of the BRET receptor constructs...48	
Figure 2.2. Average results from hPYY cannulation validation experiments.	49
Figure 2.3: Experimental paradigms used to study energy homeostasis in Chapter 4	50
Figure 3.1. Design of ligands in Chapter 3 from selected scaffolds and linkers.	81
Figure 3.2. Crude RP-HPLC analytical chromatograms	86
Figure 3.3. Illustrations of the competitive binding experiments	87
Figure 3.4. Proposed binding mode of the bivalent ligands.	88
Figure 3.5. Postulated rationale for linker-dependent preferences at the different melanocortin homodimer subtypes.	90
Figure 3.6. Illustrations of the in vitro functional pharmacology at the mMC1R, mMC3R, mMC4R, and mMC5R of the His-DPhe-Arg-Trp based ligands.	91
Figure 3.8. Correlation of IC ₅₀ (nM) vs EC ₅₀ (nM) at the different receptor subtypes for His-DPhe-Arg-Trp based ligands.	93
Figure 3.9. AlphaScreen functional Schild analysis at the mMC3R and mMC4R of both our synthetically made (CJL-1-20) and the commercially bought analog (Peptides Int) of the Ac-His-DPhe(pI)-Arg-Trp-NH ₂	94

Figure 3.10. Cumulative food intake following intracerebroventricular administration of either saline (n=16 male; 8 female) or CJL-1-87 in saline (n=8 male; 4 female) in wild type mice.....	95
Figure 4.1. In vitro serum stability of bivalent ligands and control ligands	139
Figure 4.2. Investigation of 5 nmol bivalent ligand CJL-1-87 (—●—) compared to 5 nmol monovalent ligand CJL-1-14 (—▲—) (A) on energy homeostasis in TSE metabolic cages following a cross-over nocturnal feeding paradigm	140
Figure 4.3. Investigation of 5 nmol bivalent ligand CJL-1-87 (—●—) compared to 5 nmol monovalent ligand CJL-1-14 (—▲—) (A) and saline (—■—) on energy homeostasis in TSE metabolic cages following a cross-over paradigm.....	142
Figure 4.4. A new cohort of male mice received a single treatment of saline vehicle control (—■—, n=10), 5 nmol CJL-1-14 (—▲—, n=11), or 5 nmol CJL-1-87 (—●—, n=11) in the fasting paradigm.....	145
Figure 4.5. Bioluminescence resonance energy transfer (BRET) of the mMC3R and mMC4R.....	146
Figure 4.6. Cell categories for cAMP AlphaScreen® functional assays during coexpression experiments	148
Figure 5.1. Hypothesized interaction of ligands with asymmetrically signaling melanocortin homodimers.	201
Figure 5.2. Different possible binding states of a MUmBL.	202
Figure 5.3. In vitro mouse serum stability assay to aid in the design of the MUmBLs..	203

Figure 5.4. Illustrations of the in vitro functional pharmacology at the hMC4R of MUmBLs,	204
Figure 5.5. Illustrations of a previously reported model for allosteric interactions in GPCR dimers.....	205
Figure 5.6. Illustrations of the in vitro functional pharmacology of the MUmBLs at the mMC1R, mMC3R, mMC4R, and mMC5R.....	207
Figure 5.7. The functional dose response curve of CJL-1-124 () may increase the therapeutic window versus traditional dose response curves (▼).....	208
Figure 5.8: Illustrations of the competitive binding experiments against ¹²⁵ I-NDP-MSH at the mMC3R and mMC4R.....	209
Figure 5.9: Illustrations of the ¹²⁵ I-NDP-MSH competitive binding experiments with MUmBLs compared to monovalent tetrapeptide ligands separately and in a mixture at the mMC1R.....	210
Figure 5.10. Ligand induced response of bioluminescence resonance energy transfer (BRET) signal at the mMC4R-NanoLuc and MC4R-HaloTag homodimer.....	211
Figure 5.11. The dose response effect of CJL-5-58 administered ICV on cumulative food intake in male and female wild type mice utilizing a fasting refeeding paradigm.	212
Figure 5.12. The dose response effect of CJL-5-58 administered ICV on change in body weight in male and female wild type mice utilizing a fasting refeeding paradigm.....	213
Figure 5.13. The effect of CJL-5-58 administered ICV on cumulative food intake in male and female wild type mice utilizing nocturnal feeding paradigm.....	214

Figure 5.14 The effect of **CJL-5-58** administered ICV on change in body weight (g) in male and female wild type mice utilizing nocturnal feeding paradigm..... 215

Figure 5.15. TSE metabolic cage parameters after ICV administration of 5 nmols of **CJL-5-58**, or a combination of 5 nmols **CJL-1-14** and 5 nmols **CJL-1-80** (10 nmols total combined peptide) to male wild type mice in a fasting-refeeding paradigm..... 216

Figure 5.16 TSE metabolic cage parameters after ICV administration of 5 nmols of **CJL-5-58**, or a combination of **CJL-1-14** and **CJL-1-80** (10 nmols total peptide) to male wild type mice in a fasting refeeding paradigm..... 217

Figure 5.17. TSE metabolic cage parameters after ICV administration of 5 nmols of **CJL-5-58**, or a combination of **CJL-1-14** and **CJL-1-80** (10 nmols total peptide) to male wild type mice in a nocturnal feeding paradigm (no fasting). 219

Figure 5.18: TSE metabolic cage parameters after ICV administration of 5 nmols of **CJL-5-58**, or a combination of **CJL-1-14** and **CJL-1-80** (10 nmols total peptide) to male wild type mice in a nocturnal feeding paradigm..... 220

Figure 5.19. TSE metabolic cage parameters after ICV administration of 5.0, 2.5, or 1.0 nmols of **CJL-5-58** to male MC3RKO mice in a nocturnal feeding paradigm..... 222

Figure 5.20. TSE metabolic cage parameters after ICV administration of 1.0 or 0.5 nmols of **CJL-5-58** to male MC3RKO mice in a fasting-refeeding paradigm. 224

Figure 5.21. The effect of **CJL-5-58** (5 nmols) administered ICV on cumulative food intake and body weight in male MC4RKO mice utilizing nocturnal feeding and fasting-refeeding paradigm in conventional cages..... 226

Figure 5.22. TSE metabolic cage parameters after ICV administration of 5.0 or 2.5 nmols of CJL-1-124 to male wild type mice in a nocturnal feeding paradigm.	227
Figure 5.23. TSE metabolic cage parameters after ICV administration of 5.0 or 2.5 nmols of CJL-1-124 to male MC3RKO mice in a nocturnal feeding paradigm.....	229
Figure 5.24. The effect of CJL-1-124 (5.0 and 2.5 nmols) administered ICV on cumulative food intake and body weight in male MC4RKO mice utilizing nocturnal feeding paradigm in conventional cages.....	231
Figure 6.1. The chemical structures of selected scaffolds and linkers used in Chapter 6.	259
Figure 6.2. Design of melanocortin bivalent ligands containing retro-inverso scaffolds.	260
Figure 6.3. Illustrations of the competitive binding experiments at the mMC1R (A), mMC3R (B), and mMC4R (C).....	262
Figure 6.4. In vitro serum stability of linker length bivalent analogs at 24 h (A) and retro-inverso analogs at 24 h (B) and 72 h (C)	263
Appendix Figure A-1. The chemical structures of selected scaffolds and linkers used.	301

List of Schemes

Scheme 2.1 General synthesis scheme of split resin approach.	46
Scheme 2.2. Example of resin splitting synthesis scheme.	47

Chapter 1: Introduction: What do GPCR Oligomers, Entropic Cost of Binding, Melanocortin Signaling, and the Obesity Epidemic have in Common?

Portions of the information presented in this chapter have been published previously and are currently being reproduced in part with permission from: Ericson, M. D.; Lensing, C. J.; Fleming, K. A.; Schlasner, K. N.; Doering, S. R.; Haskell-Luevano, C. Bench-Top to Clinical Therapies: A Review of Melanocortin Ligands from 1954 to 2016. *Biochim. Biophys. Acta, Mol. Basis Dis.* **2017**, in press. Copyright (2017) Elsevier B.V.¹ The primary section being reproduced from this work is **Section 1.3** and was principally written by the current author, Cody J. Lensing, with contributions from the coauthors. **Figure 1.1** was made by and used with permission from Mark D. Ericson.¹

1.1 Bivalent Ligands targeting G Protein-Coupled Receptors

Approximately 30-40% of pharmaceuticals target G protein-coupled receptors (GPCRs) making them a highly sought-after drug target.^{2, 3} Because of their therapeutic significance, novel methods of targeting GPCRs that are distinct from classical approaches are desirable. Classically, ligands targeting GPCRs were designed to bind to orthosteric sites in a monomeric fashion. One alternative to this approach would be to design ligands that target multiple GPCR orthosteric sites through multivalent binding. There has been increasing evidence that GPCRs can form dimers with themselves (homodimers) and with other GPCRs (heterodimers) as well as higher order oligomers.⁴ These oligomers may represent new drug targets with unique exploitable functions compared to their monomeric receptor forms. Therefore, the development of chemical probes to study GPCR oligomerization is of great interest.

Bivalent ligand design strategies have been developed and used to study various GPCR dimer systems including: the opioid,⁵⁻¹² gonadotropin-releasing hormone,^{13, 14} adenosine,¹⁵ cannabinoid,^{16, 17} serotonin,¹⁸⁻²⁰ dopamine,^{21, 22} chemokine,^{10, 23} oxytocin,²⁴ and melanocortin receptor systems.²⁵⁻⁴⁰ Bivalent ligands are comprised of two pharmacophores separated by a linker or spacer. The two pharmacophores are designed to target two different binding sites, such as the two orthosteric binding sites of interacting GPCRs in a dimer. This bivalent ligand approach to study GPCR dimerization was pioneered by Portoghese and coworkers studying the opioid system.^{7, 12} Since their inception, bivalent ligands have been reported to have a variety of unique pharmacological effects that are distinct from their monovalent counterparts including: increasing or decreasing binding affinity,^{19, 21, 33} positively or negatively changing functional responses,^{15, 17, 20, 26, 41} altering receptor subtype selectivity,^{8, 21} changing receptor trafficking,⁴²⁻⁴⁴ and creating tissue selectivity.^{5, 10} Specifically, heterobivalent ligands featuring pharmacophores for two different receptor types have been utilized to exploit allosteric interactions within heterodimers. This allowed for the development of ligands with novel pharmacological profiles, tissue selectivity, and different functional effects.^{10, 11, 44-48}

Of particular interest to the development of future therapeutics, there are reports indicating that bivalent ligands may avoid the undesirable side effects exhibited by classic monovalent ligands.^{10, 11, 44, 46} A previous study of heterobivalent ligands targeting the δ and μ opioid receptor heterodimers resulted in a ligand with 50-fold higher opioid agonist potency, but devoid of tolerance commonly seen with monovalent opioid ligands.¹¹ Bivalent melanocortin ligands may, therefore, be able to circumvent undesirable side

effects seen with classic monovalent ligands. To discover possibly novel biological functions of ligands created using a bivalent ligand design strategy and to investigate their utility as probes to study GPCR dimerization, this thesis work explores the application of this design strategy on the melanocortin GPCR system.

1.2 The Melanocortin Receptor System

The melanocortin receptor system is involved in various physiological functions including pigmentation,^{49, 50} sexual behavior,⁵¹ blood pressure modulation,⁵² memory,⁵³⁻⁵⁵ and energy homeostasis.⁵⁶⁻⁵⁹ Therefore, ligands targeting the melanocortin GPCRs have been utilized as probes or investigated as potential therapeutics for Alzheimer's disease,⁶⁰⁻⁶² cancer targeting,^{6, 28, 63-65} sexual function,^{51, 66} social disorders,^{67, 68} cachexia,⁶⁹⁻⁷³ and obesity.^{56, 74-76} The system contains five G_{as} protein-coupled receptor subtypes (MC1-5R) that stimulate the cAMP signal transduction pathway upon agonist binding.^{49, 77-82} The melanocortin-1-receptor (MC1R) is expressed in the skin and is primarily involved in pigmentation.^{49, 77} The melanocortin-2 receptor (MC2R) is expressed in the adrenal cortex and is involved in steroidogenesis.⁴⁹ The centrally expressed melanocortin-3 and melanocortin-4 receptors (MC3R and MC4R) are linked to energy homeostasis.^{56, 57, 83-87} Additionally, the MC4R has a role in sexual function.^{88, 89} While the exact role of the melanocortin-5 receptor (MC5R) has not been elucidated,^{90, 91} it has been linked to exocrine function in mice.⁹²

In addition to the receptors involved, the melanocortin system is comprised of both endogenous agonists and antagonists (**Figure 1.1A and B**).¹ The naturally occurring agonists are derived from the proopiomelanocortin (POMC) gene transcript and include adrenocorticotrophic hormone (ACTH), β -melanocyte stimulating hormone (β -MSH), γ -

MSH, and α -MSH (**Figure 1.1A**).⁹³ All of these ligands contain the common tetrapeptide sequence His-Phe-Arg-Trp tetrapeptide sequence. This common signal sequence has been the center of many structure activity relationship (SAR) campaigns to discover synthetic agonists (*e.g.* NDP-MSH and MTII) and antagonists (*e.g.* SHU9119) (**Figure 1.1C**).⁹⁴⁻⁹⁹ The existence of endogenous antagonists is uncommon for GPCR systems. Melanocortin endogenous antagonists include agouti (ASP) and agouti-related protein (AGRP) (**Figure 1.1B**).¹⁰⁰⁻¹⁰² Additionally, agouti and AGRP possess inverse agonist activity in some organisms,^{103, 104} directly decreasing levels of cAMP within a cell.

The melanocortin system's role in energy homeostasis is of particular interest to both academic and industrial researchers due to the current obesity epidemic. Approximately one third of Americans are clinically obese.¹⁰⁵ It is estimated that the US spends \$209.7 billion each year on obesity-related diseases.¹⁰⁶ Obesity is associated with an increased risk of developing type 2 diabetes, cancer, hypertension, osteoarthritis, asthma, depression, and myocardial infarction.¹⁰⁶ These health and economic implications demand an integrative approach of public policy, education, preventative programs, and pharmaceutical intervention to treat obesity. Melanocortin-related effects on energy homeostasis are largely thought to be mediated through the MC3R and MC4R located in the hypothalamus.^{57, 76, 107} Therefore, ligands that target the MC3R or MC4R may provide a pharmaceutical therapy to overcome the current obesity epidemic.

Initial evidence of the role of the MC4R came from the knockout (KO) mouse model.⁵⁷ Female MC4R KO mice were two times heavier as their wild-type counterparts after 15 weeks. Male MC4R KO mice were one and a half times heavier than their wildtype counterparts.⁵⁷ Importantly, these genetic trends of the MC4R's role in obesity are

observed in human epidemiological studies as well. Individuals with a loss of function mutation in the MC4R accumulate more body mass compared to normal (wild type) patients as seen in their body mass index (BMI).^{108, 109} The difference in BMI was ~8-9 kg/m² for females and ~4-5 kg/m² for males.^{108, 109} In another study, 5.8% of patients (n=500) with severe childhood obesity were identified to have a mutation in the MC4R.¹¹⁰

Although the MC3R has been identified to play a role in energy homeostasis, there is less known about it. The MC3RKO mice, MC4RKO mice, and double MC3RKO/MC4RKO mice all displayed different phenotypes indicating non-redundant roles for the MC3R and MC4R.^{58, 111} The MC3RKO mice at 4-6 months of age were reported to have increased fat mass and reduced lean mass, but were hypophagic. The MC3RKO mice were also reported to be hyperleptinemic and mildly hyperinsulinemic.⁵⁸ The double MC3RKO/MC4RKO mice become significantly heavier than either the MC4RKO mice or MC3RKO mice. This result may indicate a synergistic effect between the two receptors.^{58, 111}

Further evidence of the melanocortin system's roles in energy homeostasis can be observed in pharmacological data. Central administration of MC3R and MC4R agonist ligands results in decreased food intake and increased energy expenditure, and therefore, agonists represent potential therapeutics for metabolic disorders resulting from net positive calorie consumption (*e.g.* obesity).^{25, 56, 57, 76, 107, 112} In contrast, central administration of MC3R and MC4R antagonist ligands result in increased food intake, and therefore, antagonists represent potential therapeutics for metabolic disorders resulting from a calorie deficit (*e.g.* cachexia and anorexia).^{56, 69, 76} Teasing out the exact effects of the MC3R compared to the MC4R has been challenging. Intracerebroventricular (ICV) administration

of mixed MC3R/MC4R endogenous antagonist/inverse agonist AGRP in both MC3R and MC4R male knockout mice results in increased food intake.^{76, 113} Similarly, administration of the MC3R/MC4R agonist melanotan-II (MTII) results in decreased food intake in both MC3R and MC4R knockout mice suggesting both receptors are possible therapeutic targets.¹¹¹

Based on both genetic and pharmacological reports, many pharmaceutical companies initiated melanocortin ligand discovery programs. However, reports of cardiovascular side effects associated with MC4R ligands in humans⁵² coupled with an increase in mergers within the pharmaceutical industry led to diminished industrial investment in melanocortin ligands. Despite these setbacks, melanocortin ligands have continued to be advanced to clinical trials.¹¹⁴⁻¹¹⁷ To date, no melanocortin ligands have been FDA-approved to treat metabolic disorders. The major identified limitations of melanocortin ligands as anti-obesity therapeutics is still their undesirable effects of modulating blood pressure^{52, 118} and inducing male erections.⁶⁶

Various strategies to overcome these limitations have been proposed in the field. One approach has been attempting to identify ligands that are MC3R selective over the MC4R with the hypothesis that MC3R ligands would not possess the cardiovascular effects. This has proven challenging, but ligands with some selectivity have been reported.¹¹⁹ Other strategies that may be hypothesized include identifying allosteric modulators, biased agonist, tissue specific ligands, or other unique pharmacologies not currently reported in the literature. To identify novel pharmacologies, melanocortin ligands based on new scaffolds and different targeting strategies are needed. Therefore, we pursued utilizing bivalent ligand design strategy to target the melanocortin receptor system.

As stated above, bivalent ligands have been demonstrated to have unique functional characteristics compared to monovalent counterparts including: increasing or decreasing binding affinity,^{19, 21, 33} positively or negatively changing functional responses,^{15, 17, 20, 26, 41} altering receptor subtype selectivity,^{8, 21} changing receptor trafficking,⁴²⁻⁴⁴ and creating tissue selectivity.^{5, 10} Due to these unique characteristics, bivalent ligands may offer distinct advantages over the classical monomeric approaches or allow for the discovery of new biological functions or pharmacologies. The ideal pharmacology for an anti-obesity probe would be a melanocortin bivalent agonist ligand that has reduced effects on sexual behavior⁵¹ and blood pressure⁵² while maintaining the desirable effect of decreasing food intake.^{56-58, 74, 76} However, any novel pharmacology discovered will allow for further understanding of the melanocortin system.

1.3 Multivalent and Bivalent Ligands Targeting the Melanocortin System

Before and during this current thesis's work, research, and preparation; bivalent and multivalent ligand design strategies targeting the melanocortin receptors have been utilized. Mainly, bivalent and multivalent ligands were used only to achieve high binding affinity ligands and often functional effects on signaling pathways were not evaluated. To give an adequate introduction and review of the current state of this field (as of May 2017), we will supply a short review of reports to date. Hopefully, this will allow a thorough understanding of the current work, its context in the established literature, and its contribution to the field.

A major benefit of bivalent or multivalent ligand binding strategies is the lowered entropic cost of binding by allowing multiple binding interactions per ligand resulting in cooperative binding affinity (**Figure 1.2 A-C**).^{7, 120-124} Recent studies have suggested the

presence of melanocortin receptor dimers (or higher-order oligomers) for every known melanocortin subtype.¹²⁵⁻¹³² Furthermore, radiolabeled ligand binding studies suggested that there are two side by side receptor binding sites (indicative of homodimerization) each with different binding properties on cells expressing the melanocortin receptors.^{133, 134} This suggests targetable dimers that may be functionally relevant.^{133, 134} The reported bivalent and multivalent ligands are likely taking advantage of the dimerization or oligomerization of multiple melanocortin receptors together on the cell membrane (**Figure 1.2 D-E**).

A large portion of the prior work into bivalent and multivalent melanocortin ligands has been as probes to study melanoma. Since melanoma cells often express elevated levels of the MC1R, it was hypothesized that ligands with high MC1R affinity could be conjugated to dyes or other labels and utilized as imaging or diagnostic tools.¹³⁵⁻¹³⁹ These high affinity ligands might also be used to deliver therapeutics selectively to melanoma cells. However, this targeting strategy has been criticized because stimulation of the MC1R has been shown to increase melanocyte proliferation and, therefore, could possibly lead to melanoma growth.^{140, 141} The use of melanocortin ligands as diagnostic tools has been reviewed previously, and is not the focus of the current thesis work.¹³⁵⁻¹³⁹ The current work is focused on studying the effects of melanocortin bivalent ligands on energy homeostasis. This introduction will focus on updating the medicinal chemistry approaches that have been applied to bivalent and multivalent melanocortin ligands in general. Multivalent ligands possessing more than two pharmacophores will be reviewed first, followed by bivalent ligands containing exactly two pharmacophores.

One difficulty in understanding the pharmacology of bivalent and multivalent ligands is discerning whether the effects are from a cooperative synergistic binding mode,

or due to the effect of increasing the pharmacophore concentration without synergy effects. Large increases in binding affinity compared to the monovalent controls (>10-fold) are hypothesized to be due to a cooperative synergistic bivalent or multivalent binding mode (**Figure 1.2**). While melanocortin bivalent ligands have been shown to enhance binding affinity, rarely additional pharmacophores beyond two have been reported to result in further binding affinity gains at the melanocortin receptors as discussed below.^{28, 123}

1.3.1 Melanocortin Multivalent Ligands

Multivalent ligands are defined as ligands that feature more than two pharmacophores for the melanocortin receptors, ranging from three to several hundred. Conjugates of multiple copies α -MSH derivatives to larger biomolecules were reported starting in 1977.^{142, 143} Eberle and coworkers reported conjugating α -MSH to human serum albumin at a ratio of four and six α -MSH hormones to one molecule of albumin and showed approximately equal activity to non-conjugated α -MSH analogs in testing on *Rana pipiens* (*i.e.* frogs). Schwyzer and coworkers reported loading the tobacco mosaic virus (TMV) with approximately 400-600 molecules of α -MSH analogs, resulting in enhanced potency, affinity, resistance towards enzymatic degradation, and prolonged activity at target cells.¹⁴⁴⁻¹⁴⁹ Sharma and coworkers developed a class of multivalent fluorescent melanotropin-macromolecule conjugates.^{150, 151} They used a polyvinyl alcohol (PVA) scaffold that had an approximate molecular weight of 110,000 and 2500 hydroxyl groups available for derivation. The hydroxyl groups were conjugated to introduce 10-16 molecules of a melanocortin pharmacophore (based on NDP-MSH) and 10-16 molecules of a fluorophore (fluorescein isothiocyanate or FITC) to create macromolecular conjugates (MSH-PVA-FITC). These conjugates possessed increased binding affinity and increased

levels of melanocortin receptor detection in labeling experiments comparing different cells that did or did not express the melanocortin receptors.^{150, 151} Sharma and coworkers also developed both latex bead and polyamide bead conjugates to NDP-MSH analogs and achieved similar results as Schwyzer and coworkers.¹⁵²⁻¹⁵⁴ The latex beads were considered microspheres (~1 μm in diameter) and the polyamide beads were classified as macrospheres (40 to 100 μm in diameter). Electron and light microscopy imaging indicated that multiple latex microspheres were bound to B16/F10 mouse melanoma cells (~10-15 μm in diameter). The larger polyamide macrospheres were bound to multiple cells, a difference presumed to be due to the relative sizes of the conjugated beads and the cells.

In 2007, Newton and coworkers engineered and fused α -MSH analogs to phages and used these multivalent phage constructs to image B16-F1 mouse melanoma *in vitro* and *in vivo*.¹⁵⁵ In 2011 and 2013, Barkey and coworkers attached hMC1R selective α -MSH analogs to stabilized triblock polymer micelles through Cu-catalyzed click chemistry.^{65, 156} Though the ligand decreased binding affinity of the polymer micelles after attachment, it increased specificity for the hMC1R over the hMC4R and hMC5R.⁶⁴ Further cross-linking the targeted polymer micelles generated constructs that were used as delivery systems for contrast-enhancing gadolinium complexes of texaphyrin (Gd-Tx).⁶⁵ These agents were efficacious at penetrating and delivering the contrast agent into xenografted tumors in mice with minimal accumulation in healthy tissues, including the kidney and liver.⁶⁵

Besides conjugated multivalent ligands, additional research has focused on the design of smaller, synthetic ligands. One design strategy to create trivalent ligands has been to incorporate a lysine into the linker of bivalent ligands, providing an additional chemical handle to add another pharmacophore. This method of creating trivalent ligands has

resulted in ligands that possessed increased binding affinity over bivalent and monovalent ligands at the hMC4R, but the results were reported to not be indicative of trivalent binding.¹⁵⁷ In a different design strategy in 2011, Brabez and coworkers reported a series of trivalent melanocortin ligands with increased binding affinity in support of a trivalent cooperative binding mode. They found the optimal distance between His-DPhe-Arg-Trp tetrapeptide pharmacophores to be 24 ± 5 Å when targeting the hMC4R.²⁸ In competitive binding experiments with HEK293 cells expressing the hMC4R, the monovalent, bivalent, and trivalent analogs had IC₅₀ values of 4900, 310, and 14 nM, respectively. The increased affinity with each valency suggested that three receptors were involved in a trivalent cooperative binding mechanism with the trivalent ligand.^{28, 123} The authors noted that although cAMP signaling potency increased with each valency, the levels of cAMP signaling corresponded to receptor occupancy independent of valency. This suggested that the ligands activated cAMP signaling in a monovalent fashion and no allosterism or synergy in function was detected.²⁸ In a follow-up study, the authors conjugated multiple trivalent ligands together resulting in ligands with 6 and 9 pharmacophores.¹⁵⁸ The 6- and 9-valent compounds decreased binding affinity 3-fold at the hMC4R compared to the trivalent analog, but were approximately 100-fold more potent than the monovalent compound. These data suggest the 6- and 9- pharmacophore ligands achieved cooperative binding but three or fewer receptors were involved. The cAMP signaling was also independent of the number of pharmacophores present, as previously described. They reported that all compounds were internalized within 90 minutes, suggesting these constructs could potentially be used for drug delivery purposes.¹⁵⁸

Solanesol-derived and sucrose-derived scaffolds were utilized to make both bivalent and tetravalent ligands attached to the His-DPhe-Arg-Trp tetrapeptide sequence.^{159, 160} Moderate improvement in binding affinity at the hMC4R was observed, likely due to proximity effects and increasing the moles of pharmacophore present, but not indicative of cooperative or multivalent binding. The authors hypothesized their ligands may not possess the correct linker length or improperly presented the pharmacophores for cooperative binding.^{159, 160}

A unique strategy to synthesize multivalent ligands featuring the His-DPhe-Arg-Trp tetrapeptide was reported by Dehigaspitiya and coworkers in 2015. Linear ligands that had up to eight His-DPhe-Arg-Trp units were synthesized and separated by a (Pro-Gly)₃ linker. The binding affinities for the hMC4R were slightly enhanced in competitive binding experiments when adjusted for pharmacophore concentrations, suggesting the observed enhancement were not from cooperativity or multivalent binding.¹⁶¹

In 2015, Elshan and coworkers presented trivalent scaffolds featuring the His-DPhe-Arg-Trp tetrapeptide pharmacophore and compared them to monovalent bivalent ligands. The bivalent ligands increased binding affinity 10- to 30-fold, indicating synergistic bivalent binding affinity at the hMC4R. The trivalent ligands were reported to be only marginally better binders (~2-fold) than the bivalent ligands. This indicated that the benefits in binding for the trivalent ligands are derived from a bivalent binding mode, but that true trivalent binding was not achieved with these ligands.¹⁶² Their results suggested the optimal linker length to bridge two receptors is between 17 and 23 Å. However, considering a third receptor did not appear to be utilized, it is likely that the third pharmacophore linker is not optimized to achieve trivalent binding.¹⁶² Dehigaspitiya and

coworkers reported similar results when comparing monovalent, bivalent, trivalent and tetravalent ligands featuring the tetrapeptide His-DPhe-Arg-Trp in different scaffolds.¹⁶³ All multivalent compounds possessed 30- to 40-fold higher binding affinities at the hMC4R compared to monovalent controls, although valencies beyond two did not result in further affinity gains. This finding is consistent with bivalent binding to putative melanocortin receptor dimers, without evidence for trivalent or tetravalent binding. They also reported the optimal distance between pharmacophores was between 17 and 23 Å, as previously reported.^{162, 163}

1.3.2 Melanocortin Bivalent Ligands

Bivalent ligands are the simplest form of multivalent ligands featuring two pharmacophores separated by a linker or spacer. The two pharmacophores are intended to target two different binding sites. Bivalent ligands were first reported in the clinic by Barb and coworkers as diagnostic tools.¹⁶⁴⁻¹⁶⁷ A subclass of bivalent ligands is bitopic ligands, which target both an orthosteric and an allosteric binding site on the same receptor. To the author's knowledge, there are no known bitopic melanocortin ligands. Therefore, in this thesis the term bivalent ligand will be used exclusively for ligands that target two orthosteric binding sites on two different receptors.

Orthosteric bivalent ligands are commonly split into two classes: homobivalent ligands and heterobivalent ligands. Homobivalent ligands contain the same pharmacophore on each side of the linker. Heterobivalent ligands contain two different pharmacophores for two different GPCR types on each side of the linker. Heterobivalent ligands that contain one melanocortin pharmacophore have been developed as probes for targeting melanoma or other cancers.^{6, 168-173} These ligands feature a pharmacophore for the melanocortin

receptors and a pharmacophore for a different receptor system (including opioid receptors or cholecystinin). Monovalent binding occurs to cells expressing one receptor subtype. However, synergistic bivalent binding occurs only on cells expressing both receptor types.^{6, 168-173} If appropriate receptor pairs are selected that are co-expressed in cancer cells but not in normal cells, the synergistic bivalent binding will selectively happen on cancer cells. A fluorescent label can be conjugated in the inert linker region, resulting in high affinity ligands that can be used for cancer imaging and diagnostics. Replacement of the fluorescent label with a chemotherapeutic can result in a highly selective drug targeting strategy.^{6, 168-173} This heterobivalent ligand targeting strategy has been validated both *in vitro* and *in vivo*.^{6, 168-172} In 2012, Xu and coworkers synthesized heterobivalent ligands containing a melanocortin pharmacophore and a cholecystinin pharmacophore separated by a fluorescently-labeled synthetic linker. They observed the ligands had up to a 12-fold higher specificity for tumors co-expressing both receptors than for tumors expressing one receptor, providing a proof-of-principle for future studies.⁶ Although these ligands do hold promise, the current thesis will focus on bivalent ligands that target only the melanocortin receptor system.

This work focuses mainly on homobivalent ligands (containing two of the same pharmacophores). These are discussed in **Chapter 3**, **Chapter 4**, and **Chapter 6**. A class of bivalent ligands that are comprised of two different pharmacophores, but both targeting the melanocortin receptors, will also be discussed in **Chapter 5** and **Chapter 6**. The key differentiator between previously described heterobivalent ligands and the bivalent ligands described in **Chapter 5** and **6**, is that the ligands herein are comprised of one agonist pharmacophore and one antagonist pharmacophore on each side of the linker that both

target the same receptor. In order to differentiate from heterobivalent ligands that target two different GPCR types, we have titled this class of ligands “melanocortin unmatched bivalent ligands,” which is abbreviated MUmBLs.

Carrithers and Lerner developed one of the earliest series of homobivalent melanocortin ligands in 1996 to target two separate melanocortin receptors by crosslinking them. They utilized either an agonist pharmacophore based on α -MSH or the pharmacophore Met-Pro-DPhe-Arg-DTrp-Phe-Lys-Pro-Val tethered by a poly-lysine linker.^{26, 174} They demonstrated that the agonist bivalent ligand increased functional activity 5- to 7-fold. In the frog melanocyte dispersion assay utilized, the Met-Pro-DPhe-Arg-DTrp-Phe-Lys-Pro-Val-based monovalent ligand was reported to antagonize α -MSH mediated dispersion in a dose-dependent manner. At high concentrations, the bivalent ligand based on Met-Pro-DPhe-Arg-DTrp-Phe-Lys-Pro-Val resulted in an agonist functional response.¹⁷⁵ This was the first report demonstrating increased functional activity with melanocortin bivalent ligands targeting putative dimers.

After the above report, homobivalent ligand development primarily focused on increasing the binding affinity at the hMC4R through various bivalent ligand design strategies,^{28, 120, 123, 157, 161-163, 176-180} with some reports focusing on the MC1R and *in vivo* imaging.^{40, 180-182} While high affinity ligands are desirable for biological responses, the use of low affinity pharmacophores in bivalent ligand design allows the greatest detection of synergistic binding^{28, 40, 120, 122, 124, 157, 176, 179}. Therefore, analogs with lower initial monovalent binding affinities result in the greatest observable fold enhancements via a bivalent design strategy. Research programs primarily utilized different analogs of the agonist NDP-MSH (**Figure 1.1**). These included the tetrapeptide His-DPhe-Arg-Trp,^{28, 120,}

^{123, 157, 161-163, 176, 178, 180} six residue analogs, ^{157, 181, 182} seven residue analogs, ^{40, 177, 179} and full length NDP-MSH. ^{120, 176, 178} Antagonist analogs in which the DPhe was replaced with DNaI(2') have been utilized as well to produce antagonist analogs with increased binding affinity. ^{179, 180} There has also been one report to date in which a melanocortin agonist pharmacophore was attached to an antagonist pharmacophore via a linker that also resulted in increased binding affinity, but functional activity was not assayed. ¹⁷⁹

In the reports to date, linker optimization has been a primary goal of melanocortin homobivalent ligand design. The optimal linker length must be long enough to bridge or crosslink two receptors, but not too long to eliminate entropic gains. Various linker systems have been incorporated including poly-lysine, ^{175, 177} polyethylene glycol, ^{157, 163, 177-180} Ala-Gly, ¹⁵⁷ Pro-Gly, ^{157, 161, 177, 179, 180} rigid amino acids, ¹⁷⁶ squalene, ¹²⁰ glycerol, ¹⁶³ D-mannitol, ¹⁶³ phloroglucinol, ¹⁶² tripropargylamine, ¹⁶² 1,4,7-triazacyclononane, ¹⁶² others, ^{28, 40, 123} and mixtures of these different linker systems together. Improper linker design may result in some increased binding affinity (<10-fold) that can be attributed to simply doubling the pharmacophore concentration. ^{157, 176, 177} Greater fold enhancements (>10-fold) are observed with linkers that appear to bridge two receptors resulting in cooperative synergistic binding (**Figure 1.2 A-C**). An optimal linker length of approximately 23 ± 5 Å has been suggested by multiple studies at the hMC4R. ^{28, 162, 163, 177, 179}

An assumption in the field prior to this thesis work was that a bivalent ligand optimized for the MC4R would be effective as a diagnostic tool for melanoma (that highly expresses the MC1R), as long as a non-selective pharmacophore was incorporated. As a result, the majority of studies only investigated *in vitro* pharmacology using HEK293 cells overexpressing the hMC4R, which resulted in ligands optimized for the hMC4R. This

thesis work challenges this assumption by providing evidence that the linker systems, independent of the binding pharmacophore, displayed preferential patterns for different melanocortin receptor subtypes.¹⁸⁰ Similar trends for other GPCR systems have been reported,¹⁸³⁻¹⁸⁵ highlighting the importance of optimizing the linker and pharmacophore for a specific receptor subtype if high affinity and specificity is desired. Our work on investigating bivalent ligands' preferential binding affinities and functional activities for the different melanocortin receptor homodimers is discussed in detail in **Chapter 3**.

Binding affinity is usually the optimized parameter in melanocortin bivalent designs, but there are a few reports discussing bivalent ligand effects on functional potency. As described above, Carrithers and Lerner observed a 5- to 7-fold enhancement relative to the monovalent ligand in a functional frog-melanocyte dispersion assay (presumably through the MC1R).¹⁷⁵ Another study by Brabez and coworkers compared the effects of monovalent, bivalent, and trivalent ligands on cAMP signaling in HEK293 cells expressing the hMC4R and observed increased cAMP signaling corresponding to increased valency.²⁸ It was reported in work resulting from this thesis that although bivalent ligands increased binding affinity (14- to 25-fold), more moderate increases in cAMP signaling potency were observed (3- to 5-fold) (see **Chapter 3**). Considering that at least a doubling in functional potency would be expected due to doubling the pharmacophore concentration, these increases suggested minimal synergy in function due to bivalent ligand design.¹⁸⁰ Several hypotheses have been proposed for the possible divergences between binding affinity and functional potency, including unique $\beta\gamma$ subunit signaling, potency masking, auxiliary binding sites, signal amplification events, and asymmetric dimer signaling.^{28, 175, 180} Given the limited reports of bivalent ligands' functional effects, this thesis work sought to further

expand the characterization of the functional activities of melanocortin bivalent ligands. Our work on homobivalent ligands' functional effects both *in vitro* and *in vivo* are discussed in **Chapter 3** and **Chapter 4**. Then in **Chapter 5**, we characterize the functional effects of the designed MUmBLs to explore possible reasons for the divergences between binding affinity and functional potency. In **Chapter 6**, further structure activity relationships (SAR) are examined by exploring linker length and the incorporation of a retro-inverso pharmacophore DTrp-DArg-Phe-DHis into the bivalent ligand design.

Most of the previous *in vivo* studies on melanocortin homobivalent ligands have focused on their utility as diagnostic tools, and not on their functional efficacy.^{40, 135, 136, 164, 165, 181, 182} As noted above, the use of high affinity ligands for the MC1R coupled to dyes or radiolabeled have been identified as possible imagining tools, diagnostic tools, or targeting molecules for melanoma. To our knowledge, there were no reports of the functional effect of melanocortin bivalent ligands *in vivo* prior to our report in 2016 as presented in **Chapter 3**.²⁵ We reported that the ICV administration of melanocortin homobivalent ligand **CJL-1-87** (Ac-His-DPhe-Arg-Trp-PEDG20-His-DPhe-Arg-Trp-NH₂) in mice resulted in dose-dependent decrease in food intake.²⁵ However, comparison to the monovalent ligand Ac-His-DPhe-Arg-Trp-NH₂ suggested little improvement in a nocturnal feeding paradigm.^{25, 132, 186} To further elucidate the *in vivo* effects, we performed studies to compared the effects of **CJL-1-87** to its monovalent counterpart **CJL-1-14** (Ac-His-DPhe-Arg-Trp-NH₂) utilizing our in-house TSE metabolic cage system. These studies showed significant differences between **CJL-1-87** and **CJL-1-14** after ICV administration in a fasting-refeeding paradigm in mice.¹³² Administration of **CJL-1-87** resulted in 50% less food intake than the monovalent 2 to 8 hours post-treatment. Treatment also resulted in

significantly lowered respiratory exchange ratio (RER) as well as significantly decreased insulin, C-peptide, leptin, and resistin plasma levels compared to the monovalent ligand Ac-His-DPhe-Arg-Trp-NH₂.¹³² Further details and conclusions from these studies are presented in **Chapter 4**. In **Chapter 5**, *in vivo* data will be presented about the MUmBL compounds.

1.4 Conclusions

In summarizing the reports to date about bivalent and multivalent ligand designs for the melanocortin receptors, two key observations can be made. First, in order to observe synergistic effects, the proper pharmacophore must be used. In almost all cases, the use of tetrapeptide His-DPhe-Arg-Trp was observed to result in the greatest-fold affinity enhancements, presumably due to synergistic binding. This is likely due to the lower initial binding affinity of the monovalent tetrapeptide compared to longer analogs, which therefore allows easier detection and observation of the bivalent synergistic binding mode. The second key is the design of proper linker length to bridge putative melanocortin dimers. The greatest-fold enhancements were with linkers of approximately 23 ± 5 Å. One difficulty in estimating the exact length is that the linkers used are flexible and therefore nearly impossible to measure precisely. The estimated range for the optimal melanocortin linker is similar to that of other GPCR systems including the oxytocin (~ 25 Å),¹⁸⁷ opioid (~ 22 Å),^{11, 184, 188} and dopamine receptors (~ 25 Å).¹⁸⁵ This provides strong evidence for a common design of bivalent ligands targeting various GPCR systems and suggests this length may be the result of a common GPCR phenomenon (dimerization or high-order oligomerization). We utilized these observations from the literature as guiding principles in the bivalent ligand design throughout the current thesis.

Prior to this thesis bivalent melanocortin ligands' increased binding affinity supported their use as diagnostic tools, imaging probes, and drug delivery vehicles for melanoma, but their functional effects required further investigation. The purpose of this thesis was to provide the field with foundational work addressing the functional effects of melanocortin bivalent ligands both *in vitro* and *in vivo*, and to study in more detail their effects on energy homeostasis. **Chapter 3** and **Chapter 4** use traditional homobivalent approaches to help further advance the field. **Chapters 5** and **Chapters 6** take uncommon approaches in attempts to exploit melanocortin dimers to elicit undiscovered pharmacological effects. It seems likely that the current discoveries may be broadly applicable to various other GPCR systems. As the physiological relevancy to GPCR oligomerization is elucidated, the current medicinal chemistry strategies presented in this thesis should aid in the discovery of probes and possible therapeutics for the further understanding of GPCR pharmacology for various systems.

To address the question posed in the chapter title: “What do GPCR Oligomers, Entropic Cost of Binding, Melanocortin Signaling, and the Obesity Epidemic have in Common?” They are all key components in the goal of this thesis: To use bivalent ligands to target GPCR oligomers to decrease entropic cost of binding and elicit novel melanocortin signaling patterns in hopes of finding a solution to the obesity epidemic and other metabolic disorders.

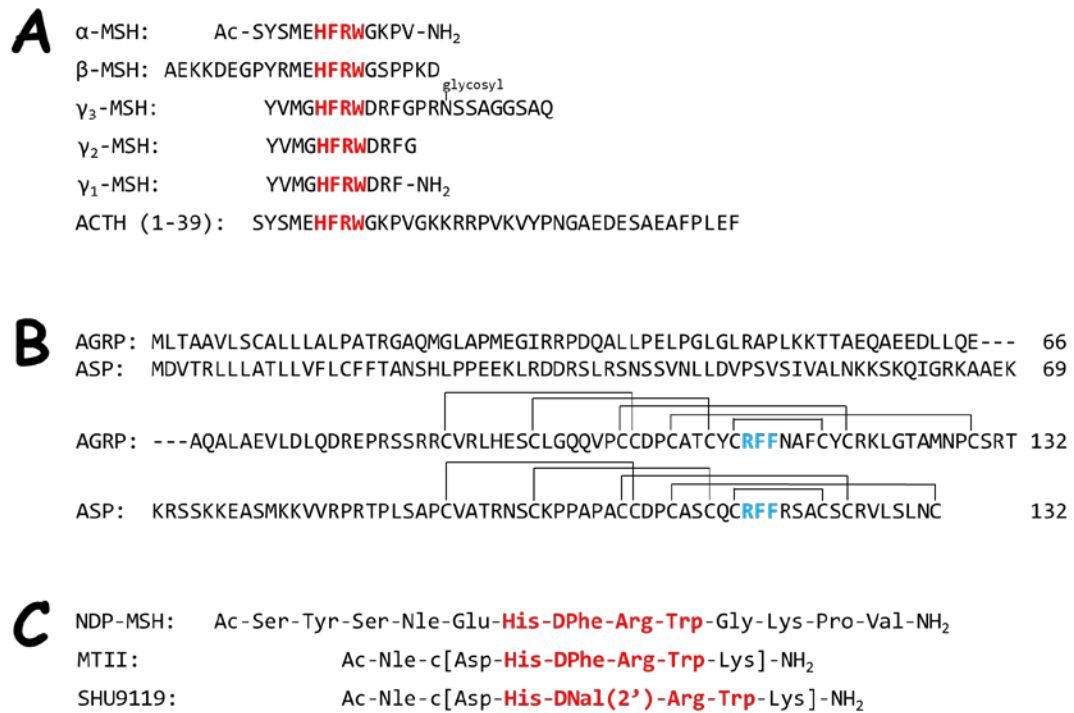


Figure 1.1: Structures of classic melanocortin ligands. (A) POMC-derived naturally occurring agonists (the common His-Phe-Arg-Trp tetrapeptide is highlighted in red). (B) The sequences of endogenous antagonists AGRP and ASP (the active Arg-Phe-Phe tripeptide is highlighted in blue). (C) The synthetic ligands NDP-MSH, MTII and SHU9119 (hypothesized pharmacophore region highlighted in red). This figure was made by Mark D. Ericson and reproduced with permission from Ericson, M. D.; Lensing, C. J.; *et. al.* Bench-Top to Clinical Therapies: A Review of Melanocortin Ligands from 1954 to 2016. *Biochim. Biophys. Acta, Mol. Basis Dis.* **2017**, in press. Copyright (2017) Elsevier B.V. ¹

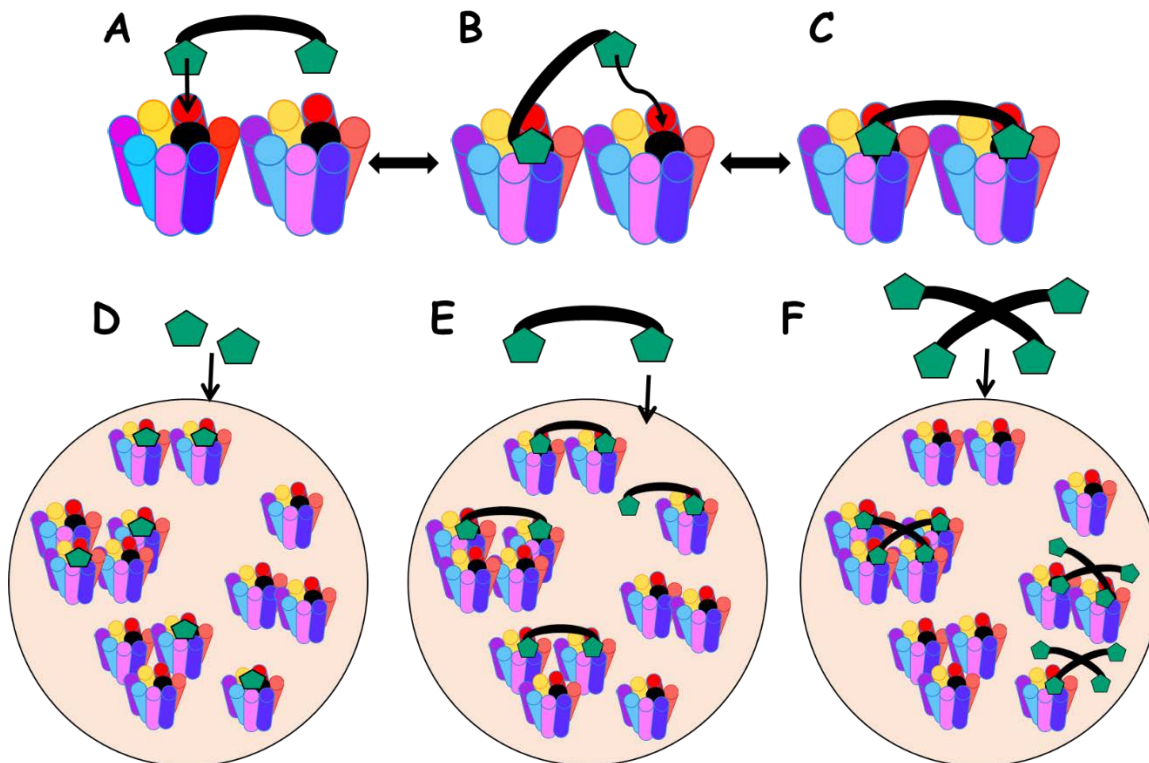


Figure 1.2. Bivalent and multivalent ligand binding modes. (A) The bivalent ligand first binds a receptor with one pharmacophore in a monovalent fashion. (B) The second pharmacophore is tethered in close proximity to the second binding site. (C) The second pharmacophore can bind the second receptor with reduced entropic cost. Similar binding mode may exist for multivalent ligands with more than two pharmacophores. (D) Monovalent ligands bind monomers, dimers, and higher-order oligomers equally. (E) Bivalent ligands bind dimers and higher-order oligomers in a cooperative synergistic fashion. (F) Multivalent ligands bind GPCR clusters in a cooperative synergistic fashion. This figure was reproduced with permission from Ericson, M. D.; Lensing, C. J.; *et. al.* Bench-Top to Clinical Therapies: A Review of Melanocortin Ligands from 1954 to 2016. *Biochim. Biophys. Acta, Mol. Basis Dis.* **2017**, in press. Copyright (2017) Elsevier B.V.¹

Chapter 2: Materials and Methods

Portions of the methods described in this chapter have been previously published, and it is being reproduced here with permission from: Lensing, C. J.; Freeman, K. T.; Schnell, S. M.; Adank, D. N.; Speth, R. C.; Haskell-Luevano, C. An *in Vitro* and *in Vivo* Investigation of Bivalent Ligands That Display Preferential Binding and Functional Activity for Different Melanocortin Receptor Homodimers. *J. Med. Chem.* **2016**, *59*, 3112-3128.²⁵ Copyright (2016) American Chemical Society. Also it is being reproduced with permission from: Lensing, C. J.; Adank, D. N.; Wilber, S. L.; Freeman, K. T.; Schnell, S. M.; Speth, R. C.; Zarth, A. T.; Haskell-Luevano, C. A Direct *In Vivo* Comparison of The Melanocortin Monovalent Agonist Ac-His-DPhe-Arg-Trp-NH₂ versus The Bivalent Agonist Ac-His-DPhe-Arg-Trp-PEDG20-His-DPhe-Arg-Trp-NH₂: A Bivalent Advantage. *ACS Chem. Neurosci.* **2017**, in press.¹³² Copyright (2017) American Chemical Society. And finally it is being reproduced with permission from: Lensing, C. J.; Adank, D. N.; Doering, S. R.; Wilber, S. L.; Andreasen, A.; Schaub, J. W.; Xiang, Z.; Haskell-Luevano, C. Ac-Trp-DPhe(p-I)-Arg-Trp-NH₂, a 250-Fold Selective Melanocortin-4 Receptor (MC4R) Antagonist over the Melanocortin-3 Receptor (MC3R), Affects Energy Homeostasis in Male and Female Mice Differently. *ACS Chem. Neurosci.* **2016**, *7*, 1283-1291.¹⁸⁹ Copyright (2016) American Chemical Society.

2.1 Chapter Overview

In the pursuit of designing, synthesizing, and evaluating melanocortin bivalent ligands many different techniques and experimental paradigms were utilized. These techniques and assay paradigms included: solid phase peptide synthesis, cell culture, cAMP Alpha Screen technology, competitive radioligand binding studies, PRESO-Tango (β -

arrestin recruitment) assays, bioluminescence resonance energy transfer (BRET) studies, *in vitro* serum stability studies, mouse breeding, ICV administration of compounds to mice, metabolism studies, hormone level studies, and more. The methods and materials for each of these techniques will be presented below. I would like to thank all my teachers, mentors, coworkers, and colleagues for their support by either teaching me these techniques or performing these experiments. I would specifically like to thank those that were or are in the Haskell-Luevano laboratory including Carrie Haskell-Luevano, Katie Henning (Freeman), Danielle Adank, Stacey Wilber, Branden Smeester, Sathya Schnell, Skye Doering, Katlyn Fleming, Katie Schlasner, Mark Ericson, Michael Powers, Mary Lunzer, Zoe Koerperich, Srinivasa Tala, and Anamika Singh. I would also like to thank those that contributed to the work from other laboratories including Adam Zarth, Erika Dahl, Radleigh Santos, and Robert Speth.

2.2 Solid Phase Peptide Synthesis

All experimental ligands were synthesized using standard solid-phase peptide synthesis. Specifically, a fluorenyl-9-methoxycarbonyl (Fmoc) methodology was utilized.^{190, 191} A CEM Discover SPS manual microwave peptide synthesizer was used to expedite couplings and deprotections especially where common sequences were present. A semi-automated synthesizer (LabTech, Louisville, KY) without the use of a microwave was also used for parallel synthesis. The 4-(2',4'-dimethoxyphenyl-Fmoc-aminomethyl)phenoxyacetyl-MBHA resin [Rink-amide-MBHA (200-400 mesh), 0.35-0.37 meq/g substitution], 2-(1H-benzotriazol-1-yl)-1,1,3,3-tetramethyluronium hexafluorophosphate (HBTU), and Fmoc-protected amino acids [Fmoc-Pro, Fmoc-Gly, Fmoc-His(Trt), Fmoc-DPhe, Fmoc-Arg(Pbf), Fmoc-Trp(Boc), and Fmoc-DNal(2')] were

purchased from Peptides International (Louisville, KY, USA). The O-(N-Fmoc-3-aminopropyl)-O'-(N-diglycolyl-3-aminopropyl)-diethyleneglycol [Fmoc-NH-(PEG)₂-COOH (20atoms) or Fmoc-NH₂-PEDG20-COOH] was purchased from Novobiochem® EMD Millipore Corp (Billerica, MA, USA). The *N,N*-diisopropylethylamine (DIEA), triisopropylsilane (TIS), 1,2-ethanedithiol (EDT), piperidine, pyridine, and trifluoroacetic acid (TFA) were purchased from Sigma-Aldrich (St. Louis, MO). Acetonitrile (MeCN), *N,N*-dimethylformamide (DMF), acetic anhydride, dichloromethane (DCM), and methanol (MeOH) were purchased from FischerScientific. All reagents were ACS grade or better and were used without further purification.

Peptides were assembled on the Rink-amide-MBHA resin in a fritted polypropylene reaction vessel (25 mL CEM reaction vessel). After resin was swelled in DCM for at least one hour, it was continually mixed by bubbling nitrogen. Subsequently, a two-step cycle of deprotection with 20% piperidine in DMF, followed by amide coupling with the Fmoc-amino acid, HBTU, and DIEA was repeated until the final peptide was synthesized on resin. Excess reagents were removed by 3-5 washes of DMF between steps. A Kaiser/ninhydrin test was utilized after each deprotection or coupling step (except with Pro residues) to indicated the presence or lack of a free primary amine.¹⁹² For Pro residues, the presence or lack of a free secondary amine was indicated by a chloranil test.^{191, 193} Removal of the Fmoc group was achieved in a two-step process using a deprotection solution of 20% piperidine in DMF. An initial two minute deprotection was performed outside of the microwave. The deprotection solution was removed by vacuum. A second aliquot of 20% piperidine was added and further deprotection was assisted by microwave heating (75°C, 30 W, 4 min).

Microwave assisted amide coupling was achieved by addition of 3.1-fold excess Fmoc-protected amino acids (5.1-fold for Arg) and 3-fold excess of HBTU (5-fold for Arg) dissolved in DMF added to the deprotected elongating peptide on the resin. The coupling reaction was initiated via addition of 5-fold excess of DIEA (7-fold for Arg) and the reaction was heated in the microwave synthesizer (75°C, 30 W or 50°C, 30 W for His) for five minutes (10 min for Arg at 75°C, 30 W). Fmoc-NH-(PEDG20)-COOH was incorporated into the peptide using the standard microwave protocol except it was allowed to cool for at least one hour post coupling to ensure the reaction went to completion.

The semi-automated synthesizer couplings were achieved by splitting dry resin with the Fmoc protected elongating peptide chain (~0.2 nmols) into a 16-well Teflon reaction block. The resin and peptide swelled for two hours in DCM, and then were deprotected by addition of 20% piperidine in DMF for two minutes. The deprotection mixture was removed, then a second aliquot of 20% piperidine was added and mixed for 18 minutes. Following a positive Kaiser test, the coupling was initiated by addition of reagents as described above. The reaction was then mixed for at least two hours at room temperature.

All N-terminal acetylated peptides were acetylated on resin after the final Fmoc deprotection by addition of 3:1 mixture of acetic anhydride to pyridine and were mixed (with a nitrogen bubbler) for 30 minutes at room temperature. After syntheses were completed, all peptides were washed with DCM at least 3 times and dried overnight in a desiccator. Simultaneous side chain deprotection and resin cleavage was accomplished via addition of 8 mL of a cleavage cocktail (91% TFA, 3% EDT, 3% TIS, 3% water) for 1.5-3 hours. The crude peptides and cleavage solution were filtered into a pre-weighed 50 mL

conical tube. The cleaved resin was rinsed with an additional 2 mL of cleavage cocktail to remove residual peptides. Peptides were precipitated using cold (4°C) anhydrous diethyl ether. The turbid mixture was vortexed and centrifuged at 4°C and 4000 RPMs for 4 minutes (Sorval Super T21 high-speed centrifuge swinging bucket rotor). The supernatant was decanted leaving the crude peptide pellet. This was then washed with cold (4°C) diethyl ether and centrifuged. This process was repeated at least 3 times until no thiol aroma was present and the peptide was dried overnight in a desiccator.

A 5-20 mg sample of crude peptide was purified by RP-HPLC using a Shimadzu chromatography system with a photodiode array detector and a semipreparative RP HPLC C₁₈ bonded silica column (Vydac 218TP1010, 1 cm x 25 cm). The solvent system for purification was either acetonitrile (MeCN) or methanol (MeOH) in water with 0.1% TFA. After purified fractions were collected, peptides were concentrated *in vacuo* and lyophilized. A purity of greater than 95% was confirmed by analytical RP-HPLC in two diverse solvent systems (10% MeCN in 0.1 % TFA/water and a gradient to 90% MeCN over 35 min; and 10% MeOH in 0.1 % TFA/water and a gradient to 90% MeOH over 35 minutes). The correct molecular mass was confirmed by ESI-MS (University of Minnesota Department of Chemistry Mass Spectrometry Laboratory).

2.3 Resin Splitting Approach

A split resin technique to allow rapid diversification was used as previously described (**Scheme 2.1**).^{25, 30} Although the specific design of the bivalent ligands will be described in detail in each chapter, in general, bivalent ligands consist of two tetrapeptide pharmacophore scaffolds connected by a linker (*e.g.* Ac-His-DPhe-Arg-Trp-PEDG20-His-DPhe-Arg-Trp-NH₂). Therefore, the synthesis of these ligands can be split into three

components: synthesis of the C-terminal pharmacophore, synthesis of the linker, and synthesis of the N-terminal pharmacophore. In the split resin approach, the initial common four amino acid residues that comprise the C-terminal pharmacophore scaffold were added to the resin. Then, the resin was split so that different linkers or spacers could be added to the C-terminal pharmacophore scaffold. Then, the resin was split further before adding the N-terminal pharmacophore for completion of the bivalent ligand. At each step along the way, the peptide could also be cleaved to provide control ligands such as the tetrapeptides used as pharmacophore scaffolds, and the tetrapeptides plus addition of the linker on to the N-terminus (**Scheme 2.1A**). The linker could be added directly to the resin to provide the tetrapeptide plus the linker on the C-terminus (**Scheme 2.1B**). When splitting resin, often a semi-automated synthesizer without the use of microwave was utilized to aid in the synthesis so that peptides could be synthesized in parallel.

The best example of this method in use was the synthesis scheme utilized for ligands in **Chapter 3**, **Chapter 4**, and **Chapter 5** (**Scheme 2.2**). In the idealized version of this method, the C-terminal tetrapeptide (*e.g.* His-DPhe-Arg-Trp) was added to the resin. An aliquot of the resin was taken, acetylated, and cleaved to yield control tetrapeptide (*e.g.* Ac-His-DPhe-Arg-Trp-NH₂). The rest of the resin was split into two additional aliquots. To one aliquot the PEDG20 linker was added and to the other the (Pro-Gly)₆ linker was added. A portion of these resins was cleaved for tetrapeptide plus linker control ligands [*e.g.* (Pro-Gly)₆-His-DPhe-Arg-Trp-NH₂ and PEDG20-His-DPhe-Arg-Trp-NH₂]. To uncleaved aliquots of the resin, a second N-terminal tetrapeptide scaffold was added. Then it was acetylated and cleaved to yield the final bivalent ligands (*e.g.* Ac-His-DNal(2')-Arg-Trp-PEDG20-His-DPhe-Arg-Trp-NH₂ and Ac-His-DPhe-Arg-Trp-PEDG20-His-DPhe-

Arg-Trp-NH₂) (**Scheme 2.2A**). In order to synthesize the C-terminus linked controls, first the linker was added to the resin. Then this was split to add different tetrapeptide pharmacophores to yield the linker controls (**Scheme 2.2B**).

It should just be mentioned that compounds synthesized early in this thesis work were synthesized linearly without splitting the resin to ensure the bivalent ligand synthesis was easily amendable to the laboratory's techniques, and for me to learn the proper techniques. For later synthesis schemes like those in **Chapter 6**, this type of synthesis plan allowed for rapid synthesis and diversification.

2.4 Cell Culture

All cells assays were performed with female HEK293 cells. Cells were maintained in Dulbecco's modified Eagle's medium (DMEM) supplemented with 10% newborn calf serum (NCS), and 1% penicillin/streptomycin in humidified atmosphere of 95% air and 5% CO₂ at 37°C. Stable cell lines were generated with wild type mMC1R, mMC4R, mMC5R, Flag-mMC3R, Flag-hMC4R DNA in pCDNA₃ expression vector (20 µg) using the calcium phosphate transfection method.¹⁹⁴ Stable populations were generated using G418 selection (0.7-1.0 mg/mL) and used in bioassays unless indicated otherwise. Experimental ligands were dissolved to a 10⁻² M stock in DMSO and stored at -20°C. Subsequent dilutions were performed in the stated assay buffer to achieve the final concentration in the well. The ligands were assayed as TFA salts.

2.5 Competitive Radioligand Binding Affinity Studies

The binding affinities of bivalent ligands in **Chapters 3-6** were evaluated by performing competitive radioligand binding assays at the mMC1R, mMC3R, and mMC4R. The mMC5R was excluded from study as its functional has not yet been fully elucidated

and our efforts are focused on understanding the melanocortin system's role in energy homeostasis. Human AGRP(87-132) or NDP-MSH peptides were radioiodinated using Na¹²⁵I following the chloramine T procedure by Robert Speth.^{25, 132, 195} Monoradioiodinated peptide was isolated from unlabeled or diradioiodinated peptide by HPLC using a C₁₈ column. It was eluted isocratically in a mobile phase of 24% acetonitrile and 76% triethylamine phosphate (pH 3.0).

HEK293 cells stably expressing the mMC1R and mMC4R were maintained as described above in **Section 2.4**. Binding experiments on the mMC3R were performed on transiently transfected HEK293 cells. Transfection was performed two days prior to the binding experiment in 10 cm plates using FuGene6 transfection reagent (15 µL/plate; Promega), Opti-Mem medium (1.7 mL/ plate; Invitrogen), and Flag-mMC3R DNA (3.33 µg/plate). One or two days preceding the experiment, cells were plated into 12-well tissue culture plates (Corning Life Sciences, Cat. # 353043) and grown to 90-100 % confluency. On the day of the assay, medium was aspirated and the cells were treated with a freshly diluted aliquot of non-labeled compound at the concentration being tested (ranging from 10⁻¹² to 10⁻⁴ M as appropriate) in assay buffer (DMEM and 0.1% bovine serum albumin (BSA)) and a constant amount of ¹²⁵I-NDP-MSH or ¹²⁵I-AGRP (100,000 cpm/well). Cells were incubated at 37° C for one hour. After which, media was gently aspirated and cells were washed gently once with assay buffer.

Buffer was gently aspirated and cells were lysed with NaOH (500 µL; 0.1M) and Triton X-100 (500 µL; 1%) for at least 10 minutes. Cell lysate was transferred to 12x75 mm polystyrene tubes and radioactivity was quantified on WIZARD² Automatic Gamma Counter (PerkinElmer). Experiments were performed with duplicate data points and

repeated in at least two independent experiments. Each experiment included unlabeled NDP-MSH or AGRP(87-132) as a positive control. Non-specific values were obtained using a 10^{-6} M unlabeled NDP-MSH or AGRP(87-132), corresponding to the respective ^{125}I -labeled peptide. Data was analyzed using the PRISM program (v4.0; GraphPad Inc.). Dose-response curves and IC_{50} values were generated and analyzed by a nonlinear regression method. The standard error of the mean (SEM) or standard deviation (SD) was derived from the IC_{50} values from at least two independent experiments.

2.6 AlphaScreen[®] cAMP Functional Bioassay

Agonist stimulation of all known melanocortin receptors results in the activation of the cAMP signaling pathway through the $G_{\alpha s}$ subunit. Melanocortin agonist activity is commonly quantified by measuring cAMP signaling.^{25, 96, 132, 196, 197} Therefore in **Chapter 3-6**, the AlphaScreen[®] cAMP technology (PerkinElmer Life Sciences, Cat #6760625M) was utilized to measure cAMP signaling after ligand stimulation in HEK293 cells stably expressing the mMC1R, mMC3R, mMC4R, and mMC5R. The AlphaScreen[®] assay was performed as described by the manufacturer and described previously by our lab.^{25, 132, 197} It is also described briefly below.

Cells were 70-95% confluent on the day of the assay. Cells were removed from 10 cm plates with Gibco[®] Versene solution. Cells were pelleted by centrifugation (Sorvall Super T21 high speed centrifuge, swinging bucket rotor) at 800 rpm for five minutes at room temperature. Medium was aspirated and cells were resuspended in Dulbecco's phosphate buffered saline solution (DPBS 1X [-] without calcium and magnesium chloride, Gibco [®] Cat # 14190-144). A 10 μL aliquot was removed for manual cell counting. After the addition of a Trypan blue dye solution (BioRad) to the cell aliquot (1:1 by volume),

cells were counted manually using a hemocytometer. Cells were again pelleted at 800 rpm for 5 minutes and DPBS was gently aspirated. The pelleted cells were then resuspended in a solution of freshly made stimulation buffer (Hank's Balanced Salt Solution [HBSS 10X [-] sodium bicarbonate] and [-] phenol red, Gibco®), 0.5 mM isobutylmethylxanthine [IBMX], 5 mM HEPES buffer solution [1M, Gibco®], 0.1% bovine serum albumin [BSA] in Milli-Q water, pH=7.4) and anti-cAMP acceptor beads (1.0 unit per well, AlphaScreen®). This resuspended cell/acceptor bead solution was added manually to a 384 well microplate (OptiPlate-384; PerkinElmer). The final concentration was 10,000 cells/well and 1.0 Unit of anti-cAMP beads/well. The equal mixture of stable mMC3R cells and stable mMC4R cells described in **Chapter 4** was 5,000 cells/well of each cell type for a total of 10,000 cells/well. Cells were stimulated for two hours in a dark laboratory drawer with ligand diluted in stimulation buffer from 10^{-13} to 10^{-4} M.

During incubation, a three-component biotinylated cAMP/streptavidin donor bead working solution was made with streptavidin donor beads (1 Unit/well, AlphaScreen®), biotinylated cAMP (1 Unit/well, AlphaScreen®), and lysis buffer (10% Tween-20, 5 mM HEPES buffer solution [1M, Gibco®], 0.1% bovine serum albumin [BSA] in Milli-Q water, pH=7.4). After the incubation, the biotinylated cAMP/streptavidin donor bead working solution was added and mixed into each well in the 384-well plate under green light and mixed well by pipetting up and down. Cells were incubated for another two hours at room temperature in the dark. The plate was read using a pre-normalized assay protocol set by the manufacturer on an EnSpire™ Alpha plate reader. All assays were performed in at least three independent experiments with duplicate data points. Each plate contained a

control ligand dose response (10^{-6} M to 10^{-12} M of NDP-MSH, α -MSH, or γ ₂-MSH), a 10^{-4} M forskolin positive control, and a no ligand assay buffer negative control.

Data was analyzed using the PRISM program (v4.0; GraphPad Inc.). Dose response curves and potency EC₅₀ values (concentration that caused 50% maximal signal) were generated and analyzed by a nonlinear regression method. Because the AlphaScreen® assay is a competition assay and to be consistent with functional data being represented as an increasing response with increasing concentration, a transformation was carried out for illustration purposes to normalize data to control compounds and flip data curves. A detailed explanation of the transformation can be found in **Section 2.7**.

Compounds that showed partial receptor activation at 100 μ M at the mMC3R or mMC4R were analyzed for antagonist properties using a Schild regression analysis.¹⁹⁸ Ligands were tested in a dose-dependent manner to inhibit NDP-MSH agonist receptor stimulation and the pA₂ values were calculated [pA₂=-log(K_i)].¹⁹⁸ The standard error of the mean (SEM) was derived from the potency values and pA₂ from at least three independent experiments.

2.7 ALPHAScreen Assay Data Normalization

The AlphaScreen® assay is a competition assay between biotinylated cAMP which is part of the assay kit and intracellular cAMP which is produced by the cells in response to agonist ligands. Because the AlphaScreen® assay is a competition assay, it results in decreasing signal with increasing cAMP functional response due to receptor activation. This is inconsistent with standard functional assays which result in increasing signal with increasing receptor activation. Therefore, data was normalized to “flip” data curves to be consistent with the literature as previously described.^{25, 197} Of note, the ligand potency

values reported were obtained prior to data normalization. Data normalization was only used for illustration purposes only and did not influence the ligand potency values.

Data was normalized by taking the raw value of each well, subtracting the averaged maximal response of NDP-MSH (normally responses at 10^{-6} and 10^{-7} M). This value was then divided by the maximal response subtracting the average minimal response (Basal values and/or values of NDP-MSH at 10^{-12}). This value was then subtracted from 1 to “flip” the response and multiplied by 100 to result in % response of NDP-MSH. The equation is as follows:

$$\% \text{ Response of NDP-MSH} = 1 - \frac{[(\text{Raw Value}) - (\text{Average Max Response})]}{[(\text{Average Minimal Response}) - (\text{Average Max Responses})]} \times 100$$

2.8 PRESTO-Tango (β -arrestin Recruitment) Assay

Melanocortin agonist stimulation is also known to result in β -arrestin recruitment and receptor desensitization.¹⁹⁹⁻²⁰¹ In order to characterize melanocortin ligand stimulated β -arrestin recruitment and to evaluate biased agonism, the PRESTO-Tango β -arrestin recruitment assay was performed on cells expressing the hMC4R in **Chapter 5**. The PRESTO-Tango assay was developed by Kroeze and coworkers for identifying biologically activate compounds by the rapid screening for most of the entire druggable GPCRome.^{202, 203} The plasmids and assay technology were kindly provided by the Bryan Roth laboratory (University of North Carolina at Chapel Hill) and are now available through ADDGENE (Kit # 1000000068). Briefly, HTLA cells (HEK293 cells that stably express a tTA-dependent luciferase reporter and a β -arrestin 2 –TEV fusion gene and were

kindly provided by Richard Axel²⁰³) were maintained in DMEM supplemented with 10% FBS, 100 U/mL penicillin, 100 µg/mL streptomycin, 2 µg/mL puromycin, and 100 µg/mL hygromycin B in humidified atmosphere of 95% air and 5% CO₂ at 37 °C.

On the first day of the assay, HTLA cells were plated at approximately 1×10^6 cells per 10 cm plate and grown to 20-40% confluency. The second day cells were transiently transfected using the calcium phosphate method with 4 µg/plate of hMC4R PRESTO-Tango plasmid construct and incubated 15-24 hours in humidified atmosphere of 97% air and 3% CO₂ at 35 °C.^{194, 202} On the third day, cells were removed from 10 cm plates using Gibco® Versene solution and pelleted by centrifugation (Sorvall Super T21 high speed centrifuge, swinging bucket rotor) at 800 rpm for five minutes at room temperature. Cells were manually counted on a hemocytometer and resuspended in 1% dialyzed FBS and 1% penicillin/streptomycin in DMEM to a final concentration of 400,000 cells/mL. Cells were plated into 384-well white wall and clear bottom microplate (ViewPlate-384 TC, PerkinElmer Cat # 6007480) for a final concentration of 20,000 cells/well and incubated in 5% CO₂ at 37 °C. On the fourth day, cells were stimulated by ligands diluted to the appropriate in well concentrations (*i.e.* 10^{-12} to 10^{-5} M) in filter-sterilized assay buffer (20 mM HEPES, 1x HBSS, water, titrated to pH 7.4 with 1 N NaOH). Stimulated cells were incubated for 18 hours in 5% CO₂ at 37 °C. On the fifth day, the assay buffer and cell medium was removed by aspiration. Then 20 µL of Bright-Glo (Promega, Cat # N1661) diluted 20-fold in assay buffer was added to each well and incubated for 15-20 minutes at room temperature. After incubation, luminescence was read on an EnSpire™ Alpha plate reader using a pre-normalized assay protocol for luminescence set by the manufacturer. Dose response curves were analyzed using the PRISM program (v4.0; GraphPad Inc.).

Potency EC₅₀ values (concentration that caused 50% maximal signal) were calculated by a nonlinear regression method.

2.9 Bioluminescence Resonance Energy Transfer (BRET) Studies

It has been supported by a variety of techniques that all known melanocortin receptors homodimerize and heterodimerize.^{125, 127, 129-131, 204-209} However, to our knowledge prior to this thesis work, no evidence has supported the existence of a MC3R-MC4R heterodimer.¹³² Based on expression patterns of mRNA in the brain and the double MC3R-MC4R KO mouse model, it was hypothesized that the MC3R-MC4R heterodimer may exist and may have functional relevancy.^{58, 81, 132, 210-212} Furthermore, there has been evidence supporting that bivalent ligands can modulate existing dimers or induce dimerization.^{213, 214} Therefore, to study the hypothesized MC3R-MC4R heterodimer, as well as to study the effects of bivalent ligands on MC4R homodimers, bioluminescence resonance energy transfer (BRET) studies were performed. This technique was utilized in **Chapter 4** and **Chapter 5**.

Specifically, a NanoBRET™ Protein:Protein Interaction System was utilized according to manufacturer's instructions to examine the association and proximity of the melanocortin receptors. Plasmids were constructed to incorporate the NanoLuc® fusion protein and the HaloTag® fusion protein onto the C-terminus of both the mMC3R and mMC4R of the plasmids described above. Competitive binding assays with ¹²⁵I-NDP-MSH demonstrate proper cell membrane expression and ligand binding (**Figure 2.1, Table 2.1**). On the first day, cells were plated in the morning into 6 well plates. In the afternoon of the same day, cells were transiently transfected with melanocortin receptor by adding FuGene6 Transfection (8 µL/well, Promega), DNA (2 µg/well) in OptiMem medium (Invitrogen) at

a total volume of 100 μ L/well. The 100 μ L/well aliquot was added to the current media in each well of the plated cells. The ratio of donor NanoLuc® to acceptor HaloTag® DNA was optimized in preliminary experiments and a ratio of 1 Receptor-NanoLuc® plasmid: 4 Receptor-HaloTag® plasmid was utilized for all following experiments. Cells were incubated with transfection reagent overnight at 37° C at 5 % CO₂. One day after the transfection, cells were re-plated into 96-well black clear bottom plates (Cat # 3603, Corning Life Sciences) at 30,000 cells in 100 μ L of assay buffer (4% FBS in OptiMem). As a negative control, a mixture of mMC4R-NanoLuc® cells and mMC3R-HaloTag® cells was made by mixing 15,000 cells of each cell type together. In these experimental conditions, the mMC4R-NanoLuc® and mMC3R-HaloTag® should not associate since they are on separate cell membranes resulting in low BRET signal.

To each well, 1 μ L of 0.1 mM HaloTag® NanoBRET™ 618 ligand was added and incubated 18-24 h at 37° C at 5 % CO₂. As a negative control, each assay also included; “no acceptor controls” in which 1 μ L of DMSO was added instead of the HaloTag® NanoBRET™ 618 ligand rendering the BRET relay system incomplete (providing the background signal). This background signal was subtracted from the final experimental signal. Plates were then developed 48 to 60 hours after transfection. To develop plates, 25 μ L of 5x solution of NanoBRET™ Nano-Glo® Substrate in Opti-MEM® was added to each well. Plates were then read within 10 min on a FlexStation® 3 plate reader (Molecular Devices) at the donor emission wavelength (460 nm) and acceptor emission wavelength (618 nm). The milli BRET Units (mBUs) were calculated by dividing the acceptor emission of 618 nm by the donor emission at 460 nm and multiplying it by 1000. All

assays were performed in at least three independent experiments with 3 to 5 replicates wells in each experiment.

In **Chapter 5**, the same protocol was followed except cells were plated in 90 μL of assay buffer instead of 100 μL to test the effects of ligands. Then, 2 hours before the plates were developed, 10 μL of a 10X aliquot of the ligand was added to each well to yield the final in well concentration (10^{-5} , 10^{-7} , or 10^{-9} M) of each compound.

2.10 Serum Stability Studies-

One critique often asserted about peptidic ligands is that they can have poor metabolic stability. Also, it has been reported that the endogenous melanocortin peptide ligand α -MSH is rapidly degraded in blood serum.⁷⁴ In order to ensure that results obtained in *in vivo* studies were due to the parent compound, it is necessary to demonstrate adequate metabolic stability of lead ligands. Furthermore, if the bivalent ligands are rapidly split into two monovalent ligands upon *in vivo* administration, the bivalent ligand design cannot be evaluated. Therefore, the lead ligands' mouse serum stability was measured *in vitro* to obtain an indication of the metabolic stability. These results are presented in **Chapter 4-6**. The experimental ligands at an initial concentration of 10 μM in mouse serum (Cat # M5905; Sigma-Aldrich) were incubated at 37 $^{\circ}\text{C}$ on an orbital shaker. At the time points 0, 0.5, 1.5, 3, 6, 8, 24, 48, and 72 h time points, a 50 μL aliquot was taken and the reaction was quenched with 150 μL of cold (4 $^{\circ}\text{C}$) 66% aqueous acetonitrile. Samples were incubated in a bucket of wet ice for 10-15 min, then centrifuged at 12900 rpm at 4 $^{\circ}\text{C}$. The supernatant was collected into pre-labeled tubes and stored at -80 $^{\circ}\text{C}$ until liquid chromatography-positive electrospray ionization-tandem mass spectrometry (LC-ESI⁺-MS/MS) analysis was performed. Liquid chromatography was carried out with a reverse-

phase linear gradient and a flow rate of 15 $\mu\text{L}/\text{min}$ on a 0.5×150 mm Zorbax SB-C18 5 μm column (Agilent, Santa Clara, CA). The gradient was from 95% aqueous TFA (0.1%) and 5% acetonitrile to 35% aqueous TFA (0.1%) and 65% acetonitrile in 15 min. This was followed by a washout and re-equilibration period at initial conditions.

Mass spectrometry was performed on a Finnigan TSQ Quantum Discovery MAX triple quadrupole mass analyzer (Thermo Scientific, Waltham, MA). Selected reaction monitoring (SRM) mass transitions were optimized for each compound from the MS/MS product ion spectra of the initial control sample. Collision energy was 35 eV and scan width was 1.0 amu. The following SRM transitions were monitored for each compound: NDP-MSH, m/z 824.2 \rightarrow 136.1; α -MSH, m/z 555.9 \rightarrow 136.1 and 833.3 \rightarrow 136.1; **CJL-1-14**, m/z 343.9 \rightarrow 110.1 and 686.7 \rightarrow 180.1; **CJL-1-87**, m/z 544.9 \rightarrow 110.2 and 816.3 \rightarrow 110.0; **CJL-5-35-4**, m/z 503.1 \rightarrow 110.1; **CJL-1-116**, m/z 482.1 \rightarrow 156.1 and 321.9 \rightarrow 156.1; **CJL-1-31**, m/z 746.8 \rightarrow 179.9; **CJL-5-35-1**, m/z 806.4 \rightarrow 172.0 and 806.4 \rightarrow 152.0; **CJL-1-41**, m/z 785.6 \rightarrow 445.1 and 524.2 \rightarrow 195.1; **CJL-5-127-7**, m/z 343.6 \rightarrow 159.1 and 343.7 \rightarrow 110.1; **CJL-5-119-1**, m/z 550.0 \rightarrow 110.1 and 550.0 \rightarrow 152.1; **CJL-5-119.2**, m/z 544.2 \rightarrow 152.0 and 816.0 \rightarrow 180.1; **CJL-5-119-3**, m/z 535.2 \rightarrow 152.1 and 535.2 \rightarrow 110.1; **CJL-9-22-4**, m/z 561.0 \rightarrow 152.1 and 841.0 \rightarrow 180.0; **CJL-5-119-5**, m/z 544.2 \rightarrow 159.1 and 544.2 \rightarrow 110.1; **CJL-5-127-2**, m/z 544.3 \rightarrow 110.1 and 816.0 \rightarrow 154.7; and **CJL-5-127-5**, m/z 544.2 \rightarrow 228.8 and 816.0 \rightarrow 110.0. All samples were run in two technical replicates. The signal intensity at time point 0 h was arbitrarily set as 100% and the % intact peptide at each time point was calculated relative to this signal. Data was graphed and half-lives were calculated using PRISM software (v 4.0; GraphPad Inc.). Mass spectrometry was

carried out in the Analytical Biochemistry Shared Resource at the University of Minnesota Masonic Cancer Center.

2.11 Animals Studies

The transition of *in vitro* assay results to *in vivo* effects is an important translational step to understand the physiological and pharmacological relevancy of newly discovered ligands. Therefore, to better understand the *in vivo* physiology of the bivalent ligands and their potential as *in vivo* probes, compounds were administered intracerebroventricular (ICV) to mice in **Chapters 3-5**. All studies were performed in accordance with the Institutional Animal Care and Use Committee (IACUC) of the University of Minnesota. The mice used were male and female wild type, MC3RKO, or MC4RKO mice with a mixed genetic background from the C57BL/6J and 129/Sv inbred strains derived for the in-house breeding colonies as previously reported.^{25, 59, 76, 107, 132, 189, 215} The specific sex and genotype is stated in the description of each assay paradigm. All mice were maintained on a reversed 12 h light/dark cycle (Lights out was at 11:00 AM) in a temperature controlled room (23-25 °C) with free access to tap water. Excluding when a fast occurred prior to injection, mice had free access to normal chow (Harlan Teklad 2018 Diet: 18.6% crude protein, 6.2% crude fat, 3.5% crude fiber, with energy density of 3.1 kcal/g). The hPYY validation experiments and the Luminex Multiplex hormone panel experiments (see below) took place in standard mouse polycarbonate conventional cages provided by the University of Minnesota's Research Animal Resources (RAR). All cages were changed weekly by lab research staff. The compounds used for animal studies were dissolved in sterile saline (0.9%; Hospira, Lake Forest, IL) to a stock solution of 10⁻² M unless specifically stated otherwise.

2.12 Cannulation Surgery and Placement Validation

Cannulation surgeries were performed to place a cannula into the lateral cerebral ventricle as previously reported.^{25, 76, 132, 189, 216} All mice were age matched to have surgeries at 8-10 weeks old. Mice were anesthetized with a mixture of xylazine (5 mg/kg) and ketamine (100 mg/kg) administered intraperitoneally (IP). Mice were placed in a stereotaxic apparatus (David Kopf Instruments), which was used to guide the cannula placement. A 26-gauge cannula (Cat # 8IC315GS4SPC; PlasticsOne, Roanoke, VA) was placed into the lateral cerebral ventricle at the coordinates 1.0 mm lateral and 0.46 mm posterior to bregma and 2.3 mm ventral to the skull.²¹⁷ Dental cement (C&B-Metabond Adhesive Cement Kit # S380) followed by Lang's Jet™ Denture Repair Kit (Jet Denture Repair Powder, Ref #1220; Jet Liquid, Ref # 1403) was used to secure the cannula. Flunixin meglumine (FluMeglumine, Clipper Distribution Company) and 0.5 mL of 0.9% saline (Hospira, Lake Forrest, IL) was administered subcutaneously after surgery to aid in recovery. Mice were given at least seven days to recover before cannula validation. Mice were housed individually after surgery and for the remainder of the experiments.^{25, 76, 132, 189, 216}

Cannula placement was verified by evaluating the increase in feeding after the ICV administration of 2.5 µg of human (h)PYY₃₋₃₆ (Cat # H8585; Bachem) as described previously.^{25, 76, 107, 132, 189, 216} Each mouse received a saline treatment and a hPYY treatment on different days separated in a cross-over design nocturnal feeding paradigm. There was at least a 3-day washout period between administration to ensure that normal feeding patterns and body weight returned as hPYY is well documented to have only an acute response. In the nocturnal feeding paradigm utilized in this entire thesis, compound or

saline is administered two hours prior to lights out ($t = 0$ h) with free access to food and water throughout the entire experiment. Food intake and body weight were manually measured 2, 4, and 6 hours after hPYY or saline administration. A mouse with a validated, properly placed cannula consumed at least 0.75 g more food after hPYY administration compared to saline administration at the 4 h time point. Data from a standard validation experiment is provided in (**Figure 2.2**). This validation experiment was performed for the TSE metabolic cage studies described in **Chapter 4**. In this experiment an average mouse ate 0.4 ± 0.1 g at the 4 h time point after saline administration compared to 1.6 ± 0.1 g after hPYY administration

2.13 In Vivo Energy Metabolism Studies

A TSE PhenoMaster metabolic cage system was utilized to study more thoroughly the effects of bivalent ligands on energy homeostasis. Normally, the effects on food intake and body weight were first characterized in standard mouse polycarbonate conventional cages. Then, a new cohort of mice with validated cannula placement were transitioned into sealed metabolic home cages and allowed one week to acclimate to the TSE cages and environment. The TSE PhenoMaster metabolic cage system (TSE Systems, Berlin Germany) was configured to measure food intake, water intake, oxygen uptake, carbon dioxide production, and locomotor activity (beam break) in 15 minute bins. After the acclimation period, the indicated amount (nmols) of compound in 3 μ L of saline was delivered two hours prior to lights out ($t=0$ hr) through the implanted cannula using an infusion internal cannula (Cat# 8IC315IS4SPC; PlasticsOne, Roanoke, VA) in either a satiated nocturnal feeding paradigm or a fasting refeeding paradigm as described above.²⁵

132, 189, 215, 218

All experiments followed a cross-over paradigm in which the mouse received saline and compound on different days with a washout period in between. In Chapter 4, a three-group crossover design paradigm was utilized to assess the differences between **CJL-1-14**, **CJL-1-87**, and saline (**Figure 2.3A**). The nocturnal paradigm is described above. In the fasting-refeeding paradigm utilized throughout this thesis, food was removed from the mice at the start of the lights out on the previous day ($t = -22$ h) for a 22-hour fast. Two hours before lights out on the day of the assay ($t = 0$ h), mice received the indicated dose (nmols of compound or saline vehicle control) and food was returned to the cage (**Figure 2.3B**). After compound administration ($t=0$ h), TSE cages were “resumed” to collect data in 15 minute intervals until the conclusion of the experiment.

The cumulative food and water intakes were reported in two hour increments. The energy expenditure and RER were calculated from the oxygen uptake and carbon dioxide production. The oxygen uptake, carbon dioxide production, and locomotor activity were recorded in 15-minute bins. The RER of four 15-minute recordings were averaged for each reported hourly RER. Similarly, the four 15-minute energy expenditure readings (kcal/h) were normalized to the animals' pre-treatment weight (kcal/kg/h) and were then averaged into one-hour bins. Activity measurements were the ambulatory activity (X_A) defined as consecutive beam breaks of two different X-axis beams. Activity readings of the four 15-minute intervals were summed for each one-hour bin. Figures were made using PRISM software (v 4.0; GraphPad Inc.). Statistical analysis was performed using SPSS V23 software (IBM) utilizing a multivariate general linear model followed by a Bonferroni *post hoc* test. Statistical significance was defined as $p < 0.05$. Results are presented as Mean \pm SEM.

2.14 Body Composition Studies

In **Chapter 4**, the effects of lead bivalent ligand **CJL-1-87** and its monovalent counterpart **CJL-1-14** is evaluated for its effects on lean and fat mass and on metabolic hormones.¹³² In these studies an additional cohort of 32 male age matched littermate mice (saline, n=10; 5 nmol **CJL-1-14**, n=11; 5 nmol **CJL-1-87**, n=11) remained in standard mouse polycarbonate conventional cages. This cohort was used for both body composition analysis and Luminex Milliplex assays in a block design. Food intake and body weight were manually measured using a standard top-loading laboratory balance at time points -22, 0, 2, 4, and 6 hours. The amount of lean body mass and fat mass was measured using an EchoMRI-100H™ (Echo Medical Systems LLC, Houston TX, USA) at time points -22, 0, and 6 hours. The lean body mass percentage and body fat mass percentage were calculated based on the amount of lean mass or fat mass measured divided by the manually recorded weight immediately prior to the MRI measurements. Results are presented as the Mean ± SEM.

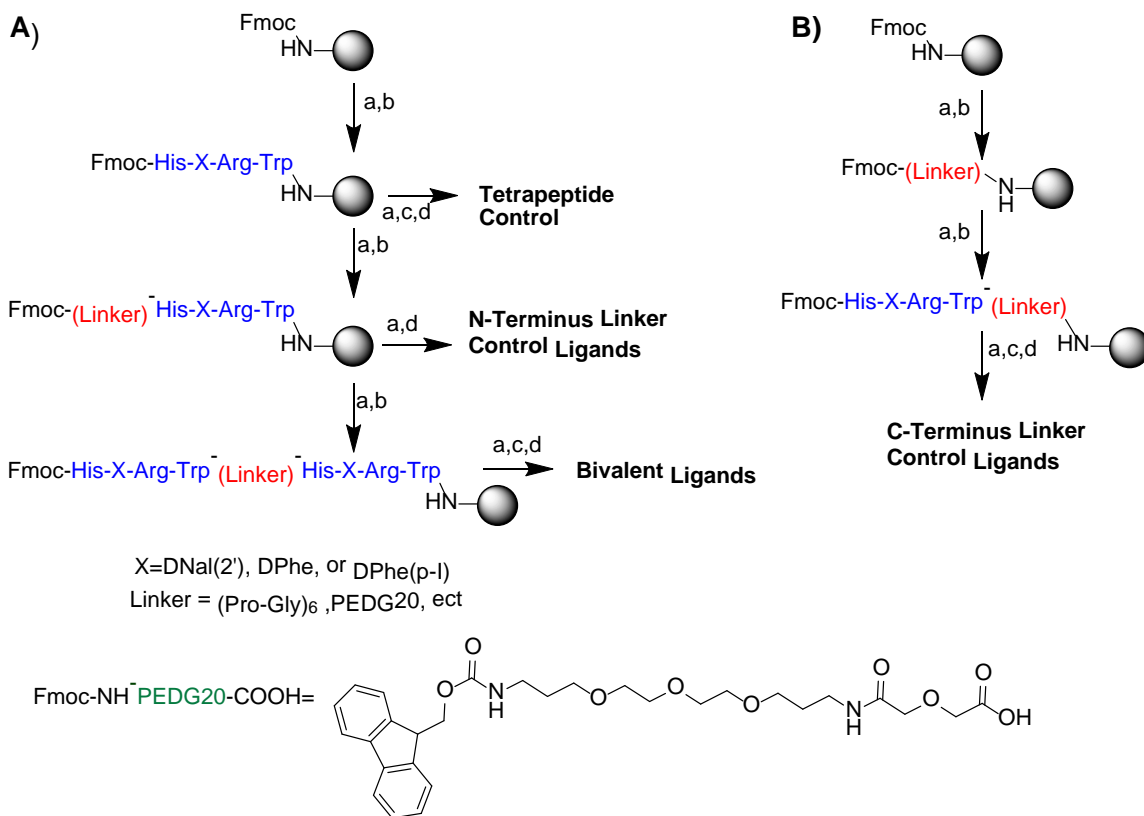
2.15 Luminex Milliplex Hormone Panel Studies

A Luminex Milliplex assay was utilized to assess the effects of lead compound **CJL-1-87** on metabolic hormone regulation in **Chapter 4**. Trunk blood of the second cohort was collected six hours after treatment using 1.5 mL EDTA-K2 coated tubes (Milian, USA) and placed on ice. To prevent hormone degradation, a series of inhibitors was added to each EDTA-K2 coated tube. DPPIV (Cat. No. DPP4, EMD Millipore Corporation, Billerica, MA) was added at a concentration of 10 µL/mL of whole blood. Pefabloc/AEBSF (Product No. 11873601001, Roche, Indianapolis, IN) was added at 1 mg/mL of whole blood. Protease Inhibitor Cocktail (Part No. P8340, Sigma-Aldrich, St.

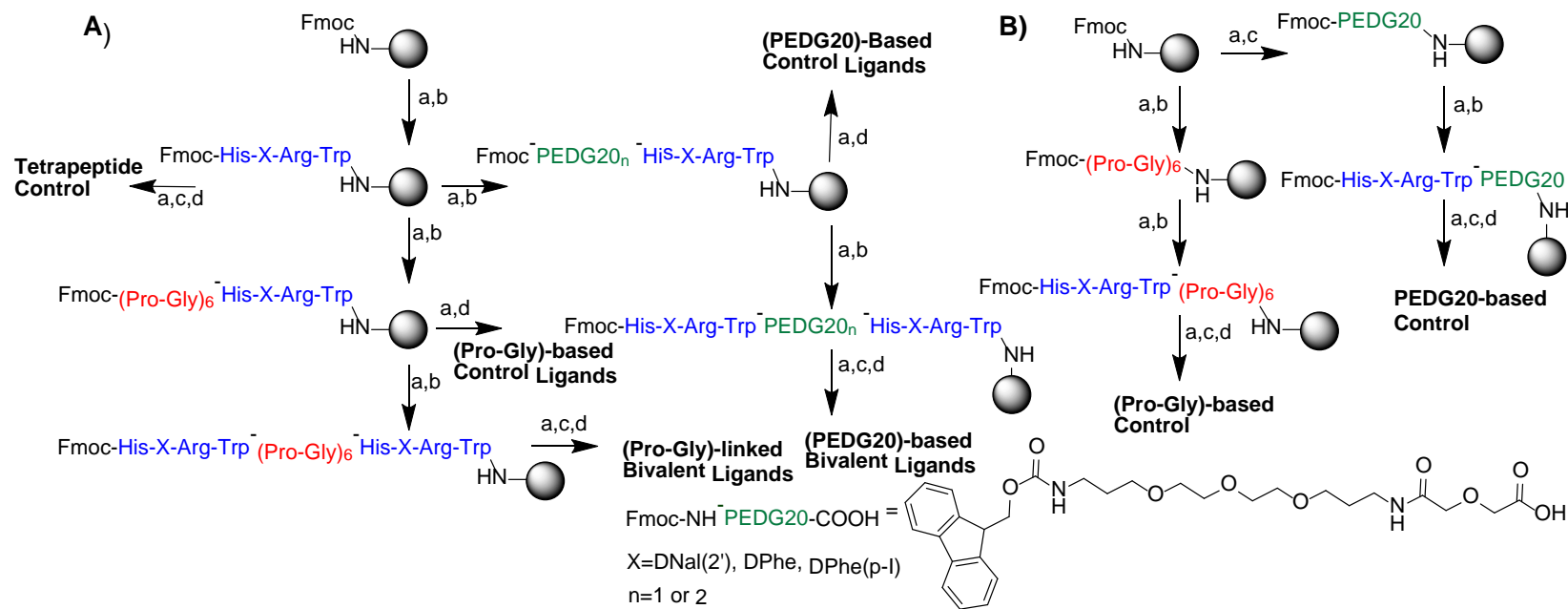
Louis, MO) was added at 10 $\mu\text{L}/\text{mL}$ of whole blood. Aprotinin (Part No. A6279, Sigma-Aldrich, Indianapolis, IN) was added at 500 KIU/ mL of whole blood. The total whole blood collected per tube was about 500 μL . Whole blood samples were spun at 10,000 rpm for 10 minutes at 4 $^{\circ}\text{C}$. Plasma was collected from the supernatant and aliquoted to avoid multiple freeze/thaw cycles. The samples were then frozen at -20 $^{\circ}\text{C}$ until they were assayed. Plasma hormone levels were measured in duplicate from a 10 μL serum sample using the Mouse Metabolic Hormone Magnetic Bead Panel Milliplex Kit (Cat. No. MMHMAG-44K, EMD Millipore Corporation, Billerica, MA), which is commercially available. Hormone levels were read and acquired using Magpix instrument and Luminex xPonent 4.2 software (Cat. No. 40-072, EMD Millipore Corporation, Billerica, MA). Data was analyzed using GraphPad Prism.

2.16 Data Analysis

All *in vitro* data was analyzed utilizing PRISM program (v 4.0; GraphPad Inc.). The *in vivo* data was analyzed utilizing SPSS (v 23; IBM), but was graphed using the PRISM program. Statistical significance was considered $p < 0.05$. Data analysis is discussed in more detail at the end of each assays' experimental section.



Scheme 2.1 General synthesis scheme of split resin approach. A) As a bivalent ligand is synthesized, the resin can be split at various points to produce control ligands including the tetrapeptide scaffold by itself and the tetrapeptide with the N-terminus linker. Also, the resin can be split such that a different linker can be added and/or a different second pharmacophore scaffold can be added. B) The C-terminus linker controls must be synthesized separately. The resin can still be split to add different pharmacophores onto the same linker. (a) 20 % piperidine in DMF (b) Fmoc-NH-AA-COOH or Fmoc-NH-PEDG20-COOH, HBTU, DIEA in DMF. Repeat (a) and (b) to achieve desired sequence. When Fmoc-NH-PEDG20-COOH was incorporated, reaction was allowed to proceed for an extra hour at room temperature. (c) 75% acetic anhydride/ 25% pyridine. (d) Cleavage with 91% TFA, 3% EDT, 3% TIS, 3% water for 1.5-3 hours.



Scheme 2.2. Example of resin splitting synthesis scheme. This scheme was utilized to make ligands in **Chapter 3**, **Chapter 4**, and **Chapter 5**. (A) The synthesis of N-terminal linker controls and bivalent ligands by microwave synthesis. (B) Synthesis of C-terminal linker controls using a semi-automated synthesizer (a) 20 % piperidine in DMF (b) Fmoc-NH-AA-COOH or Fmoc-NH-PEDG20-COOH, HBTU, DIEA in DMF. Repeat (a) and (b) to achieve desired sequence. When Fmoc-NH-PEDG20-COOH was incorporated, reaction was allowed to proceed for an extra hour at room temperature. (c) 75% acetic anhydride/ 25% pyridine. (d) Cleavage with 91% TFA, 3% EDT, 3% TIS, 3% water for 1.5-3 hours. This scheme has been adapted with permission from Lensing, C.J. *et al*, *J. Med. Chem.* **2016**, 59, 3112-3128.²⁵ Copyright (2016) American Chemical Society.

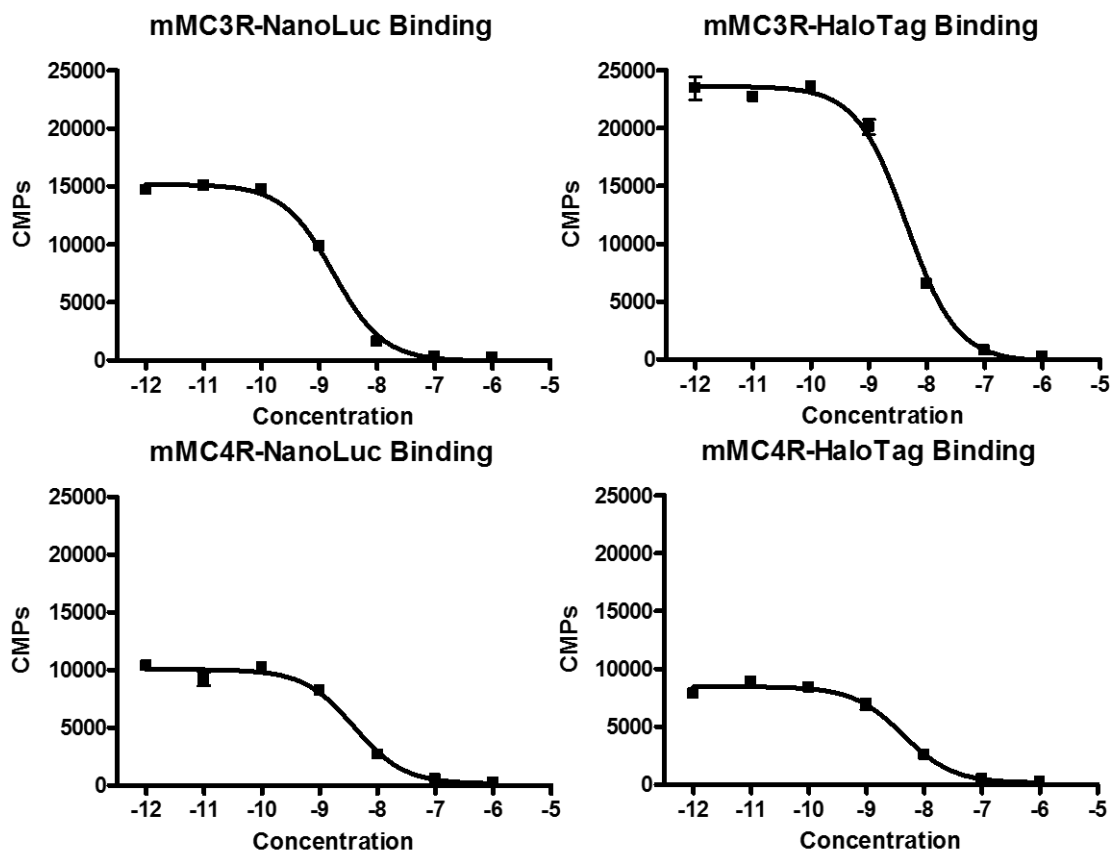


Figure 2.1. Representative radioligand binding curves of the BRET receptor constructs. Unlabeled NDP-MSH was used to displace ¹²⁵I-NDP-MSH in a dose-response manner to calculate the IC₅₀ values. The reported errors are the standard error of the mean (SEM) determined from two replicate wells in a single experiment. This figure has been reproduced with permission from Lensing, C. J. *et. al*, *ACS Chem. Neurosci.* **2017**, in press.¹³² Copyright (2017) American Chemical Society.

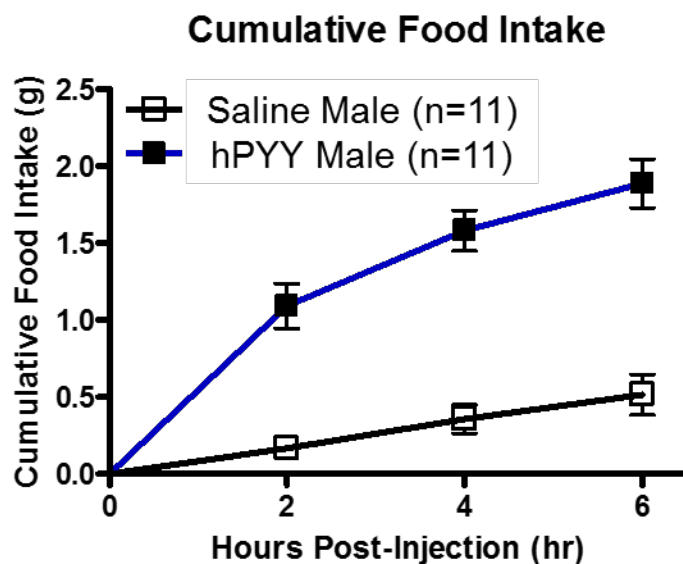


Figure 2.2. Average results from hPYY cannulation validation experiments. This experiment was performed to identify validated mice for use in TSE metabolic cage studies described in Chapter 4. Mice were administered 2.5 μg of human (h)PYY3-36 two hours before lights out. Food intake was measured manually. Validated mice ate at least 0.8 g more food after hPYY administration compared to saline administration at the 4 h time point. On average mice ate 0.4 ± 0.1 g at the 4 h time point after saline administration compared to 1.6 ± 0.1 g after hPYY administration in this experiment. Statistical analysis not shown. This figure has been reproduced with permission from Lensing, C. J. *et. al*, *ACS Chem. Neurosci.* **2017**, in press.¹³² Copyright (2017) American Chemical Society.

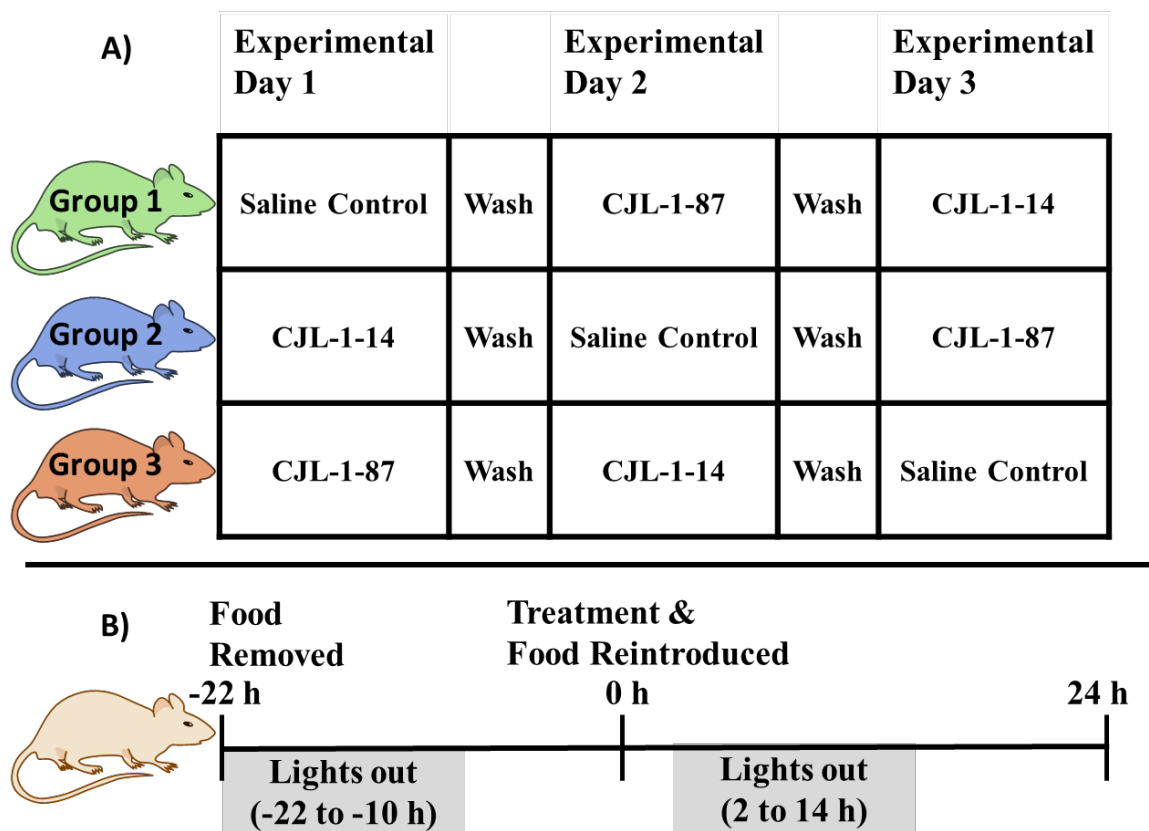


Figure 2.3: Experimental paradigms used to study energy homeostasis in Chapter 4. A) Head to head three-way crossover design of experimental groups. Similarly, a two-way cross-over was also used in this thesis work. B) Fasting-refeeding experimental paradigm used throughout this thesis work. This figure has been reproduced with permission from Lensing, C. J. *et. al*, *ACS Chem. Neurosci.* **2017**, in press.¹³² Copyright (2017) American Chemical Society.

	NDP-MSH IC₅₀ (nM)
	Mean±SEM
mMC3R-NanoLuc®	1.1±0.7
mMC3R-HaloTag®	3.1±1.4
mMC4R-NanoLuc®	2.8±1.1
mMC4R-HaloTag®	2.5±1.8

Table 2.1. Competitive radioligand binding assays on the BRET receptor constructs.

Unlabeled NDP-MSH was used to displace ¹²⁵I-NDP-MSH in a dose-response manner to calculate the IC₅₀ values. The reported errors are the standard error of the mean (SEM) determined from at least two independent experiments. This table has been reproduced with permission from Lensing, C. J. *et. al*, *ACS Chem. Neurosci.* **2017**, in press.¹³²

Copyright (2017) American Chemical Society.

**Chapter 3: The Design, Synthesis, *In Vitro*, and *In Vivo* Investigation of
Homobivalent Ligands that Display Preferential Binding and Functional Activity
for Different Melanocortin Receptor Homodimers**

Portions of the studies presented in this chapter have been previously published and are currently being reproduced with permission from: Lensing, C. J.; Freeman, K. T.; Schnell, S. M.; Adank, D. N.; Speth, R. C.; Haskell-Luevano, C. An *in Vitro* and *in Vivo* Investigation of Bivalent Ligands That Display Preferential Binding and Functional Activity for Different Melanocortin Receptor Homodimers. *J. Med. Chem.* 2016, 59, 3112-3128.²⁵ Copyright (2016) American Chemical Society. All peptides were designed, synthesized, purified, and analytically characterized by Cody Lensing under the supervision of Carrie Haskell-Luevano. The *in vitro* pharmacology studies were performed by Cody Lensing, Katie Freeman, and Sathya Schnell, all members of the Haskell-Luevano lab group. *In vivo* studies were performed by Cody Lensing and Danielle Adank. Katlyn Fleming aided in the interpretation of the pharmacology of **CJL-1-20** (Ac-His-DPhe(pI)-Arg-Trp-NH₂) and presented the following poster at the Chemistry and Biology of Peptides Gordon Research Conference: Fleming, K. A.; Doering, S. R.; Lensing, C. J.; Freeman, K. T.; Tala, S. R.; Haskell-Luevano, C. "A Parallel Comparison of the Functional Efficacy of Melanocortin Peptides in Two Diverse *In Vitro* Assays." Radiolabeled ¹²⁵I-NDP-MSH was prepared by Robert Speth.

3.1 Chapter Overview

Pharmacological probes for the melanocortin receptors have been utilized for studying various disease states including cancer, sexual function disorders, Alzheimer's disease, social disorders, cachexia, and obesity. This study focused on the design and synthesis of bivalent ligands to target melanocortin receptor homodimers. Lead ligands (**CJL-1-87** and **CJL-1-31**) increased binding affinity by 14- to 25-fold and increased cAMP signaling potency by 3- to 5-fold compared to their monovalent counterparts. Unexpectedly, different bivalent ligands showed preferences for particular melanocortin receptor subtypes depending on the linker that connected the tetrapeptide scaffolds suggesting structural differences between the various dimer subtypes. Homobivalent compound **CJL-1-140** possessed a functional profile that was unique from its monovalent counterparts providing evidence of the discrete effects of bivalent ligands.

3.2 Introduction

As stated in **Chapter 1**,¹ the melanocortin receptor system is involved in various physiological functions including pigmentation,^{49, 50} sexual behavior,⁵¹ blood pressure modulation,⁵² memory,⁵³⁻⁵⁵ and energy homeostasis.⁵⁶⁻⁵⁹ The system contains five G_{as} protein-coupled receptor subtypes (MC1-5R) that stimulate the cAMP signal transduction pathway upon agonist binding.^{49, 77-82} Ligands targeting the melanocortin G protein-coupled receptors (GPCRs) have been utilized as probes, and investigated as potential therapeutics for Alzheimer's disease,⁶⁰⁻⁶² cancer targeting,^{6, 28, 63-65} sexual function,^{51, 66} social disorders,^{67, 68} cachexia,⁶⁹⁻⁷³ and obesity.^{56, 74-76} Due to the wide range of

pharmacological effects, the development of ligands with new scaffolds, unique functional properties, or more selective profiles are needed as *in vitro* and *in vivo* probes for the various melanocortin dependent functions.

Bivalent ligands have been shown to offer access to properties and pharmacological profiles which are unique from classic monovalent ligands. The growing acceptance of GPCR dimers as pharmacological targets has fostered the development of bivalent ligands to target them. There have been several reports establishing that all known subtypes of melanocortin receptors form homodimers.^{125, 127, 129-131, 204, 206} Competitive binding studies suggested that melanocortin receptors have two side by side binding sites (presumably on different receptors) each with different binding properties which may indicate targetable homodimers.^{205, 219} Bivalent ligands offer a potential avenue to target melanocortin GPCR dimers and investigate their functional effects both *in vitro* and *in vivo*. Since Portoghese and coworkers pioneered bivalent ligands targeting GPCRs,⁷ bivalent ligands have been developed for various GPCR systems including the opioid,^{5, 7-9, 11} serotonin,¹⁸⁻²⁰ adenosine,¹⁵ cannabinoid,^{16, 17} chemokine,²³ dopamine,²¹ and melanocortin receptors.²⁶⁻³⁷ Bivalent ligands have been demonstrated to have a variety of different pharmacological effects as compared to their monovalent counterparts including: increasing or decreasing binding affinity,^{19, 21, 33} positively or negatively changing functional responses,^{15, 17, 20, 26, 41} altering receptor subtype selectivity,^{8, 21} changing receptor trafficking,⁴²⁻⁴⁴ and creating tissue selectivity.^{5, 10} Due to these unique characteristics, bivalent ligands can offer distinct advantages and/or disadvantages over the classical monomeric approach.

Melanocortin bivalent ligands with various designs and linkers have increased binding affinity for human (h)MC4R expressed in HEK293 cells.^{27, 29-37} There had not previously been a report of bivalent ligands' pharmacologies using the cloned MC1R, MC3R, and MC5R cell lines prior to this thesis work.²⁵ Studying bivalent ligands' effects at each receptor subtype is important for understanding ligand selectivity and for transitioning molecules to more complicated whole animal models that are expressing multiple receptor isoforms. Furthermore, there has been no investigation of bivalent ligands' effects on the cloned mouse receptors prior to this thesis work.^{25, 132} Results obtained from the cloned mouse receptors are advantageous to inform the use of melanocortin bivalent ligands in the developed mouse models⁵⁶⁻⁵⁹ and represent an important translational step in the development of bivalent ligands as pharmacological probes.

Reports of melanocortin bivalent ligand's effects on functional activity have been limited. The early functional activity study showed effects on frog-melanophore cells and used an unoptimized linker.²⁶ In this system, an agonist bivalent ligand increased agonist signal. They also reported a bivalent ligand based on an antagonist monovalent pharmacophore that unexpectedly became a full agonist at high concentrations.²⁶ Another report described bivalent ligands as having increased potency in cAMP accumulation assays in HEK293 cells expressing the hMC4R.²⁸ To the best of our knowledge, these were the only two functional studies of bivalent ligands at the melanocortin receptors reported prior to this thesis work.^{26, 28} While these preliminary studies with frog melanophores and

hMC4R cell lines illustrate the uniqueness and utility of melanocortin bivalent ligands, further functional studies such as the one presented in this chapter at other receptor subtypes would help advance melanocortin bivalent ligands as potentially selective and potent pharmacological probes.²⁵

Given the lack of studies reporting bivalent ligands' effects at different melanocortin receptor subtypes, there had been little understanding of how different linkers and design strategies affect binding and functional selectivity between the different melanocortin receptor isoforms. One objective of this study in this chapter was to investigate receptor subtype preference patterns by screening in parallel the different melanocortin receptors (the MC2R was excluded since it is reported to only be stimulated by ACTH)⁴⁹ with bivalent ligands using different design strategies. Furthermore, in order for the bivalent ligands to be suitable *in vivo* functional probes for mouse studies, their effects must be characterized at the mouse melanocortin receptors otherwise interpretation of *in vivo* mouse studies would be confounding. The current study reports the design and synthesis of a library of agonist, partial agonist, and antagonist melanocortin homobivalent ligands which underwent *in vitro* binding and functional evaluation at the mouse (m)MC1R, mMC3R, mMC4R, and mMC5R subtypes. It also gives, to the best of our knowledge, the first *in vivo* functional evaluation of a melanocortin bivalent ligand.²⁵

3.3 Results and Discussion:

3.3.1 Design

It was hypothesized that appropriately designed bivalent ligands can be used to target melanocortin receptor dimers, and that there may be differences in the receptor subtype homodimer pharmacological profiles. Our approach throughout this thesis was to target receptor homodimers by creating bivalent ligands comprised of two pharmacophore scaffolds connected with two different linkers (**Figure 3.1**). The previously reported tetrapeptides Ac-His-DPhe-Arg-Trp-NH₂,^{96, 98} Ac-His-DNal(2')-Arg-Trp-NH₂,^{97, 220} and Ac-His-DPhe(pI)-Arg-Trp-NH₂,^{97, 220} were selected as the scaffold templates to incorporate into the bivalent ligands. These tetrapeptides are based on His-Phe-Arg-Trp which is the minimal messaging sequence of the endogenous melanocortin hormones.^{96, 99, 221, 222} Truncation studies of the potent and enzymatically stable peptide NDP-MSH (Ac-Ser-Tyr-Ser-Nle-Glu-His-DPhe-Arg-Trp-Gly-Lys-Pro-Val-NH₂) have previously shown the tetrapeptide Ac-His-DPhe-Arg-Trp-NH₂ to be the most active fragment.⁹⁶

The Ac-His-DPhe-Arg-Trp-NH₂ peptide has previously been reported to have a high nanomolar to low micromolar binding affinity at the melanocortin receptors.⁹⁸ Herein, it is postulated that the incorporation of the His-DPhe-Arg-Trp scaffold into bivalent ligands would retain the relatively potent agonist functional effects, but would have a lower binding affinity than bivalent ligands containing longer peptides scaffolds would. This is an important consideration in the design strategy presented, since bivalent ligands based off of low affinity scaffolds often allow easier detection of synergistic binding effects as

discussed in **Chapter 1**.^{1, 27, 122, 223} This allows for detection of larger increases in binding affinity which is characteristic of bivalent ligands targeting dimers.^{7, 31, 47} Incorporation of the tetrapeptide His-DPhe-Arg-Trp into bivalent ligands had already been reported to significantly increase binding at the hMC4R.³³ This thesis' design and experiments advance the field by examining the binding and functional effects of bivalent ligands based on this tetrapeptide with different linkers at the various melanocortin receptor subtypes. The previous report studied bivalent ligands that contained 14 atom, 19 atom, and 38 atom linkers separating the two His-DPhe-Arg-Trp scaffolds;³³ the design herein utilizes 20 atom, 36 atom, and 40 atom linkers connecting the same scaffolds. The small extensions in our design can significantly change activity, as bivalent ligands are quite sensitive to linker length.^{10, 11, 224, 225} For example, single atom linker extensions previously resulted in noteworthy changes (>500-fold) in the *in vivo* potency in a series of bivalent ligands tested for antinociception.¹⁰ A two-atom linker extension in a bivalent ligand previously increased potency by 1100-fold.²²⁵

Carrithers and Lerner reported that bivalent ligands containing antagonist monomers yields an agonist bivalent ligand at high concentrations in a functional frog melanocyte dispersion assay.²⁶ This result leads to the present hypotheses that bivalent ligands based on antagonist and partial agonist monomers may result in unique pharmacological profiles with general activity trends that could be exploited in future bivalent ligand design. In order to study the effects of antagonist and partial agonist based bivalent ligands, the DPhe in the agonist scaffold was substituted to a DNal(2') or a

DPhe(pI) to yield the His-DNal(2')-Arg-Trp and Ac-His-DPhe(pI)-Arg-Trp-NH₂ tetrapeptide scaffolds. The His-DNal(2')-Arg-Trp tetrapeptide has previously been reported to be a mMC3R/mMC4R antagonist, with partial activity at the mMC3R, and full agonist activity at the mMC1R and mMC5R.^{97, 220} To our knowledge, the binding affinity of this tetrapeptide had not been previously reported, but it was assumed that the binding affinity would be similar to Ac-His-DPhe-Arg-Trp-NH₂ in that it would have a low enough affinity to detect synergistic binding modes when used in homobivalent ligands. The Ac-His-DPhe(pI)-Arg-Trp-NH₂ tetrapeptide was reported to be a full double digit to single digit nanomolar agonist at the mMC1R, mMC4R, and mMC5R, but an antagonist ($pA_2 = 7.25 \pm 0.18$) with some agonist activity (40% receptor activation at 100 μ M) at the mMC3R.^{97, 220} Of note, the reported pharmacology of these compounds was from a CRE/ β -galactosidase reporter gene assay,^{97, 196, 220} but most of the studies in this thesis utilize an AlphaScreen cAMP technology to measure receptor activation. There were some assay differences between compounds that will be discussed more thoroughly below in **Section 3.3.4.1.**

Both a polyethylene diamine diglycolic acid (PEDG, but also referred to in the literature as PEGO or PEG₂) and an alternating proline-glycine (Pro-Gly) linker system were selected for this study based upon previous work of Hruby and coworkers demonstrating these linker systems enhance binding affinity at the hMC4R.^{30, 31, 33, 168, 170} It was hypothesized that different linker systems and lengths may have varying effects at the different receptor homodimer subtypes. The PEDG linker is flexible with good

solubility. Both a 20 atom PEDG20 linker and a 40 atom PEDG20-PEDG20 linker have previously been reported to have increased binding affinity at the hMC4R when joining seven residue analogs of the NDP-MSH scaffold.³¹ The Pro-Gly linker is a semi-rigid linker system with the Pro giving the linker rigidity and the Gly giving the linker flexibility. A linker system of 36 atoms based on six repeats of Pro-Gly has been shown to be an effective linker system for targeting the hMC4R.^{30, 31, 168} The PEDG20, PEDG20-PEDG20, and (Pro-Gly)₆ have previously been estimated to be 4-18 Å, 8-36 Å, and 10-20 Å, respectively.^{31, 63} The PEDG20 linker was selected for the Ac-His-DNal(2')-Arg-Trp-NH₂ series and Ac-His-DPhe(pI)-Arg-Trp- NH₂ series based on solubility, ease of synthesis, and preliminary functional results. Although the metabolic stability was not tested at the time of the current study, it has previously been shown that adding polyethylene glycol to a peptide can increase metabolic stability.^{226, 227} By incorporating the polyethylene glycol-like PEDG20 into our design, we hypothesized it may increase the likelihood of identifying a suitable *in vivo* probe. Serum stability assays examining the effects of linker design were performed later, validating this hypothesized design strategy, and will be discussed in detail in **Chapter 4** and **Chapter 6**.¹³²

3.3.2 Peptide synthesis

All compounds were synthesized on Rink-amide-MBHA resin using standard Fmoc-chemistry and solid phase synthesis methodology utilizing both a semi-automated synthesizer and a microwave synthesizer as described in **Chapter 2**.^{190, 191, 228} Similar to a strategy previously employed,³⁰ the resin was split at various points in the synthesis to

produce the desired linker controls (**Scheme 2.1** and **2.2**). This strategy allowed the production of the desired control ligands (*i.e.* the tetrapeptides and the tetrapeptides with the linker attached) in route to the synthesis of the bivalent ligands. This strategy was also used to derivatize control ligands with the linker attached to the N-terminus of the DPhe, DNal(2'), and DPhe(pI) compounds. The control compounds synthesized in this fashion also served as controls for the MUmBL compounds discussed in **Chapter 5**.

Peptides were cleaved off of the resin using triisopropylsilane, 1,2-ethanedithiol, and water in trifluoroacetic acid (TFA). A cleavage time of 3 hours caused significant degradation of **CJL-1-116**. Interestingly, the major degradation product and pure **CJL-1-116** had the same retention time by analytical RP-HPLC in acetonitrile and aqueous TFA (0.1%) (**Figure 3.2A**), but clear peak separation could be seen by analytical RP-HPLC in methanol and aqueous TFA (0.1%) (**Figure 3.2B**) illustrating the importance of using two diverse solvent systems (*e.g.* acetonitrile and methanol) when assessing compound purity. Mass spectrometry revealed the mass of the desired product (mass of 961.6) and the mass of the impurity (mass of 685.4). The impurity peak possessed the same mass and had similar retention times as the parent tetrapeptide Ac-His-DPhe-Arg-Trp-NH₂ that could indicate the degradation of the linker. Co-injection of purified **CJL-1-14** with crude sample of **CJL-1-116** from the 3-hour cleavage resulted in increased relative intensity of the impurity peak demonstrating the similar retention times of **CJL-1-14** and the impurity (**Figure 3.2C**). A shorter cleavage time of 1.5 hours resulted in minimal degradation products of **CJL-1-116** as seen by analytical HPLC in methanol and aqueous TFA (0.1%)

(Figure 3.2D). A shorter cleavage time was also used for **CJL-1-132** and minimal degradation was observed. The remaining peptides reported were synthesized with little difficulty. All final ligands were purified to greater than 95% pure and their mass was confirmed by ESI-MS (Table 3.1). Further details can be found in the in **Chapter 2**.

Although bivalent **CJL-5-64**, Ac-His-DPhe(pI)-Arg-Trp-(PEDG20)-His-DPhe(pI)-Arg-Trp-NH₂, was synthesized and purified, it could not be successfully dissolved after lyophilization. Attempted solvents to dissolve the peptide included DMSO, water, 20% Solutol®HS (Sigma, Cat # 42966) in water, neat acetic acid, and mixtures of these solvents. Compound **CJL-5-64** did seem to dissolve in large amounts of methanol or acetonitrile but these solvent systems would not be applicable to the current whole cell assays or *in vivo* assays. The reason for the lack solvation of **CJL-5-64** was never understood completely. Retention times in HPLC were similar to readily dissolvable compounds ($K'_{MeCN} = 6.0$, $K'_{MeOH} = 10.5$) indicating it was not an issue of hydrophobicity. The current hypothesis is that a noncovalent “side-on” interaction of the negatively charged I atom with the electropositive aromatic plane that results in polymerization or aggregation.²²⁹ This would need to be experimentally validated and tested. Because of the solubility issues and the assay differences observed with Ac-His-DPhe(pI)-Arg-Trp-NH₂ (**CJL-1-20**) that will be discussed below, **CJL5-64** was excluded from the bioassays and any further development. It will, therefore, not be discussed further.

3.3.3 ¹²⁵I-NDP-MSH Competitive Binding Affinity Studies

The ligands' ability to competitively displace ¹²⁵I-NDP-MSH was studied in HEK293 cells signally expressing each of the melanocortin receptors. The results are summarized in Table 3.2 and illustrated in Figure 3.3. The varying effects of the linker, pharmacophore, and receptor subtype are summarized below.

3.3.3.1 *Linker effects*

The addition of the linker to the monovalent tetrapeptide scaffold affected binding of the ligand depending on the type of linker, site of addition (N- or C-terminus), and receptor subtype. At the mMC1R, the linkers had minimal effects on binding (**Figure 3.3A and D**) and the difference between control ligand **CJL-1-14**, **CJL-1-80**, or **CJL-1-20** and their corresponding linker control ligands are within experimental error. Changes less than 3-fold were considered to be within experimental error associated with the assay (in our hands). At the mMC3R, the addition of a linker to the tetrapeptides resulted in equal or increased binding affinity (**Figure 3.3B and E**). Most notable was the addition of the PEDG20 to the C-terminus and (Pro-Gly)₆ to the N-terminus of the Ac-His-DPhe-Arg-Trp-NH₂ scaffold in compounds **CJL-5-35-4** and **CJL-1-41**. The addition of this linker resulted in increased mMC3R binding affinity of *ca.* 6- and 9-fold, respectively, as compared to its monovalent counterpart **CJL-1-14** (**Table 3.2**). The addition of the PEDG20 to the N-terminus of Ac-His-DPhe(p-I)-Arg-Trp-NH₂ in compound **CJL-5-009** resulted in a 3-fold increase in binding affinity compared to its monovalent counterpart **CJL-1-20**. At the mMC4R, the (Pro-Gly)₆ linker reduced the binding affinity by 4-fold compared to **CJL-1-**

14 when added to the C-terminus in compound **CJL-5-35-1** (**Figure 3.3C** and **F**). In contrast, the PEDG20 linker when added to the C-terminus in **CJL-5-35-4** resulted in a 3-fold increased binding affinity compared to **CJL-1-14**. All other linker control compounds resulted in less than 3-fold changes at the mMC4R compared to their monovalent counterpart.

It is worth noting that there were changes in binding affinity when the linker was added to the C-terminus of the peptide, which has been seldom investigated when studying melanocortin bivalent ligands. The present SAR study demonstrated that the site of linker addition to either the C-terminus or N-terminus is an important consideration when designing bivalent ligands.

3.3.3.2 Bivalent Ligands

All His-DPhe-Arg-Trp based bivalent ligands had increased binding affinity (3- to 25-fold) compared to the parent tetrapeptide **CJL-1-14**. The SAR of the His-DPhe-Arg-Trp based bivalent ligands at the different receptor subtypes was an intriguing finding. At the mMC1R, the most enhanced compound was the (Pro-Gly)₆ linked compound **CJL-1-31** (**Figure 3.3A**). Its binding affinity increased by 14-fold compared to monovalent ligand **CJL-1-14**. The PEDG20 linked compounds **CJL-1-87** and **CJL-5-72** resulted in a 6- and 3-fold increased binding affinity, respectively. At the mMC3R, the (Pro-Gly)₆ and PEDG20 linkers had the greatest effect (**Figure 3.3B**). It was observed that **CJL-1-31** and **CJL-1-87** possessed *c.a.* 25- and 23-fold increased binding affinity, respectively, compared to **CJL-1-14**. Compound **CJL-5-72** resulted in an 8-fold increased binding

affinity compared to **CJL-1-14**. At the mMC4R, the PEDG20 linked bivalent ligand **CJL-1-87** increased binding affinity 22-fold as compared to the monovalent counterpart **CJL-1-14** (**Figure 3.3C**). Compounds **CJL-1-31** and **CJL-5-72** possessed 6- and 4-fold increased binding affinity, respectively, as compared to **CJL-1-14**.

In the Ac-His-DNal(2')-Arg-Trp-NH₂ series, bivalent ligand **CJL-1-140** resulted in 4-fold increased binding affinity at both the mMC1R and mMC3R as compared to its monovalent counterpart **CJL-1-80** (**Figure 3.3D and E**). The binding affinity of compound **CJL-1-140** was within experimental error of the binding affinity of **CJL-1-80** at the mMC4R (**Figure 3.3F**). It was postulated that no increase in binding affinity was observed at the mMC4R because of the potent binding affinity of Ac-His-DNal(2')-Arg-Trp-NH₂ scaffold that potentially masked multivalent interactions.^{27, 122, 223} The lower binding affinity of the Ac-His-DPhe-Arg-Trp-NH₂ scaffolds allows easier detection of the enhancements in the binding affinity. As Kiessling and Lamanna explain, an “increase in apparent affinity of a multivalent display of middle-affinity epitopes quickly exceeds measurable binding constants and is indistinguishable from multivalent scaffolds of high-affinity ligands. In contrast, the increase in functional affinity between multivalent displays of weakly versus more weakly interacting epitopes falls within a range discernible by most biological systems.”²²³

The increased binding affinity (14- to 25-fold) of the lead bivalent ligands in the Ac-His-DPhe-Arg-Trp-NH₂-based series support the hypothesis that these ligands are binding in a synergistic bivalent mode utilizing a second binding site. The second binding

site could be either an auxiliary binding site on the same receptor or an orthosteric binding site on a neighboring receptor.^{223, 230} The use of Occam's razor directs us to the latter possibility since it has been observed that melanocortin receptors dimerize,^{125, 127, 129-131, 204, 206} and therefore, a neighboring orthosteric binding site should be readily accessible for synergistic binding versus an unknown auxiliary binding site for the His-DPhe-Arg-Trp pharmacophore.

In the proposed bivalent binding mode, the first binding interaction of one pharmacophore is postulated to tether the second pharmacophore to the receptor surface. If the linker has the correct properties (*e.g.* length, flexibility) to orientate the second pharmacophore into a tandem binding site (*i.e.* a GPCR dimer), the second binding interaction proceeds with lowered entropic cost (**Figure 3.4**).^{7, 230} Based on these results, the PEDG20-PEDG20 linker in compound **CJL-5-72** may be too long to tether the second pharmacophore in the correct location of the second binding site, and therefore, loses the entropic gains of the bivalent design reflected in the lower fold changes in binding affinity at all receptor subtypes.⁷ These results help validate the use of this design strategy in **Chapters 4-6**.

An interesting trend observed was the differential effects of the (Pro-Gly)₆ and PEDG20 linkers at the melanocortin receptor subtypes. Compound **CJL-1-31** with the (Pro-Gly)₆ linker resulted in the greatest fold increase in ligand binding affinity at the mMC1R (14-fold) and notable fold increase at the mMC3R (25-fold), but lower fold changes at the mMC4R (6-fold). Ligand **CJL-1-87** with the PEDG20 linker resulted in the

greatest fold increase in binding affinity at the mMC4R (22-fold) and notable fold increase at the mMC3R (23-fold), but lower fold increase at the mMC1R (6-fold). In this study, it was identified that the mMC1R has a preference for the (Pro-Gly)₆ linker, the mMC4R has preference for the PEDG20 linker, and the mMC3R bound well with both of the two linkers (**Figure 3.5**).

The receptor subtype differences observed with compounds **CJL-1-31** and **CJL-1-87** are not due to the binding scaffold or the binding pocket since these remain constant when comparing the bivalent ligands to the monovalent counterparts at each receptor subtype. In addition, the tetrapeptide plus linker control ligands resulted in minimal increased binding affinity (<4-fold) at the mMC1R and mMC4R suggesting that the linker by itself is not the driving factor for the bivalent ligands increased activity. At the mMC3R, the linker control ligands did result in increased binding affinity (≤ 9 -fold), but their affinities were lower than the affinities of the lead bivalent ligands and are likely not the primary driving factor for the increased mMC3R binding affinities of the bivalent ligands. Instead the bivalent ligand-receptor differences are conjectured to be due to differences in the physiochemical nature of the linker (*e.g.* flexibility, length, ect.) and how these may change the presentation of the pharmacophore to the tandem binding site.

Based upon these results it can be postulated that there are differences how the tandem binding sites of different melanocortin homodimer subtypes present themselves. For example, if the mMC1R homodimer has more distance between the two binding sites than a mMC4R homodimer, the (Pro-Gly)₆ linker (36 atoms, $\sim 8\text{-}36 \text{ \AA}^{31, 63}$), that is

hypothesized to be longer based on atom length than the PEDG20 linker (20 atoms, ~4-18 Å^{31, 63}), would favor the mMC1R homodimer and the PEDG20 would favor the mMC4R. To be consistent with the data, the mMC3R homodimer would have an intermediate distance between their two binding sites compared to the mMC1R and mMC4R homodimers, and therefore would show enhanced binding with both linker systems (**Figure 3.5**). It should be noted that the flexibility of the linkers makes prediction of their exact lengths in solution difficult, and this is just a hypothesis to explain the trends observed.

This idealized situation only accounts for the distance between tandemly arranged binding pockets and the linker's length. Other factors including the linker's other physiochemical properties, the two pharmacophores' orientations, and the binding pockets' accessibility may play a role in the binding affinity preferences observed. Nevertheless, these data suggest bivalent ligands could be exploited to achieve selectivity between the different melanocortin homodimers. This is, to our knowledge, the first indication of ligand preference patterns (albeit not selectivity) between the melanocortin homodimer-subtypes; however this phenomenon has been observed in several other bivalent ligand systems targeting GPCR systems.^{8, 21} For example, Kuhhorn and coworkers previously observed different linker systems connecting bivalent ligands resulted in varying dopamine receptor subtype specificity.²¹ In addition, Portoghese and coworkers synthesized bivalent ligands with different selectivity profiles for the μ , κ , and δ opioid receptors based on single glycol unit linker extensions.⁸ Given these three examples of differential binding of bivalent

ligands, it suggests that ligand selectivity between different receptor homodimer subtypes, as opposed to monomer orthosteric selectivity, may be a general phenomenon among GPCRs. However, more investigation into melanocortin receptor homodimerization (or higher-order oligomerization) will be necessary. The current study reports foundational work and results in novel chemical probes for future studies for both melanocortin GPCR homodimers and heterodimers.

3.3.4 Functional cAMP Accumulation Studies

The AlphaScreen[®] cAMP Assay Technology was utilized to examine the ligands ability to stimulate intracellular cAMP signaling in live HEK293 cells stably expressing the mMC1R, mMC3R, mMC4R, and mMC5R. Compounds which did not produce full activation at 100 μ M (compared to maximal NDP-MSH signal) were analyzed for antagonist properties via a Schild analysis at the mMC3R and mMC4R.¹⁹⁸ The results of the studies are summarized in **Tables 3.2** and **3.3** as well as illustrated in **Figures 3.6** and **3.7**.

As anticipated, compounds with greater binding affinity tended to have greater functional potency. However, plotting the EC₅₀ values versus IC₅₀ values of His-DPhe-Arg-Trp ligands suggested that binding affinity does not correlate linearly to function at the mMC1R and mMC3R with R² values of 0.22 and 0.75, respectively (**Figure 3.8**). At the mMC4R, it does appear to correlate linearly (R² value of 0.95) such that a ligand's EC₅₀ potency is approximately 10-fold more potent compared to its IC₅₀ binding affinity. Although some of the poor correlation could be due to inherent experimental error, these

data show that binding affinity and cAMP accumulation functional potency observed do not necessarily correlate within receptor isoforms highlighting the importance of studying both a ligand's binding affinity and functional potency in complementary assays. A more detailed description of the functional activity with the linker control compounds and the bivalent compounds is discussed below.

3.3.4.1 Discrepancies between cAMP Functional Assays

Comparison of the current studies to past literature results reported by our laboratory revealed some discrepancies between the functional potency and efficacy of monovalent tetrapeptides presumably due to differences in the assay paradigms. In the literature studies, a CRE/ β -galactosidase reporter gene assay was utilized to evaluate the pharmacology instead of the AlphaScreen[®] cAMP Assay Technology currently used.^{97, 220} Compound **CJL-1-14**, Ac-His-DPhe-Arg-Trp-NH₂, was a strong agonist and gave comparable results to previous reports using the CRE/ β -galactosidase reporter gene assay by our laboratory (**Table 3.3**).^{97, 220} Furthermore, the other control agonist compounds (*i.e.* NDP-MSH, α -MSH, and γ -MSH) presented currently have comparable activities compared previous literature reports in the CRE/ β -galactosidase reporter gene assay.^{97, 220}

The results obtained with compound **CJL-1-80**, Ac-His-DNal(2')-Arg-Trp-NH₂ at the mMC1R and mMC3R were similar to literature values reported (**Table 3.4**).^{97, 220} At the mMC4R, **CJL-1-80** resulted in a very similar pA₂ value to those reported pervious, but it resulted in some agonist activity at 100 μ M that was not previously observed.^{97, 220} This agonist activity at high concentrations is likely not physiologically relevant as

concentrations exceeding 10 μ M are unlikely to be achieved in the brain. This also could be an assay artifact from some sort of assay interference observed at high concentrations. This hypothesis that it is an assay artifact was supported by the preliminary work of Katie Henning (Freeman) utilizing the AlphaScreen™ TruHits™ assay kit (data not shown). However, a major pharmacological difference was observed with **CJL-1-80** at the mMC5R. In the current AlphaScreen Assay, **CJL-1-80** resulted in only 75% receptor activation at 100 μ M relative to NDP-MSH. In previous studies using the CRE/ β -galactosidase reporter gene assay, **CJL-1-80** was reported to be a double-digit nanomolar agonist.⁹⁷ This suggests that these results are not solely due to assay artifacts and that these two assays are not completely equivalent. Our laboratory is primarily interested in the mMC3R and mMC4R and its role in energy homeostasis. However, if designing ligands for the mMC5R, this discrepancy must be included in data interpretation.

Compound **CJL-1-20**, Ac-His-DPhe(pI)-Arg-Trp-NH₂, resulted in comparable pharmacology at the mMC1R, mMC3R, and the mMC5R as previous literature reports.⁹⁷ ²²⁰ However, compound **CJL-1-20** was a nanomolar antagonist ($pA_2 = 8.6 \pm 0.1$) with some partial activity. In previous reports, Ac-His-DPhe(pI)-Arg-Trp-NH₂ was reported to be a nanomolar agonist at the mMC4R in the CRE/ β -galactosidase reporter gene assay.^{97, 220} This contrast of **CJL-1-20** being an agonist in the CRE/ β -galactosidase reporter gene assay but an antagonist in the AlphaScreen assay warranted further investigation.

In order to investigate, Ac-His-DPhe(pI)-Arg-Trp-NH₂ was purchased from Peptides International for a direct comparison to the synthesized compound, **CJL-1-20**.

The two compounds were then assayed in parallel in the AlphaScreen Assay to compare the cAMP signaling results directly (**Figure 3.9**). A very similar pharmacological profile was observed with both compounds. Also the compounds had matching masses and retention times by analytical RP-HPLC. This confirmed that the compound differences between the reported pharmacology,^{97, 220} and the observed current results are not due to our synthesis of the compound. It seems likely that the discrepancy is due to an assay difference between the CRE/ β -galactosidase reporter gene assay and the cAMP AlphaScreen assay.

In order to understand why there may be assay-dependent differences, it is necessary to understand how the assays work. In the CRE/ β -galactosidase reporter gene assay, the receptor is stimulated which activates adenylate cyclase. The adenylate cyclase amplifies the signal by converting ATP to cAMP. Then cAMP activates protein kinase A (PKA) which then phosphorylates cAMP response element binding protein (CREB) resulting in further signal amplification. In the CRE/ β -galactosidase reporter gene assay, cells are transfected with a plasmid with five CRE promoters that drives β -galactosidase expression in another amplification step. In a final amplification step after cell lysis, the β -galactosidase cleaves the colorless *ortho*-nitrophenyl- β -galactoside (ONPG) into galactose and brightly yellow colored *ortho*-nitrophenol. A dose-dependent increase in color conversion can be analyzed as a functional curve.¹⁹⁶ In contrast, the AlphaScreen assay measures cAMP by direct competition for a cAMP antibody such that binding disrupts a

signal relay system. Increased cAMP production by the cell results in decreased signal due to disruption in a dose-dependent manner.

Due to the inherent differences in the assay, several hypotheses can be proposed to explain the discrepancies between the two assays. First, the several additional signal amplification steps may result in greater signal from weak or partial agonists allowing them to reach maximal signal and be observed as full agonists. Second, the AlphaScreen has only a 2-hour compound stimulation whereas the CRE/ β -galactosidase reporter gene assay has a 6-hour compound stimulation. The differences observed may be time-dependent differences. Third, the cAMP AlphaScreen should only be affected by the $G_{\alpha s}$ -coupled signaling pathway. In addition to $G_{\alpha s}$ -coupled signaling pathway, the CRE/ β -galactosidase reporter gene assay is known to be stimulated through the $G_{\alpha q}$ -coupled signaling pathway that also results in CREB phosphorylation.¹⁹⁶ Discrepancies could be a result of this alternative signaling cascade (possibly through biased agonism). Fourth, if any compound-dependent assay interference was occurring in either assay, it may be different between the two assays considering the assay conditions are different (*e.g.* room temperature vs 37° C, gain of function versus loss of function, incubation times, gene reporter vs bead reporter).

Further research into the reason for the exact assay discrepancies is warranted. In the current thesis, we treated the two assays as complementary. Therefore, consistent results in the two assays was treated as a way of confirming compound pharmacology at that receptor subtype. Compounds based off **CJL-1-14** (Ac-His-DPhe-Arg-Trp-NH₂) and **CJL-1-80** (Ac-His-DNal(2')-Arg-Trp-NH₂), especially at the mMC3R and mMC4R,

normally resulted in consistent results in both assays and, therefore, were the focus of the current thesis work. Compounds that were inconsistent between the two assays were treated as suspect and, therefore, were avoided for further study and inclusion in design. These included compounds designed based on **CJL-1-20** (Ac-His-DPhe(pI)-Arg-Trp-NH₂). However, some *in vitro* work was performed with compounds that contain the His-DPhe(pI)-Arg-Trp pharmacophore were included in this chapter and in **Chapter 5** to aid in future efforts to understand the assay discrepancies and melanocortin ligand design (See the **Appendix** for pharmacology information). After all, hindsight is 20/20.

3.3.4.2 Linker Effects

There were five situations in which the addition of a linker to the tetrapeptide scaffold resulted in noteworthy changes in agonist activity. Changes less than 3-fold were considered to be within the intrinsic experimental error associated with this functional assay (in our hands). The attachment of the (Pro-Gly)₆ linker to the C-terminus in **CJL-5-35-1** decreased the potency of the Ac-His-DPhe-Arg-Trp-NH₂ by 5-fold at the mMC4R and mMC5R (**Table 3.3, Figure 3.6G and H**). In contrast, at the mMC5R the attachment of PEDG20 to the C-terminus in **CJL-5-35-4** resulted in 5-fold increased functional potency (**Table 3.3, Figure 3.6H**). Also attachment of the PEDG20 to the C-terminus of His-DPhe(pI)-Arg-Trp as seen in compound **CJL-5-35-6** resulted in a 10-fold increase in agonist potency at the mMC5R. Compound **CJL-5-35-6** also resulted in a 3-fold increase in antagonist potency at the mMC3R (**Table 3.4**).

These data indicated that the C-terminus of His-DPhe-Arg-Trp is amendable to changes, but sensitive to modifications. These findings reinforced the importance of including C-terminal linker controls in bivalent ligand studies.

3.3.4.3 Bivalent Ligands

At the mMC1R, the bivalent ligand **CJL-1-31**, based off of the His-DPhe-Arg-Trp scaffold, resulted in 3-fold increased agonist potency as compared to its monovalent counterpart **CJL-1-14** (**Figure 3.6A**). At the mMC3R, ligands **CJL-1-87** and **CJL-1-31** (that possessed 23- and 25-fold increased binding affinity) resulted in 5- and 3-fold increased agonist potency, respectively, as compared to **CJL-1-14** (**Figure 3.6B**). At the mMC4R, bivalent ligand **CJL-1-87** resulted in 4-fold increased potency as compared to the parent tetrapeptide **CJL-1-14** (**Figure 3.6C**). At the mMC5R, bivalent ligand **CJL-1-87** resulted in a 3-fold increased potency as compared to the monovalent control **CJL-1-14** (**Figure 3.6D**). However, this data was confounded by the 5-fold increased potency of linker control compound **CJL-5-35-4** compared to **CJL-1-14** (**Figure 3.6H**). It is therefore hard to interpret whether increased potency at this receptor subtype is due to the addition of the linker or because of the bivalent design.

At the mMC1R, bivalent ligand **CJL-1-140**, derived from the His-DNal(2')-Arg-Trp tetrapeptide, decreased agonist potency 5-fold as compared to the monovalent counterpart **CJL-1-80** (**Figure 3.7A**). This is the only bivalent ligand that displayed a decreased potency; an unanticipated result since the binding affinity of this ligand was increased as compared to its monovalent counterpart **CJL-1-80**. At the mMC3R, ligand

CJL-1-140 increased receptor efficacy relative to NDP-MSH, resulting in an 80% maximal signal at 100 μ M compared to monovalent ligand's 45% signal (**Figure 3.7B**). The ligand was analyzed via a Schild analysis for antagonist activity but showed no change in antagonist potency as compared to the monovalent ligand **CJL-1-80** (**Table 3.4**). At the mMC4R, bivalent ligand **CJL-1-140** showed increased receptor efficacy showing 85% maximal signal at 100 μ M relative to NDP-MSH compared 40% maximal signal by the monovalent ligand **CJL-1-80** (**Figure 3.7C**). The ligand was also analyzed by a Schild analysis, but showed minimal change in antagonist potency compared to the monovalent ligand **CJL-1-80** (**Table 3.4**). At the mMC5R, ligand **CJL-1-140** displayed full agonist pharmacology ($EC_{50} = 790$ nM) and increased receptor efficacy as compared to **CJL-1-80** that showed 75% agonist signal at 100 μ M relative to NDP-MSH (**Figure 3.7D**).

A thought-provoking pattern with the bivalent ligands based on the His-DNal(2')-Arg-Trp scaffold was observed: compound **CJL-1-140** increased efficacy at the mMC3R, mMC4R, and mMC5R as compared to the monovalent control ligand **CJL-1-80**. This trend observed of a monovalent scaffold that possessed relatively low agonist efficacy and potent antagonism being converted to a bivalent ligand showing increased agonist efficacy at high concentrations was previously seen by Carrithers and Lerner.²⁶ They observed this trend in a frog skin melanocyte dispersion assay with a bivalent ligand that consisted of the nonapeptide antagonist scaffold Met-Pro-DPhe-Arg-DTrp-Phe-Lys-Pro-Val¹⁷⁴ linked with a polylysine linker.²⁶ The current study extends this finding by showing a similar trend at the individually cloned mMC3R, mMC4R, and mMC5R subtypes. Interestingly, bivalent

ligand **CJL-1-140** also showed decreased agonist potency at the mMC1R despite an increased binding affinity. The ligand had a receptor functional profile different than the original monovalent ligand **CJL-1-80** in which its agonist potency increased at the mMC3R, mMC4R, and mMC5R yet decreased at the mMC1R. Since the region of the ligand which purportedly binds the receptor is not changing from the monovalent ligand, the pharmacology of **CJL-140** is a result of joining the two scaffolds.

This SAR is unique from classical monovalent ligand SAR and demonstrates that bivalent ligands can create unique pharmacologies. The conversion observed at the mMC3R and mMC4R of monovalent scaffolds with relatively low agonist efficacy and potent antagonism to a bivalent ligand with increased agonist efficacy, yet similar antagonism, may be just one potential functional consequence of bivalent compounds targeting the melanocortin receptors. Furthermore, the observation that **CJL-1-140** possessed increased binding affinity at the mMC1R but decreased functional potency once again emphasizes the importance of studying both the binding and function of bivalent ligands.

It should be noted that the fold increases observed in functional potency (3- to 5-fold) were not as pronounced as the fold increases observed in binding affinity (14- to 25-fold). There are several possibilities for why the increased binding affinities did not translate to larger increases in functional potency. First, similar to discussion above about the smaller fold increases observed with Ac-His-DNaI(2')-Arg-Trp-NH₂ based compounds' binding affinity, the Ac-His-DPhe-Arg-Trp-NH₂ scaffold's potent nanomolar

agonist efficacy could be masking functional increases. Second, binding affinity is a molecular recognition event whereas functional potency is a signaling transduction event and is dependent on a conformational change of the receptor. The tethered bivalent ligands could cause a change in the orientation of the second pharmacophore in the second binding pocket in which it can still bind to the receptor, but it does not activate the cAMP signal transduction pathway as effectively. Third, the bivalent ligand could be binding in an auxiliary binding site that has minimal functional effects. Fourth, the lower fold changes in functional potency could be a result of asymmetric signaling of the two receptors present in the dimer. It could be postulated that the first binding event activates cAMP signal transduction through the first receptor, but the second binding event does not activate the cAMP pathway. The second binding could result in no conformational change of the second receptor, or a different conformational change that results in biased signaling through a different pathway (*e.g.* β -arrestin recruitment). This would result in a lack of increase in functional activity in spite of increased bivalent ligand binding. This type of asymmetry in GPCR dimers was previously observed by Han and coworkers.²³¹ They observed that an agonist binding a single dopamine D2 receptor resulted in maximal functional activation, while an agonist binding the second receptor in the GPCR dimer blunted signaling.²³¹ This final hypothesis led to the design of the MUmBLs that will be discussed in **Chapter 5**.

3.3.5 *In Vivo* ICV Administration Studies

Although there have been reports of melanocortin bivalent ligands as *in vivo* imaging tools,³⁸⁻⁴⁰ to the best of our knowledge, the *in vivo* functional effects of melanocortin bivalent ligands had not been reported prior this thesis work.^{25, 132} Given the unique characteristics of bivalent ligands compared to their monovalent counterparts that were not explicitly tested (*e.g.* altering receptor trafficking⁴²⁻⁴⁴ and creating tissue selectivity⁵), it is important to demonstrate that the *in vitro* pharmacology translated to the *in vivo* pharmacology.

In order to better understand the functional effects of melanocortin bivalent ligands and their potential as *in vivo* probes, the intracerebroventricular (ICV) administration of bivalent ligand **CJL-1-87** was performed in mice. The central administration of melanocortin ligands has previously been used to study their effect on the centrally located MC3R and MC4R. Specifically, ICV administration of melanocortin agonists has been reported to decrease food intake and antagonists to increase food intake.^{56, 76, 107} Compound **CJL-1-87** was selected for study since it showed the greatest potency and binding affinity at the mMC3R and mMC4R.

Treatment of mice with **CJL-1-87** was well tolerated and resulted in a dose dependent decrease in food intake after ICV administration as anticipated for an agonist compound (**Figure 3.10**). The treatment strategy followed a cross-over paradigm described in **Chapter 2 (Table 3.5)**. A significant decrease in food intake was observed in male mice 2, 4, 6, and 8 hours after 5 nmols of **CJL-1-87** was administered (**Figure 3.10A**). No

significant effect in male mice was seen for later time points (24-72 hours) (**Figure 3.10C**). No significant differences were observed in female mice at 2, 4, 6, and 8 hour time points (**Figure 3.10B**). A significant decrease in food intake was observed 24 hours post-treatment in female mice ($p < 0.05$), but no significant effect was observed at the 48 and 72 hour time points (**Figure 3.10D**). No significant effect on body weight was observed in either female or male mice.

These data are consistent with the *in vitro* data that **CJL-1-87** acts as a melanocortin agonist at the centrally expressed melanocortin receptors. The monovalent counterpart, Ac-His-DPhe-Arg-Trp-NH₂, was previously shown to decrease food intake 3, 4, 5, 6, 16, and 24 hours after administration of a 2 nmol dose.⁷⁶ An interesting observation between the two studies is the longer-lasting effect previously reported with Ac-His-DPhe-Arg-Trp-NH₂ at 24 hours which was not observed with **CJL-1-87** in male mice in the current study. This may indicate a difference in the physiological effects of the compound *in vivo* and may be due to any number of reasons including increased receptor desensitization, increased compensation pathways, changes in hormone signaling, or increased metabolic degradation of the compound. Additional experiments were performed to examine differences observed in these preliminary experiments, and are the focus of **Chapter 4**.

A previous study showed that Ac-His-DPhe-Arg-Trp-NH₂ at the 2.0 nmol dose had similar results to **CJL-1-87** at the 5 nmol dose at 4 and 6 hours after administration. These results would indicate that the *in vitro* functional results (as opposed to binding results) are more indicative of the *in vivo* effects in the current nocturnal satiated feeding paradigm.

However, there are key differences between the current study and the previous study that should be mentioned. Firstly, the food intake after saline administration in the previous study was significantly lower than in the current study at the 6 and 24 hour time points ($p < 0.05$). Secondly, different mouse chow was used. The previous study utilized Harlan Teklad 8604 containing 4% fat and 3.30 kcal/g digestible energy, whereas, Harlan Teklad 2018 containing 6.2 % fat and 3.1 kcal/g digestible energy was used in the current study. This difference in chow may have been responsible for the differences in saline food intake, since a mouse eating Harlan Teklad 8604 would need to consume less chow to achieve the same caloric intake. There were also varying environment factors including the animal facilities, the lab staff, frequency of measurements, and type of nesting material. Subtle changes in experimental conditions have been shown to result in differences in animal behavior.²³²⁻²³⁵ Given these factors, a direct head to head comparison study of the monovalent **CJL-1-14** and the bivalent ligand **CJL-1-87** would be necessary to draw more definitive conclusions. This was performed and will be discussed in detail in **Chapter 4**.

The current report advanced the field by indicating that melanocortin bivalent ligands are suitable to probe for melanocortin effects *in vivo*. In the current study, there does not appear to be a dramatic advantage between monovalent ligand **CJL-1-14** and bivalent ligand **CJL-1-87**. However, only one experimental paradigm of food intake was evaluated. Since bivalent ligands show increased binding affinity compared to their monovalent counterparts, they may be beneficial in conditions that the ligand is competing with the natural antagonist AGRP for binding such as in a fasting state which was indeed

the case when evaluated in **Chapter 4**. The bivalent ligands developed currently may also be exploited as imaging tools as described previously,^{6, 38-40, 63} but for the centrally located receptors. This would be especially useful if bivalent ligands featuring selective scaffolds for different melanocortin receptor subtypes were used for imaging the isoforms' locations in the brain. Bivalent ligands are also uniquely poised to study melanocortin receptor dimerization *in vivo*. The use of **CJL-1-87** to decrease food intake in mice demonstrates its utility as a probe for metabolic diseases such as obesity. Additionally, the current study's finding that melanocortin bivalent are well tolerated and functionally active *in vivo* indicates that they will also be useful probes for other disease states in which the melanocortin system plays a role including Alzheimer's disease,^{60, 61} sexual function,^{51, 66} and social disorders.^{67, 68} In deed, this preliminary study laid the groundwork for the more comprehensive study performed in **Chapter 4**.¹³²

3.4 Conclusion:

This thesis chapter validated that melanocortin bivalent ligands can be utilized to increase receptor binding affinity and functional potency. It also identified a preference of the receptor subtypes for different bivalent ligand linkers indicating differences in the homodimer subtypes. It laid the foundational work that was used in **Chapter 5** and **Chapter 6** in which different medicinal chemistry design strategies were utilized to further the SAR of melanocortin bivalent ligands. Furthermore, compound **CJL-1-87** resulted in significant decreased feeding *in vivo* upon ICV administration which was consistent with its agonist *in vitro* pharmacology. We utilized these preliminary *in vivo* results to design

and perform a more thorough assessment of **CJL-1-87**'s *in vitro* and *in vivo* pharmacology in **Chapter 4**. This foundational work can also be applied to the various fields in which melanocortin ligands are currently under investigation as pharmacological probes and potential therapeutics. Specifically, our *in vivo* results indicate bivalent ligands' utility in studying melanocortin-dependent metabolic disease states. It also serves as a foundation for the development of melanocortin bivalent ligands as functional pharmacological probes for melanocortin receptor homodimers and heterodimers (as discussed further in **Chapters 4-6**).

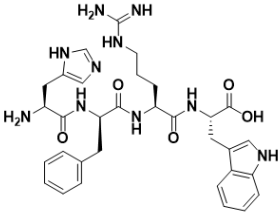
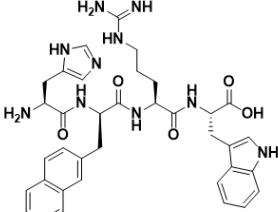
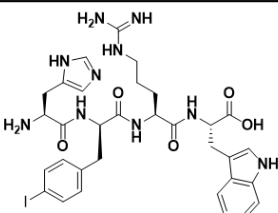
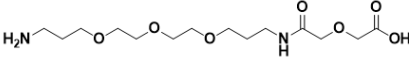
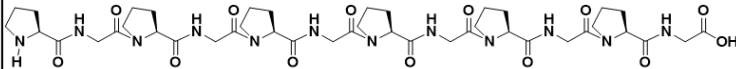
Selected Scaffolds	
His-DPhe-Arg-Trp	
His-DNal(2')-Arg-Trp	
His-DPhe(pI)-Arg-Trp	
Selected Linkers	
(PEDG20)	
(Pro-Gly) ₆	
Compound #	Structure of Ligands
CJL-1-14	Ac-His-DPhe-Arg-Trp-NH ₂
CJL-5-35-4	Ac-His-DPhe-Arg-Trp-(PEDG20)-NH ₂
CJL-1-116	(PEDG20)-His-DPhe-Arg-Trp-NH ₂
CJL-5-35-1	Ac-His-DPhe-Arg-Trp-(Pro-Gly) ₆ -NH ₂
CJL-1-41	(Pro-Gly) ₆ -His-DPhe-Arg-Trp-NH ₂
CJL-1-31	Ac-His-DPhe-Arg-Trp-(Pro-Gly) ₆ -His-DPhe-Arg-Trp-NH ₂
CJL-1-87	Ac-His-DPhe-Arg-Trp-(PEDG20)-His-DPhe-Arg-Trp-NH ₂
CJL-5-72	Ac-His-DPhe-Arg-Trp-(PEDG20)-(PEDG20)-His-DPhe-Arg-Trp-NH ₂
CJL-1-80	Ac-His-DNal(2')-Arg-Trp-NH ₂
CJL-5-35-5	Ac-His-DNal(2')-Arg-Trp-(PEDG20)-NH ₂
CJL-1-132	(PEDG20)-His-DNal(2')-Arg-Trp-NH ₂
CJL-1-140	Ac-His-DNal(2')-Arg-Trp-(PEDG20)-His-DNal(2')-Arg-Trp-NH ₂
CJL-1-20	Ac-His-DPhe(pI)-Arg-Trp-NH ₂
CJL-5-35-6	Ac-His-DPhe(pI)-Arg-Trp-(PEDG20)-NH ₂
CJL-5-009	(PEDG20)-His-DPhe(pI)-Arg-Trp-NH ₂
CJL-5-64	Ac-His-DPhe(pI)-Arg-Trp-(PEDG20)-His-DPhe(pI)-Arg-Trp-NH ₂

Figure 3.1. Design of ligands in Chapter 3 from selected scaffolds and linkers. This figure has been adapted with permission from Lensing, C.J. *et al*, *J. Med. Chem.* **2016**, 59, 3112-3128.²⁵ Copyright (2016) American Chemical Society.

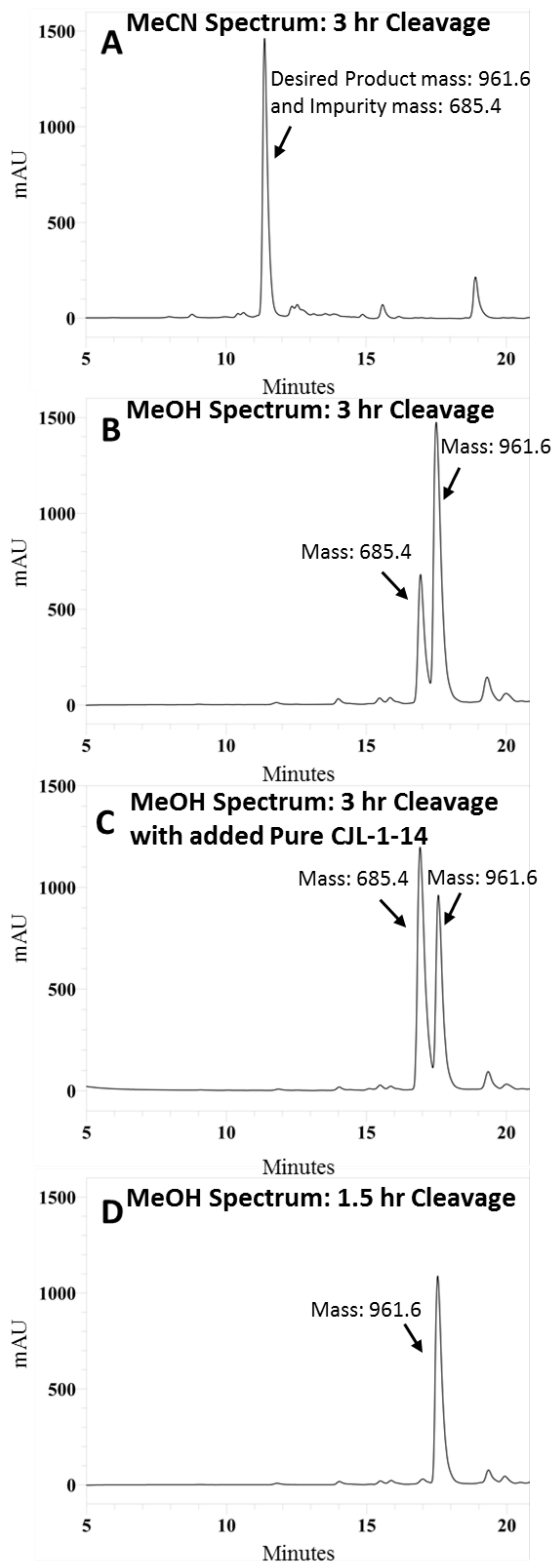


Figure 3.2. Crude RP-HPLC analytical chromatograms at 214 nm of **CJL-1-116** (mass of 961.6) in a gradient from 10% to 90% MeCN or MeOH in water containing 0.1 % trifluoroacetic acid at a flow rate of 1.5 mL/min over 35 minutes (5 to 20 minutes are shown) using an analytical Vydac C18 column (Vydac 218TP104). (A) Analytical HPLC trace in MeCN of crude peptide **CJL-1-116** after a three hour cleavage which shows only one major peak. A major impurity peak (mass of 685.4) is masked in this chromatogram. (B) Analytical HPLC trace in MeOH of crude peptide **CJL-1-116** after a three hour cleavage which identifies both the desired product and an impurity peak masked in MeCN chromatogram. (C) Co-injection of crude **CJL-1-116** from three hour cleavage with purified **CJL-1-14** (mass of 685.4) increases the intensity of the impurity peak demonstrating similar retention times. (D) A shorter cleavage time of 1.5 hours diminishes degradation product giving better crude peptide purity. This figure has been adapted with permission from Lensing, C.J. *et al*, *J. Med. Chem.* **2016**, 59, 3112-3128.²⁵ Copyright (2016) American Chemical Society.

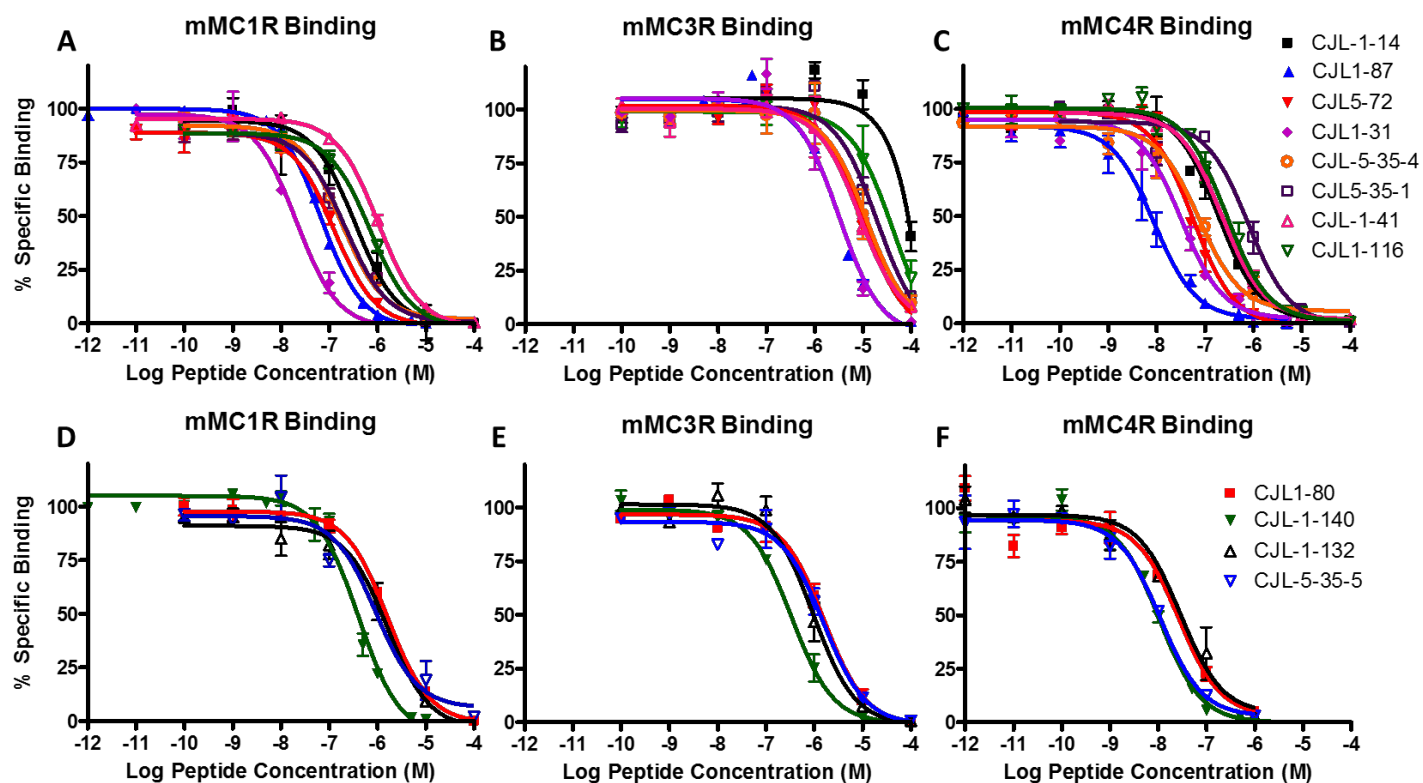


Figure 3.3. Illustrations of the competitive binding experiments at the mMC1R, mMC3R, and mMC4R. Top figures shows the His-DPhe-Arg-Trp-based ligands. The bottom figures show the His-DNal(2')-Arg-Trp-based ligands. This figure has been adapted with permission from Lensing, C.J. *et al*, *J. Med. Chem.* **2016**, 59, 3112-3128.²⁵ Copyright (2016) American Chemical Society.

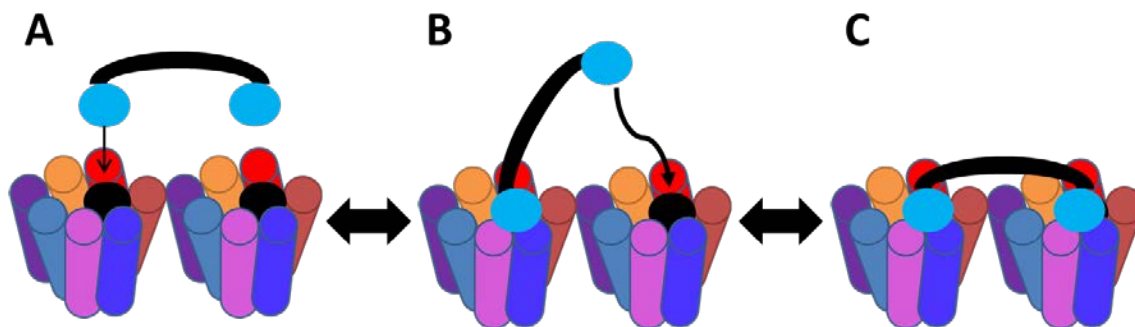


Figure 3.4. Proposed binding mode of the bivalent ligands. (A) First pharmacophore engages GPCR dimer or two neighboring binding sites. (B) The first binding event tethers the second pharmacophore in close proximity to the second binding site significantly increasing the likelihood of the second binding event. (C) The second pharmacophore binds with low entropic cost. This figure has been reproduced with permission from Lensing, C.J. *et al*, *J. Med. Chem.* **2016**, 59, 3112-3128.²⁵ Copyright (2016) American Chemical Society.

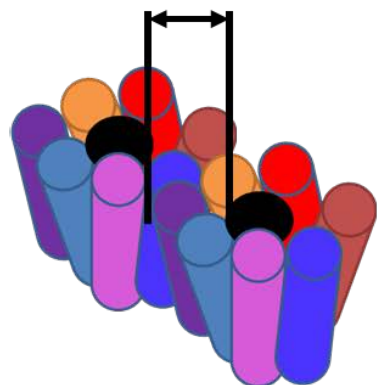
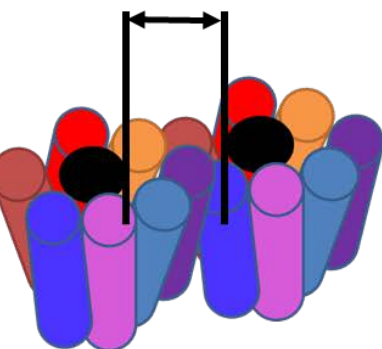
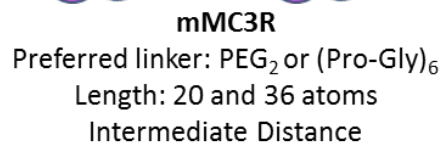
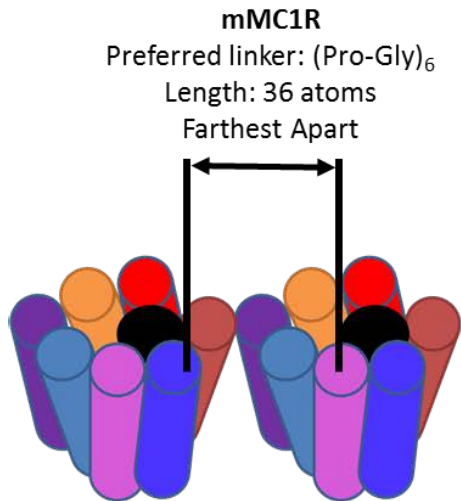


Figure 3.5. Postulated rationale for linker-dependent preferences at the different melanocortin homodimer subtypes. The different linker systems had varying effects on enhancing binding or functional responses depending on which receptor subtype was expressed. Since the linkers connect the same pharmacophore, it appears the differences are due to the linkers' physicochemical properties such as linker length. These differences suggest that there are differences between the various subtypes of melanocortin receptor dimers such as the distance between tandem binding sites (see text). The figure demonstrates how different distances between tandem binding sites would show preference for the different length linker systems. This figure has been reproduced with permission from Lensing, C.J. *et al*, *J. Med. Chem.* **2016**, 59, 3112-3128.²⁵ Copyright (2016) American Chemical Society.

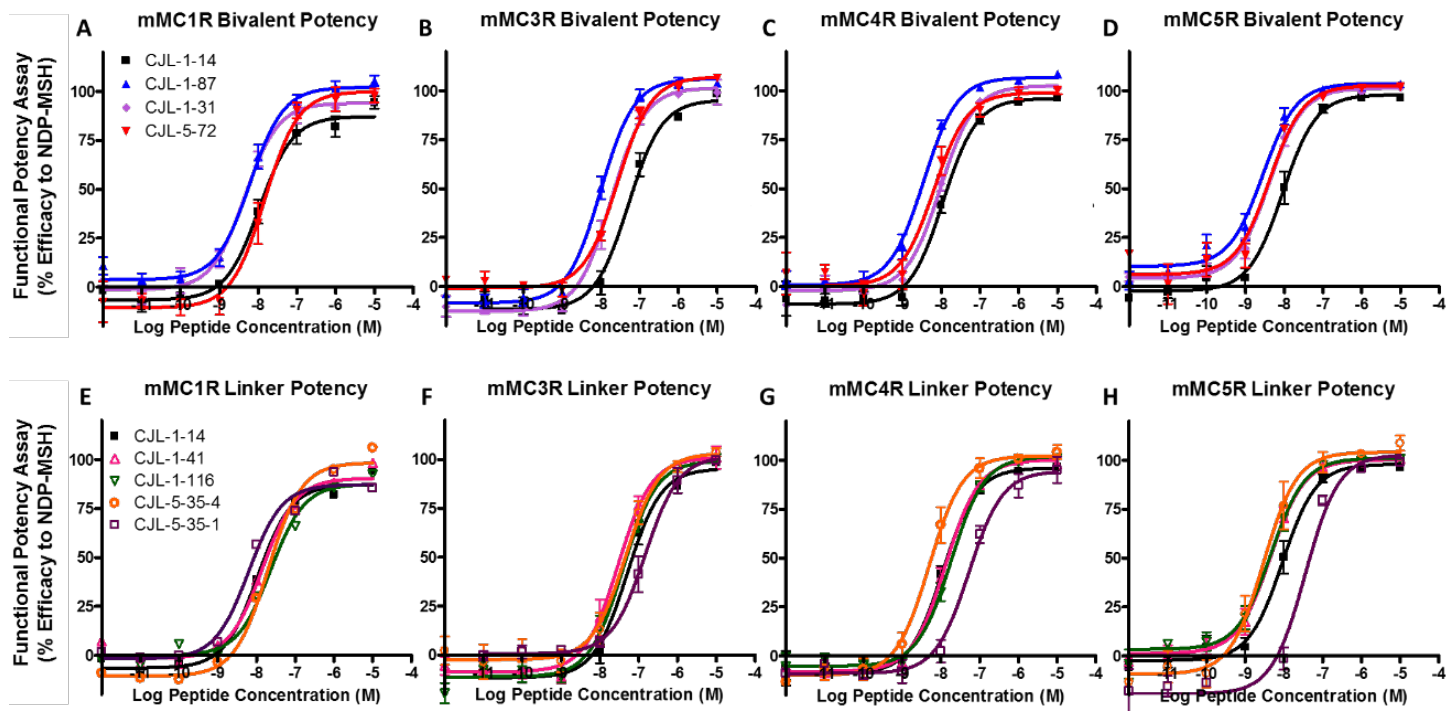


Figure 3.6. Illustrations of the in vitro functional pharmacology at the mMC1R, mMC3R, mMC4R, and mMC5R of the His-DPhe-Arg-Trp based ligands. Top figures show the bivalent ligands compared to the control peptide **CJL-1-14**. The bottom figures show the effects of the linkers plus pharmacophore compared to control peptide **CJL-1-14**. This figure has been adapted with permission from Lensing, C.J. *et al*, *J. Med. Chem.* **2016**, 59, 3112-3128.²⁵ Copyright (2016) American Chemical Society.

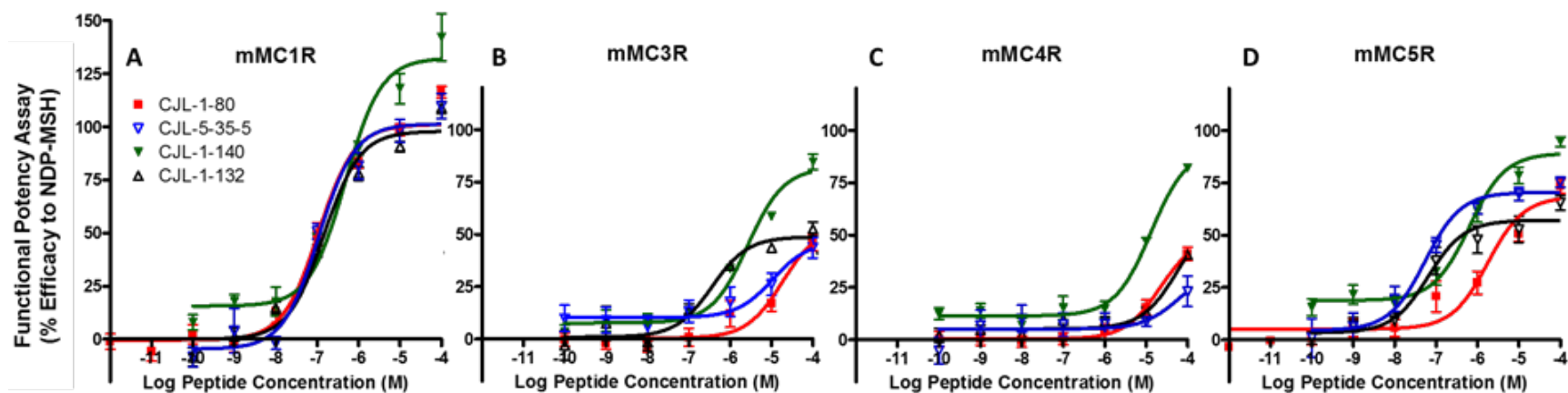


Figure 3.7. Illustrations of the in vitro functional agonist pharmacology at the mMC1R, mMC3R, mMC4R, and mMC5R of the His-DNal(2')-Arg-Trp based ligands. This figure has been adapted with permission from Lensing, C.J. *et al*, *J. Med. Chem.* **2016**, 59, 3112-3128.²⁵ Copyright (2016) American Chemical Society.

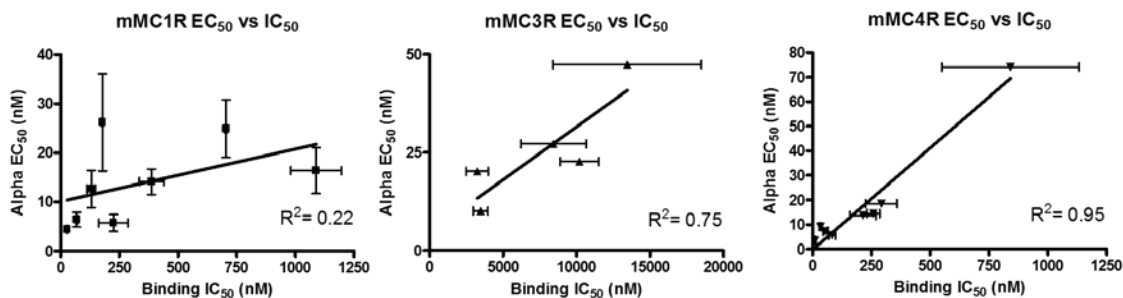


Figure 3.8. Correlation of IC₅₀ (nM) vs EC₅₀ (nM) at the different receptor subtypes for His-DPhe-Arg-Trp based ligands. The mMC4R had a relatively linear correlation between receptor activation and ligand binding. At the mMC1R there appears to be relatively little correlation. The lack of correlation stresses the importance of studying ligands' binding affinity and functional effects in complementary assays. Data is shown as mean ± SEM. This figure has been reproduced with permission from Lensing, C.J. *et al*, *J. Med. Chem.* **2016**, 59, 3112-3128.²⁵ Copyright (2016) American Chemical Society.

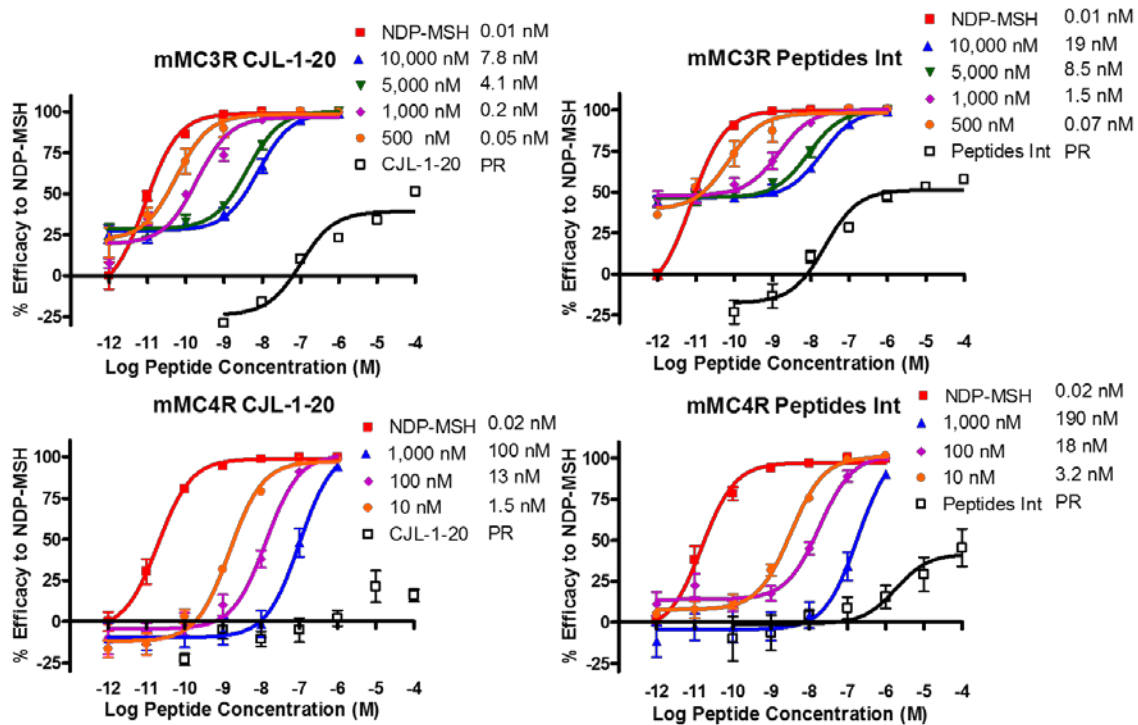


Figure 3.9. AlphaScreen functional Schild analysis at the mMC3R and mMC4R of both our synthetically made (**CJL-1-20**) and the commercially bought analog (Peptides Int) of the Ac-His-DPhe(pI)-Arg-Trp-NH₂. The pharmacology matches for both **CJL-1-20** and the Peptides International bought version confirming the pharmacology discrepancies were not a result of improper synthesis. All structural analysis performed also confirmed the proper structure. Data is shown as mean \pm SEM calculated from two independent experiments.

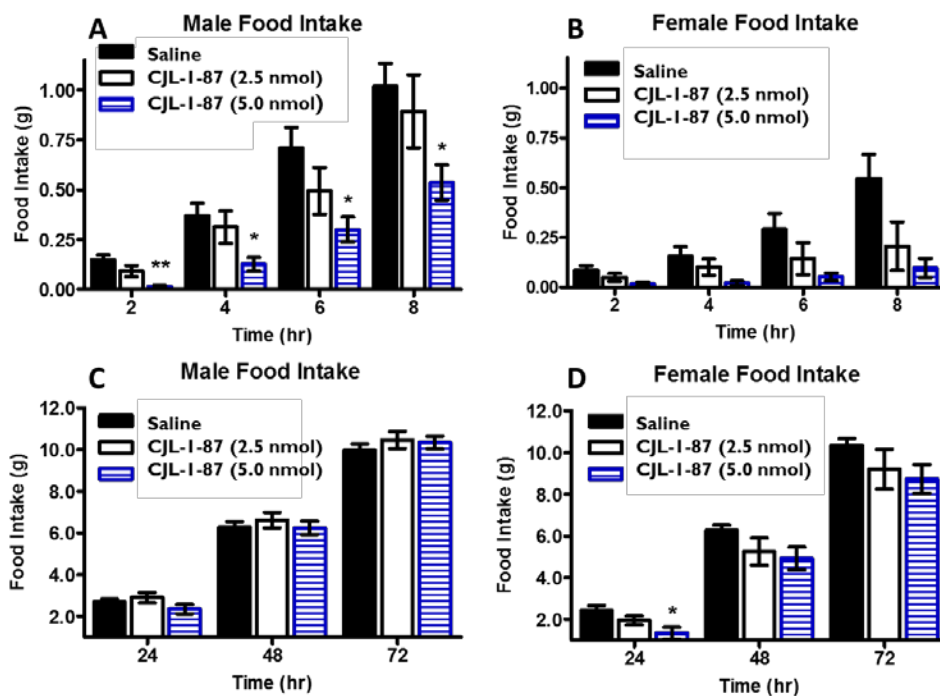


Figure 3.10. Cumulative food intake following intracerebroventricular administration of either saline (n=16 male; 8 female) or **CJL-1-87** in saline (n=8 male; 4 female) in wild type mice. (A) Male dose response of food intake in first 8 hours as appear in primary manuscript (appears here for comparison.) (B) Female dose response of food intake in first 8 hours. Data is not significant. (C) Male dose response of food intake between 24-72 hours. Data is not significant. (D) Female dose response of food intake between 24-72 hours. The 24 hr time point is significant ($p < 0.05$). Data is shown as mean \pm SEM. Data was analyzed using the PRISM program (v4.0; GraphPad Inc.) by a one-way ANOVA followed by a Bonferroni post test in order to compare individual doses to saline administration. * $p < 0.05$, ** $p < 0.01$. This figure has been adapted with permission from Lensing, C.J. *et al*, *J. Med. Chem.* **2016**, 59, 3112-3128.²⁵ Copyright (2016) American Chemical Society.

Comp.	Structure	HPLC <i>k'</i> (Syst. 1)	HPLC <i>k'</i> (Syst. 2)	Mass (calcd.)	Mass (obs.)	Purity %
CJL-1-14	Ac- His-DPhe-Arg-Trp -NH ₂	3.2	5.5	685.34	685.39	>99%
CJL-5-35-4	Ac- His-DPhe-Arg-Trp -(PEDG20)-NH ₂	4.6	8.3	1003.52	1003.70	>95%
CJL-1-116	(PEDG20)- His-DPhe-Arg-Trp -NH ₂	4.0	6.4	961.51	961.57	>96%
CJL-5-35-1	Ac- His-DPhe-Arg-Trp -(Pro-Gly) ₆ -NH ₂	4.3	8.5	1609.79	1610.00	>97%
CJL-1-41	(Pro-Gly) ₆ - His-DPhe-Arg-Trp -NH ₂	3.6	6.2	1567.78	1568.28	>95%
CJL-1-31	Ac- His-DPhe-Arg-Trp -(Pro-Gly) ₆ - His-DPhe-Arg-Trp -NH ₂	4.9	7.4	2237.10	2237.18	>99%
CJL-1-87	Ac- His-DPhe-Arg-Trp -(PEDG20)- His-DPhe-Arg-Trp -NH ₂	4.0	7.9	1629.83	1629.80	>99%
CJL-5-72	Ac- His-DPhe-Arg-Trp -(PEDG20)-(PEDG20)- His-DPhe-Arg-Trp -NH ₂	5.2	9.5	1949.01	1949.00	>95%
CJL-1-80	Ac- His-DNal(2')-Arg-Trp -NH ₂	4.3	7.5	735.36	735.30	>98%
CJL-5-35-5	Ac- His-DNal(2')-Arg-Trp -(PEDG20)-NH ₂	4.7	8.6	1053.54	1053.70	>95%
CJL-1-132	(PEDG20)- His-DNal(2')-Arg-Trp -NH ₂	5.2	8.3	1011.53	1011.59	>98%
CJL-1-140	Ac- His-DNal(2')-Arg-Trp -(PEDG20)- His-DNal(2')-Arg-Trp -NH ₂	6.4	10.9	1729.86	1730.03	>95%
CJL-1-20	Ac- His-DPhe(p-I)-Arg-Trp -NH ₂	3.4	6.1	811.2	811.4	>99%
CJL-5-35-6	Ac- His-DPhe(p-I)-Arg-Trp -(PEDG20)-NH ₂	4.7	8.7	1129.4	1129.6	>96%
CJL-5-009	(PEDG20)- His-DPhe(p-I)-Arg-Trp -NH ₂	4.5	8.0	1087.4	1087.3	>98%
CJL-5-64	Ac- His-DPhe(p-I)-Arg-Trp -(PEDG20)- His-DPhe(p-I)-Arg-Trp -NH ₂	6.0	10.5	1881.6	1881.6	>97%

Table 3.1. Analytical data for peptides synthesized in this Chapter 3. HPLC k' = (peptide retention time - solvent retention time) / solvent retention time. System 1 is a 10% to 90% gradient of acetonitrile in water containing 0.1% trifluoroacetic acid over 35 minutes at a flow rate of 1.5 mL/min, and system 2 is the same gradient with methanol replacing acetonitrile. Product purity was determined by integrating the area under the curves of the chromatograms collected at 214 nm. The solvent system that resulted in the lowest purity was used for the purity % in the table above. Mass observed was calculated from the M+1 or (M+2)/2 peak. This table has been adapted with permission from Lensing, C.J. *et al*, *J. Med. Chem.* **2016**, 59, 3112-3128.²⁵ Copyright (2016) American Chemical Society.

Compound Number	mMC1R			mMC3R			mMC4R			Selectivity Ratios 1R:3R:4R
	IC ₅₀ (nM)			IC ₅₀ (nM)			IC ₅₀ (nM)			
	Mean ± SEM	n	Fold Diff	Mean ± SEM	n	Fold Diff.	Mean ± SEM	n	Fold Diff	
NDP-MSH	0.31±0.08	6		4.18±0.61	14		1.09±0.12	19		1:13:4
CJL-1-14	388±52	2	1	60% @100 μM	2	1 ^a	214±55	6	1	1:374:1
CJL-5-35-4	178±4	2	2	13400±5100	2	6	83±14	4	3	2:162:1
CJL-1-116	705±6	2	0.6	78% @100 μM	3	ND	292±67	4	0.7	2:ND:1
CJL-5-35-1	225±63	2	2	85% @100 μM	2	ND	841±290	2	0.3	1:ND:4
CJL-1-41	1090±110	3	0.4	8430±230	2	9	258±27	2	0.8	4:33:1
CJL-1-31	27.5±2.2	2	14	3250±760	2	25	33±5.1	3	6	1:119:1
CJL-1-87	68.6±5.3	3	6	3470±510	2	23	9.9±2.9	4	22	7:351:1
CJL-5-72	131±18	2	3	10200±1300	2	8	54±10	2	4	2:190:1
CJL-1-80	1630±120	2	1	1430±190	2	1	26.0±3.4	2	1	63:55:1
CJL-5-35-5	997±190	2	2	1310±120	2	1	10.7±0.6	2	2	94:123:1
CJL-1-132	1870±220	4	1	999±290	2	1	21.8±1.9	3	1	85:46:1
CJL-1-140	430±40	3	4	350±80	5	4	10.4±0.03	2	2	41:34:1
CJL-1-20	190±10	2	1	780±90	2	1	6.0±1.2	2	1	31:130:1
CJL-5-35-6	130±10	2	1	550±10	2	1	2.7±0.4	2	2	48:203:1
CJL-5-009	460±170	3	0.4	230±70	2	3	13.5±5.0	3	0.4	34:17:1
CJL-5-64	NS			NS			NS			

Table 3.2. Summary of competitive binding experiments for compounds evaluated at the mouse melanocortin receptors. The experimental compounds were used to displace ¹²⁵I-NDP-MSH in a dose-response manner to calculate the IC₅₀ values. % represent the amount of ¹²⁵I-NDP-MSH signal reduction at 100 μM. The “n” column represents the number of independent experiments performed. The reported errors are the standard error of the mean (SEM). ND means not determined. ^aFold difference for mMC3R was calculated based on an estimated IC₅₀ of 80,000 nM for **CJL-1-14**. Compound **CJL-5-64** was not soluble (NS)

in bioassay solvents. This table has been adapted with permission from Lensing, C.J. *et al*,
J. Med. Chem. **2016**, 59, 3112-3128.²⁵ Copyright (2016) American Chemical Society.

Compound	mMC1R		mMC3R		mMC4R		mMC5R		Selectivity
	Agonist EC ₅₀ (nM)		Agonist EC ₅₀ (nM)		Agonist EC ₅₀ (nM)		Agonist EC ₅₀ (nM)		Ratios
	Mean±SEM	Fold Diff.	1R:3R:4R:5R						
NDP-MSH	0.03±0.01 ^a		0.24±0.01 ^a		0.46±0.04 ^a		0.31±0.03 ^a		1:9:18:12
α-MSH	0.15±0.05		0.76±0.05		4.0±0.9		0.59±0.03		1:5:28:4
γ-MSH	1090±300		34.6±4.0		869±66		35.1±18.7		31:1:25:1
CJL-1-14	14.1±2.6 ^a	1	55.5±12.2 ^a	1	13.7±1.9 ^a	1	9.8±2.7 ^a	1	1:4:1:1
CJL-5-35-4	26.2±9.9	0.5	47.4±12.7	1	5.7±2.9	2	2.1±0.3	5	13:23:3:1
CJL-1-116	24.9±5.9 ^a	0.6	30.9±7.5 ^a	2	18.5±2.9 ^a	0.7	3.9±1.3 ^a	2	6:8:5:1
CJL-5-35-1	5.7±.7	2	107±66	0.5	74.1±14.1	0.2	52.4±10.3	0.2	1:19:13:9
CJL-1-41	16.4±4.7 ^a	0.9	27.2±5.2 ^a	2	14.5±2.7 ^a	0.9	4.9±1.2 ^a	2	3:6:3:1
CJL-1-31	4.4±0.6 ^a	3	20.2±4.0 ^a	3	9.2±1.0 ^a	1	3.8±0.9 ^a	2	1:5:2:1
CJL-1-87	6.4±1.5 ^a	2	10.1±2.5 ^a	5	3.6±0.5 ^a	4	3.1±0.6 ^a	3	1:3:1:1
CJL-5-72	12.6±3.8	1	22.7±3.7	2	7.3±2.1	2	4.0±0.2	2	3:6:2:1

Table 3.3 Summary of functional experiments for His-DPhe-Arg-Trp-based compounds evaluated at the mouse melanocortin receptors. AlphaScreen[®] assays were performed to determine relative potency of compounds to induce cAMP signaling. The reported errors are the standard error of the mean (SEM) determined from at least three independent experiments. Changes less than 3-fold were considered to be within the inherent experimental assay error. ^a denotes six or more independent experiments. This table has been adapted with permission from Lensing, C.J. *et al*, *J. Med. Chem.* **2016**, 59, 3112-3128.²⁵ Copyright (2016) American Chemical Society.

Compound	mMC1R		mMC3R		mMC4R		mMC5R
	Agonist EC ₅₀ (nM)		Agonist EC ₅₀ (nM)	Antagonist (pA ₂)	Agonist EC ₅₀ (nM)	Antagonist (pA ₂)	Agonist EC ₅₀ (nM)
	Mean±SEM	Fold Diff.	Mean±SEM	Mean±SEM	Mean±SEM	Mean±SEM	Mean±SEM
CJL-1-80	98.4±32.2 ^a	1	45% at 100 μM	6.04±0.09	40% at 100 μM	8.09±0.04	75% at 100 μM
CJL-5-35-5	112±19	0.9	40% at 100 μM ^a	6.14±0.06	20% at 100 μM ^a	8.39±0.08	PA, 70% at 100 μM
CJL-1-132	139±17 ^a	0.7	PA, 50% at 100 μM ^a	6.07±0.18	40% at 100 μM ^a	7.97±0.29	PA, 65% at 100 μM ^a
CJL-1-140	563±142 ^a	0.2	80% at 100 μM ^a	6.08±0.11	85% at 100 μM ^a	7.68±0.37	786±185 ^a
CJL-1-20	12±2	1	55% at 100 μM ^a	6.79±0.08	50% at 100 μM	8.57±0.08	2.75±1.15
CJL-5-35-6	9.5±1.7	1	PA, 60% at 100 μM	7.30±0.07	PA, 45% at 100 μM	8.67±0.05	28±12
CJL-5-009	30±6	0.4	PA, 60% at 100 μM	7.01±0.22	PA, 45% at 100 μM	8.49±0.24	4.5±1.6
CJL-5-64	NS		NS	NS	NS	NS	NS

Table 3.4 Summary of functional experiments for His-DNal(2')-Arg-Trp and the His-DPhe(p-I)-Arg-Trp based compounds evaluated at the mouse melanocortin receptors. AlphaScreen[®] assays were performed to determine relative potency of compounds to induce cAMP signaling. The reported errors are the standard error of the mean (SEM) of at least three independent experiments. Antagonist activity was evaluated at only the mMC3R and mMC4R with all compounds based on the His-DNal(2')-Arg-Trp and the His-DPhe(p-I)-Arg-Trp pharmacophores. The pA₂ values were calculated by a Schild analysis in which NDP-MSH was in a standard dose response (10⁻¹² to 10⁻⁶) and three doses of antagonist were used to shift the agonist dose response. PA indicates partial agonist activity was observed. Percentage (%) indicate the amount of activity relative to maximal NDP-MSH response was observed at 100 μM. ^a denotes six or more independent experiments. A bar graph representation of the partial functional responses and the associated error can be seen in the supplemental information. Compound **CJL-5-64** was not soluble (NS) in bioassay solvents. This table has been adapted with permission from Lensing, C.J. *et al*, *J. Med. Chem.* **2016**, 59, 3112-3128.²⁵ Copyright (2016) American Chemical Society.

	Group 1	Group 2
Day 1	Saline	CJL-1-87 (5 nmol)
Day 2	CJL-1-87 (5 nmol)	Saline
Day 3	Saline	CJL-1-87 (2.5 nmol)
Day 4	CJL-1-87 (2.5 nmol)	Saline

Table 3.5 Latin-square (Cross-over) paradigm used for in vivo feeding experiments in Chapter 3. All animals received both compound and saline in this order. The same animals were used throughout the experiment. There was at a least 6 day washout period between injections. This table has been adapted with permission from Lensing, C.J. *et al*, *J. Med. Chem.* **2016**, 59, 3112-3128.²⁵ Copyright (2016) American Chemical Society.

Chapter 4: A Direct *In Vivo* Comparison of The Melanocortin Monovalent Agonist Ac-His-DPhe-Arg-Trp-NH₂ versus The Bivalent Agonist Ac-His-DPhe-Arg-Trp-PEDG20-His-DPhe-Arg-Trp-NH₂: A Bivalent Advantage

Portions of the studies presented in this chapter have previously been published and are currently being reproduced with permission from: Lensing, C. J.; Adank, D. N.; Wilber, S. L.; Freeman, K. T.; Schnell, S. M.; Speth, R. C.; Zarth, A. T.; Haskell-Luevano, C. A. Direct *In Vivo* Comparison of The Melanocortin Monovalent Agonist Ac-His-DPhe-Arg-Trp-NH₂ versus The Bivalent Agonist Ac-His-DPhe-Arg-Trp-PEDG20-His-DPhe-Arg-Trp-NH₂: A Bivalent Advantage. *ACS Chem. Neurosci.* 2017.¹³² Copyright (2017) American Chemical Society. All animal studies were performed by Cody Lensing, Danielle Adank, and Stacey Wilber. Competitive binding assays were performed by Cody Lensing, Katie Freeman, and Sathya Schnell. BRET assays were performed by Katie Freeman with Cody Lensing contributing to the design of the experiments. AlphaScreen assays were performed by Cody Lensing. Radiolabeled compounds were prepared by Robert Speth. All experimental compounds were synthesized and prepared by Cody Lensing. Serum stability studies were performed by Cody Lensing and Adam Zarth.

4.1 Chapter Overview:

As discussed in **Chapter 1** and **Chapter 3**,^{1, 25} bivalent ligands targeting putative melanocortin receptor dimers have been developed and characterized *in vitro*, however studies of their functional *in vivo* effects have been limited. This chapter compares the effects of homobivalent ligand **CJL-1-87**, Ac-His-DPhe-Arg-Trp-PEDG20-His-DPhe-

Arg-Trp-NH₂, to monovalent ligand **CJL-1-14**, Ac-His-DPhe-Arg-Trp-NH₂ on energy homeostasis in mice after administration into the lateral ventricle of the brain, based on the initial *in vivo* results presented in **Chapter 3**. Bivalent ligand **CJL-1-87** had noteworthy advantages as an anti-obesity probe over **CJL-1-14** in a fasting-refeeding *in vivo* paradigm. Treatment with **CJL-1-87** significantly decreased food intake compared to **CJL-1-14** or saline (50% less intake 2 to 8 hours after treatment). Furthermore, **CJL-1-87** treatment decreased the respiratory exchange ratio (RER) without changing the energy expenditure indicating that fats were being burned as the primary fuel source. Additionally, **CJL-1-87** treatment significantly lowered body fat mass percentage 6 hours after administration ($p < 0.05$) without changing the lean mass percentage. The bivalent ligand significantly decreased insulin, C-peptide, leptin, GIP, and resistin plasma levels compared to levels after **CJL-1-14** or saline treatments. Alternatively, ghrelin plasma levels were significantly increased. Serum stability of **CJL-1-87** and **CJL-1-14** ($T_{1/2} = 6.0$ h and 16.8 h, respectively) was sufficient to permit physiological effects.

The differences in binding affinity of **CJL-1-14** compared to **CJL-1-87** are speculated as a possible mechanism for the bivalent ligand's unique effects. We also provide *in vitro* evidence for the formation of a MC3R-MC4R heterodimer complex, for the first time to our knowledge, that may be an unexploited neuronal molecular target. Regardless of the exact mechanism, the advantageous ability of **CJL-1-87** compared to **CJL-1-14** to increase *in vitro* binding affinity, increase the duration of action in spite of decreased serum stability, decrease *in vivo* food intake, decrease mice's body fat percent,

and differentially affect mouse hormone levels demonstrates the distinct characteristics achieved from the current melanocortin agonist bivalent design strategy.

4.2 Introduction

As discussed in **Chapter 1**,¹ bivalent ligand design strategies have been utilized to develop novel ligands for various GPCR systems including the opioids,⁵⁻¹² gonadotropin-releasing hormone receptor,^{13, 14} adenosine,¹⁵ cannabinoid,^{16, 17} serotonin,¹⁸⁻²⁰ dopamine,^{21, 22} chemokine,^{10, 23} oxytocin,²⁴ and melanocortin receptor systems.²⁵⁻⁴⁰ There has been increasing evidence that heterobivalent ligands featuring pharmacophores for two different receptors can be an efficacious targeting strategy for heterodimers and results in unique properties *in vivo*.^{10, 11, 46, 225} Reports of homobivalent ligands containing two pharmacophores for the same receptor have shown them to possess distinct characteristics *in vitro* compared to monovalent ligands. Reports of homobivalent ligands' *in vivo* functions compared to their monovalent counterparts are sparser.^{24, 25, 132, 236, 237} Because bivalent ligands can have unique functional characteristics compared to monovalent ligands that are not easily assayed *in vitro* (*i.e.* alterations of receptor trafficking⁴²⁻⁴⁴ or tissue selectivity^{5, 10}), it is important to establish their *in vivo* functional significance. This *in vivo* data can be used to guide future bivalent drug design strategies and identify molecular probes for *in vivo* mechanism of action hypothesis driven research. A recent report demonstrated that homobivalent ligands targeting the oxytocin receptor system exhibited 40- and 100-fold greater potency in zebrafish and mice, respectively, establishing that a homobivalent design strategy can have noteworthy advantages *in vivo*.²⁴

There have been several reports of bivalent ligands targeting the melanocortin receptor system.²⁵⁻⁴⁰ Many of these studies focus on the development of bivalent ligands for their use as high affinity imaging tools or targeting agents for melanoma.²⁸⁻⁴⁰ Given that chemical probes for the five melanocortin receptor subtypes (MC1-5R) have been utilized to study several diseases and disorders including Alzheimer's disease,⁶⁰⁻⁶² sexual function disorders,^{51, 66} social disorders,^{67, 68} cachexia,^{69-73, 189} and obesity;^{25, 56, 76} it is of interest to study the biological functions of bivalent ligands targeting these receptors. The limited reports of the *in vitro* functional effects of melanocortin homobivalent ligands have all shown increased functional potency (up to 16-fold).^{25, 26, 28} Although melanocortin bivalent ligands have been used *in vivo* as imaging tools;³⁸⁻⁴⁰ to our knowledge no other laboratories beside us have reported on the functional effects of melanocortin homobivalent ligands *in vivo* to date.^{25, 132}

As reported in **Chapter 3**, our melanocortin homobivalent ligands possessed increased binding affinity of 14- to 25-fold, and increased *in vitro* functional potency of 3- to 5-fold depending on the individual melanocortin receptor subtype compared to monovalent control counterparts.²⁵ Specifically, compound **CJL-1-87**, Ac-His-DPhe-Arg-Trp-PEDG20-His-DPhe-Arg-Trp-NH₂, was the most potent bivalent ligand at the melanocortin 3 receptor (MC3R) and melanocortin 4 receptor (MC4R). This compound consists of two monovalent agonist His-DPhe-Arg-Trp tetrapeptide scaffolds connected through a 20-atom polyethylene diamine diglycolic acid linker (PEDG20). It had an increased binding affinity of 23- and 22- fold, and an increased functional potency of 5-

and 4-fold compared to its monovalent counterpart **CJL-1-14**, Ac-His-DPhe-Arg-Trp-NH₂, at the MC3R and MC4R, respectively. As predicted, administering **CJL-1-87** directly into the brain dose-dependently decreased food intake demonstrating its *in vivo* efficacy at the MC3R and/or MC4R (as seen in **Chapter 3**).²⁵

The MC3R and MC4R are centrally located and are implicated in the melanocortin system's role in energy homeostasis.^{57, 76, 107} Agonist stimulation of the MC3R and MC4R decreases food intake and increases energy expenditure. Therefore, agonist ligands may be potential therapeutics for the treatment of obesity.^{57, 76, 107, 112} It is hypothesized that the distinct pharmacological profile of agonist homobivalent ligand **CJL-1-87** may be advantageous *in vivo* compared to monovalent agonist ligands by enhancing desirable effects such as decreasing food intake and weight loss while hopefully minimizing undesirable side effects. However, given the lack of studies directly comparing the effects of melanocortin monovalent and bivalent ligands *in vivo*; exploratory *in vivo* studies are necessary to characterize the physiological profile of homobivalent ligands, assess their side effect profiles, and guide future design and *in vitro* SAR studies. Direct comparison of bivalent ligand **CJL-1-87** to monovalent ligand **CJL-1-14** may provide insight into the advantages and disadvantages of a melanocortin bivalent ligand design strategy in the development of anti-obesity therapeutics. These studies may also help further elucidate the complex melanocortin pharmacology within the brain and particularly the role of the MC3-MC4 receptor homo- and heterodimerization. Furthermore, understanding the *in vivo* pharmacology of homobivalent ligands is of utmost importance when attempting to

decipher the effects of more complex bivalent ligands such as the MUmBLs presented in **Chapter 5**.

Previously published literature pertinent to comparing **CJL-1-87** to its monovalent counterpart was inconclusive as to whether there is any significant advantages or disadvantages of the bivalent ligand **CJL-1-87** over the monovalent ligand **CJL-1-14** *in vivo*.^{25, 76} Thus it is necessary to perform direct head to head comparison studies in different experimental paradigms to draw definitive conclusions.^{25, 76} In the current chapter, evidence is provided that the melanocortin bivalent agonist ligand **CJL-1-87** possesses distinct advantages in a mouse fasting-refeeding paradigm compared to its monovalent counterpart **CJL-1-14** including: decreased *in vivo* food intake, reduced *in vivo* body fat percentage, and differentially effected mouse hormone levels. These data have led us to postulate two possible mechanisms to explain the differences in the *in vivo* pharmacology between **CJL-1-14** and **CJL-1-87**. The first possible mechanism is that **CJL-1-87** can compete more effectively with endogenous antagonist agouti-related peptide (AGRP) in the fasting state due to its increased binding affinity compared to **CJL-1-14**. The other possible mechanism is that **CJL-1-87** is targeting melanocortin dimers. To test this hypothesis, bioluminescence resonance energy transfer (BRET) studies were performed and support MC3R-MC4R heterodimer formation *in vitro*. This heterodimer may be a novel neuronal target for treating metabolic disorders, but its physiological relevancy remains to be determined. Although the exact molecular mechanism accounting for the differences observed *in vivo* remains unclear, the studies presented in the current chapter

provide direct evidence that the ICV administration of bivalent ligand **CJL-1-87** and monovalent control **CJL-1-14** result in different effects on energy homeostasis in mice in the fasting-refeeding experimental paradigm.

4.3 Results and Discussion:

4.3.1 In Vitro Mouse Serum Stability Assays

In order to assess the metabolic stability of the peptides, *in vitro* mouse serum stability assays were performed as described in **Chapter 2 (Figure 4.1)**. As reported previously, α -MSH was rapidly degraded with less than 1% intact peptide remaining following a 6 h incubation (**Figure 4.1**).^{74, 94, 238} It had a half-life of 0.9 h which is comparable with previous literature reports in rat serum.⁷⁴ Compound **CJL-1-14**, Ac-His-DPhe-Arg-Trp-NH₂, was the most stable peptide in mouse serum and had a half-life of 16.8 h. After incubation in mouse serum for 72 hours 12% of the Ac-His-DPhe-Arg-Trp-NH₂ peptide remained intact. The next most stable peptides were the linker control peptides **CJL-5-35-4** and **CJL-1-116** that have a PEDG20 linker added to the N-terminus or C-terminus to Ac-His-DPhe-Arg-Trp-NH₂. They possessed half-lives of 12.5 h and 10.6 h, respectively. This supports the hypothesis that the PEDG20 linker is not rapidly degraded in mouse serum. The PEDG20-based bivalent ligand **CJL-1-87** had similar stability to NDP-MSH, the enzymatically stable analog of α -MSH.^{94, 238} Compound **CJL-1-87** and NDP-MSH had half-lives of 6.0 and 5.1 h, respectively. Considering NDP-MSH is currently approved for clinical use in the European Union,¹¹⁷ the similar half-lives of **CJL-**

1-87 and NDP-MSH suggest that **CJL-1-87** would have a reasonable metabolic stability for *in vivo* applications.

The current results demonstrate that the bivalent ligand **CJL-1-87** is metabolized faster by the serum proteases present in the mouse serum than its monovalent counterpart **CJL-1-14**. This implies that the bivalent ligand **CJL-1-87** would be at a disadvantage to the monovalent ligand **CJL-1-14** if *in vivo* metabolic stability is desired. In order to interpret the data completely, it must be noted that it would be necessary to metabolically inactivate both pharmacophores of **CJL-1-87** before it was rendered completely pharmacologically inactive. For example, if the N-terminal His-DPhe-Arg-Trp was cleaved by serum proteases, the C-terminal His-DPhe-Arg-Trp would retain activity at the melanocortin receptors similar to that of **CJL-1-116** (cAMP signaling EC₅₀ = 31 nM and 19 nM at the mMC3R and mMC4R, respectively) until the C-terminal His-DPhe-Arg-Trp was metabolized.²⁵ In the current thesis, only the loss of fully intact peptide was monitored to give an indication of metabolic stability. Further studies into the rate of functional inactivation of the peptides will be necessary to determine how fast pharmacological activity is lost, but is outside the scope of the current study.

The previously reported bivalent ligands that were synthesized using a (Pro-Gly)₆ linker were included in the current study for comparison of the linker design for future *in vivo* applications.²⁵ The linker control ligands with the tetrapeptide and the (Pro-Gly)₆, **CJL-5-35-1** and **CJL-1-41**, and the bivalent ligand **CJL-1-31** were rapidly degraded (**Figure 4.1**). There was ≤ 2% intact peptide of **CJL-1-41**, **CJL-1-31**, and **CJL-5-35-1**

remaining after 0.5 h (**Figure 4.1**). It is unclear currently whether the loss of intact peptide results in loss of functional melanocortin activity or if the linker is merely being degraded rapidly while the active His-DPhe-Arg-Trp pharmacophore remains intact. Nevertheless, the current results validate the previous hypothesis that although a Pro-Gly based linker may be useful for determining *in vitro* pharmacology,²⁵ its use is limited for *in vivo* applications to study bivalent design strategies unless rapid degradation is desired. It should also be noted that if a Pro-Gly linker system is used for *in vitro* applications in any bivalent design strategy for any receptor system, the supplementation of assay buffer with serums [*i.e.* fetal bovine serum (FBS), newborn calf serum (NCS)] may result in rapid degradation of the linker system.

Beyond the useful data obtained about the bivalent design strategy and metabolic stability, the current data demonstrates for the first time that the Ac-His-DPhe-Arg-Trp-NH₂ is more stable in mouse serum than NDP-MSH (**Figure 4.1**). This suggests that Ac-His-DPhe-Arg-Trp-NH₂ is less susceptible to common proteases found in mouse serum and supports further research into the tetrapeptide scaffold.

4.3.2 The Effect of ICV Administration of CJL-1-14 versus CJL-1-87 on Mouse Energy Homeostasis

A direct head to head *in vivo* crossover experimental paradigm (**Figure 2.3A**) was designed to compare 5 nmol monovalent **CJL-1-14** to 5 nmol bivalent **CJL-1-87** utilizing the TSE Phenotypic metabolic cages configured to measure food intake, water intake, changes in CO₂ and O₂, and beam break activity. In a nocturnal satiated paradigm in which

compound was administered ICV two hours before lights out and food is available *ad libitum*, no significant differences were observed in food intake, water intake, energy expenditure, respiratory exchange ratio (RER) values, or activity between **CJL-1-14** and **CJL-1-87** (**Figure 4.2**). The observation of approximately equal food intake in this paradigm was consistent with the previous reports of food intake after **CJL-1-14** and **CJL-1-87** treatment in the literature, and no further experiments utilizing this experimental paradigm were performed.^{25, 76} However, significant differences between bivalent ligand **CJL-1-87** and monovalent ligand **CJL-1-14** were observed on food intake and RER values when utilizing a fasting-refeeding paradigm (**Figure 4.3**).

In the fasting-refeeding paradigm, food was removed from mice immediately before the lights out cycle on the previous day. Treatment occurred two hours prior to lights out and food was reintroduced (**Figure 2.3B**). Due to the fast, a hyperphagic response occurs during refeeding and this robust response can aid in the detection of effects. However, fasting can also mask subtle effects due to the strong desire to eat.²¹⁸ During fasting many hormone levels change to promote feeding. Of important relevance to the melanocortin system, the endogenous MC3R/MC4R antagonist agouti-related peptide (AGRP) is upregulated in the hypothalamic regions that are also innervated by proopiomelanocortin (POMC) neurons.^{113, 239-241} AGRP blocks the agonism of endogenous melanocortin agonist peptides (*e.g.* α -MSH, β -MSH, γ -MSH, ACTH) and is also known to function as an inverse agonist at the MC4R to increase feeding and lower energy expenditure.^{76, 113, 242} In addition, fasting upregulates several other hormones including

ghrelin, corticosterone, and neuropeptide Y (NPY) while several hormones are also downregulated including insulin, leptin, and resistin (for a review see Jensen, 2013.²⁴³) These changes in hormonal expression levels are hypothesized to drive the hyperphagic response. Although the maximal signal and, therefore, signal to noise is increased in a fasting-refeeding paradigm compared to a nocturnal feeding paradigm due to the increased baseline or control food intake, achieving a measurable decrease in food intake can sometimes be challenging. This is because the experimental compounds need to overcome these robust hormone changes to have observable activity.

In the current fasting-refeeding experiments, food intake after 5 nmol **CJL-1-87** compared to saline administration was significantly reduced between 2 to 16 hours after ICV administration as expected for a melanocortin receptor agonist (**Figure 4.3B**). Approximately 50% less food was consumed compared to saline and 5 nmol **CJL-1-14** at the 2-8 hour time points. Notably, there was no significant difference in food intake after fasting between **CJL-1-14** and saline groups. Compared to **CJL-1-14** food intake after **CJL-1-87** treatment was significantly reduced at every time point from 2 to 24 hours after compound administration (**Figure 4.3B**). It is worth noting that the current experiments were performed in a crossover design paradigm, such that all 11 age matched male mice included in the study were administered saline, 5 nmol **CJL-1-14** and 5 nmol **CJL-1-87** on different days with a washout period of one week in between administrations and no mice were excluded.

The RER was determined by dividing the volume of CO₂ produced by the volume of O₂ consumed by an animal.^{189, 244, 245} Because the oxidation of carbohydrates or fatty acids produces different amounts of CO₂ for each O₂ molecule utilized, the RER indicates whether mice are using carbohydrates or fats as the primary fuel source. RER values of about 1.0 indicate that carbohydrates are the primary fuel source being utilized, whereas values of approximately 0.7 indicate that fats are primarily being utilized.^{189, 244, 245} The RER in the current experiment was indirectly calculated by measuring the amount of CO₂ and O₂ entering and exiting the sealed metabolic cages as previously described.^{132, 189, 244, 245}

During the fast, RER values for all groups dropped to slightly above 0.7 indicating that fats are primarily being used as a source of energy (**Figure 4.3C**). This is expected due to the lack of carbohydrates available from food during the fast that results in a reliance of fat storage for energy, an effect previously described.^{246, 247} At the 0 h time point, the compound or saline is administered and food is reintroduced to the cage. A rapid increase in the RER is observed in the saline treatment group until the fuel source is primarily carbohydrates during the initial dark cycle as anticipated. Treatment with both **CJL-1-87** and **CJL-1-14** resulted in a more gradual increase in RER (**Figure 4.3C**). Significant reduction of RER values was observed 2-9 and 11 hours after **CJL-1-87** treatment compared to after saline treatment during the first dark cycle. Significant reduction in RER values were observed 5-9 and 11-15 hours after **CJL-1-87** treatment compared to **CJL-1-14** treatment. The compound-specific reduction in RER suggests that the mice are using

more fats after **CJL-1-87** administration compared to either saline or **CJL-1-14**. No significant differences in energy expenditure (kcal/kg/h) was observed between any treatment groups (**Figure 4.3D**). The energy expenditure taken together with the RER data indicates that the mice are burning approximately the same amount of calories upon different treatments, however the **CJL-1-87** treated mice appear to be utilizing more fats for their energy in lieu of carbohydrates (**Figure 4.3C-D**).

During the following light cycle (t = 14-26 h), the RER decreased for all groups most likely due to decreased feeding and decreased activity that is expected with nocturnal feeders like mice. The RER increases again preceding and during the second dark cycle (t = 26-38 h). Although no clear trend was observed in food intake beyond 24 hours, the RER was still significantly lower after **CJL-1-87** treatment compared to saline or **CJL-1-14** at time points 27-34 h (**Figure 4.3C**). This second time period of significantly decreased RER in the absence of decreased food intake suggests that compound **CJL-1-87** has long-lasting effects on energy homeostasis that do not appear to directly correlate to food intake. This is not observed with the monovalent ligand **CJL-1-14**.

The length of time that **CJL-1-87** affected energy homeostasis was unexpected since the initial nocturnal paradigm studies presented in **Chapter 3** showed no significant effects on food intake past 8 hours with this compound,²⁵ and less than 3% of the **CJL-1-87** remained intact after 24 hours in the *in vitro* serum stability assays (**Figure 4.1**). However, the serum stability studies give only an indication of the metabolic stability of **CJL-1-87** in the brain as the proteases present in the cerebrospinal fluid (CSF) may be

different than those in the serum. Another factor in the interpretation of the long lasting effects on RER of **CJL-1-87** is the rate of clearance from the ventricular system of the brain into the peripheral. Although the rate of clearance is currently unknown for **CJL-1-87** and **CJL-1-14**, it has previously been reported that CSF emptying time and compound clearance from the CSF is rapid after ICV administration.²⁴⁸⁻²⁵⁰ These data suggest the long-lasting response was the result of a pharmacological effect due to receptor binding, and not due to the drug being present in the cerebrospinal fluid (CSF) for an extended period of time. It could be that once **CJL-1-87** is bound to a receptor, it avoids degradation and clearance from the brain while promoting long lasting effects, or that the binding of **CJL-1-87** to melanocortin receptors may cause unique downstream signaling cascades not observed with its monovalent counterpart. Either way, the increased duration of action on RER with increased utilization of fat stores for energy is a distinct characteristic of the bivalent ligand that is not observed with the monovalent ligand. Further studies into the CSF clearance rate of **CJL-1-87** and **CJL-1-14** as well as studies thoroughly characterizing the absorption, distribution, metabolism, and excretion of these ligands will be necessary to draw clear conclusions about the long-lasting (>24 h) effects.

Whenever an experiment's measurements are based on loss of function, it can raise questions about assay artifacts. In this particular assay paradigm, it may be questioned whether the reduction in food intake and RER are a consequence of an adverse reaction or toxicity to **CJL-1-87**. In order to address this concern, mice were monitored visually for at least 2 hours post treatment and no adverse reactions in any of the three treatment groups

were observed. Additionally, no significant effect was observed between saline, **CJL-1-87** or **CJL-1-14** on locomotor activity (beam breaks), water intake (mL), or energy expenditure (kcal/h/kg) (**Figure 4.3D-F**). If sick-like behavior or toxicity were suspect for the observed decrease in food intake and RER, it would be expected that these other parameters would be lowered as well. In particular, locomotor activity, as quantified by infrared beam breaks along the side of the cages (X-axis), would be negatively affected because a sick mouse would typically be hunched and inactive in the corner of the cage (**Figure 4.3E**). The lack of effect observed on activity between all treatment groups supports that visceral illness or other adverse reactions were not likely to be contributing factors to the significant effects observed.

4.3.3 The Effect of ICV Administration of CJL-1-14 and CJL-1-87 on Body Composition

To study the effect of **CJL-1-87** and **CJL-1-14** on body composition and metabolically active hormone levels in the blood plasma of mice, a new cohort of 32 male age matched mice (saline, n=10; **CJL-1-14**, n=11; **CJL-1-87**, n=11) underwent cannulation surgery and placement validation as previously discussed in **Chapter 2**. The animals were administered a single treatment of saline vehicle control, 5 nmol **CJL-1-14**, or 5 nmol **CJL-1-87** and sacrificed 6 h post-treatment in the fasting-refeeding paradigm described above but in conventional cages (**Figure 2.3B**). Once again, **CJL-1-87** treatment decreased food intake as compared to **CJL-1-14** and saline (**Figure 4.3B, Figure 4.4A**). As expected the decreased food intake was accompanied by a significant reduction in the

amount of weight gained after the food was reintroduced with **CJL-1-87** treatment compared to **CJL-1-14** for the first 6 h post-treatment (**Figure 4.4B**). Mice treated with **CJL-1-87** gained back 55% less weight than saline and **CJL-1-14** treated mice 6 h post fast. The **CJL-1-87** treated mice also gained significantly less weight than saline treated mice 4 and 6 h post-fast (**Figure 4.4B**).

The amount of lean mass and fat mass was measured pre-fast, immediately before compound administration, and 6 h post-administration just before sacrificing the animals using an EchoMRI-100H system. There were no significant differences between the saline, **CJL-1-14**, and **CJL-1-87** treatment in their effect on body percentage of lean mass before the fast, at compound administration, or 6 h after compound administration (**Figure 4.4C**). There were no significant differences in body fat mass percentage before the fast, or immediately before treatment between saline, **CJL-1-14**, and **CJL-1-87** as expected. The body fat percentage was significantly lower in mice that received **CJL-1-87** treatment compared to saline treatment 6 h post-administration (**Figure 4.4D**). Mice treated with **CJL-1-87** gained back 45% less fat mass 6 h after the fast compared to saline treated mice. Mice treated with **CJL-1-14** gained back 15% less fat mass compared to saline treated mice, however there were no significant differences in body fat percentage between **CJL-1-14** compared to saline or **CJL-1-87**. The decreased body fat percentage after **CJL-1-87** treatment is consistent with the lowered RER values in the metabolic cage studies supporting the hypothesis that fat, and not carbohydrates, is the primary fuel source after **CJL-1-87** treatment (**Figure 4.3C**).

4.3.4 The Effect of ICV Administration of CJL-1-14 and CJL-1-87 on Hormone Levels

The same 32 mice from the body composition studies were sacrificed and trunk blood was collected 6 h post ICV treatment with saline, 5 nmol **CJL-1-14**, or 5 nmol **CJL-1-87**. The plasma was analyzed using a multiplex Luminex Milliplex system to assess six hormones and one cytokine: insulin, C-peptide, leptin, ghrelin, glucose-dependent insulinotropic polypeptide (GIP), resistin, and interleukin 6 (IL-6) (**Figure 4.4 E-K**). Mice treated with **CJL-1-87** had significantly lower levels of insulin, C-peptide, leptin, GIP and resistin compared to mice receiving either saline or **CJL-1-14** (**Figure 4.4E-H and K**). Also **CJL-1-87** treated mice had significantly lower levels of IL-6 compared to saline, but there was no significant difference between **CJL-1-14** and **CJL-1-87** treatment (**Figure 4.4J**). Mice receiving **CJL-1-87** had significantly increased ghrelin levels compared to mice receiving saline or **CJL-1-14** (**Figure 4.4I**). Mice receiving **CJL-1-14** had significantly reduced C-peptide, leptin, GIP, and IL-6 compared to mice receiving saline (**Figure 4.4F-H and J**).

The differences in metabolic hormone levels observed between all three treatment groups demonstrate unique effects of the melanocortin bivalent agonist ligand design. The unique effects were evident in the significant differences in the levels of insulin, C-peptide, leptin, GIP, ghrelin, and resistin between **CJL-1-14** treatment and **CJL-1-87** treatment (**Figure 4.4E-I and K**). It should be noted that although the same molar amount of peptide (5 nmols) was administered, the bivalent ligand **CJL-1-87** contains twice as many

pharmacophores. It could, therefore, be hypothesized that differences between **CJL-1-14** and **CJL-1-87** on C-peptide, leptin, and GIP were due to a “dose-dependent” effect of the pharmacophores (**Figure 4.4F, H, and I**). However, this is an intricate argument, since a similar “dose-dependent” effect was not observed with insulin, ghrelin, IL-6, or resistin. Doubling of the pharmacophores could be a contributing factor, but the complexity of the *in vivo* pharmacology suggests that the effects are due to characteristics of **CJL-1-87** that are distinct from **CJL-1-14**. The unique characteristics may originate from the bivalent design strategy, differences in receptor selectivity (*e.g.* MC3R vs MC4R as discussed in **Chapter 3**), different receptors being responsible for the different responses (*e.g.* hormone release vs food intake), or the different distribution of **CJL-1-87** and **CJL-1-14** after ICV delivery. Further experimentation will be necessary to determine the exact neuronal mechanism of action of the observed *in vivo* response differences. However, it is clear that in the current fasting-refeeding *in vivo* experimental paradigm that **CJL-1-87** behaviors differently than its monovalent counterpart. Possible *in vitro* molecular mechanisms focused on how the bivalent ligand **CJL-1-87** may be interacting with melanocortin dimers will be discussed below.

The effects of the melanocortin ligands on the hormone plasma levels are consistent with previous literature reports (**Table 4.1**).²⁵¹⁻²⁶³ For example, it has previously been reported that melanocortin agonists decreased insulin serum and plasma levels, regardless of food intake.²⁵¹⁻²⁵³ This is consistent with the decreased insulin levels observed herein with **CJL-1-87** treatment, albeit no effect was observed with **CJL-1-14** treatment (**Figure**

4.4E). As would be anticipated, C-peptide was also decreased by melanocortin agonism (**Figure 4.4F**), because insulin and C-peptide are produced in equimolar amounts from the cleavage of proinsulin.^{254, 255} Similarly, decreased leptin levels in the serum or plasma have been reported following administration of melanocortin agonists as observed herein (**Figure 4.4G**).^{252, 253} There is also evidence that melanocortin agonist administration decreases GIP, similar to the current results (**Figure 4.4H**).²⁵⁶ At least two studies have reported that the melanocortin agonist MTII has no effect on resistin serum levels although one study found that resistin mRNA expression was upregulated after MTII treatment.^{257, 258} Also, the MC3R and MC4R antagonist SHU9119 was reported to increase resistin serum levels making interpretation of the data inconclusive.^{257, 258} The significant decrease in resistin levels after **CJL-1-87** treatment appears to be a unique effect of the bivalent ligand compared to the monovalent ligand **CJL-1-14** and the previous studies (**Figure 4.4K**).^{257, 258} Previous studies reported melanocortin agonists decreasing IL-6 gene expression and secretion after administration in mice which is also consistent with the current results (**Figure 4.4J**).²⁵⁹⁻²⁶¹ However, this effect is confounded by conflicting data indicating that α -MSH increases IL-6 expression.²⁶² Although ghrelin is usually thought of as an upstream regulator of the melanocortin pathway, there is some evidence that α -MSH can directly affect the release of ghrelin (**Figure 4.4I**).²⁶³ It is therefore unclear if the current increase in ghrelin after **CJL-1-87** treatment is a direct pharmacological effect or an effect of the decreased food intake.

Although the above literature provides evidence that some of the changes in hormone levels may be from activation of melanocortin receptors, it is possible that some of the changes in hormones are due to lowered refeeding of **CJL-1-87** treated mice. During the fasting state prior to compound administration, the lack of food intake is likely to cause a decrease in the serum concentration of insulin, C-peptide, leptin, resistin, and GIP.^{243, 256, 264-266} Inversely, ghrelin is normally elevated during fasting and decreased after food intake (**Table 4.1**).^{243, 267} IL-6 is also thought to be increased during fasting.²⁶⁸ While it is possible that direct pharmacological agonism causes the changes in the plasma hormone levels after compound administration, the decrease in food intake resulting from **CJL-1-87** administration may slow the rate of change in hormones levels from the fasting state. However, such slowing cannot explain the significantly reduced plasma levels of C-peptide, leptin, GIP and IL-6 observed with **CJL-1-14** treated mice compared to saline treated mice that had the same food intake. This indicates that these hormone changes are a direct effect of agonizing the melanocortin receptors with **CJL-1-14**. The effects of **CJL-1-87** on hormone levels may be attributed to pharmacological agonism of the melanocortin receptors, decreased food intake, or some combination of both. Regardless, it appears that **CJL-1-87** has physiological effects that significantly reduce food intake after fasting in spite of the increased levels of the orexigenic peptide ghrelin and the decreased levels of the anorexigenic peptides leptin and insulin.

4.3.5 ¹²⁵I-AGRP Competitive Binding Studies

Although the bivalent ligand **CJL-1-87** is advantageous in reducing food intake, body weight, and fat mass gained when utilizing a fasting-refeeding paradigm compared to **CJL-1-14**, the exact molecular mechanism is unclear. Two major hypotheses can be envisioned based on the bivalent design concept: 1) The *c.a* 20-fold increased binding affinity of **CJL-1-87** compared **CJL-1-14** discussed in **Chapter 3** helps it compete more effectively with endogenous AGRP that is upregulated in the fasting state. 2) The bivalent ligands are interacting with melanocortin homodimers or heterodimers in a unique fashion that is different than the monovalent counterpart. In order to investigate how effectively **CJL-1-87** can displace AGRP, competitive radioligand binding assays using ¹²⁵I-AGRP(87-132) were performed (**Table 4.2**). Results from **Chapter 3** for **CJL-1-14** and **CJL-1-87** competition against ¹²⁵I-NDP-MSH and results from antagonist monovalent tetrapeptide Ac-His-DNal(2')-Arg-Trp-NH₂ and antagonist homobivalent ligand **CJL-1-140**, Ac-His-DNal(2')-Arg-Trp-(PEDG20)-His-DNal(2')-Arg-Trp-NH₂, are provided for easier comparison (**Table 4.2**).²⁵

At the mMC4R, the IC₅₀ values obtained by competing experimental ligands against ¹²⁵I-AGRP(87-132) are within experimental error (less than 3-fold change) of those obtained by competing against ¹²⁵I-NDP-MSH in **Chapter 3**.²⁵ Bivalent ligand **CJL-1-87** had a 17-fold higher binding affinity when competing against ¹²⁵I-AGRP(87-132) compared to its monovalent counterpart **CJL-1-14** at the mMC4R. At the mMC3R, the experimental agonist ligands tended to be better at displacing ¹²⁵I-AGRP(87-132)

compared to ^{125}I -NDP-MSH. In fact, compound **CJL-1-14** and **CJL-1-87** had approximately a 10-fold shift in the IC_{50} values obtained when displacing ^{125}I -AGRP(87-132) compared to ^{125}I -NDP-MSH at the mMC3R. Unlabeled NDP-MSH and antagonist ligand Ac-His-DNal(2')-Arg-Trp-NH₂ had less than 3-fold changes in IC_{50} values to compete ^{125}I -NDP-MSH and ^{125}I -AGRP(87-132). Homobivalent antagonist **CJL-1-140** had nearly a 3-fold shift in its IC_{50} value when competing against ^{125}I -AGRP(87-132) compared to the value obtained when competing against ^{125}I -NDP-MSH in **Chapter 3**. The homobivalent agonist ligand **CJL-1-87** had an 18-fold higher binding affinity compared to its monovalent counterpart **CJL-1-14** when both are competing against ^{125}I -AGRP(87-132) at the mMC3R (**Table 4.2**). This increase in binding affinity of the agonist ligands when competing against ^{125}I -AGRP(87-132) compared to ^{125}I -NDP-MSH at the mMC3R and not the mMC4R may implicate that the mMC3R has increased regulation in reducing refeeding from the fasting state. This observation is consistent with a previous report that MC3R knockout mice have lowered food intake after fasting compared to wild type mice.²⁴⁰

During fasting, the expression of endogenous MC3R and MC4R antagonist/ inverse agonist AGRP is upregulated and promotes a state of hunger that drives refeeding.^{113, 239-241} This may allow melanocortin agonists to have two functional effects by both activating the melanocortin receptors, and functionally antagonizing AGRP's orexigenic effects by blocking the endogenous AGRP from binding the melanocortin receptors. This dual action may be able to explain a mechanism of how bivalent ligand **CJL-1-87** has more significant

effects in the fasting-refeeding paradigm than the monovalent ligand **CJL-1-14**, but not in the nocturnal paradigm. Although **CJL-1-87** was previously reported in **Chapter 3** to possess only about 3- to 5-fold increased agonist potency to stimulate cAMP signaling compared to **CJL-1-14**,²⁵ the increased *in vitro* binding affinity of 17- to 18-fold may increase **CJL-1-87**'s ability to compete effectively with AGRP *in vivo*. In the nocturnal paradigm in which there would be lower amounts of AGRP present, the increase in binding affinity would be less of a driving force in decreasing feeding and, therefore, **CJL-1-14** and **CJL-1-87** would have more similar *in vivo* effects based on the closer functional cAMP potencies.^{25, 76} However, in the fasting state there would be a higher concentration of AGRP and the ability of **CJL-1-87** to compete with and antagonize AGRP's orexigenic effects would become increasingly important. Monovalent ligand **CJL-1-14** may not have a strong enough binding affinity to effectively compete with AGRP and antagonize its orexigenic effects, whereas **CJL-1-87** with a 17- to 21-fold increased binding affinity at both the mMC3R and mMC4R would block the orexigenic effects of AGRP *in vivo* resulting in significantly decreased refeeding.

It should be noted that although the hypothesized binding affinity mechanism may explain the current observation of bivalent ligand **CJL-1-87**'s advantages in the fasting paradigm over the monovalent ligand **CJL-1-14**, this proposed mechanism does not exclude the possibility that melanocortin receptor dimerization is also responsible. In fact, the increased binding affinity of **CJL-1-87** is hypothesized to be a result of synergistic bivalent binding at melanocortin dimers.²⁵ It is possible that the dimerization of

melanocortin receptors may play a functional role beyond synergistic bivalent binding in the pharmacology of **CJL-1-87** which will be discussed further below. Regardless of the exact mechanism, it does appear that the bivalent design strategy is responsible either by synergistic binding, or by targeting melanocortin dimers for the ability of the bivalent ligand, and not the monovalent ligand, to decrease feeding in the fasting-refeeding paradigm.

4.3.6 Bioluminescence Resonance Energy Transfer (BRET) Supports mMC3R-mMC4R Heterodimerization

The second hypothesis for the significant differences between **CJL-1-14** and **CJL-1-87** in the fasting-refeeding paradigm could be the interaction of the compounds with melanocortin receptor dimers. Portoghese and coworkers have demonstrated that bivalent ligands can be designed to selectively target opioid heterodimers.⁵⁻¹¹ It has previously been supported that the melanocortin receptors can form homodimers, heterodimers, or higher-order oligomers utilizing various techniques to demonstrate proximity and association.^{125, 127, 129-131, 204-209} Furthermore, it has recently been demonstrated that coexpression of the MC1R and MC5R can create ligand-dependent signal modulation providing evidence that melanocortin heterodimerization can have functional consequences.²⁰⁹ Considering that the bivalent ligands were designed to interact with melanocortin receptor dimers, it is possible that the unique *in vivo* effects of **CJL-1-87** versus **CJL-1-14** could be from bivalent binding specifically to homodimers or heterodimers. In order to explore whether these effects could be mediated through a MC3R-MC4R heterodimer, bioluminescence

resonance energy transfer (BRET) studies were undertaken to show association of the two receptors. Additionally, cAMP-based AlphaScreen experiments were performed on cells coexpressing both the mMC3R and mMC4R to begin elucidating the possible functional significance of a mMC3R-mMC4R heterodimer.

BRET is a biophysical technique that can be used to demonstrate the association of two proteins. It has previously been utilized to show that the mMC3R and mMC4R are in close proximity suggesting that they form homodimers or higher-order oligomers.^{130, 204, 205} It has also been shown that the hMC1R closely associates with the hMC3R by BRET suggesting heterodimerization.²⁰⁴ To our knowledge, the MC3R and MC4R have never been studied by BRET for heterodimerization prior to this thesis work.¹³² In rats, mRNA of both the MC3R and MC4R have been detected in select regions of the brain such as the anteroventral periventricular (AVPV), ventral premammillary (PMV), and posterior hypothalamic nuclei suggesting possible *in vivo* coexpression.^{81, 211, 212} Also *in vitro* coexpression of the MC3R and MC4R in neuronal cells colocalize on the cell membrane suggesting heterodimerization is possible.²¹¹ This hypothesized heterodimer may explain some of the ambiguous pharmacology of the melanocortin system such as the mechanism of the synergistic effects observed in the MC3R-MC4R double knockout mice as discussed in the **Chapter 1**.^{1, 58, 210} Furthermore, due to the differential expression profile of the mMC3R and mMC4R, ligands that would target a mMC3R-mMC4R heterodimer could be developed to be tissue selective acting only in the distinct regions within the brain that

coexpress the receptors. Further studies will be needed to demonstrate whether individual neurons do in fact coexpress the MC3R and MC4R.

BRET studies were performed on HEK293 cells expressing only the mMC3R, only the mMC4R, or coexpressing the mMC3R and mMC4R (**Figure 4.5**). The Promega NanoBRET™ Protein:Protein interaction system was utilized with limited modifications to develop mMC3R and mMC4R fused to both the NanoLuc® fusion protein and the HaloTag® fusion protein. HEK293 cells expressing the mMC3R-NanoLuc® and the mMC3R-HaloTag® resulted in a BRET ratio of 90 ± 5 mBU, supporting mMC3R homodimerization. This data is similar to a previous result observed with a slightly different BRET system that showed a BRET ratio of 350 mBU with the hMC3R. The decrease in signal currently observed might be explained by differences in assay paradigms including using Cos-7 cells, the human receptors, or DeepBlueC substrate.²⁰⁴ HEK293 cells expressing the mMC4R-NanoLuc® and the mMC4R-HaloTag® resulted in a high BRET ratio of 100 ± 10 mBU. This is in good agreement with previous results reported by two independent laboratories using different BRET conditions (*e.g.* using Cos-7 cells versus HEK293 cells) that reported BRET ratios of 75 mBU and 110 mBU with the hMC4R.^{130, 205}

HEK293 cells that were transfected to coexpress mMC4R-NanoLuc® and the mMC3R-HaloTag® gave a high BRET ratio of 150 ± 10 mBU (**Figure 4.5**). As a negative control, a plate of cells was transiently transfected with the mMC4R-NanoLuc® and a separate plate was transfected with mMC3R-HaloTag®. These cells were mixed in equal

amounts and assayed together which resulted in minimal BRET signal (1.6 ± 0.5 mBU). This suggested that BRET signal was indeed from specific mMC3R-mMC4R interactions on the same cell membrane, and not from non-specific interactions of the receptors being assayed at the same time. As a further negative control, unrelated mouse double minute 2 (MDM2)-NanoLuc® and the mMC3R-HaloTag® were coexpressed as well as mMC4R-NanoLuc® and the p53-HaloTag® that resulted in minimal signal (7.7 ± 4.0 mBU and 3.4 ± 0.3 mBU, respectively).

The increased signal from mMC4R-NanoLuc® and mMC3R-HaloTag® coexpression compared to singly expressed mMC3R or mMC4R suggests that the mMC3R and the mMC4R form heterodimers in addition to homodimers. The ratio of homodimers to heterodimers is yet to be determined. It also should be noted that the relative BRET signal could be affected by the expression levels of the transiently transfected receptors which was not quantified in this study. It is also possible that higher-order oligomers are responsible for the high BRET signal of both homodimers and heterodimers as it is possible that the receptors could form tetramers (or even higher-order oligomers) that are “heterodimers” of the homodimer species. This would cause strong BRET signal of both homo- and heterodimers as observed herein.

4.3.7 Coexpression of mMC3R and mMC4R effects on Functional Potency

Based upon the BRET data indicating mMC3R-mMC4R heterodimerization, cAMP AlphaScreen assays were performed on cells coexpressing both the mMC3R and mMC4R to elucidate any functional significance. In these experiments, HEK293 cells

stably expressing one receptor subtype were transiently transfected with the second receptor subtype to achieve dual expressing cells (**Figure 4.6**). To determine if the effects were due to the receptors being expressed on the same cell membrane (**Figure 4.6 C, and D**) versus the receptors being assayed together; an equal mixture of both individual stable cells lines was assayed as a control (**Figure 4.6 E**). Five cell categories (*i.e.* stable mMC3R cells, stable mMC4R cells, stable mMC3R cells transiently expressing the mMC4R, stable mMC4R cells transiently expressing the mMC3R, and an equal mixture of stable mMC3R cells and stable mMC4R cells) were screened in parallel at the same time to control for inherent day to day assay variability (**Figure 4.6, Table 4.3**). Only cells that coexpressed the mMC3R and mMC4R could possibly contain mMC3R-mMC4R heterodimers (**Figure 4.6 C and D**), whereas the mixture of mMC3R stable cells with mMC4R stable cells would contain no heterodimers even though both cell types are assayed together (**Figure 4.6 E**). At least three independent experiments were performed on separate days. The EC₅₀ values for ligands NDP-MSH, α -MSH, MTII, **CJL-1-87**, and **CJL-1-14** at the singly expressed mMC3R and mMC4R were consistent with the field.^{25, 269, 270}

The EC₅₀ values for the four monovalent ligands (*i.e.* NDP-MSH, α -MSH, MTII, and **CJL-1-14**) were within the inherent experimental error (<3-fold difference) when comparing the coexpressing cells (with possible heterodimers) to the mixed stable cell category (with no possible heterodimers) (**Table 4.3**). The values obtained for coexpressed cell lines corresponded well with the most potent EC₅₀ value at the individually expressed cells lines (*i.e.* stable mMC3R or stable mMC4R cells) as expected based on the principle

of the harmonic mean.²⁷¹ This indicates that there is no observable effect on the potency of these monovalent compounds (in our hands) of the mMC3R and mMC4R being coexpressed in the same cells compared to on different cells. Although it should be noted that the monovalent ligand **CJL-1-14** was observed to trend towards increased potency (2.5 fold increase) when the mMC4R stable cells were transiently transfected with the mMC3R plasmid, but this is within the inherent 3-fold experimental error associated with these assays in our laboratory.

Bivalent ligand **CJL-1-87** possessed subnanomolar potency that was over 3-fold more potent compared to results achieved with the stable cell mixture when the mMC3R was transiently transfected into the stable mMC4R cell line (**Table 4.3**). These results may suggest that the bivalent ligand induced a synergistic effect during coexpression of the mMC3R and mMC4R presumably through a mMC3R-mMC4R heterodimer. However, the increase observed was slight (3-fold) especially considering the monovalent **CJL-1-14** resulted in a trending increase as well (2.5-fold). Also the opposite transfection order in which stable mMC3R cells were transiently transfected with the mMC4R did not result in a difference (see **Section 4.3.8** for further discussion). Therefore, these results are currently inconclusive, but warrant further studies to establish the functional effects of melanocortin coexpression, and whether the mMC3R-mMC4R heterodimer may be a future neuronal molecular drug target.

4.3.8 Coexpression of mMC3R and mMC4R Effects on Functional Potency and Discussion of Expression Levels

One noteworthy trend observed in the cAMP functional coexpression experiments is that for all compounds coexpression of the mMC3R transiently in mMC4R stable cells resulted in slightly more potent EC₅₀ values than the opposite transfection order in which stable mMC3R cells were transiently transfected with the mMC4R plasmid (**Table 4.3**). This was especially true with dosing of **CJL-1-14** and **CJL-1-87** that both resulted in about 2-fold differences in EC₅₀ values. Although this is within experimental error of 3-fold, these changes are still worth discussing as they are consistent and may indicate that further study will be necessary.

These differences likely have to do with the ratio of the amount of mMC3R and mMC4R expressed on the cell surface. It is dogma in the field that transient transfection results in a greater expression of receptors on the cell membrane than selected stable receptor populations of cells. Therefore, when the mMC3R is transiently transfected into the stable mMC4R cells, it is anticipated that more mMC3R than mMC4R would be expressed on the cell surface. If heterodimers do exist on the cell surface, the relative concentration of each receptor would be hypothesized to affect the equilibrium of the ratios of mMC3R monomers, mMC4R monomers, mMC3R homodimers, mMC4R homodimers, and mMC3R-mMC4R heterodimers (or how they compose higher-order oligomers). Considering **CJL-1-87** has 45- to -350 fold higher binding affinity (depending on the radioligand used) at the mMC4R compared to the mMC3R, these shifts in equilibrium

between dimer species would affect how much of the dosed **CJL-1-87** is binding mMC4R homodimers, mMC3R homodimers, or mMC3R-mMC4R heterodimers. To our knowledge, there is no technology feasibly capable of distinguishing how much of a ligand is binding to each of the different dimer states at this time. However, the increased potency in the coexpression system suggests that the heterodimerization of the mMC3R-mMC4R could play a role in the altered *in vivo* effects of **CJL-1-87** compared to **CJL-1-14**, and that the mMC3R-mMC4R heterodimer may be a future neuronal molecular drug target.

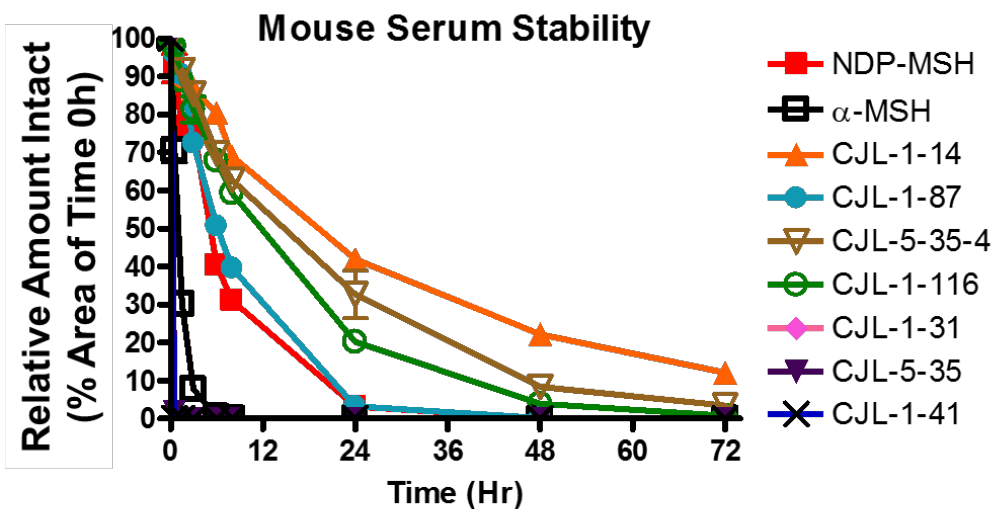
4.4 Conclusions

The studies in the current chapter demonstrate that the homobivalent ligand **CJL-1-87** has a distinct pharmacological *in vivo* profile compared to the monovalent control ligand **CJL-1-14**. The findings reported here, along with **Chapter 3**,^{25, 132} provide new knowledge of molecular probes for future anti-obesity drug design and *in vivo* mechanism of action studies. The bivalent ligand **CJL-1-87** had an increased ability to reduce food intake, promote fat utilization, modulate metabolic hormones, and decrease percent body fat when utilized in a mouse fasting-refeeding experimental paradigm as compared to the monovalent control ligand **CJL-1-14**. This extended the results in **Chapter 3** that **CJL-1-87** has *c.a.* 20-fold increased binding affinity and moderately increased functional activity *in vitro*.²⁵ However, *in vivo* paradigm-specific effects of **CJL-1-87** could not have been predicted by *in vitro* assays from **Chapter 3**. Compound **CJL-1-87** appears to be effective at reducing food intake in spite of peripheral hormone signals that stimulate hunger and refeeding including elevated ghrelin levels and depressed insulin and leptin levels.

It is postulated that the current *in vivo* differences reported herein, between **CJL-1-87** and **CJL-1-14**, are due to the bivalent ligand design strategy. Two possible mechanisms to explain the distinct pharmacology of **CJL-1-87** compared to **CJL-1-14** based on the homobivalent ligand design have been presented. In the first proposed mechanism, the lowered entropy of the bivalent ligand binding allows **CJL-1-87** to compete more effectively at displacing the endogenous MC3R/MC4R antagonist AGRP (that is upregulated in the fasting state) resulting in both agonism of the melanocortin receptors and antagonism of the orexigenic effects of AGRP. The monovalent ligand **CJL-1-14** has a lower binding affinity and is speculated to not compete as effectively with endogenous AGRP. In the second proposed mechanism, it is postulated that **CJL-1-87** interacts with melanocortin receptor homo- and/or heterodimers in a distinct molecular mechanism as compared to the monovalent counterpart **CJL-1-14**. The unique pharmacology observed *in vivo* may be a result of interacting with MC3R homodimers, MC4R homodimers, or MC3R-MC4R heterodimers that were all identified to form during *in vitro* BRET studies. It is possible that both of these postulated mechanisms play a synergistic role in the present *in vivo* observations. However, additional experimental studies are necessary to validate the postulated physiological significance of melanocortin dimers *in vivo*.

The result presented herein provides “proof-of-concept” and a foundation that homobivalent ligands can achieve unique *in vivo* effects that are discrete from their monovalent counterparts. These results validate melanocortin homobivalent ligands as a

design strategy for therapeutically relevant compounds towards the treatment of energy homeostasis disorders such as obesity or cachexia. The advantage of **CJL-1-87** compared to **CJL-1-14** is increased *in vitro* binding affinity, increased *in vivo* functional potency, increased duration of action, decreased food intake after fasting, decreased body fat percentage, and differentially altered metabolic hormone levels. These findings justified further study of the SAR of melanocortin homobivalent ligands as presented in **Chapter 6**. This chapter also allows for better understanding for the of the *in vivo* pharmacology of the MUmBLs that will be presented in **Chapter 5**.



Analog	Half-Life (hr)
NDP-MSH	5.1
α -MSH	0.9
CJL-1-14	16.8
CJL-1-87	6.0
CJL-5-35-4	12.5
CJL-1-116	10.6
CJL-1-31	0.1
CJL-5-35-1	0.1
CJL-1-41	0.1

Analog	Structure	Amount of Intact Peptide (%)								
		0.5 hr	1.5 hr	3 hr	6 hr	8 hr	24 hr	48 hr	72 hr	
NDP-MSH	Ac-Ser-Try-Ser-Nle-Glu- His-DPhe-Arg-Trp -Gly-Lys-Pro-Val-NH ₂	92	77	76	40	31	3	0	0	
α -MSH	Ac-Ser-Try-Ser-Met-Glu- His-Phe-Arg-Trp -Gly-Lys-Pro-Val-NH ₂	71	30	8	1	0	0	0	0	
CJL-1-14	Ac- His-DPhe-Arg-Trp -NH ₂	99	90	87	80	69	42	22	12	
CJL-1-87	Ac- His-DPhe-Arg-Trp -(PEDG20)- His-DPhe-Arg-Trp -NH ₂	96	90	72	51	40	3	0	0	
CJL-5-35-4	Ac- His-DPhe-Arg-Trp -(PEDG20)-NH ₂	101	92	85	70	63	33	8	3	
CJL-1-116	(PEDG20)- His-DPhe-Arg-Trp -NH ₂	98	89	81	68	59	20	4	1	
CJL-1-31	Ac- His-DPhe-Arg-Trp -(Pro-Gly) ₆ - His-DPhe-Arg-Trp -NH ₂	0	0	0	0	0	0	0	0	
CJL-5-35-1	Ac- His-DPhe-Arg-Trp -(Pro-Gly) ₆ -NH ₂	2	0	0	0	0	0	0	0	
CJL-1-41	(Pro-Gly) ₆ - His-DPhe-Arg-Trp -NH ₂	0	0	0	0	0	0	0	0	

Figure 4.1. *In vitro* serum stability of bivalent ligands and control ligands. Ligands (10 μ M) were incubated in mouse serum and monitored for degradation of the parent molecule by LC-ESI⁺-MS/MS. The PEDG20 based compounds were relatively metabolically stable, whereas (Pro-Gly)₆ based compounds were rapidly degraded. Half-lives were calculated from two technical replicates of the *in vitro* serum stability assays. This figure has been adapted with permission from Lensing, C. J. *et. al*, *ACS Chem. Neurosci.* **2017**, in press.¹³²
Copyright (2017) American Chemical Society.

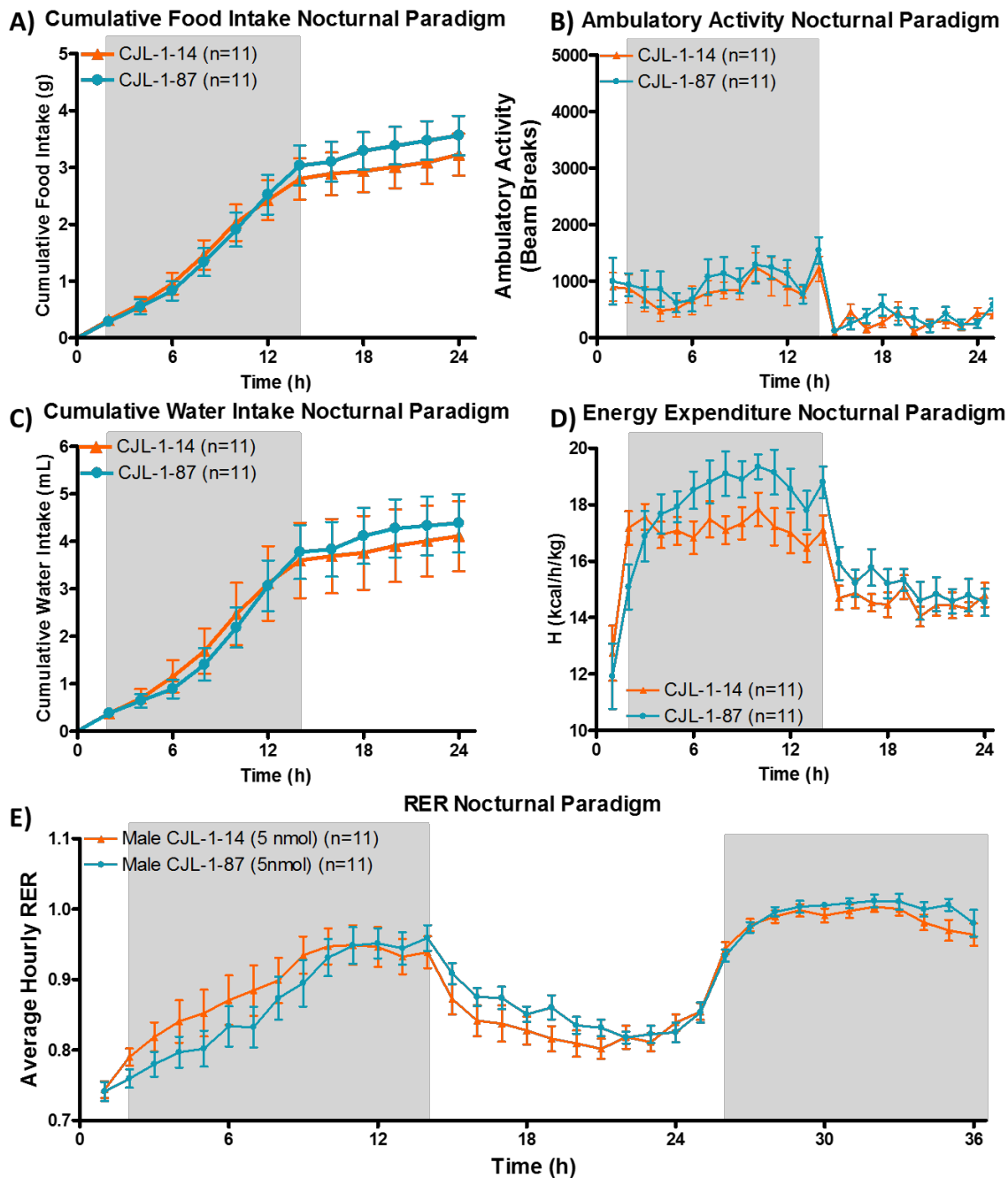


Figure 4.2. Investigation of 5 nmol bivalent ligand **CJL-1-87** (●) compared to 5 nmol monovalent ligand **CJL-1-14** (▲) (A) on energy homeostasis in TSE metabolic cages following a cross-over nocturnal feeding paradigm (Figure 2.3A). Treatment was given

ICV at time 0 h, and food was available *ad libitum* throughout the entire experiment. No significant effects were observed on any parameters. Grey boxes represent lights off. Because no significant differences were observed, no further experiments with this paradigm were performed.

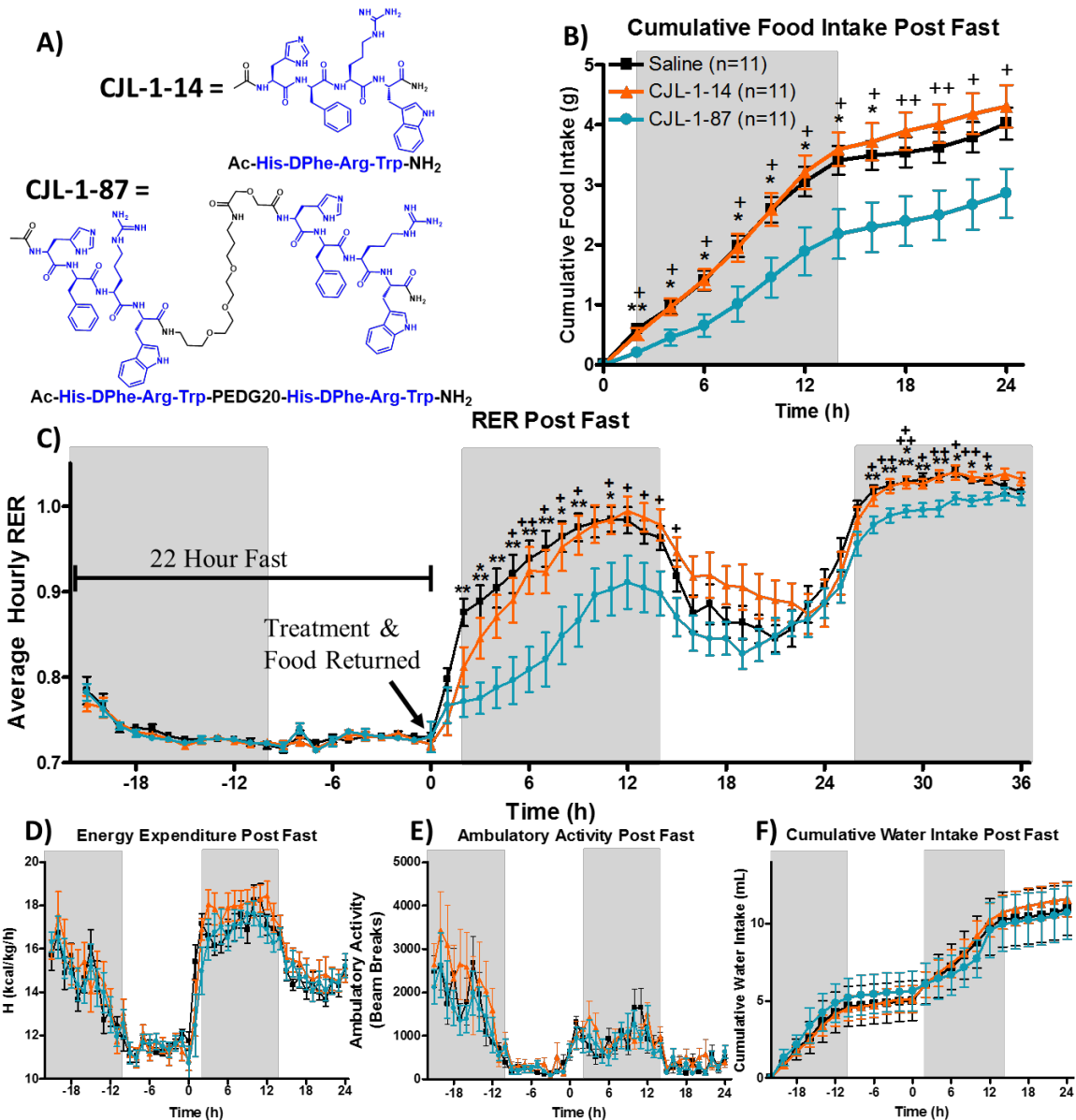


Figure 4.3. Investigation of 5 nmol bivalent ligand **CJL-1-87** (●—) compared to 5 nmol monovalent ligand **CJL-1-14** (▲—) (A) and saline (■—) on energy homeostasis in TSE metabolic cages following a cross-over paradigm (Figure 2.3A). Male mice were fasted starting at the previous light cycle (t=-22 h) until 2 h prior to the light cycle (t=0 h). Treatment was given ICV at time 0 h and food was returned immediately thereafter (Figure

2.3B). Cumulative food intake (B) was significantly reduced by **CJL-1-87** compared to saline and **CJL-1-14**. The RER (C) was significantly reduced after **CJL-1-87** treatment compared to saline and **CJL-1-14**. No significant effects were observed between saline, **CJL-1-14**, and **CJL-1-87** on energy expenditure (D), ambulatory activity (E), or water intake (F). No significant effects were observed on any parameters past 24 h other than RER and, therefore, data is not shown. Grey boxes represent lights off. * $p < 0.05$; ** $p < 0.01$, *** $p < 0.001$ for **CJL-1-87** compared to saline. + $p < 0.05$; ++ $p < 0.01$, +++ $p < 0.001$ **CJL-1-87** for compared to **CJL-1-14**. This figure has been reproduced with permission from Lensing, C. J. *et. al*, *ACS Chem. Neurosci.* **2017**, in press.¹³² Copyright (2017) American Chemical Society.

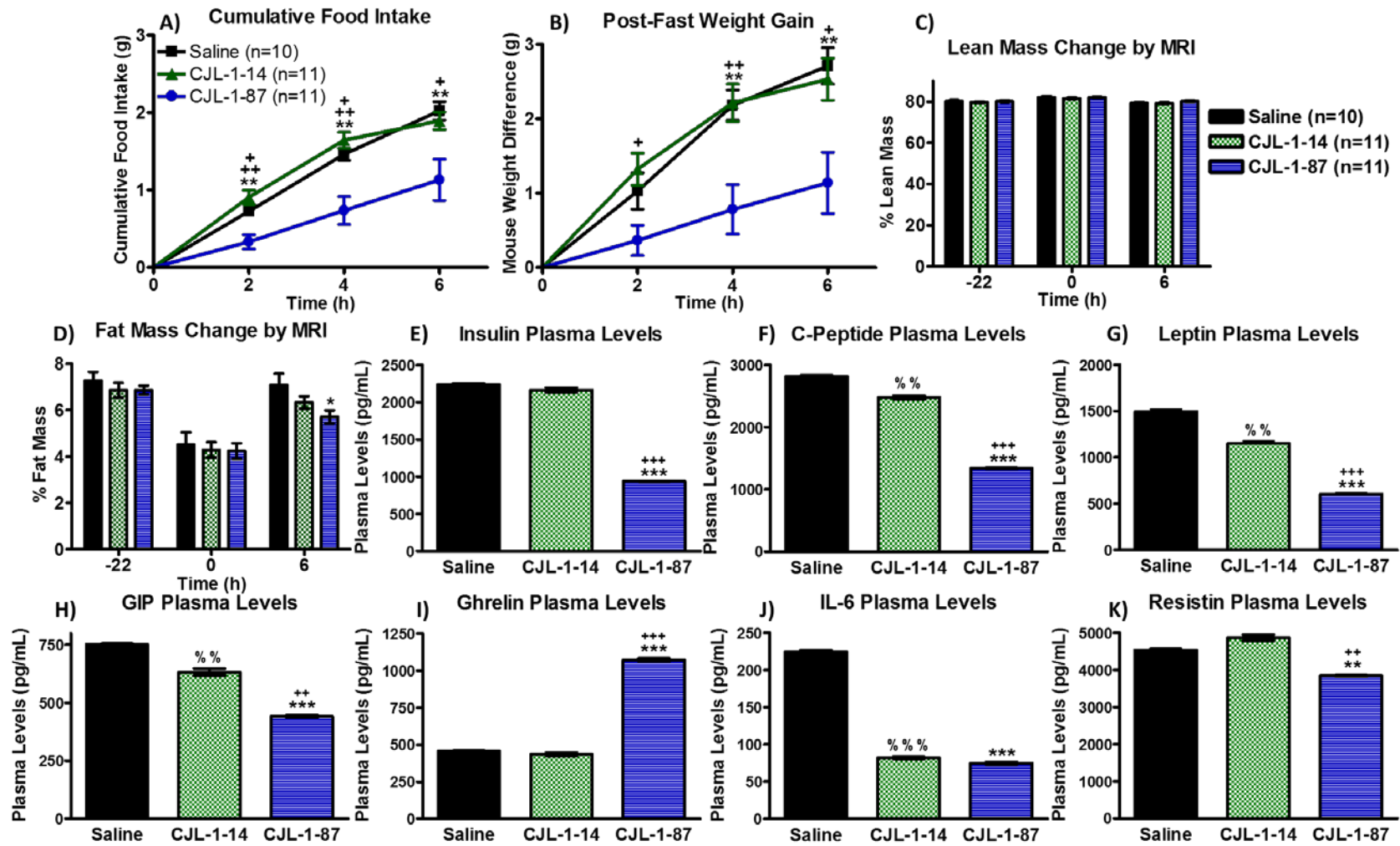


Figure 4.4. A new cohort of male mice received a single treatment of saline vehicle control (■, n=10), 5 nmol **CJL-1-14** (▲, n=11), or 5 nmol **CJL-1-87** (●, n=11) in the fasting paradigm used above (**Figure 2.3B**). **CJL-1-87** treatment resulted in lowered refeeding food intake (A) corresponding to slower regain of body weight (B) measured manually. Measurements using an EchoMRI-100H system showed no change in lean body mass percentage (C), but a significant decrease in body fat mass percentage was observed 6 h after treatment with **CJL-1-87**. (D). Mice were sacrificed 6 h post-treatment and their trunk blood was analyzed using an Luminex Milliplex systems to examine insulin (E), C-peptide (F), leptin (G), GIP (H), ghrelin (I), IL-6 (J), and resistin (K). Hormone and cytokine levels are reported as pg per mL of plasma. Time 0 h was defined as the time of treatment. *p<0.05; **p<0.01; ***p<0.001 for **CJL-1-87** compared to saline. +p<0.05; ++p<0.01; +++p<0.001 for **CJL-1-87** compared to **CJL-1-14**. % p<0.05; %% p<0.01; %%% p<0.001 for **CJL-1-14** compared to saline. This figure has been reproduced with permission from Lensing, C. J. *et. al*, *ACS Chem. Neurosci.* **2017**, in press.¹³² Copyright (2017) American Chemical Society.

Melanocortin Receptor BRET Study

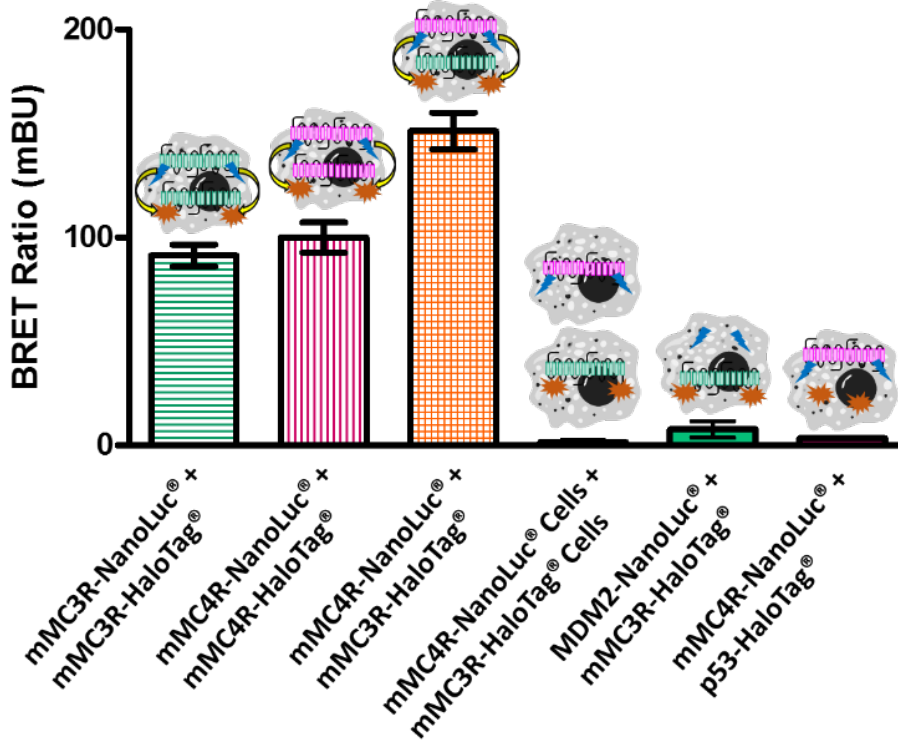


Figure 4.5. Bioluminescence resonance energy transfer (BRET) of the mMC3R and mMC4R. As previously shown in similar systems, coexpression of the mMC3R-NanoLuc® and the mMC3R-HaloTag® result in high BRET signal supporting homodimerization. Similar results were achieved when the mMC4R-NanoLuc® and the mMC4R-HaloTag® were coexpressed. When the mMC4R-NanoLuc® and the mMC3R-HaloTag® are coexpressed an even higher BRET signal is observed suggesting heterodimerization. Cells expressing mMC4R-NanoLuc® were mixed with cells expressing the mMC3R-HaloTag® in equal amounts and produced minimal signal. As a negative control, unrelated mouse double minute 2 (MDM2)-NanoLuc® and the mMC3R-HaloTag® are coexpressed as well as mMC4R-NanoLuc® and the p53-HaloTag®. Both

resulted in minimal signal. Receptors were expressed at a 1:4 donor NanoLuc® plasmid to acceptor HaloTag® plasmid. Data are the mean \pm standard error of the mean (SEM) determined from three independent experiments, except for the mMC4R-NanoLuc® and the mMC3R-HaloTag® coexpression which was performed in six independent experiments. This figure has been reproduced with permission from Lensing, C. J. *et. al*, *ACS Chem. Neurosci.* **2017**, in press.¹³² Copyright (2017) American Chemical Society.

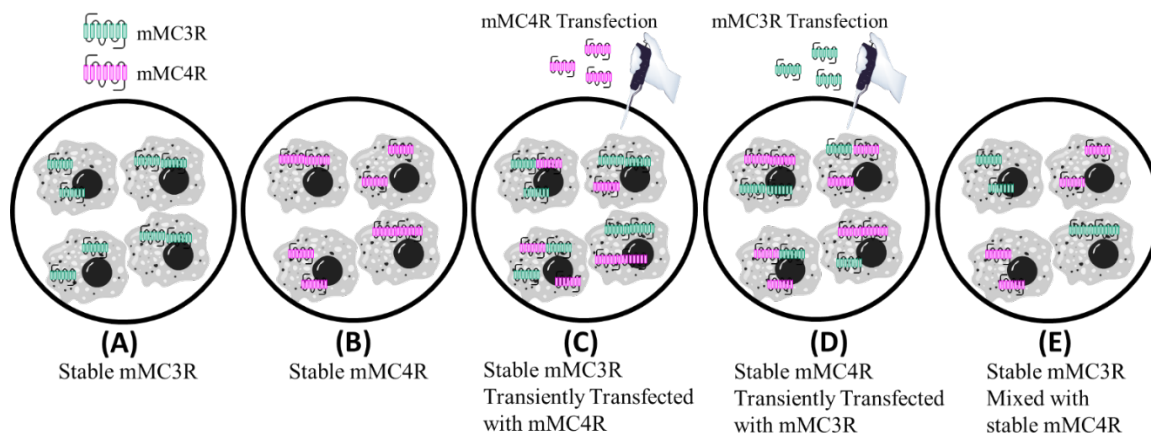


Figure 4.6. Cell categories for cAMP AlphaScreen® functional assays during coexpression experiments (**Table 4.3**). (A) Cells stably expressing mMC3R. (B) Cells stably expressing the mMC4R. (C) Cells stably expressing the mMC3R that were then transiently transfected with mMC4R plasmid. (D) Cells stably expressing the mMC4R that were then transiently transfected with mMC3R plasmid. (E) Cells stably expressing the mMC3R were mixed 1:1 with cells stably expressing the mMC4R. This mixture cannot contain MC3R-MC4R heterodimers. This figure has been reproduced with permission from Lensing, C. J. *et. al*, *ACS Chem. Neurosci.* **2017**, in press.¹³² Copyright (2017) American Chemical Society.

Hormone	Fasting from Lit.	Fasting Citations	MC Agonism from Lit.	MC Agonism Citations	CJL-1-14 (Current Study)	CJL-1-87 (Current Study)
Insulin	↓	243, 265	↓	251-253	↔	↓↓↓
C-Peptide	↓	243, 254, 255, 265	↓	251-255	↓↓	↓↓↓
Leptin	↓	243, 265	↓	252, 253	↓↓	↓↓↓
GIP	↓	256, 266	↓	256	↓↓	↓↓↓
Ghrelin	↑	243, 267	? ↑	263	↔	↑↑↑
IL-6	↑	268	? ↓	259-262	↓↓↓	↓↓↓
Resistin	↓	243, 264	?	257, 258	↔	↓↓

Table 4.1. Summary of the effects of fasting and melanocortin (MC) receptor agonism on hormone and cytokine levels from the literature (Lit.) and the current study. Results from fasting and melanocortin (MC) agonism are from the literature with citations referenced directly to their right. A question mark (?) indicates conflicting results. Results from 5 nmol **CJL-1-14** and **CJL-1-87** treatments are summarized from the current study. In the current studies, the significance of treatment compared to saline treatment is

indicated such that one arrow is $p < 0.05$, two arrows are $p < 0.01$, and three arrows are $p < 0.001$. This table has been adapted with permission from Lensing, C. J. *et. al*, *ACS Chem. Neurosci.* **2017**, in press.¹³² Copyright (2017) American Chemical Society.

Compound	Structure	¹²⁵ I-NDP-MSH IC ₅₀ (nM) ^a		¹²⁵ I-AGRP IC ₅₀ (nM)	
		mMC3R	mMC4R	mMC3R	mMC4R
		Mean±SEM	Mean±SEM	Mean±SEM	Mean±SEM
NDP-MSH		4.2±0.6	1.1±0.1	3.3±0.08	2.6±0.09
CJL1-14	Ac-His-DPhe-Arg-Trp-NH ₂	60% @100 μM	210±60	6200±1700	130±20
CJL1-87	Ac-His-DPhe-Arg-Trp-(PEDG20)-His-DPhe-Arg-Trp-NH ₂	3500±500	9.9±3	330±40	7.5±2
CJL1-80	Ac-His-DNal(2')-Arg-Trp-NH ₂	1400±200	26±3	660±20	12±4
CJL1-140	Ac-His-DNal(2')-Arg-Trp-(PEDG20)-His-DNal(2')-Arg-Trp-NH ₂	350±80	10±0.03	120±10	11±2

Table 4.2: The experimental compounds were used to displace either ¹²⁵I-NDP-MSH or ¹²⁵I-AGRP in a dose-response manner to calculate the IC₅₀ values. The % represents the amount of ¹²⁵I-NDP-MSH signal reduction at 100 μM. The reported errors are the standard error of the mean (SEM) determined from at least two independent experiments. ^aThe IC₅₀ values obtained by competition with ¹²⁵I-NDP-MSH were reported previously in **Chapter 3**, but are included herein for easier comparison.²¹ This table has been adapted with permission from Lensing, C. J. *et. al*, *ACS Chem. Neurosci.* **2017**, in press.¹³² Copyright (2017) American Chemical Society.

Agonist cAMP Based Alpha Screen Results EC ₅₀ (nM)					
Compound	mMC3R	mMC4R	mMC3R Trans mMC4R	mMC4R Trans mMC3R	mMC3R Mixed with mMC4R
	Mean±SEM	Mean±SEM	Mean±SEM	Mean±SEM	Mean±SEM
NDP-MSH	0.13±0.02	0.46±0.07	0.19±0.03	0.12±0.01	0.13±0.02
α-MSH	0.21±0.02	3.1±0.7	0.27±0.05	0.20±0.03	0.19±0.03
MTII	0.10±0.02	0.11±0.03	0.09±0.02	0.06±0.01	0.08±0.02
CJL1-14	23±3	8.5±1	7.7±1	4.0±0.5	9.9±2
CJL1-87	2.6±0.4	1.2±0.3	1.4±0.3	0.63±0.1	2.0±0.4

Table 4.3: Functional cAMP AlphaScreen® assays were performed to determine in vitro potency of compounds to induce cAMP signaling in five cell categories (**Figure 4.6**): (A) stable mMC3R cells, (B) stable mMC4R cells, (C) stable mMC3R cells transiently transfected with mMC4R, (D) stable mMC4R cells transiently transfected with mMC3R, and (E) an equal mixture of stable mMC3R cells and mMC4R cells. All assays and cell categories were run in parallel. The reported standard error of the mean (SEM) was determined from at least three independent experiments. This table has been adapted with permission from Lensing, C. J. *et. al*, *ACS Chem. Neurosci.* **2017**, in press.¹³² Copyright (2017) American Chemical Society.

Chapter 5: Developing Biased Unmatched Bivalent Ligands (BUmBLs) to Target Asymmetrically Signaling Melanocortin-4 Receptor Homodimers

All peptides were designed, synthesized, purified, and analytically characterized by Cody Lensing under the supervision of Carrie Haskell-Luevano. The *in vitro* pharmacology studies were performed by Cody Lensing, Katie Freeman, and Sathya Schnell, all members of the Haskell-Luevano lab group. Radiolabeled ^{125}I -NDP-MSH was prepared by Robert Speth. All animal studies were performed by Cody Lensing, Danielle Adank, and Stacey Wilber. BRET assays were performed by Katie Freeman with Cody Lensing contributing to the design of the experiments. Serum stability studies were performed by Cody Lensing and Adam Zarth.

5.1 Chapter Overview

A major limitation in understanding the functional relevance of homodimerization of G protein-coupled receptors (GPCRs) has been the limited number of molecular tools to assess asymmetric signaling within dimer pairs comprised of the same receptor type. In the chapter, we present melanocortin unmatched bivalent ligands (MUmBLs) as tools for studying asymmetric function of melanocortin receptor homodimers. MUmBLs contain one agonist pharmacophore and one antagonist pharmacophore designed to target a melanocortin homodimer pair such that one protomer is occupied by an agonist and other one by an antagonist pharmacophore. Utilizing this design strategy to target the melanocortin-4 receptor (MC4R), first in class biased unmatched bivalent ligands (BUmBLs) were discovered. The BUmBLs displayed biased agonism in which they

potently stimulated cAMP signaling, but resulted in minimal activation of the β -arrestin recruitment pathway. After *in vitro* characterization, the lead BUmBL (**CJL-5-58**) was evaluated *in vivo* for its effect on energy homeostasis in mice utilizing TSE Phenotypic metabolic cages. These studies indicate a unique pharmacology purportedly due to the BUmBL design strategy employed demonstrating *in vivo* that the agonist pharmacophore overrides the antagonist pharmacophore in the regulation of food intake behavior. To the best of our knowledge, we report the first single compound design strategy to pharmacologically target melanocortin receptor allosteric signaling that occurs between putative GPCR homodimers that can be applied easily both *in vitro* and *in vivo* to other GPCR systems.

5.2 Introduction

G protein-coupled receptors (GPCRs) are highly sought after drug targets in the pharmaceutical industry with approximately 30-40% of drugs targeting them.^{2, 3} Classically, medicinal chemists targeted GPCRs as monomeric units; however increasing evidence has shown GPCRs form dimers with themselves (homodimers) and with other GPCRs (heterodimers).^{4, 272} Targeting GPCR homodimers' and heterodimers' distinct and exploitable functions may yield a revolution in GPCR targeting therapeutics. Although ligands targeting heterodimers have shown much promise in both *in vitro* and *in vivo* preclinical studies,^{10, 11, 44, 46, 48} there has been limited development of ligands targeting the allostereism that can occur within homodimers.

Pharmacologically targeting homodimers possess a unique conundrum: How do you target and detect a homodimer when the two receptors comprising it are structurally similar, usually respond to the same ligands, and appear to have the same propensity to signal in standard cell culture assays? Various groups have devised clever strategies around these problems to demonstrate the functional consequences of asymmetric homodimers.^{207, 231, 273-287} Some of these groups focus on demonstrating subtle changes in pharmacology utilizing strategically designed *in vitro* experiments and other groups exploited receptor mutation strategies in order to differentiate between the two protomers making up the dimer.^{207, 231, 273-287} For example, Han and coworkers in 2009 combined different receptor-G protein fusions and various mutant receptors to demonstrate allosteric modulation within a dopamine homodimer.²³¹ They reported that the D2 dopamine receptor homodimers are maximally activated upon a single agonist binding a single protomer in the dimer pair. When a second agonist binds the second protomer, it blunts the signal. If an inverse agonist binds the second protomer, it actually enhances the signal beyond agonist alone.²³¹ In a different strategy, Teitler and coworkers developed pseudo-irreversible inactivators and reactivators that can be used to block only one of the protomers within the dimer pair in order to demonstrate the crosstalk within wild type serotonin homodimers.²⁷⁴ This approach can and has been used to demonstrate the allosteric regulation within homodimers in native tissue samples, however application of this technique *in vivo* would be difficult given the multiple dosing regimen necessary and, therefore, would have very limited therapeutic applications.²⁷⁴ Although these reports provide critical proof of the relevancy

and functional significance of asymmetric signaling homodimers, the techniques employed are limited by their use of receptor mutations or subtle pharmacological differences that make adaption of the approaches to *in vivo* applications difficult and therapeutic applications inexecutable. Ideally, a pharmacological approach is needed to target and exploit allosteric communication between homodimers with a single chemical entity that could be used to examine the *in vivo* effects of native asymmetric GPCR homodimers in order to study their potential as therapeutic targets.

As discussed in **Chapter 1**, one approach to pharmacologically targeting GPCR dimers is utilizing bivalent ligands. This approach was pioneered Portoghese and coworkers targeting the opioid receptors.^{7, 12} Heterobivalent ligands featuring pharmacophores for two different receptor types have been utilized to exploit allosteric interactions within heterodimers to develop ligands with novel pharmacological profiles, tissue selectivity, and different functional effects.^{10, 11, 44-47} However, to our knowledge, no one has exploited the allosteric communication that may occur between homodimers with bivalent ligands to produce novel pharmacologies. In the current report, we exploit the allosteric communication between melanocortin-4 receptor (MC4R) homodimers with melanocortin unmatched bivalent ligands (MUmBLs) to produce biased agonists. Unmatched bivalent ligands (UmBLs) have an agonist pharmacophore on one side of the bivalent ligand connected to an antagonist pharmacophore through an inert linker. We use the term UmBLs to separate this class of ligands from heterobivalent ligands that also have different pharmacophores on each side of the bivalent ligand, but are usually used to target

different receptor types. This type of ligand design has been proposed and reported previously, however, to our knowledge they have not been used to successfully exploit asymmetric signaling of GPCR homodimers.^{22, 30, 288} One of the best examples of the UmBL strategy was reported by Kühhorn and coworkers. They reported UmBLs targeting the dopamine D₂ receptors that had some agonist efficacy (13% maximal) and did not induce receptor internalization suggesting biased agonism may be possible with this design strategy, although they conclude “ligand bias” was not accomplished.²²

In **Chapter 3** and **Chapter 4**, both agonist and antagonist homobivalent ligands targeting the melanocortin receptor system were described.^{25, 132} It is hypothesized that ligands that target melanocortin homodimers may have unique effects from the current monovalent approaches, and may, therefore circumvent some side effects. In these chapter, we show that an agonist homobivalent ligand produces a distinct *in vivo* pharmacological profile compared to monovalent counterpart suggesting that targeting melanocortin dimers may have therapeutic relevancy.¹³² Furthermore, biased ligands would be valuable pharmacological probes to elucidate which signaling pathway is responsible for the various melanocortin dependent effects (*i.e.* lowered food intake vs increased blood pressure). In this chapter, we report the design and synthesis of MUmBLs to target asymmetrically signaling melanocortin homodimers. We study the *in vitro* effects of these ligands in competitive binding assays, functional cAMP assays, and β -arrestin recruitment assays. A biased agonist for cAMP pathway over the β -arrestin pathway was discovered which has not been reported in the literature for the melanocortin receptors to date. Lead ligand **CJL-**

5-58 was studied *in vivo* using mice housed in TSE Phenotypic metabolic cages to demonstrate unique effects on energy homeostasis presumably due to the bivalent ligand design. The current study provides novel molecular probes for the melanocortin receptors as well as an *in vitro* and *in vivo* proof-of-concept of using the BUmBL design strategy to target asymmetrically signaling homodimers. This innovative design strategy that could be applied to various GPCR systems for the creation of biased ligands.

5.3. Results and Discussion

5.3.1 Design and Synthesis

As discussed in **Chapter 3**, homobivalent ligands targeting melanocortin receptors have previously resulted in increased binding affinity (~14 to 25-fold) consistent with a synergistic binding mode resulting from receptor dimer binding.^{25, 26, 28-31, 33-37, 132} In spite of an increased binding affinity, we have observed much smaller fold increases in cAMP based functional activity (3 to 5-fold).²⁵ Hruby and coworkers noted similar effects with melanocortin bivalent ligands in which cAMP accumulation was not as dramatically increased with synergistic multivalent binding.²⁸ One possibility for the incongruity between binding affinity increases and functional signaling increases with bivalent ligands may be due to allostery between the melanocortin receptors within homodimers.²⁵

A new paradigm can be hypothesized that one receptor within the melanocortin homodimer might be responsible for cAMP signaling and the other receptor might be responsible for signaling through a different cellular pathway (*e.g.* β -arrestin recruitment pathway) (**Figure 5.1A-B**). It would then follow that the increased binding would not

necessarily result in an increase in functional agonist activity observed in a cAMP assay, since the effect of the second binding event is not detected by this cellular assay paradigm. Furthermore, there has been reports of asymmetry within melanocortin homodimers in both binding experiments and functional assays.^{205-207, 219} In order to exploit this possibility of asymmetric homodimers, we designed and synthesized MUmBLs that contained the known agonist melanocortin moiety His-DPhe-Arg-Trp on one side of the molecule,^{96, 98} and the known MC3R and MC4R antagonist moiety His-DNal(2')-Arg-Trp^{97, 289} connected by three different linker systems previously validated in **Chapter 3 (Table 5.1)**.^{25, 30, 31, 168} We also synthesized and biologically evaluated MUmBLs that contained the His-DPhe(p-I)-Arg-Trp moiety on one side of the molecule. Due to the discrepancies with the tetrapeptide Ac-His-DPhe(p-I)-Arg-Trp-NH₂ between the cAMP AlphaScreen assay and CRE/ β -galactosidase reporter gene assay described thoroughly in Chapter 3 Section 3.4.1, the biological results of these His-DPhe(p-I)-Arg-Trp containing MUmBLs are difficult to interpret. Therefore, these peptides will not be discussed further, but their characterization and functional assessment can be found the appendix.

Because bivalent ligands presumably occupy both orthosteric binding sites in a receptor dimer due to synergistic binding, a MUmBL is postulated to occupy one receptor within a homodimer pair with an agonist pharmacophore and the other receptor within the same homodimer with an antagonist pharmacophore (**Figure 5.1C**). This assumes approximately equal binding affinities of the pharmacophores, and low enough concentrations of ligand so that intermolecular competition does not occur. The MUmBLs

should favor a bivalent binding mode supported in Chapter 3 pushing the equilibrium towards occupation of one receptor with agonist and the other receptor with antagonist in the homodimer, but other binding states probably exist in equilibrium (**Figure 5.2**). It should also be noted, that we are currently assuming that only orthosteric binding is occurring, because allosteric binding has never been reported with either the His-DPhe-Arg-Trp or the His-DNal(2')-Arg-Trp pharmacophores even though they both have been extensively studied as tetrapeptides and in standard control ligands NDP-MSH and SHU9119.⁹⁴⁻⁹⁷ Both of these tetrapeptides are also direct competitors of ¹²⁵I-NDP-MSH and ¹²⁵I-AGRP(87-132) that further validates an orthosteric binding mode.^{1, 25, 132}

Ligands **CJL-1-124**, **CJL-5-74**, and **CJL-1-63** feature the His-DPhe-Arg-Trp scaffold on the C-terminus and the His-DNal(2')-Arg-Trp scaffold on the N-terminus (**Table 5.1**). Since the molecules are not symmetric, the opposite composition of **CJL-1-124** was designed and synthesized with the His-DNal(2')-Arg-Trp scaffold on the C-terminus and His-DPhe-Arg-Trp scaffold on the N-terminus in compound **CJL-5-58**. In particular, the construction of **CJL-5-58** with the PEDG20 linker system was selected because this linker system was previously shown to be optimal in homobivalent ligands compared to the PEDG20-PEDG20 or Pro-Gly linker systems at the mMC4R.^{25, 30} Also in **Chapter 4**, the PEDG20 linker was shown to be more metabolically stable than the Pro-Gly linker system and would allow *in vivo* applications.¹³² In an *in vitro* mouse serum stability assay, **CJL-5-58** had similar serum stability (half-life = 6.9 h) as the previously reported **CJL-1-87** confirming the PEDG20 linker selection (**Figure 5.3**).¹³²

Bivalent melanocortin ligands featuring agonist and antagonist pharmacophores were synthesized previously and were reported to possess increased binding affinity.³⁰ These ligands provide evidence that UmBLs can bind hMC4R homodimers, but no functional activity was evaluated.^{30, 290} Therefore, the effects of functional asymmetric homodimers could not be detected. In the current study, all compounds were synthesized using standard Fmoc chemistry utilizing solid-phase synthesis methodology.^{191, 228, 291} A split resin approach for control ligands and bivalent ligands was performed as described in **Chapter 2**.²⁵ The ligands were purified to >95% by semi-preparative RP-HPLC and their mass was confirmed by ESI-MS (**Table 5.2**). The inclusion of compound from Chapter 3 and Chapter 4 are provided for easier comparison currently.

5.3.2 Biased Signaling at the hMC4R

Upon agonist stimulation, melanocortin receptors are known to signal through a G α_s -protein mediated signaling pathway that results in intracellular cAMP accumulation. Agonist stimulation of the melanocortin receptors also results in β -arrestin recruitment and receptor desensitization.¹⁹⁹⁻²⁰¹ In order to evaluate the ligands efficacy and potency to stimulate cAMP signaling, the ALPHAScreen™ cAMP Assay Technology was utilized to assess live HEK293 cells stably expressing human (h)MC4R.^{292, 293} All ligands that contained the His-DPhe-Arg-Trp pharmacophore, including the MUmBLs, were single-digit or sub-nanomolar agonists in the cAMP assay (**Table 5.1, Figure 5.4A**). The most potent ligand (besides control ligand NDP-MSH) was the bivalent ligand **CJL-1-87** that had an EC₅₀ of 570 pM and was 3-fold more potent than its monovalent counterpart **CJL-**

1-14. This result was similar to that previously observed in **Chapter 3** with **CJL-1-87** at the mouse (m)MC4R.²⁵ The ligands that only contained the His-DNal(2')-Arg-Trp antagonist scaffold were not able to elicit a full response when tested up to 10 μ M. Homobivalent ligand **CJL-1-140** with two His-DNal(2')-Arg-Trp resulted in 70% cAMP accumulation of that seen with NDP-MSH at 10 μ M which is also consistent with previous reports at the mouse receptors in **Chapter 3**.²⁵ These results suggest that there is minimal species variation within the monovalent and homobivalent ligands currently tested.

The MUmBLs (*i.e.* **CJL-1-63**, **CJL-5-58**, **CJL-1-124**, and **CJL-5-74**) were all single digit nanomolar potent agonists at the hMC4R. For comparison with the MUmBLs, as a control an equal mixture of tetrapeptides **CJL-1-14** + **CJL-1-80** was assayed and resulted in an agonist dose response curve with an EC₅₀ of 1.9 \pm 0.2 nM. In order to give the best comparison to the MUmBLs, 1 nM of the tetrapeptide mixture contained 1 nM **CJL-1-14** and 1 nM **CJL-1-80** (for a final concentration of 2 nM total peptide) was tested. This would be directly comparable to 1 nM of a MUmBL when looking at final pharmacophore concentration. From this data, it appears that antagonist scaffold His-DNal(2')-Arg-Trp is not capable of effecting the cAMP agonist pharmacology of His-DPhe-Arg-Trp agonist scaffold when mixed in equal portions.

Theoretically, if both the agonist scaffold and antagonist scaffolds compete equally for binding, then at 100% receptor occupancy 50% of the receptors would be occupied by agonist tetrapeptide scaffold and 50% would be occupied by the antagonist tetrapeptide scaffold (**Figure 5.2 A-B, E-J**). Based on this assumption, the MUmBLs full cAMP agonist

pharmacology would be achieved by only 50% receptor occupancy by the agonist scaffold at the receptors, since the antagonist scaffold would be occupying approximately 50% of the receptors. This is consistent with both the spare receptor theory,^{294, 295} and the hypothesis presented above for asymmetric signaling homodimers in which ~50% of the receptors are responsible for β -arrestin recruitment and 50% are responsible for cAMP signaling (**Figure 5.1**). In practice, the MUmBLs may be binding to the melanocortin receptor monomers, dimers, and/or higher-order oligomers and may not be binding in exactly equal amounts of agonist and antagonist due to intermolecular competition. (**Figure 5.2**)

It was, therefore, hypothesized that the second binding event within the GPCR dimer may be responsible for a different functional response. It has previously been observed that β -arrestin recruitment of one protomer within the AT₁ angiotensin receptor homodimer can be allosterically regulated by selective stimulation of the other protomer.²⁸² In order to examine if β -arrestin recruitment to the hMC4R was regulated differently by MUmBLs versus agonist or antagonist homobivalent ligands, we utilized the PRESTO-Tango assay developed by Roth and colleagues.^{202, 203} The PRESTO-Tango technology is an open-source resource that has been utilized to identify ligands for orphan receptors based on β -arrestin recruitment. This assay has previously been validated at the hMC4R that agonist stimulation results in β -arrestin recruitment.²⁰² In agreement with these results, classic monovalent agonist ligands result in the recruitment of β -arrestin and high signal (**Table 5.1, Figure 5.4B-C**). The classical melanocortin control agonists NDP-MSH, MTII

and the tetrapeptide Ac-His-DPhe-Arg-Trp-NH₂ all resulted in maximal β -arrestin recruitment with MTII being the most potent ligand. The linker control and homobivalent ligands that featured only the His-DPhe-Arg-Trp pharmacophore all resulted in maximal β -arrestin recruitment relative to NDP-MSH control. Among the linker controls, compound **CJL-5-35-4** with the PEDG20 linker on the C-terminus resulted in a 5-fold increase in β -arrestin recruitment compared to the tetrapeptide **CJL-1-14**. This ligand also resulted in a 3-fold increase in the cAMP signaling assay. The other PEDG20 linker compound **CJL-1-116** resulted in less than a 3-fold increase in β -arrestin recruitment compared to **CJL-1-14**. The His-DPhe-Arg-Trp that utilized the Pro-Gly linker system did result in a decrease in the potency for β -arrestin recruitment in spite of them retaining their full cAMP pathway functional activity.

The ligands containing only the antagonist His-DNal(2')-Arg-Trp pharmacophore resulted in minimal β -arrestin recruitment consistent with a classical antagonist pharmacology. The tetrapeptide Ac-His-DNal(2')-Arg-Trp-NH₂ resulted in 30% response at 10 μ M compared to the maximal efficacy of NDP-MSH. The other linker control ligands and the bivalent ligand **CJL-1-140** resulted in equal or lower β -arrestin recruitment. This result was not surprising given the antagonist nature of these compounds and that antagonists have previously been reported to result in minimal β -arrestin recruitment and receptor internalization.¹⁹⁹⁻²⁰¹

Interestingly, the MUmBLs resulted in minimal β -arrestin recruitment. The most potent MUmBL was **CJL-1-63** that resulted in 55% maximal efficacy at 10 μ M compared

to NDP-MSH. All other MUmBLs resulted in less β -arrestin recruitment. Because these ligands still potently stimulate cAMP signaling but result in minimal β -arrestin recruitment, it supports the current hypothesis that one pharmacophore is responsible for the activation of the cAMP pathway, but the other pharmacophore is responsible for the β -arrestin recruitment. When a bivalent ligand is comprised of an agonist pharmacophore and an antagonist pharmacophore, it should bind to a GPCR dimer in equal portions. The agonist pharmacophore would then signal effectively through the cAMP pathway, but the antagonist pharmacophore would block the β -arrestin recruitment pathway (**Figure 5.1**). The current results are not consistent with the current dogma in the field, however, these results may be explained by the asymmetric allosteric signaling within GPCR homodimers.

Although there have been reports of biased agonists at different melanocortin pathways including cAMP, calcium mobilization, and receptor internalization,²⁹⁶⁻²⁹⁸ to the best of our knowledge the MUmBLs are the first melanocortin biased agonists for the cAMP pathway over the β -arrestin recruitment pathway. Biased ligands for GPCRs have been of interest for future drug development due their distinct pharmacology and functional selectivity.^{299, 300} In particular, it is hypothesized that biased ligands stabilize a specific conformation of the receptor that favors one signaling pathway over another.^{299, 300} We currently hypothesize similarly that the MUmBLs stabilize specific dimer conformational states (as opposed to monomeric receptor conformational states) that results in the cAMP-signaling biased agonism.

An explanation of the biased agonism is through a model for allosterically interacting receptor dimers (**Figure 5.5**).^{301, 302} In this model, one receptor within a dimer can allosterically stabilize the other receptor within the dimer to different conformations. These different conformations are thought to be dynamic in that the receptors oscillate between the different states even with no ligand present.³⁰¹ However, it is postulated that with no ligand bound both receptors are conformationally open to cAMP signaling upon agonist stimulation (**Figure 5.5A**). After the first agonist binding event, a conformational change occurs which induces cAMP signaling pathway (**Figure 5.5B**) and this conformational change allosterically modifies the second receptor to have a propensity to signal through the β -arrestin pathway (**Figure 5.5E**). For this reason, monovalent agonist ligands, homobivalent agonist ligands, and the MUmBLs all produce full agonist cAMP induction, since the first agonist binding event is similar. After the first agonist binding event, the second receptor in the dimer is hypothesized to have structural bias for β -arrestin recruitment upon agonist binding. Therefore, the second agonist binding event results in β -arrestin recruitment (**Figure 5.5F**). This is the same for monovalent and homobivalent agonist ligands since both result in a second agonist binding event and this is observed in full β -arrestin recruitment results (**Figure 5.4**). However, the MUmBLs result in an antagonist binding the second receptor instead of another agonist. The MUmBL's antagonist pharmacophore prevents β -arrestin recruitment that results in minimal signal in the PRESTO-Tango assay (**Figure 5.5G-I**).

There is an assumption above that the agonist tetrapeptide scaffold of the MUmBLs binds first before the antagonist tetrapeptide scaffold, but in practice the order of binding is not determined (**Figure 5.5J-L**). However, antagonist scaffolds restrict the GPCR from accessing conformational states that result in GPCR signaling (*i.e.* G-protein or β -arrestin). Therefore, even if the antagonist does bind first to the receptor dimer pair (**Figure 5.5K**), it would not induce G-protein signaling. Instead it would still require the first agonist binding event to the second receptor in the dimer pair to occur that would result in cAMP signaling (**Figure 5.4A**), and allosteric modulation to the β -arrestin ready state. However, the antagonist scaffold would already be bound to the dimer, and would block β -arrestin recruitment resulting in minimal PRESTO-Tango signal (**Figure 5.4B**).

This interpretation of the data is based on the model for allosteric interaction in receptor dimers that has previously been reported.^{301, 302} However, to add further complexity to the current model, it has been supported that GPCRs oscillate between monomeric, dimeric, and high-order oligomeric states and models that include these states have also been proposed (**Figure 5.2**).^{301, 302, 206, 207, 214} Also the MUmBLs may bind in various different ways such that antagonist scaffold displaces the agonist scaffolds or vice versa resulting in more agonist scaffolds bound than antagonist scaffolds. These different conformational states may help explain the β -arrestin recruitment observed at higher concentrations of the MUmBLs. It is predicted that similar states are present in various GPCR systems, and that a biased unmatched bivalent ligand (BUmBL) design strategy

could be applied to any asymmetric GPCR homodimer system for the creation of biased ligands.

This model may help explain a variety of observations in the field related to melanocortin dimerization and oligomerization. For example, Piechowski and coworkers reported in 2013 that disruption of hMC4R homodimerization leads to increased cAMP signaling capacity (or efficacy) although receptor expression was unchanged.²⁰⁶ This can be explained by the current model of asymmetric homodimers (**Figure 5.1**), since disruption of the dimer to monomers would increase the amount of receptors capable of accessing the cAMP signaling states (**Figure 5.5 B**). In other words, with more monomers there would be less receptors being allosterically modulated to signal through β -arrestin recruitment since the asymmetric signaling could not occur. Therefore, more receptors would signal through the cAMP signaling pathway upon agonist binding increasing signaling capacity. To experimentally establish this hypothesis further, a concerted effort of pharmacological intervention, receptor mutagenesis and other techniques would be necessary. For this thesis, we are delighted that using the hypothesis of asymmetrically signaling melanocortin homodimers allowed for the creation of first-in-class biased agonists for the cAMP signaling over the β -arrestin recruitment, even if the hypothesis still needs further validation.

5.3.3 Characterization of cAMP Signaling at the Mouse Melanocortin Receptors

Initial *in vivo* evaluations are often performed in mouse models, therefore, we evaluated the MUmBLs ability to promote cAMP signaling in HEK293 cells stably

expressing the mouse (m)MC1R, mMC3R, mMC4R, and mMC5R. The MC2R was excluded from the study as it has been reported to only be stimulated by ACTH.⁴⁹ The mouse receptor pharmacology for control ligands (except **CJL-5-35-2**) and homobivalent ligands were previously discussed in **Chapter 3**,²⁵ but are also included for complete comparison in **Table 5.3** and **Table 5.4** and **Table 5.5**. In order to compare the pharmacology of the MUmBLs, a tetrapeptide mixture of **CJL-1-14** and **CJL1-80** in equal proportions was assayed as controls as discussed above.

Similar to the hMC4R, the MUmBLs displayed some agonist activity at all four receptors subtypes (**Table 5.3, Figure 5.6**). At the mMC1R, both the Ac-His-DPhe-Arg-Trp-NH₂ and Ac-His-DNal(2')-Arg-Trp-NH₂ function as agonists ($EC_{50} = 14$ nM and 98 nM, respectively). Functional data from the mixture of **CJL-1-14** and **CJL-1-80** were equipotent as the most potent agonist monovalent ligand **CJL-1-14**. Changes <3-fold were considered to be within the intrinsic error of the assay (in our hands). Similar potency was observed with MUmBL compounds **CJL-1-63**, **CJL-5-58**, and **CJL-1-124** at the mMC1R (**Figure 5.6A**). Compounds **CJL-1-14**, **CJL-5-58**, and **CJL-1-124** were more than 3-fold potent compared to **CJL-5-74**. In Chapter 3, we observed that the 40 atom PEDG20-PEDG20 linker was not optimal for bivalent binding most likely due to linker being too long,²⁵ and the non-optimal linker may be responsible for the decreased potency of **CJL-5-74**. At the mMC5R, all MUmBL compounds were comparable to the mixture of **CJL-1-14** and **CJL-1-80** in their cAMP potency (**Figure 5.6D**).

At the mMC3R, the mixture of **CJL-1-14** and **CJL-1-80** seemed to match the functional activity of **CJL-1-14** from 10^{-11} to 10^{-7} M, but began plateauing at 75% max efficacy of NDP-MSH at 10 μ M. (**Table 5.3, Figure 5.6B**). This loss of max efficacy is postulated to be due to the antagonism of the **CJL-1-80** ($pA_2=6.04$, $K_i= 912$ nM) in the mixture which is known to possess a more potent binding affinity than **CJL-1-14** at the mMC3R (**Table 5.3**).²⁵ Unlike the control mixture, all MUmBLs resulted in full nanomolar cAMP agonist activity ($EC_{50} = 15-30$ nM) at the mMC3R. Compounds **CJL-1-63** and **CJL-1-124** were >3-fold more potent than the tetrapeptide **CJL-1-14** alone, and **CJL-5-58** and **CJL-5-74** trended towards increased potency. This suggests the MUmBL design at the mMC3R favors **CJL-1-14** tetrapeptide's agonism overriding **CJL-1-80** tetrapeptide's antagonist properties which is consistent with the hypothesized asymmetry of melanocortin homodimers (**Figure 5.1**).

At the mMC4R, the mixture of **CJL-1-14** and **CJL-1-80** resulted in partial agonism with a max efficacy of 50% at 10 μ M. (**Table 5.3, Figure 5.6C**). This decrease in max efficacy likely resulted due to the competition between the strong full agonism of **CJL-1-14** ($EC_{50} = 14$ nM) with the strong antagonism of **CJL-1-80** ($pA_2 = 8.09$, $K_i = 8.1$ nM) at the mMC4R. Interestingly, unlike the mMC3R, two MUmBLs, **CJL-1-124** and **CJL-5-74**, have similar pharmacologies as the tetrapeptide mixture both resulting in partial agonism. However, MUmBLs **CJL-5-58** and **CJL-1-63** were both potent agonist with EC_{50} values of about 13 nM. The partial agonist properties observed with both the mixture of **CJL-1-14** and **CJL-1-80** and the MUmBLs **CJL-1-124** and **CJL-5-74** demonstrates a species

difference between the mouse and human MC4R. This demonstrates the importance of performing *in vitro* pharmacology on species specific receptors for *in vivo* interpretation. The partial agonism of bifunctional ligands possessing agonist pharmacophores and antagonist pharmacophores were predicted by simulation data by Zhu in 2005.³⁰³ However, the full agonism observed with **CJL-5-58** and **CJL-1-63** was unexpected. The pharmacology differences between **CJL-5-58** and **CJL-1-63** compared to **CJL-1-124** and **CJL-5-74** were also unexpected considering these differences were not observed at the other four receptor types assayed (*i.e.* mMC1R, mMC3R, mMC5R, and hMC4R). Both of these pharmacologies have much interest as pharmacology probes. Especially considering this design strategy should be applicable to various GPCR systems.

In contemplating the usefulness of intentionally designing partial agonists such as **CJL-1-124** and **CJL-5-74**, we thought about their possible ability to increase a therapeutic window. This design of partial agonist GPCR UmBLs may offer an approach to increase the therapeutic window of GPCR ligands, since these compounds resulted in 50% receptor activation for a wider dose response window compared to standard agonist compounds (**Figure 5.7**). This may happen in cases where full functional activation may result in side effects or characteristics that lead to abuse (*e.g.* euphoria), however partial functional activation is therapeutic. Partial agonisms may therefore allow the drug to remain in the therapeutic window for much longer without side effects and result in easier dosing.

In contrast to this partial agonism, **CJL-5-58** and **CJL-1-63** were observed to be full nanomolar potent agonists with similar pharmacologies to monovalent ligand **CJL-1-**

14 ($EC_{50} = 14$ nM). The full agonism observed at the mMC3R with all MUmBLs and at the mMC4R with **CJL-5-58** and **CJL-1-63** is consistent with the hypothesis that only one receptor in a dimer pair needs agonist activation for full cAMP signal transduction, but not the second receptor in the putative GPCR dimer. In an idealized bivalent binding mode, each dimer is occupied by one bivalent ligand assuming equal binding affinity of both pharmacophores. In the case of MUmBLs, each mMC3R or mMC4R homodimer is hypothesized to have one receptor occupied by the His-DPhe-Arg-Trp agonist pharmacophore or His-DNal(2')-Arg-Trp antagonist pharmacophore. This results in full cAMP signaling from the His-DPhe-Arg-Trp agonist pharmacophore, but the His-DNal(2')-Arg-Trp antagonist pharmacophore results in minimal β -arrestin recruitment (**Figure 5.1C**). Furthermore, given the consistent pharmacology with the human and mouse receptor isoforms and the better metabolic stability of the PEDG20 linker (**Figure 5.3**), **CJL-5-58** stands out as a lead ligand for *in vivo* characterization.

The most interesting part of the MUmBL SAR is the comparison of **CJL-5-58** and **CJL-1-124** at the mMC4R that possess the same linker system, but **CJL-5-58** resulted in a full agonist response curve in cAMP signaling ($EC_{50} = 14 \pm 6$ nM) and **CJL-1-124** resulted in a partial agonist (55% activation at 10 μ M). The difference between the two ligands is that the His-DNal(2')-Arg-Trp antagonist is on the N-terminus of **CJL-1-124** but on the C-terminus of **CJL-5-58**; and the His-DPhe-Arg-Trp pharmacophore is present C-terminus in **CJL-5-58** and the N-terminus of **CJL-1-124**. Since the current ligands are not symmetrical, this suggest the three-dimensional orientation of the pharmacophores effects

the *in vitro* receptor pharmacology at the mMC4R but not at any of the other melanocortin receptors examined in this study.

For the sake of comparison based on the site of attachment of the linker to the pharmacophore (N- versus C-terminus), compound **CJL-5-58** can be thought to be comprised of **CJL5-35-4** and **CJL-1-132**. Compound **CJL-1-124** can be considered to be comprised of **CJL5-35-2** and **CJL-1-116**. The His-DPhe-Arg-Trp based compound **CJL-5-35-4** ($EC_{50}= 5.7\pm 2.9$) with the PEDG20 linker on the C-terminus as seen in **CJL-5-58** was 3-fold more potent at the mMC4R than **CJL-1-116** ($EC_{50}= 18.5\pm 2.9$) with the PEDG20 linker on the N-terminus as seen in **CJL-1-124**. The His-DNal(2')-Arg-Trp based compound **CJL-1-132** ($pA_2=7.97\pm 0.29$) with the PEDG20 linker on the N-terminus as seen in **CJL-5-58** resulted in 15% maximal agonist activation at 10 μ M at the mMC4R compared to the 10% observed with **CJL-5-35-5** ($pA_2=8.38\pm 0.08$) with the PEDG20 linker at the C-terminus as seen in **CJL-1-124** (Table 5.4). The components that comprise **CJL-5-58** do appear to have more propensity for agonism, however, these small differences are postulated not to be the driving force between the large pharmacological differences observed at the mMC4R. In order to examine the pharmacology of these compound in more detail, competitive displacement binding assays were performed.

5.3.4 ¹²⁵I-NDP-MSH Competitive Binding Assays.

Competitive radioligand binding assays were utilized to further understand the *in vitro* molecular pharmacology of the MUmBL design strategy at the mMC3R and mMC4R (Table 5.3, Figure 5.8, Figure 5.9). Although ligand development towards the mMC1R

was not the focus of the current study, the binding data was included since the MC1R has been identified as a drug target and a potential melanoma diagnostic target (**Figure 5.9**).^{117, 158} It has previously been shown that bivalent ligands can dramatically increase the binding affinity compared to monovalent ligands due to a synergistic binding event and lowered entropic cost of binding.^{7, 25}

At the mMC1R, the MUmBLs resulted in increased binding affinity even compared to the tightest binding tetrapeptide scaffold **CJL-1-14**. Compound **CJL-1-63** with the (Pro-Gly)₆ linker resulted in a 7-fold decreased IC₅₀ value which was the highest binding affinity for the mMC1R among the MUmBLs (**Table 5.3, Figure 5.9**). This was consistent with previous results that the mMC1R preferred the (Pro-Gly)₆ linker over the PEDG20 and PEDG20-PEDG20 linker systems in homobivalent ligands (**Table 5.5**).²⁵ It should be noted that the binding affinities of the tetrapeptide scaffolds **CJL-1-14** and **CJL-1-80** that make up the MUmBLs are different by more than 4-fold at all the receptor subtypes examined in this study. In theory, this difference in binding affinity of the tetrapeptide scaffolds results in the higher affinity scaffold on one side of the MUmBL acting as a “targeting” region to bring the lower affinity scaffold to the second binding site in the homodimer assuming all binding is orthosteric. The entropic gains from a bivalent binding mode for the lower affinity tetrapeptide scaffold (*i.e.* His-DNal(2’)-Arg-Trp at the mMC1R, or His-DPhe-Arg-Trp at the mMC3R and mMC4R) would be much greater than the gains for the tighter binding tetrapeptide scaffold (*i.e.* His-DPhe-Arg-Trp at the mMC1R, or His-DNal(2’)-Arg-Trp at the mMC3R and mMC4R). This is observed in

compound **CJL-1-63** at the mMC1R that has a 28-fold increase in binding affinity compared to **CJL-1-80**, but only a 7-fold increase in binding affinity compared to **CJL-1-14**. Regardless, the increased binding affinity of the MUmBLs are consistent to that observed from synergistic bivalent binding modes. *1, 7, 25, 132, 230*

At the mMC3R, the MUmBL's also resulted in an increased binding affinity compared to the monovalent ligand **CJL-1-14** with IC₅₀ values that are 130 to 480-fold lower (**Table 5.3, Figure 5.8A**). When comparing the MUmBL's to the higher affinity tetrapeptide scaffold **CJL-1-80** at the mMC3R, the MUmBL's ligands had lower fold increases ranging from 3 to 8-fold. This supports the hypothesis that His-DNal(2')-Arg-Trp scaffold is functioning as a targeting moiety to bring the His-DPhe-Arg-Trp scaffold to the putative homodimer. Further evidence of the MUmBLs' synergistic binding can be observed by comparing the mixture of **CJL-1-14** and **CJL-1-80** that represent the same amount of tetrapeptide scaffold as the MUmBL's without being linked together. All the MUmBLs resulted in greater than 10-fold increased binding affinity as compared to the tetrapeptide monomeric **CJL-1-14** and **CJL-1-80** mixture. The tightest binding MUmBL, **CJL-1-63**, possessed a 40-fold increased binding affinity compared to the mixture of **CJL-1-14** and **CJL-1-80** which supports the hypothesis of synergistic binding due to bivalent ligand design (**Table 5.3, Figure 5.8A**).

At the mMC4R, the MUmBLs resulted in a 14- to 30-fold increased binding affinity compared to monovalent ligand **CJL-1-14** (**Table 5.3, Figure 5.8B**). This supports that the His-DNal(2')-Arg-Trp scaffold is acting as a "targeting" moiety to deliver the agonist

scaffold His-DPhe-Arg-Trp to the putative melanocortin homodimer. When the MUmBLs are compared to **CJL-1-80**, only ligand **CJL-1-124** had an increase in binding affinity above the 3-fold inherent error of the assay. The reason why a substantial increase in binding affinity might not have been observed when compared to the Ac-His-DNal(2')-Arg-Trp-NH₂ tetrapeptide is because **CJL-1-80** is already a strong nanomolar binder and may mask further increases in binding affinity. This has been described by others utilizing high affinity scaffolds in bivalent and multivalent ligands.^{27, 122, 223} This type of masking was explained in more detail in **Chapter 3 Section 3.3.3.2** as it was observed with a homobivalent ligand **CJL-1-140** in which increased binding affinity was observed at the mMC1R and mMC3R, but not at the mMC4R.²⁵

Analysis of the binding data helps interpret the functional cAMP assay data at the mMC4R. Comparison of **CJL-5-58** and **CJL-1-124** in which the only difference is that the orientation of the tetrapeptide scaffolds are switched, but one is a full agonist and the other is a partial agonist in cAMP signaling in spite of similar binding affinities. In order to understand the difference between these two ligands, the effect of the site of attachment of the linker on the two different tetrapeptide scaffolds must be considered. Compound **CJL-5-58** can be thought of being comprised of **CJL-5-35-4** with the linker attached to the C-terminus of the His-DPhe-Arg-Trp scaffold and **CJL-1-132** with linker attached to the N-terminus of the His-DNal(2')-Arg-Trp scaffold. Conversely, **CJL-1-124** can be thought of as being comprised of **CJL-1-116** and **CJL-5-35-5** with the contrasting attachments of the linker to each scaffold (**See structures in Table 5.1**).

The linker control ligands, **CJL-5-35-4** and **CJL-1-132**, for **CJL-5-58** have comparable binding affinities to each other at the mMC4R (**Figure 5.8C, Table 5.5**). Compound **CJL-1-132** possessed 4-fold increased binding affinity compared to **CJL-5-35-4**. In comparison, the linker control ligands, **CJL-1-116** and **CJL-5-35-5**, for **CJL-1-124** have notable differences in binding affinities. The IC₅₀ value for **CJL-5-35-5** is 27-fold lower than the IC₅₀ value for **CJL-1-116** at the mMC4R (**Figure 5.8D, Table 5.5**). This suggests that **CJL-5-35-5** is a tighter binder than **CJL-1-116**. It could be postulated that the differences in the balance (*i.e.* 4-fold difference compared to 27-fold difference) of the linker control ligands' binding affinities within the bivalent ligands are responsible to the difference in the functional cAMP dose response curves. At higher concentrations of **CJL-1-124**, the compound may start competing against itself for receptor occupancy, such that the higher affinity side of the ligand [*i.e.* Ac-His-DNal(2')-Arg-Trp-(PEDG20)] would be displacing the lower affinity side for binding (**Figure 5.2D**). This may result in a lack of binding of the agonist pharmacophore to the receptors and may cause the partial agonism to occur since more than 50% of the total receptors (the level necessary for full receptor cAMP signaling based on asymmetric homodimer hypothesis) will be bound by His-DNal(2')-Arg-Trp instead of by agonist. In contrast, compound **CJL-5-58** has a much more balanced binding profile of the two sides (*i.e.* 4-fold difference in control ligands), and competition of the pharmacophores should not as readily favor one over the other. Therefore, it can be postulated that approximately equal binding of both tetrapeptides would occur, and that at 100% receptor occupancy approximately 50% of the receptors

would be occupied by the His-DPhe-Arg-Trp scaffold and 50% would be occupied by the His-DNal(2')-Arg-Trp scaffold (**Figure 5.2E-H**). Then based on these assumptions and the hypothesis of asymmetric MC4R homodimer, no plateau would arise because 50% of the receptors would be occupied by the agonist His-DPhe-Arg-Trp scaffold which is all that is necessary to achieve full cAMP signaling (**Figure 5.1C**, **Figure 5.5I** and **Figure 5.5L**).

5.3.5 Ligand Dependent Modulation of BRET Signal

Bioluminescence resonance energy transfer (BRET) has been routinely used to assess GPCR dimerization.³⁰⁴ Specifically, the MC3R and MC4R have been reported to result in high basal BRET signal supporting the formation of homodimers as discussed in **Chapter 4**.^{130, 132, 204, 205} Furthermore, BRET has been utilized to support the existence of hMC1R-hMC3R and mMC3R-mMC4R heterodimers.^{132, 204} It has also been suggested that ligand treatment can increase or decrease GPCR dimerization which should be detectable with changes in BRET signal.^{18, 213, 214, 305-308} However, these reports vary depending on the receptor system and ligands used.³⁰⁵ For example, agonist treatment at the somatostatin receptor 2 has been reported to cause the homodimers to dissociate into monomers.³⁰⁶ Whereas at the vasopressin V_{1a}, agonist ligand had no observable effect on dimerization ratio.³⁰⁷ There are also several examples of bivalent ligand treatment resulting in increased BRET signal suggesting they are inducing or increasing dimerization.^{18, 213, 214, 308} In previous reports focused on melanocortin receptors, no significant effect of agonist or antagonist ligand was reported for the hMC1R, hMC3R, or hMC4R

homodimerization.^{130, 204} However, in the BRET study involving the hMC4R, there does appear to be a trend towards decreasing BRET signal after agonist dosing, albeit not significant. After dosing α -MSH at 1 μ M the mean BRET signal decreased by approximately 20% compared to basal BRET signal of the hMC4R.¹³⁰ Because of the potential of our compounds to be modulating the dimer or oligomer state or changing the dimer conformational state (**Figure 5.5**), we investigated the response of BRET signal from mMC4R homodimers in response to ligand treatment.

Ligands α -MSH, **CJL-1-14**, and **CJL-1-87**, that have full agonist activity in both the cAMP signaling assay and the β -arrestin recruitment assay, resulted in a dose dependent decrease in BRET signal (**Figure 5.10**). Dosing these ligands at 10 μ M resulted in a significant 15% reduction in BRET signal compared to basal signal. In contrast, ligands **CJL-1-80** and **CJL-1-140** contain only the antagonist tetrapeptide scaffold and have minimal functional agonist activity in both the cAMP signaling assay and the β -arrestin recruitment assay. These antagonist-based ligands resulted in no significant changes in BRET signal from basal levels. In addition, the equal mixture of agonist **CJL-1-14** and antagonist **CJL-1-80** resulted in no significant changes from basal signal. The MUmBLs, **CJL-1-124** and **CJL-5-58**, resulted in a significant effect in which dosing at 10 μ M resulted in approximately an 8% reduction in BRET signal compared to basal signal (**Figure 5.10**).

The reduction of BRET signal observed with agonist containing ligands could be the result of two different mechanisms: 1) The dimerization or oligomerization is being

disrupted and moving towards a lower oligomer state (*e.g.* dimers to monomers). 2) A conformational change is occurring within the intact dimer or higher-order oligomer in which the NanoLuc®-donor and the HaloTag®-acceptor are being orientated such that the BRET signal is being reduced (*e.g.* moving further away or dipole orientation is incorrect.)³⁰⁹ It is currently difficult to determine which of these two possibilities are the driving force for the BRET signal reduction observed in our studies. Regardless, it is apparent that some sort of conformational change is occurring that effects the BRET signal which relates with a ligand's agonist activity both for cAMP and for β -arrestin recruitment. These changes match the proposed asymmetric signaling of MC4R homodimers (**Figure 5.1, Figure 5.5**). It follows from the proposed model that at basal levels in which only assay buffer is added (**Figure 5.5A**), no conformational changes have occurred. With the addition of agonist ligand and the first binding event, cAMP signaling pathways are activated and a conformational change occurs that effects BRET signal (*c.a.* 7-8% change) (**Figure 5.5B or E**). This is observed with all ligands that contain an agonist scaffold including α -MSH, **CJL-1-14**, **CJL-1-87**, **CJL-1-124**, and **CJL-5-58** (**Figure 5.10**). The second agonist binding event is hypothesized to result in an additional conformational change at the second receptor in the homodimer, and this is postulated to be responsible for the maximal observed decrease in BRET signal (*c.a.* 15%) (**Figure 5.5F**). This is observed with ligands α -MSH, **CJL-1-14**, and **CJL-1-87** because they result in the second conformational change with in the homodimer due to a second agonist binding event on the second receptor. However, the second receptor in the homodimer pair is postulated to

be bound by an antagonist scaffold with ligands **CJL-5-58** and **CJL-1-124** (**Figure 5.1C**) and, therefore, the full conformational change to the homodimer does not occur (**Figure 3I**) resulting in the lack of β -arrestin recruitment (**Figure 2B-C**) and the only 50% maximal change in BRET signal (*i.e.* 7-8% change instead of 15%) (**Figure 5.10**).

Although further experimental work will be necessary to determine the exact dimer conformational changes that are occurring, the current studies support the hypothesis that the bias agonism observed currently with **CJL-5-58** is the results of a conformational change of the dimeric state as correlate with the changes observed in the BRET signal. These conformational changes could be changes in the oligomeric number (*e.g.* dimers to monomers), orientation of the receptors within a dimer pair (*e.g.* which transmembrane helixes are interacting), or changes in the cellular location of the receptors (*e.g.* receptor internalization).^{10, 206, 207} Further elucidation of these mechanisms will be necessary.

5.3.6 MUmBLs Effects on Energy Homeostasis in Mice

The novel *in vitro* pharmacological profile of the MUmBLs warranted further evaluation *in vivo* to study their effects on energy homeostasis and physiological consequences. In particular, compound **CJL-5-58** was selected due to its biased agonism at the hMC4R, consistent pharmacology in cAMP accumulation assays between the mouse and human isoforms, and the increased serum stability of a PEDG20 linker compared to a Pro-Gly linker (**Figure 5.3**).¹³² We selected to administer the compound intracerebroventricularly (ICV) directly into the lateral ventricle of the brain in order to

avoid the confounding effects of metabolism and brain delivery and to be consistent with previous work in the field.^{1, 25, 76, 107, 132, 189}

5.3.6.1 Preliminary Food Intake Studies of CJL-5-58 in Mice

The initial dose response studies were performed in “conventional” standard mouse cages in which all measurements were taken manually. Compound **CJL-5-58** resulted in no signs of adverse effects at doses of 2.5 nmols and 5.0 nmols in the conventional cage experiments. Compound **CJL-5-58** resulted in a dose dependent decrease in food intake when refeeding was measured after a 22 hour fast. Significant decreases in food intake were observed at 2, 4, 6, and 8 hours after compound administration in male mice (**Figure 5.11A**), and 2 and 4 hours in female mice (**Figure 5.11B**). Consistent with the decreased food intake, male mice receiving **CJL-5-58** in the fasting refeeding paradigm did not return to their pre-fasting weights as quickly as the saline controls. A significant difference was observed in the change in weight of the male mice after compound administration at time points 2, 4, 6, 8, and 24 hours after compound administration (**Figure 5.12A**). Only the 2 hour time point was significant in female mice (**Figure 5.12B**).

Interestingly, no statistically significant effect on either food intake or body weight was observed with **CJL-5-58** at a 5.0 nmol dose in a nocturnal free-feeding paradigm (**Figure 5.13** and **Figure 5.14**). In the nocturnal feeding paradigm, mice have free access to food the entire course of the experiments, and compound is administered 2 hours before lights out.^{25, 132, 189} Since mice consume approximately 70% of their food during the dark cycle with their biggest meal being soon after lights out, this paradigm should measure the

effect on food intake with minimal disruption of homeostasis.²¹⁸ However, in the fasting-refeeding paradigm, mice are fasted from the start of the previous dark cycle until 2 hours before lights out. At which point mice were administered the compound and food was returned. This disrupts the normal homeostasis of the mice by putting them in a fasting state, but the fast creates a robust re-feeding response that can help to detect significant effects.^{132, 218} Specific to the melanocortin system, expression of endogenous antagonist AGRP is upregulated upon fasting.^{113, 239, 241}

In **Chapter 4**, we observed that agonist homobivalent ligand **CJL-1-87** has a significantly greater effect in a fasting-refeeding paradigm than monovalent agonist **CJL-1-14**, even though they have similar effects in a nocturnal feeding paradigm.¹³² This was hypothesized to be the result of either increased binding affinity of **CJL-1-87** or due to specific interactions *in vivo* with melanocortin homo- or heterodimers, but the exact mechanism remains unclear.¹³² It can be hypothesized that the differences between paradigms observed is due to similar mechanisms as that proposed previously for **CJL-1-87**. For example, **CJL-5-58**'s potent binding affinity ($IC_{50} = 14$ nM) may allow it to compete more effectively against endogenous ligands for binding. In the fasting paradigm, compound **CJL-5-58** is directly competing with agouti-related peptide (AGRP) which is an endogenous MC3R/MC4R antagonist whose expression levels are upregulated during fasting.^{113, 239, 241} It, therefore, may be hypothesized that **CJL-5-58** achieves its effects in the fasting state by blocking the orexigenic effects of AGRP, and not from melanocortin agonist action. Indeed, food intake after **CJL-5-58** is consistent between the nocturnal

paradigm and the fasting paradigm suggesting that it maintains consistent feeding patterns regardless of endogenous homeostasis regulation.

5.3.6.2 Effects of CJL-5-58 *In Vivo*

In order to better characterize the effects of **CJL-5-58** on energy homeostasis, it was decided to perform compound administration in TSE Phenotypic metabolic cages that are configured to automatically measure water intake, food intake, changes in the CO₂ and O₂ levels within the cages, and beam break activity. A new cohort of littermate age match male mice was cannulated and acclimated to the TSE metabolic cages for one week. Consistent with the conventional cage data, the administration of 5 nmols of **CJL-5-58** resulted in a decrease in food intake up to 12 hours after administration in the fasting paradigm (**Figure 5.15A**). Because no consistent long term effects (>24 hours) were observed at any parameters measured, the discussion will be focused on the first 24 hours, with the majority of effects observed within the first 12 hours. (For full time course, see **Figure 5.16**). A decrease in water intake was observed with 5 nmols of **CJL-5-58** at time points 4, 6, 8, 10, and 12 hours after compound administration in the fasting paradigm (**Figure 5.15C**). This was not surprising since water intake correlates directly to food intake and is known to decline during fasting paradigms.²¹⁸ It is, therefore, difficult in the current study to know if the decrease in water intake is a consequence of decreased food intake after **CJL-5-58** administration or a direct pharmacological effect. As observed in the conventional cages, no significant effect was observed with the administration of **CJL-5-**

58 in the nocturnal feeding paradigm (**Figure 5.17A, Figure 5.18A**). Also no difference in water intake was observed in the nocturnal paradigm (**Figure 5.17C**).

As discussed in **Chapter 4**, melanocortin ligands have previously been reported to effect the respiratory exchange ratio (RER), with agonist compounds decreasing the RER, and antagonist compounds increasing the RER.^{112, 216, 242, 310} The RER can be measured indirectly utilizing TSE metabolic cage system by measuring the amount of CO₂ and O₂ entering and exiting the sealed cages. A RER value of *c.a.* 0.7 gives an indication that fats are the primary fuel source that the animal is utilizing.^{35,118,127,128} A RER value of *c.a.* 1.0 gives an indication that carbohydrates are the primary fuel source the animal is utilizing.^{132, 189, 244, 245} As expected, during the fast a baseline RER value of slightly above 0.7 was observed (**Figure 5.15B, Figure 5.16B**). This value has been reported previously in the literature,^{132, 246, 247} and is purportedly due to the lack of carbohydrates available for energy during a fast that results in a reliance of fat storage as the primary energy source. After saline treatment and the return of food, the RER value increases rapidly towards 1.0 as the mice consume food and the consumed carbohydrates become the primary fuel source through the first dark cycle. Administration of **CJL-5-58** resulted in more gradual increase in RER from the 0.7 baseline value to 1.0. A significantly lower RER was observed for the first 9 hours and at 17 hours after compound **CJL-5-58** administration compared to saline (**Figure 5.16B**). The lowered RER values support a hypothesis that in addition to eating less, the mice were burning more fats instead of carbohydrates. In the nocturnal feeding paradigm, compound administration resulted in significantly lowered RER values only

until 2 hours after administration supporting a hypothesis that the pharmacological effect of **CJL-5-58** is amplified by fasting (**Figure 5.17B**, **Figure 5.18B**).

Melanocortin ligands have been reported to effect the energy expenditure such that agonists increase the amount of calories burned as seen in **Chapter 4**, and antagonist decrease the amount of calories burned.^{112, 216, 242, 310} In the fasting paradigm, the energy expenditure decreases rapidly during fasting which is consistent with the mice conserving energy (**Figure 5.15D**). The baseline energy expenditure is *c.a.* 12 kcal/h/kg prior to treatment. Following saline treatment and the reintroduction of food, energy expenditure increases rapidly in rate up to *c.a.* 17-19 kcal/h/kg. After the administration of the 5 nmol dose of **CJL-5-58**, energy expenditure also increases to *c.a.* 17-19 kcal/h/kg, however, the increase is more gradual and the energy expenditure remains significantly lower for the first 3 hours post-treatment. The mice's rate of energy expenditure eventually recovered and an increased energy expenditure is observed 15, 17, and 21 hours after compound administration compared to saline (**Figure 5.15D**). This is interesting, because all other parameters are consistent with **CJL-5-58** functioning as an agonist *in vivo*, but **CJL-5-58** effects on energy expenditure is consistent with it functioning as an antagonist. The decrease in energy expenditure may be due to the robust decrease in food intake that keeps the mice in an energy conservative state.

Another hypothesis for the lowered energy expenditure may be the biased signaling of **CJL-5-58** for the cAMP signaling pathway over the β -arrestin recruitment pathway. It could be hypothesized that the β -arrestin pathway is responsible for classic agonist effect

to increase energy expenditure. Therefore, **CJL-5-58**, with minimal β -arrestin recruitment, results in a more gradual change in energy expenditure from baseline. However, further experimentation is necessary before hypothesis could be validated. In the nocturnal paradigm, an increase in energy expenditure was observed 5, 13, 15, and 16 hours after treatment which is consistent with agonist function (**Figure 5.17D**, **Figure 5.18D**).

Of note some adverse reactions were observed during the TSE cage experiments that were not observed during the conventional cage experiments (**Table 5.6**). These adverse reactions began with the individual mouse putting its tail upright in the air then increased sporadic activity about 15-30 minutes post-compound administration. Then the mouse went through 10-15 second bouts of “barrel roll” type behavior. This behavior was repeated 2-3 times with approximately 4-5 minutes between bouts. At which point the mouse either died, or completely recovered. All mice were completely recovered within two hours (unless there was death).

During the fasting paradigm, four adverse reactions were observed within 30 minutes of injection, and one mouse died about 2 hours post-injection. During the nocturnal paradigm there was a total of 2 adverse reactions and one mouse died 30 minutes post-administration. Mice experiencing adverse reactions recovered rapidly (<1 hr). Due to the lack of significant effects observed in the nocturnal paradigm group as well as in the ambulatory activity measurements in both paradigms (**Figure 5.16**, **Figure 5.18**), the adverse reactions observed do not seem to be having a significant effect on the parameters measured during the experiments. If the effects of the compound were due to toxicity, it

would be expected that the mice receiving compound in the nocturnal paradigm would be adversely effected as well, and decreases in food intake, RER, energy expenditure, and water intake would be observed after compound administration. Furthermore, visceral illness and toxicity is usually accompanied by decreased activity, however no significant differences were observed in activity between saline and **CJL-5-58** in the fasting paradigm in the TSE cages. In the nocturnal paradigm, an increase in activity was observed during the first 5 hours after administration which is inconsistent with toxic effects associated with a compound.

5.3.6.3 Effects of Co-administration of CJL-1-14 and CJL-1-80 *In Vivo*

In order to help elucidate if the *in vivo* effects were due to the MUmBL design or were due to the co-treatment of an agonist and antagonist, co-administration experiments were performed in the same mice as the **CJL-5-58** experiment with 5 nmols of **CJL-1-14**, Ac-His-DPhe-Arg-Trp-NH₂, and 5 nmols of **CJL-1-80**, Ac-His-DNal(2')-Arg-Trp-NH₂, that would reconstitute the 10 nmols of tetrapeptide scaffolds administered with **CJL-5-58** at the 5 nmol dose. In the fasting paradigm and the nocturnal paradigm, no statistically significant effect on food intake or water intake were observed compared to saline within 24 hours of administration expect for in the 2 hours timepoint in the nocturnal paradigm (**Figure 5.15A and C, Figure 5.17A and C**). There was a significant decrease in food intake 2 hours post-administration compared to saline in the nocturnal paradigm, but no other time points were significant. These data are consistent with the hypothesis in the field that co-administration of an antagonist with an agonist cancels out the effects on food intake.⁵⁶

No significant effect was observed in energy expenditure between saline and co-administration of **CJL-1-80** and **CJL-1-14** in the fasting paradigm (**Figure 5.15D**, **Figure 5.16D**). In the nocturnal paradigm, there was a significant effect on energy expenditure observed 19 hours after administration, but no other time point was significant (**Figure 5.17D**, **Figure 5.18**). The RER was significantly lower than saline in the fasting paradigm at the 1 hour and 4 hour time points (**Figure 5.15B**). The RER was also lower in the nocturnal paradigm at 1-4 hour time points (**Figure 5.17B**).

A direct comparison of **CJL-5-58** to the co-administration of **CJL-1-14** and **CJL-1-80** reveals some differences. There were significant differences in the food intake at 2 and 4 hour time points in the fasting paradigm comparing **CJL-5-58** to the tetrapeptide combination. There were significant differences in RER at the 2, 3, 6, and 7 hour time points in the fasting paradigm. Energy expenditure was also significantly higher for **CJL-5-58** at the 13 and 17 hour time points in the fasting paradigm. In the nocturnal paradigm, no significant differences were observed for any parameter between the co-administration of the tetrapeptide combination and **CJL-5-58**.

The combination of **CJL-1-14** and **CJL-1-80** resulted in more adverse observations than **CJL-5-58**. In the fasting paradigm, three mice died after compound administration. In the nocturnal paradigm, one mouse died. As with **CJL-5-58**, in the energy homeostasis parameters measured compound toxicity was not observed. If compound toxicity was suspected for the *in vivo* effects on energy homeostasis, it would be expected that decreases in food intake and water intake would be observed in both the fasting paradigm and the

nocturnal paradigm. Furthermore, ambulatory activity resulted in very little significant changes compared to saline. The only significant changes observed in ambulatory activity were at hours 18 and 19 post-administration. It would be expected in the case of compound toxicity, a more significant effect on activity would be observed.

5.3.6.4 CJL-5-58 Administration into Melanocortin Knockout Mice

In order to more clearly understand the effects of the biased agonism at the MC4R, the effects of administration of **CJL-5-58** was explored in MC3R knockout (KO) mice and MC4RKO mice. In male MC3RKO mice, a significant decrease in food intake was observed in the nocturnal feeding paradigm (**Figure 5.19**). Food intake was decreased at time points 2-12 hours after compound ICV administration at the 5 nmol. Furthermore, RER was significantly decreased at time points 1-5, 8 and 12 hours after compound administration. Also significant increased RER was observed 18, 19, and 24 hours after 2.5 nmol compound administration. Finally, energy expenditure was significantly reduced at time points 1-3 hrs after 5 nmol administration compared to saline. After 2.5 nmol **CJL-5-58** administration, energy expenditure was significant reduced 1-8 and 13 hours post-treatment. It must be taken into account that adverse reactions were also observed at the 2.5 and 5 nmol concentrations which may be a confounding factor in interpretation of this data (**Table 5.6**). Adverse reactions included two mice dying after the 5 nmol dose. It should also be noted that although no significant reductions in activity were observed, the activity for **CJL-5-58** at 5 nmols trended towards being lowered ($p=0.069$) and the error with the activity at 2.5 nmols is high. The large error in activity may serve as an indication

of toxicity. It is currently difficult to decipher whether the adverse reactions observed are due to paradigm effects, genotype difference, or compound toxicity. No adverse reactions were observed at the 1 nmol dose in the nocturnal paradigm, however, no significant effects were observed at the 1 nmol dose.

The effects of **CJL-5-58** on male MC3RKO mice in a fasting-refeeding paradigm were evaluated for comparison with wild type mice. However due to the adverse reactions observed with higher dosing in the nocturnal paradigm, the effects were only evaluated at 0.5 and 1 nmols (**Figure 5.20**). Significant reduction in food intake was observed at 2 and 4 hour time points after the 1.0 nmol **CJL-5-58**. Significant reductions in energy expenditure were observed in the fasting paradigm at time points 1 and 2 hours at the 1 nmol dose. RER was significantly reduced at 2 and 3 hours after the 1 nmol administration of **CJL-5-58**. The only significant effect observed at 0.5 nmol dosing was a significant increase in RER at time point 24 hours. No other parameters were significantly affected by administration of 0.5 nmols of **CJL-5-58**. It should be noted that some minor signs of adverse reactions (such as tail going upright without barrel rolls) were observed with administration of **CJL-5-58** at 1 nmol in the fasting paradigm that could confound these results (**Table 5.6**).

In male MC4RKO mice, **CJL-5-58** was administered at 5 nmols in both a nocturnal paradigm and a fasting-refeeding paradigm in standard conventional cages (**Figure 5.21**). The dose was well handled in the nocturnal paradigm, but minimal effect was observed. There was an immediate reduction in food intake 2 hours after compound administration.

There was also a significant increase in body weight 6 hours after compound administration. In the fasting-refeeding paradigm, administration of **CJL-5-58** at 5 nmols resulted in decreased food intake at 2, 4, 6, 8 and 24 hours after compound administration with no effect on mouse body weight. Mice looked healthy in the nocturnal paradigm, however some signs of adverse reactions (such as tail going upright without barrel rolls) were observed in the fasting-refeeding paradigm (**Table 5.6**).

Due to the observed adverse physiological effects that were observed in the different housing and different genotypes (**Table 5.6**), the exact *in vivo* pharmacology for MUmBL **CJL-5-58** will need further elucidation. However, there are some key conclusions that may be drawn. First the adverse reactions seem to be acute and short-term (<1 h), suggesting that longer effects are due to the ligands on-target pharmacology. Second, the observed adverse reactions were increased during the fasting-refeeding paradigm, suggesting the adverse reactions are paradigm related and probably has a very specific pharmacological cause that remains to be identified. Third, the adverse behaviors appeared to be more notable in the MC3RKO mice, followed by the wild type mice, and minimal in the MC4RKO mice. This may suggest the melanocortin pathway may play a role, but experimental evidence would be necessary.

In Chapter 4, homobivalent ligand **CJL-1-87**, which differs from **CJL-5-58** by substitution of one the DNal(2') to DPhe, had no observable adverse reactions in similar mouse studies.^{31,32} Compound **CJL-1-87** also had similar cAMP functional activity and binding affinity as **CJL-5-58** (**Table 5.3**), and therefore,^{25, 132} it may be hypothesize that

the lack β -arrestin recruitment may be associated with the adverse reactions observed with **CJL-5-58**. It may be hypothesized that biased agonism of the cAMP pathway over the β -arrestin recruitment results in amplification of toxicity known to melanocortin ligands such as their effects on the cardiovascular system.⁵² Experimental evidence of the cardiovascular effects and molecular probes which favor the β -arrestin over the cAMP pathway will be necessary to confirm this hypothesis, but are lacking in the field to date. Although the current adverse effects are less than ideal in future drug design, they have been reported for full disclosure and good scientific practice. Further study in the effect of **CJL-5-58** *in vitro* as well as methods of targeting homodimers will be necessary to determine how to properly exploit these the asymmetric signaling of homodimers to reduce side effects.

5.3.6.5 Administration of CJL-1-124 to WT, MC3RKO, and MC4RKO Mice in Metabolic Cages

In order to study the effects of the orientation of the tetrapeptide scaffolds at the N-terminus and the C-terminus *in vivo*, **CJL-1-124** was administered to wild type, MC3RKO, and MC4RKO mice and parameters about their energy homeostasis was recorded using TSE phenotypic metabolic cages. In preliminary conventional cages experiments, strong adverse effects as described above were observed after compound administration in the fasting paradigm, therefore only the nocturnal paradigm was performed. No significant effect on male wild type mice was observed in the nocturnal paradigm at either the 2.5 nmol or 5 nmol dose of **CJL-1-124** compared to saline on food intake, water intake, or activity (**Figure 5.22**). Compound **CJL-1-124** did appear to cause a dose dependent

decrease in RER at the first 2 hours after compound administration. Energy expenditure appeared to be lowered by both the 2.5 nmol and the 5 nmol dose of **CJL-1-124** for the first 3 hours after administration compared to saline. Furthermore, it was observed that the 2.5 nmol dose of **CJL-1-124** significantly increased the energy expenditure 15, 18, 20, and 24 hours post compound administration compared to saline. There were some signs of adverse reactions observed at higher 5 nmol dose in the wild type nocturnal paradigm.

The administration of 2.5 nmols or 5.0 nmols **CJL-1-124** to male MC3RKO mice resulted in no significant changes in food intake or water intake (**Figure 5.23**). Energy expenditure was significantly reduced 1-6 hours after administration of 5.0 nmols of **CJL-1-124**. A significant increase in energy expenditure was observed 15 hours after compound administration. A significant reduction in energy expenditure was observed 1 and 2 hours after administration of 2.5 nmols of **CJL-1-124**, and a significant increase at 19 hours after compound administration. The RER was significantly increased from 15-21 and 24 hours after administration of 5 nmols of **CJL-1-124**. The RER of was significantly increased from 16-17, 19, 22, and 24 hours after administration of 2.5 nmols of **CJL-1-124**. The activity was significantly increased at 15 hours after 5 nmols of **CJL-1-124**, otherwise no significant changes were observed in the male MC3RKO mice. The administration of **CJL-1-124** to MC4RKO mice resulted in minimal significant change in food intake or body weight. The only significant change was the increase in food intake observed 2 hours after administration of 2.5 nmol **CJL-1-124** (**Figure 5.24**). It should again be noted that some

signs of toxicity were observed in the MC3RKO and the MC4RKO mice including animal death after administration

5.4 Conclusions

There is a growing amount of evidence that GPCR homodimers are functionally relevant and are possible pharmaceutical targets. A broadly applicable drug design strategy that targets homodimers, as opposed to monomeric receptors, would theoretically double the amount GPCR drug targets. Although various labs have presented different techniques and proof of concepts for methods to target asymmetrically signaling GPCR homodimers,^{231, 273-286} these techniques would be difficult to adapt to therapeutic design and *in vivo* applications. The current report presents a design strategy that targets asymmetric homodimers that should be easily amendable to various GPCR systems and *in vivo* targeting applications.

In the current report, we designed bivalent ligands that contained an agonist tetrapeptide scaffold and antagonist tetrapeptide scaffold for the MC4R. The MUmBL design strategy aims at occupying each of the two receptors within the homodimer with a different pharmacophore such that an agonist pharmacophore and an antagonist pharmacophore each occupy one of the two receptors within each homodimer. This design strategy produced biased ligands at the hMC4R in which the cAMP signaling pathway was robustly activated at nanomolar concentrations ($EC_{50} \sim 2$ to 6 nM) but the β -arrestin pathway was only partially activated at a concentration of $10 \mu\text{M}$. To our knowledge, these are the first melanocortin biased ligands favoring cAMP signaling over β -arrestin

recruitment and will be valuable chemical probes to study melanocortin signaling in the disease states and disorders in which the melanocortin receptors are implicated including: cancer,^{6, 28, 63, 156, 158} skin pigmentation disorders,¹¹⁷ social disorders,^{67, 68} sexual function disorders,^{66, 114, 116} Alzheimer's disease,^{61, 62} cachexia^{69, 70, 72, 73}, and obesity.^{25, 56, 76, 107}

We then functionally characterize the MUmBLs at the mouse melanocortin receptors. Two of the compounds showed species difference in which a partial agonist dose response curve was observed at the mMC4R. Furthermore, the partial agonist curve was present when assaying an equal mixture of the individual tetrapeptide pharmacophore scaffolds, and therefore, is not a result of the BUmBL design strategy. This identified **CJL-5-58** as the lead ligand for *in vivo* evaluation due to its biased agonism at the hMC4R, consistent pharmacology in cAMP signaling assays between the mouse and human receptors, and the increased serum stability of a PEDG20 linker compared to a Pro-Gly linker.¹³²

The evaluation of **CJL-5-58** in mice identified that it decreased food intake, water intake, and RER values in a fasting paradigm which is consistent with it functioning as an agonist in the cAMP signaling *in vitro* assays. However, the ligand did result in a decreased energy expenditure which is more consistent with it functioning as an antagonist like that seen in its β -arrestin recruitment assay results. There were significant differences observed between the administration of bivalent **CJL-5-58** compared with the administration of an equal mixture of the tetrapeptide pharmacophores ligands, **CJL-1-14** and **CJL-1-80**, suggesting that the bivalent design strategy is at least partially responsible for the *in vivo*

effects. This suggests we are indeed targeting asymmetric homodimers *in vivo*, although further experimental evidence would be necessary to confirm these results.

Some adverse reactions were observed in the current mouse studies with the administration of both **CJL-5-58** and the co-administration of **CJL-1-14** and **CJL-1-80**. Although these adverse reactions did not appear to effect the parameters measured (*i.e.* activity, food intake, water intake, RER, and energy expenditure), the adverse reactions cannot be ignored and have been reported for full disclosure and good scientific practices. Historically, one of the most detrimental side effects of melanocortin agonist ligands is their ability to increase blood pressure and heart rate that is thought to be mediated through MC4R neuronal pathways.^{52, 311} It could be conceived that by reducing β -arrestin dependent desensitization, we are increasing the MC4R acute cardiovascular effects resulting in short-term (<60 minutes) adverse effects, but with minimal effects on our longer parameter measurements (≥ 60 minutes). This might be an indication that the opposite type of biased ligand in which the β -arrestin recruitment pathway is selectively activated over the cAMP pathway would be preferable. Further elucidation in the pharmacology of biased melanocortin ligands will be necessary, but the current report provides the field with the first-in-class biased ligand that favors the cAMP pathway over the β -arrestin pathway.

Furthermore, the UmBL methodology presented currently should be applicable to various other GPCRs and can easily accommodate the plethora of well-studied and developed selective agonists and antagonists for various GPCR systems. This bivalent

ligand targeting method should allow for biased ligands or unique pharmacologies at various receptors by combining known agonists and antagonists with an effective linker. Considering the wide array of GPCRs that are already reported to exist as allosterically modulated or asymmetric homodimers (including the vasopressin,²⁸⁷ dopamine,²³¹ adenosine,²⁸⁶ metabotropic glutamate,²⁷⁹ and serotonin receptors²⁷³) this strategy should be broadly applicable. In order to effectively synthesize UmBLs for other receptor systems, it will be necessary to perform some standard medicinal chemistry to optimize the connection points of the linker to the pharmacophores, optimize the linker properties, and optimize the orientation of the pharmacophores. In the current study, it was important to have a balance in the binding affinity of the agonist side of the UmBL and the antagonist side of the UmBL. The unbalance ligand, **CJL-1-124**, did not appear to give a significant difference as compared to unlinked pharmacophores most likely due to competition of the stronger binding side of the UmBL.

The exact pharmacology achieved through the UmBLs design strategy will be as diverse as the allosteric mechanisms between different GPCR homodimers. For example, based on the results of Han and coworkers it can be hypothesized that UmBLs targeting the dopamine D2 receptor would result in increased receptor activation beyond just monovalent agonist alone. This is because allosteric cross-talk of a second agonist protomer was shown to blunt activation, so the occupation of the second protomer with an antagonist instead of an agonist should increase signal activation.²³¹ In contrast if the UmBL approach was applied to the metabotropic glutamate receptor, it would be

hypothesized to result in lower than full receptor activation of agonist alone as Kniazeff and coworkers observed that one agonist can partially activate a dimeric unit but two agonists are required for full activation.²⁷⁹ Finally, it has been reported that the vasopressin V_{1b} receptor signals through both the G_{q/11}-inositol phosphate (IP) and the cAMP pathways.²⁸⁷ It was hypothesized by OrceI and coworkers in 2009 that “the IP pathway could be activated by the binding of either one or two AVP molecules to a single receptor dimer... By contrast, cAMP production could only be turned on upon the binding of two ligands to a dimer.” Their observations and hypothesis is consistent with asymmetric homodimers such that the IP pathway is activated by the first agonist binding event and the cAMP pathway is activated second agonist binding event (similar to **Figure 5.1**).²⁸⁷ Therefore, if the UmBL design strategy was applied to ligands targeting the vasopressin V_{1b} receptor, it would be predicted to result in biased ligands in which the agonist pharmacophore would activate the IP pathway, and the antagonist pharmacophore would block the cAMP pathway activation within the homodimer. The UmBL design approach could also be applied to GPCR systems in which asymmetry between homodimers has not been identified, or even systems in which homodimerization has not yet been observed. In these situations, designed UmBLs could be evaluated for their ability to induce signaling in multiple signaling pathways (*e.g.* cAMP, Ca⁺, kinase signaling, β-arrestin signaling, *ect.*), in order to identify asymmetrically signaling GPCR homodimers.

In conclusion, the UmBL design approach reported herein has been used to progress the melanocortin field by supplying the first known biased ligands for cAMP pathway over

β -arrestin recruitment pathway. This chapter also provided functional pharmacological evidence of asymmetric homodimerization that complements previous BRET studies supporting homodimerization,^{132, 204} radioligand binding studies suggesting asymmetry of melanocortin homodimers propensity to bind ligands,^{205, 219} and functional reports demonstrating the significance of melanocortin oligomerization.^{206, 207} In a much broader sense, the UmBL approach provides a medicinal chemistry design strategy for the future advancement of GPCR pharmacology that can be applied to various receptor systems.

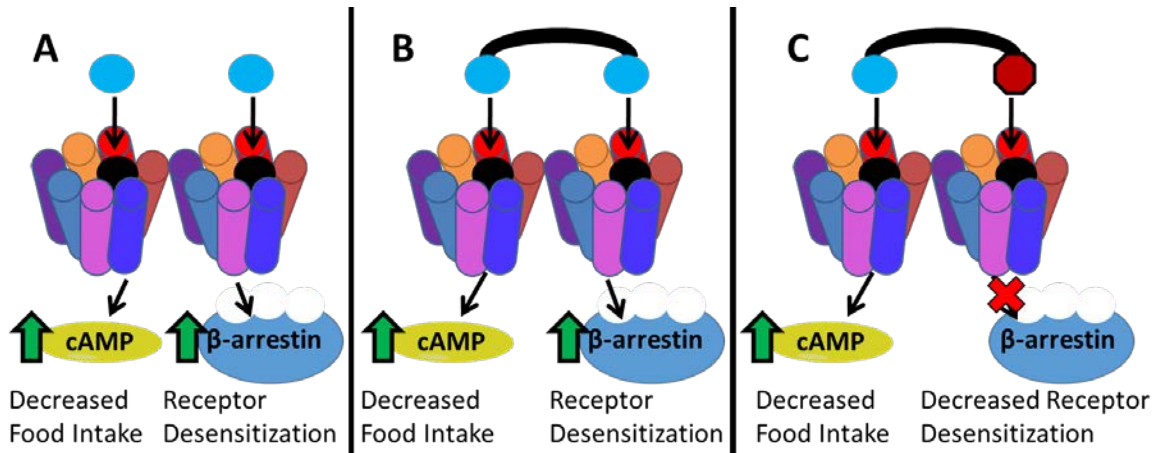


Figure 5.1. Hypothesized interaction of ligands with asymmetrically signaling melanocortin homodimers. A) Monovalent agonist ligands (blue circle) could occupy both receptors and result in both cAMP signaling and β -arrestin recruitment. B) Agonist homobivalent ligands (blue circle connected with black linker) could result in similar functional cAMP assays as monomeric ligands in spite of increased binding affinities due to asymmetric signaling. C) Working paradigm herein in which biased unmatched bivalent ligands (BUMBLs) containing an agonist pharmacophore (blue circle) and antagonist pharmacophore (red octagon) are postulated to result in biased signaling by agonizing one signaling pathway while antagonizing the other pathway when bound to the asymmetrical homodimer.

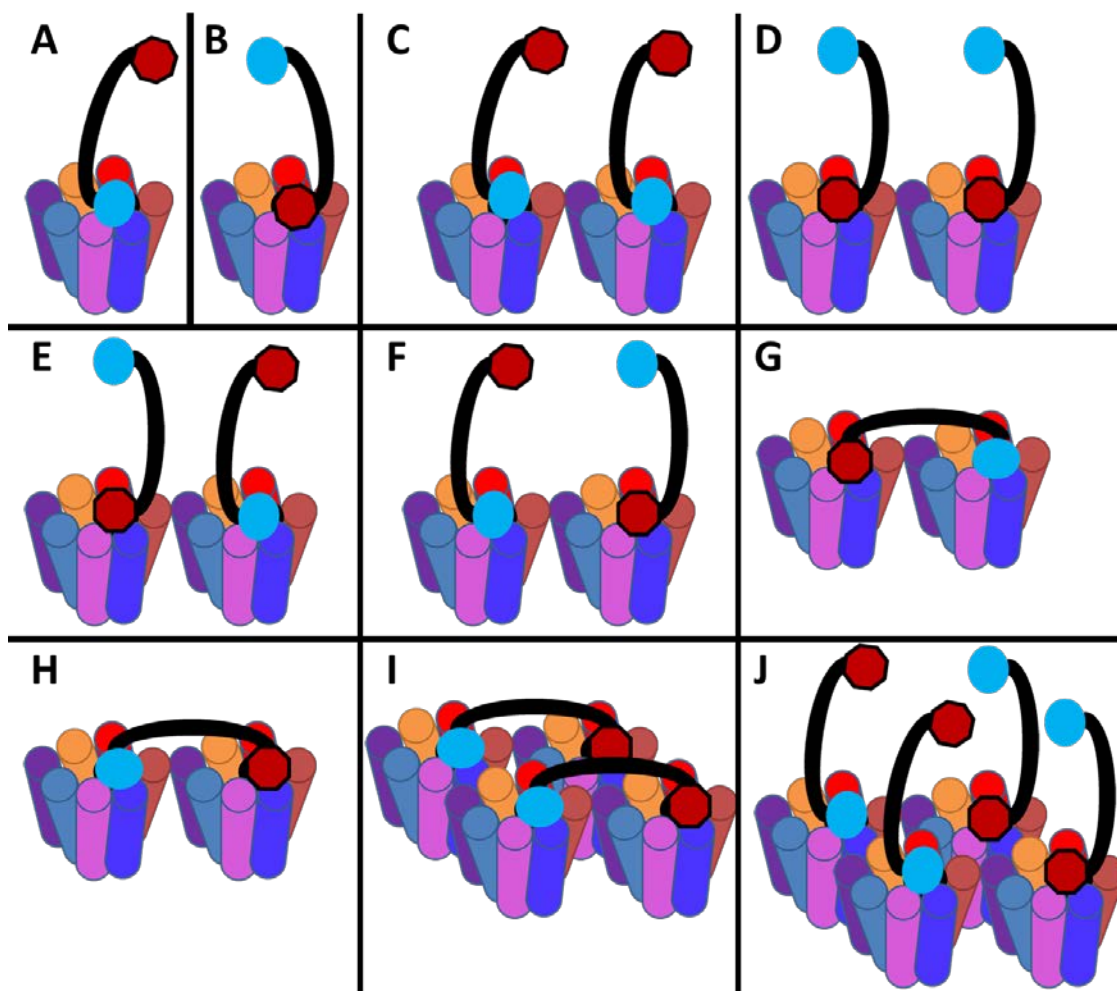


Figure 5.2. Different possible binding states of a MUMBL. The MUMBL can bind to a monomer with either the agonist scaffold (A) or the antagonist scaffold (B). The MUMBL can bind to a dimer in a monomeric fashion (C-F) or a bivalent fashion (G-H). Finally higher-order oligomers may exist in which the MUMBLs can bind in a bivalent fashion (I), a monomeric fashion (J), or some combination of both. It is postulated that some combination of all these states exist, however, bivalent binding to dimers or higher-order oligomers should be favored due to the synergist binding mode of bivalent ligands that was supported in Chapter 3.²⁵

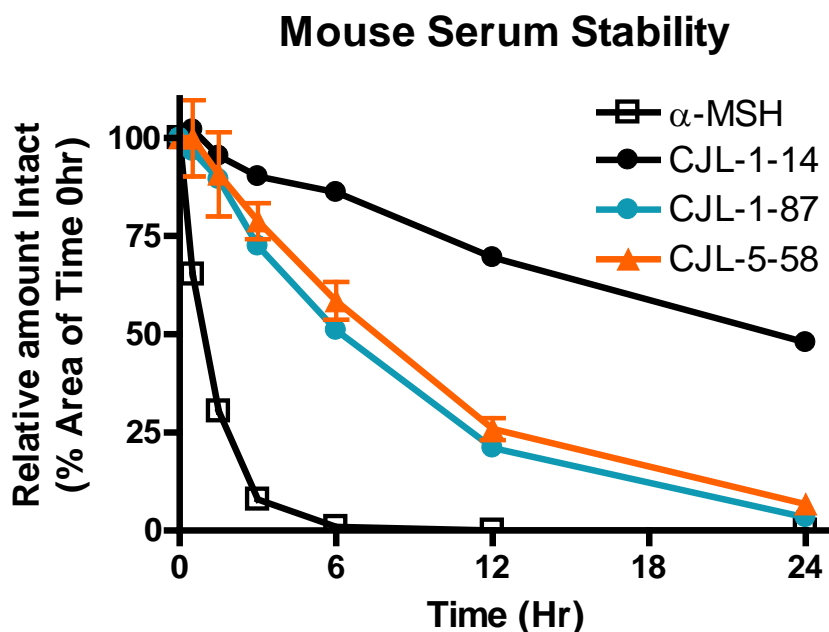


Figure 5.3. *In vitro* mouse serum stability assay to aid in the design of the MUmBLs. Ligands (10 μ M) were incubated in mouse serum and monitored for degradation of the parent molecule by LC-ESI+-MS/ MS. Results from α -MSH, **CJL-1-87**, and **CJL-1-14** were within error of previously reported results in Chapter 4.¹³² MUmBL/BUmBL **CJL-5-58** had a similar metabolic stability in two technical replicates as **CJL-1-87** suggesting adequate metabolic stability for *in vivo* evaluation. The signal intensity at time point 0 h was arbitrarily set as 100% and the percent of intact peptide at each time point was used to calculate the relative amount intact. For full methods see Chapter 2.¹³²

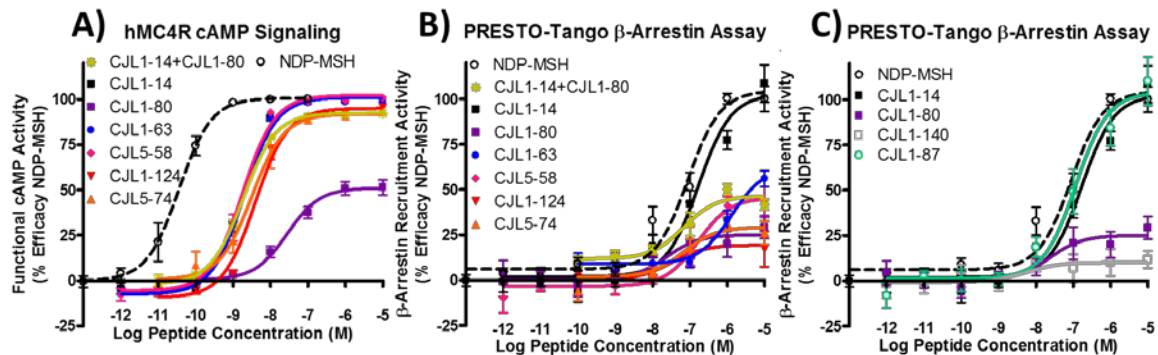


Figure 5.4. Illustrations of the *in vitro* functional pharmacology at the hMC4R of MUmBLs, A) The cAMP signaling potency was determined by AlphaScreen® assays. B and C) The β -arrestin recruitment potency was determined by PRESTO-Tango assays.²⁰² The * symbol represents the two monovalent tetrapeptides Ac-His-DPhe-Arg-Trp-NH₂ and Ac-His-DNal(2')-Arg-Trp-NH₂ assayed together each at the indicated M concentration such that pharmacophore concentration is the same as the bivalent pharmacophore concentration. Functional cAMP data was normalized as discussed in experimental section to show tradition dose response curve with increasing response at increasing agonist concentration.

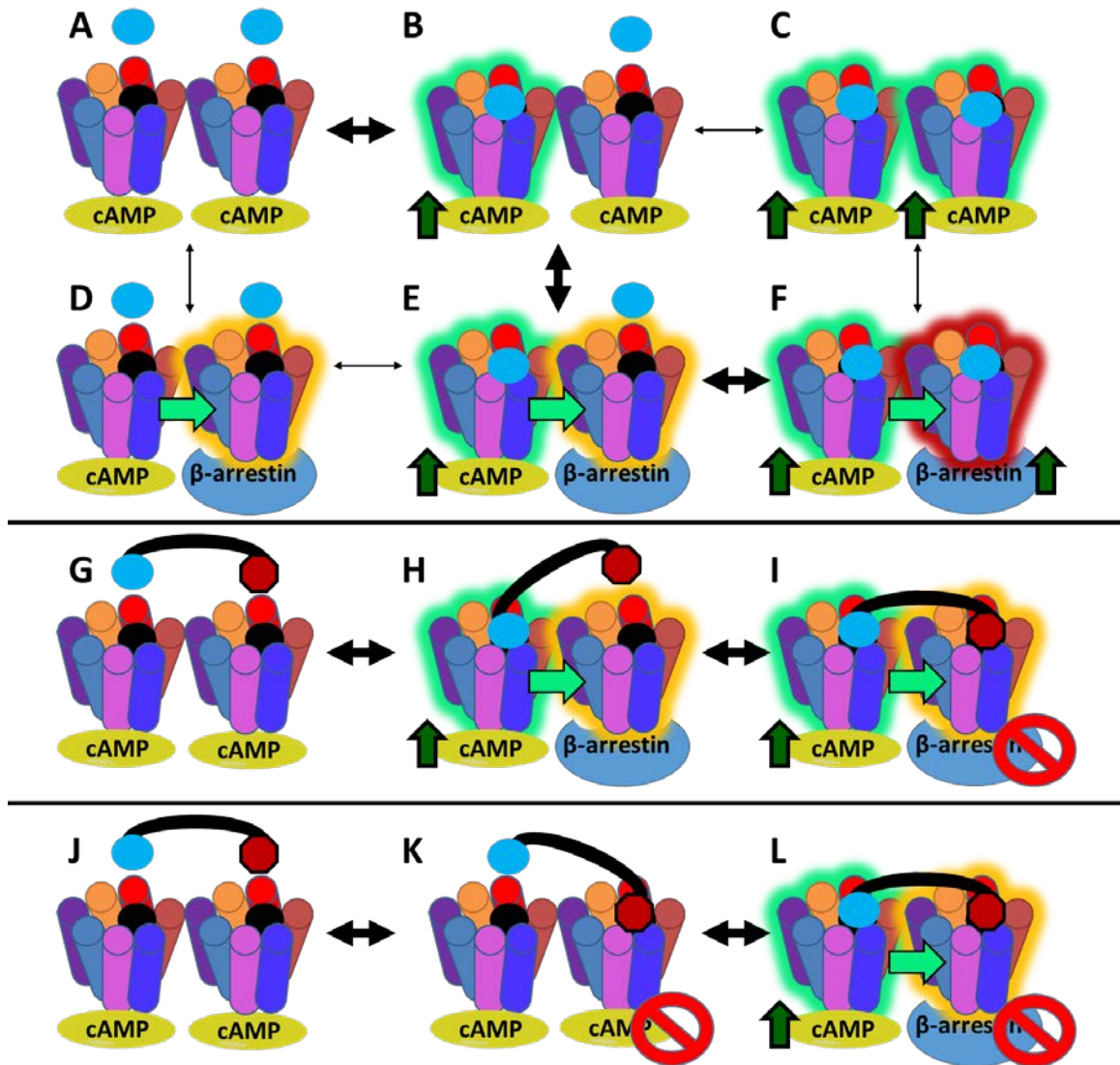


Figure 5.5. Illustrations of a previously reported model for allosteric interactions in GPCR dimers. (Durrux 2005, Casdao 2007).^{301, 302} In this model, GPCRs oscillate through different conformational states. Different conformations have different propensity to signal through cAMP or through β -arrestin. Signaling is represented by green arrows (**B, C, E, F, H, I, L**). Conformational changes are represented based on receptor highlighting (**B, C, D,**

E, F, H, I, L). The binding of an agonist pharmacophore to one receptor that signals through cAMP stabilizes the second receptor's conformation to increase its propensity to signal through the β -arrestin recruitment pathway (**State E**). Therefore, the second agonist binding event results in β -arrestin recruitment (**State F**). The BUmBL design strategy can be used to block the β -arrestin recruitment by increasing the likelihood of an antagonist pharmacophore binding the second receptor in the homodimer (**States G-I**). Even if the opposite binding order occurs, the antagonist blocks β -arrestin recruitment since it is already bound to the receptor after the agonist induces a conformational change (**States J-L**). This model assumes that the receptors are in GPCR dimers, but they are likely in an equilibrium as monomers and higher order oligomers.^{214, 301, 302} This model also assumes that the bivalent synergistic binding mode is favored with MUmBLs due to the decreased entropic cost of binding of the second pharmacophore.²⁵ It is possible that MUmBLs compete in monovalent fashion (**Figure 5.2**), but then the increased binding affinity observed below would not be expected.

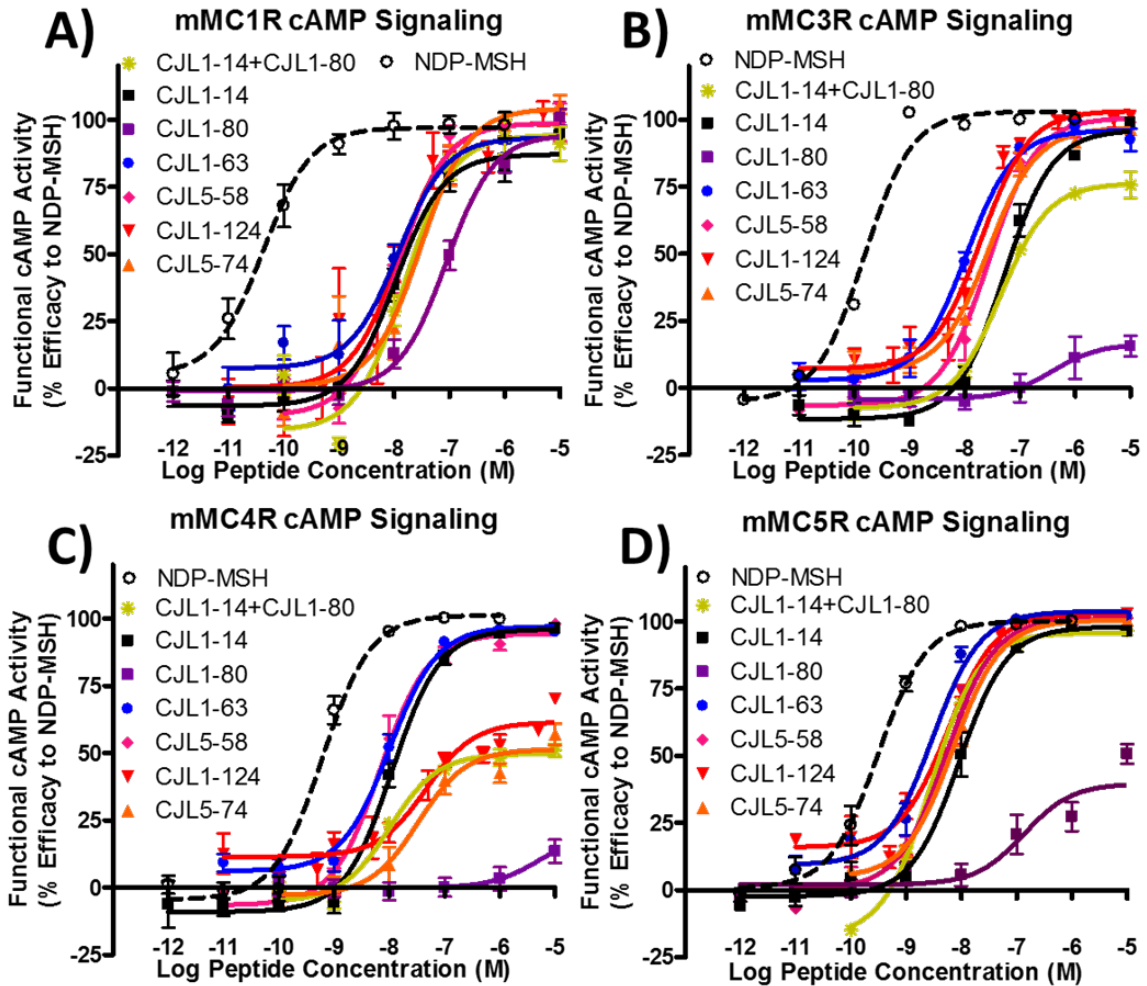


Figure 5.6. Illustrations of the *in vitro* functional pharmacology of the MUMBLs at the mMC1R, mMC3R, mMC4R, and mMC5R expressed in HEK293 cells. The cAMP signaling potency was determined by AlphaScreen® assays. The reported errors are the standard error of the mean (SEM) determined from at least three independent experiments. Functional cAMP data was normalized as discussed in experimental section to show tradition dose response curve with increasing response at increasing agonist concentration.

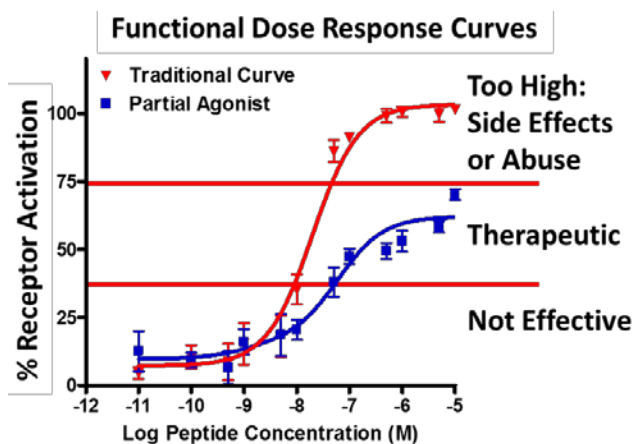


Figure 5.7. The functional dose response curve of **CJL-1-124** () may increase the therapeutic window versus traditional dose response curves (▼). For example, if the ligand is effective at 40% receptor activation, but has side effects above 60 % receptor activation, the ligand with the traditional curve can only be given at doses between ~10 nM to 25 nM to be active without side effects. Ligand **CJL-1-124** can be given at doses between ~50 nM to 5,000 nM to be active without side effects. However, this is speculative and would need to be confirmed experimentally.

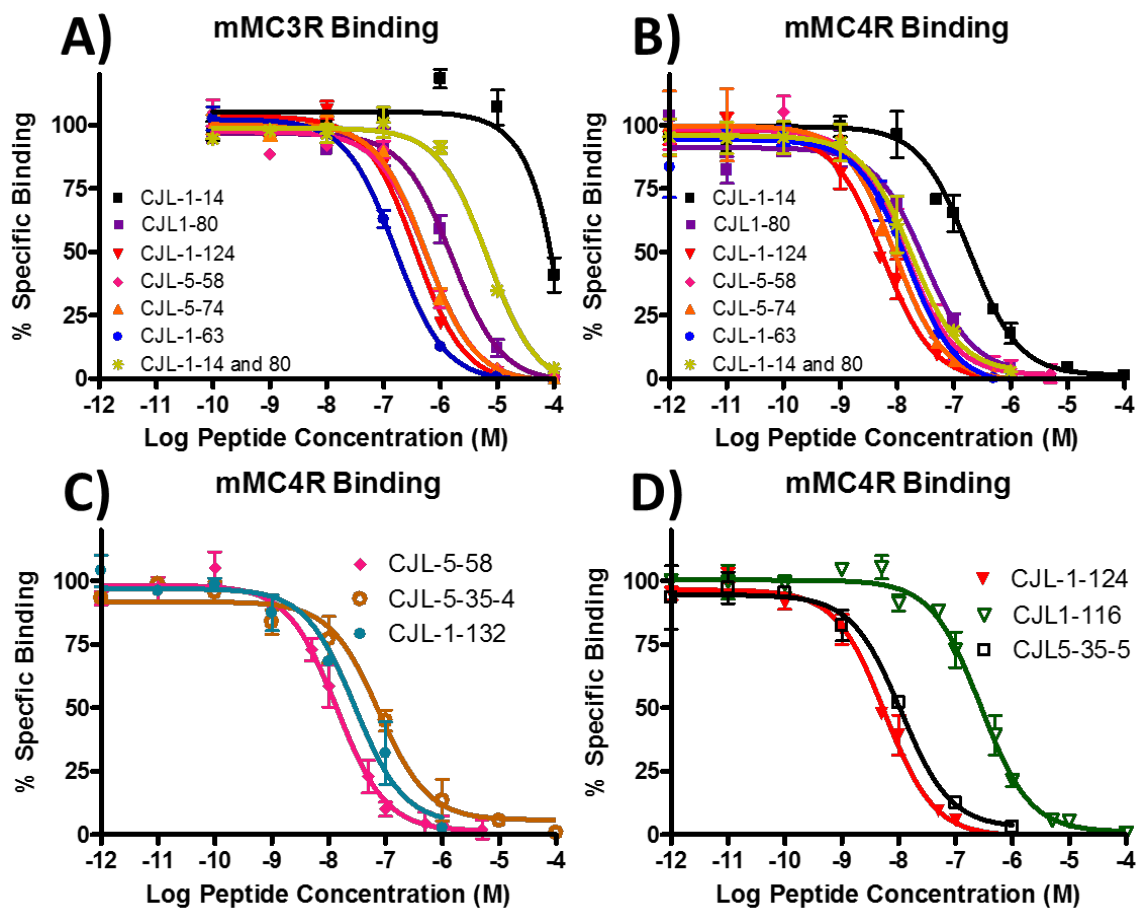


Figure 5.8: Illustrations of the competitive binding experiments against ^{125}I -NDP-MSH at the mMC3R and mMC4R. Top panels: MUmBL ligands compared to monovalent tetrapeptide ligands separately and in a mixture at the mMC3R (A) and mMC4R (B). Bottom panels: Comparing the linker control ligands **CJL-1-116** and **CJL-5-35-5** that comprise MUmBL **CJL-1-124** (D), there is a notable difference in binding affinity (27-fold difference). However, linker control ligands **CJL-5-35-4** and **CJL-1-132** that comprise MUmBL **CJL-5-58**, are much more balanced with only a 4-fold difference (C). Data is shown as mean \pm SEM of at least two independent experiments.

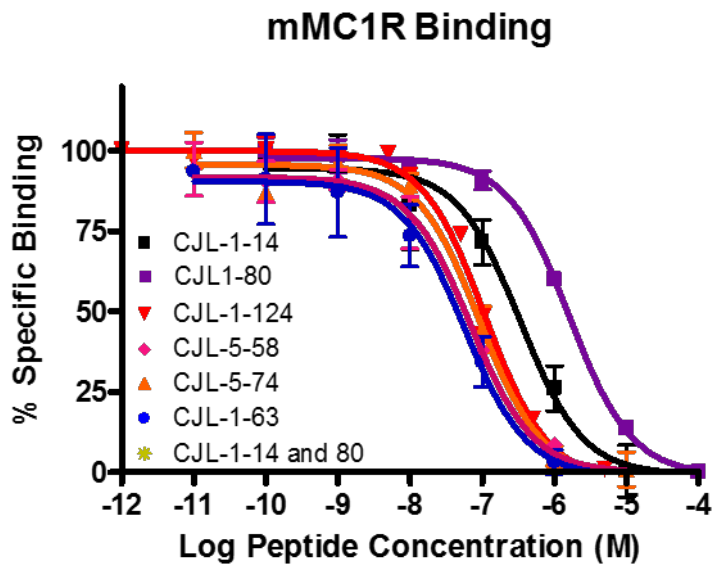


Figure 5.9: Illustrations of the ^{125}I -NDP-MSH competitive binding experiments with MUmBLs compared to monovalent tetrapeptide ligands separately and in a mixture at the mMC1R. For IC₅₀ values see **Table 2** or **Supplemental Table 2**.

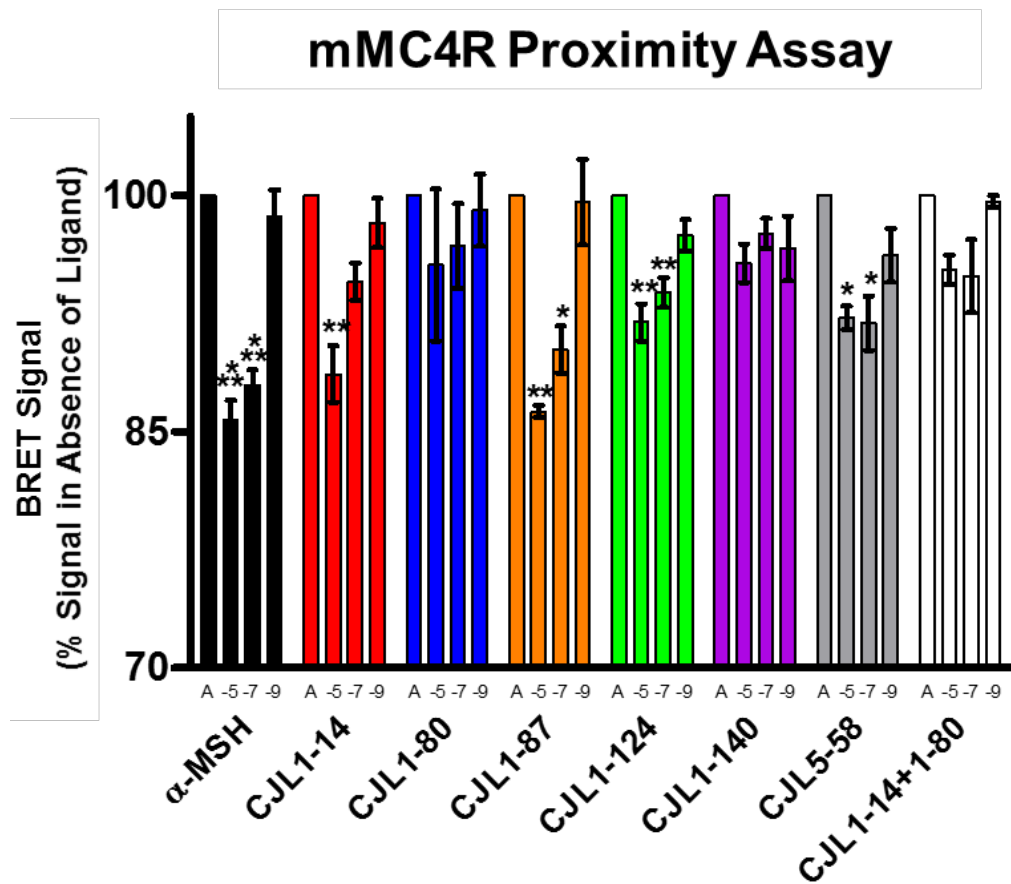


Figure 5.10. Ligand induced response of bioluminescence resonance energy transfer (BRET) signal at the mMC4R-NanoLuc and MC4R-HaloTag homodimer. Maximal BRET signal (100%) was defined as the signal measured when assay buffer (A) was added. Each ligand was dosed at 10^{-5} , 10^{-7} and 10^{-9} M. Significance was determined using a one-way ANOVA to determine overall significance upon treatment followed by a Bonferroni post-hoc test to compare each ligand concentration to assay buffer control (A). * $p < 0.05$, ** $p = 0.01$, *** $p < 0.001$. Data shown as the mean \pm standard error of the mean (SEM) determined from three independent experiments.

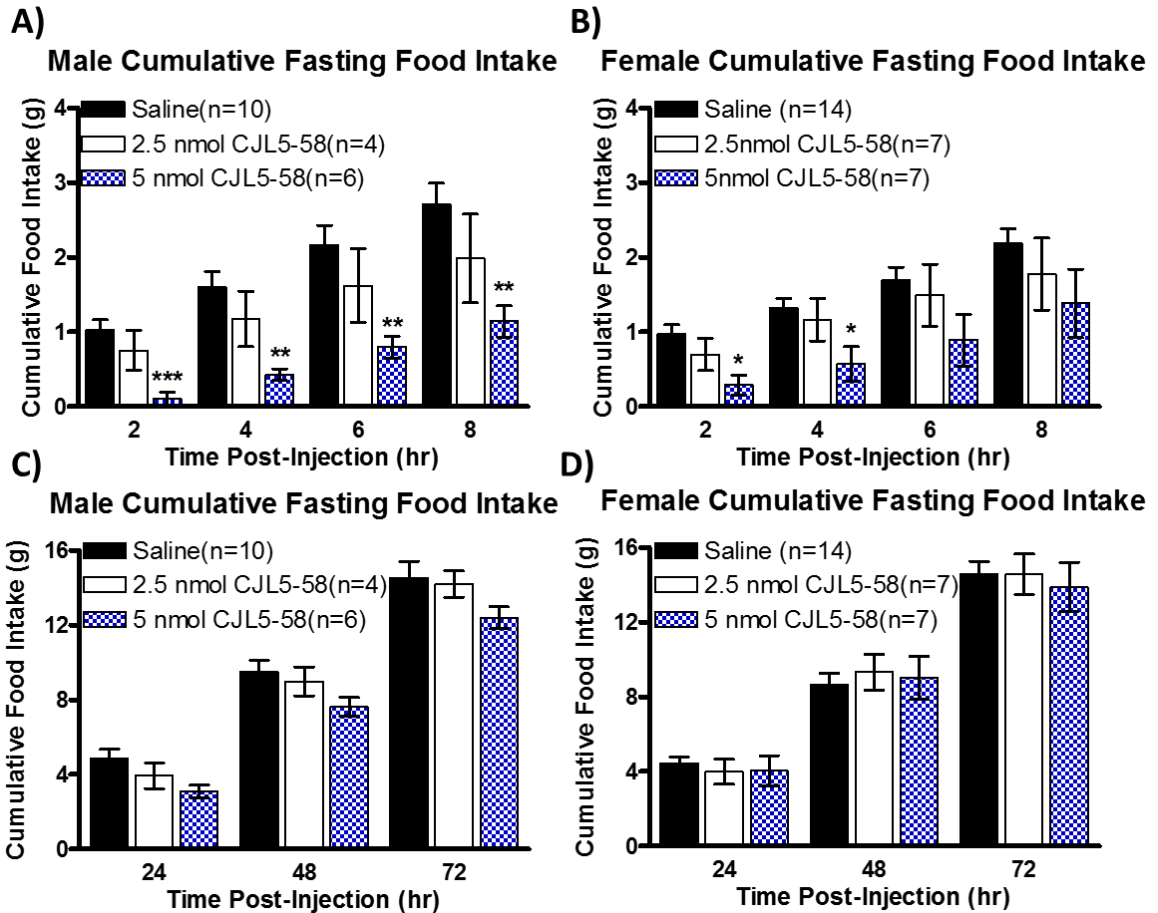


Figure 5.11. The dose response effect of **CJL-5-58** administered ICV on cumulative food intake in male and female wild type mice utilizing a fasting refeeding paradigm. The littermate age matched mice were fasted for 22 hours prior to treatment and the reintroduction of food. Data is shown as mean \pm SEM. Data was analyzed using the SPSS (v23, IBM) using a multivariate general linear model followed by a Bonferroni's *post hoc* test. * $p < 0.05$, ** $p = 0.01$, *** $p < 0.001$ for **CJL-5-58** compared to saline. For body weight information see **Figure 5.12**.

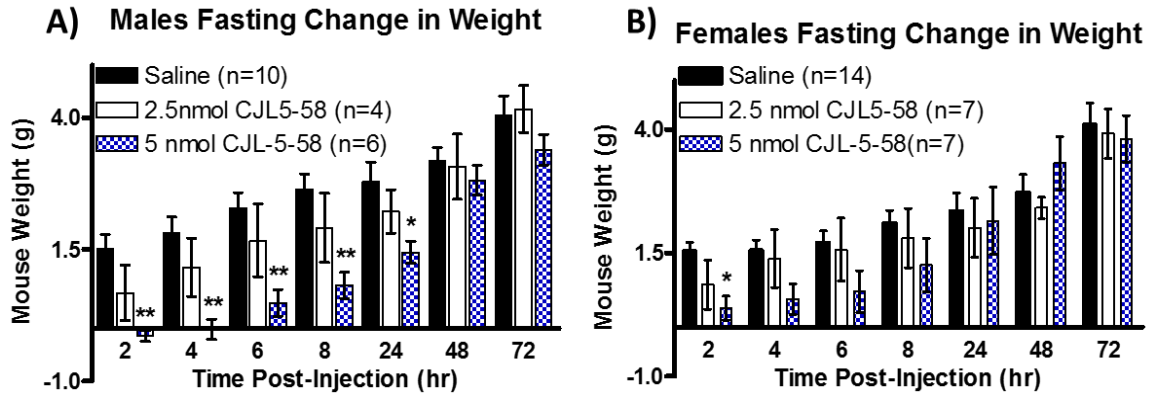


Figure 5.12. The dose response effect of **CJL-5-58** administered ICV on change in body weight in male and female wild type mice utilizing a fasting refeeding paradigm. Data is shown as mean \pm SEM. Data was analyzed using the SPSS (v23, IBM). * $p < 0.05$, ** $p = 0.01$, *** $p < 0.001$ for **CJL-5-58** compared to saline. For food intake information see **Figure 5.11**.

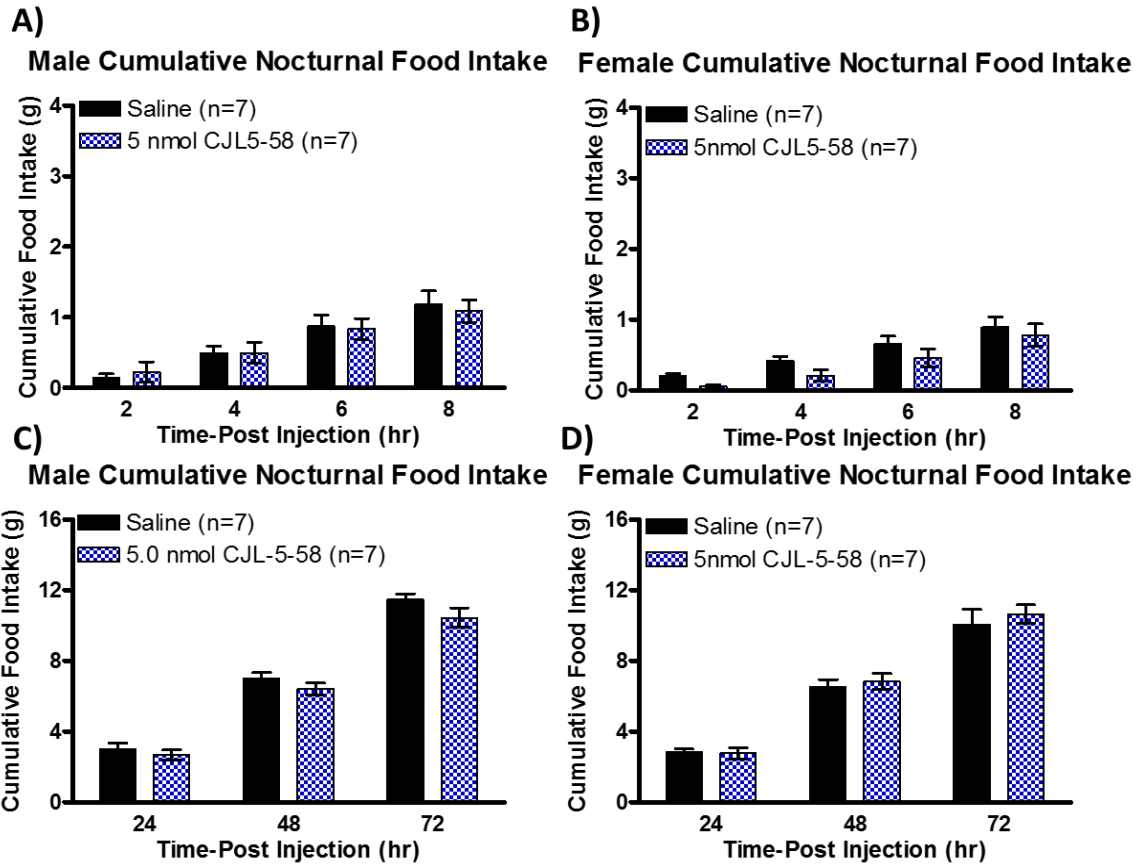


Figure 5.13. The effect of **CJL-5-58** administered ICV on cumulative food intake in male and female wild type mice utilizing nocturnal feeding paradigm. Satiated mice were treated 2 hours prior to lights out. Data is shown as mean \pm SEM. Data was analyzed using the SPSS (v23, IBM) using a multivariate general linear model followed by a Bonferroni's *post hoc* test.. * $p < 0.05$, ** $p = 0.01$, *** $p < 0.001$ for **CJL-5-58** compared to saline.

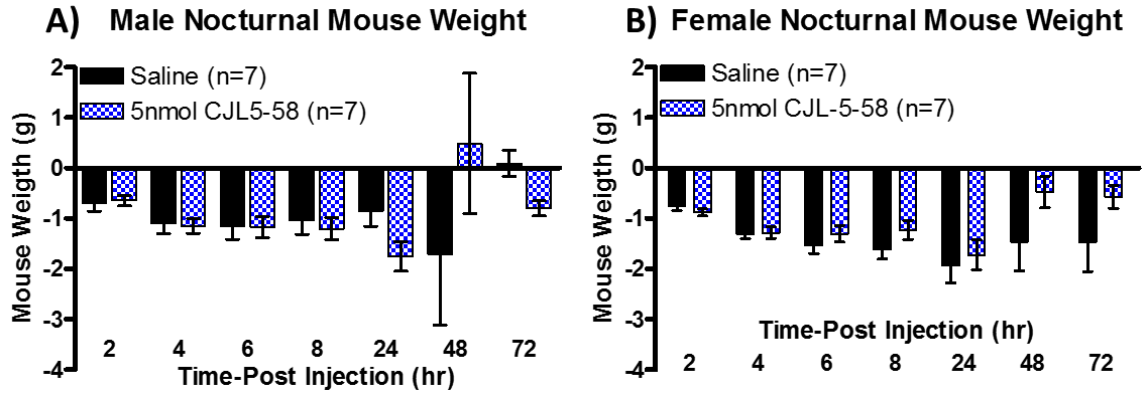


Figure 5.14 The effect of **CJL-5-58** administered ICV on change in body weight (g) in male and female wild type mice utilizing nocturnal feeding paradigm. Data is shown as mean \pm SEM. Data was analyzed using the SPSS (v23, IBM). * $p < 0.05$, ** $p = 0.01$, *** $p < 0.001$ for **CJL-5-58** compared to saline.

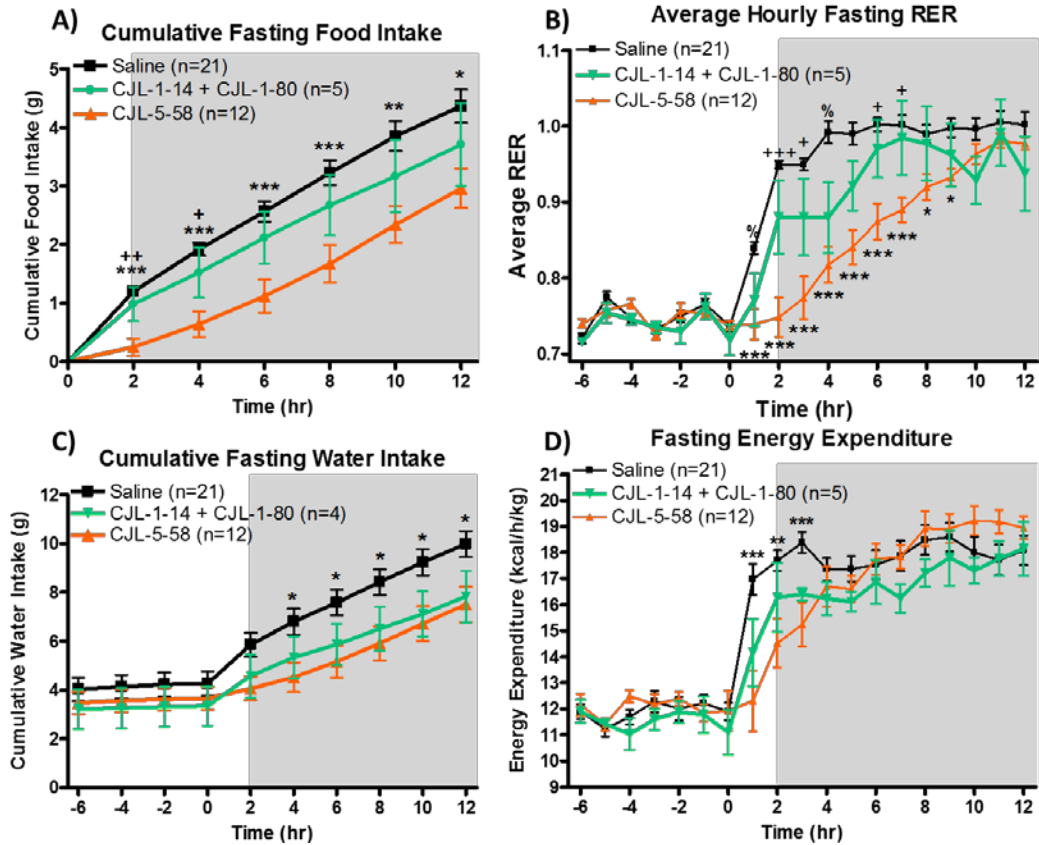


Figure 5.15. TSE metabolic cage parameters after ICV administration of 5 nmols of **CJL-5-58**, or a combination of 5 nmols **CJL-1-14** and 5 nmols **CJL-1-80** (10 nmols total combined peptide) to male wild type mice in a fasting-refeeding paradigm. The littermate age matched mice were fasted for 22 hours. Data is shown as mean \pm SEM. Data was analyzed using the SPSS (v23, IBM) using a multivariate general linear model followed by a Bonferroni's *post hoc* test. * $p < 0.05$, ** $p = 0.01$, *** $p < 0.001$ for **CJL-5-58** compared to saline. % $p < 0.05$, %% $p = 0.01$, %%% $p < 0.001$ for saline compared to co-administration of **CJL-1-14** and **CJL-1-80**. + $p < 0.05$, ++ $p = 0.01$, +++ $p < 0.001$ for **CJL-5-58** compared to co-administration of **CJL-1-14** and **CJL-1-80**. For all parameters from -18 to 24 hours, see **Figure 5.16**.

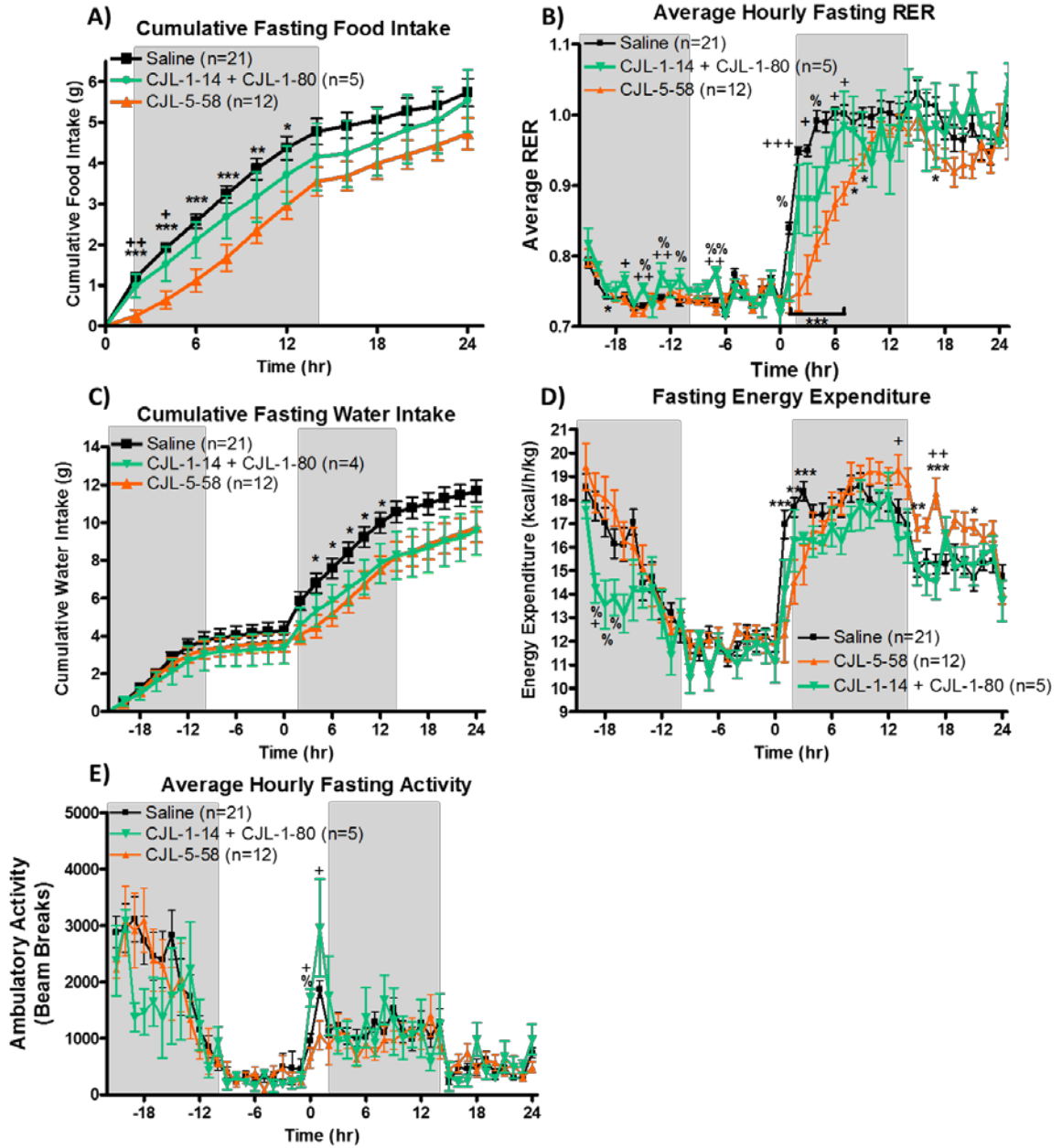


Figure 5.16 TSE metabolic cage parameters after ICV administration of 5 nmols of **CJL-5-58**, or a combination of **CJL-1-14** and **CJL-1-80** (10 nmols total peptide) to male wild type mice in a fasting refeeding paradigm. The littermate age matched mice were fasted for 22 hours. Data is shown as mean \pm SEM. Data was analyzed using the SPSS (v23,

IBM). * $p < 0.05$, ** $p = 0.01$, *** $p < 0.001$ for **CJL-5-58** compared to saline. % $p < 0.05$, %% $p = 0.01$, %%% $p < 0.001$ for saline compared to co-administration of **CJL-1-14** and **CJL-1-80**. + $p < 0.05$, ++ $p = 0.01$, +++ $p < 0.001$ for **CJL-5-58** compared to co-administration of **CJL-1-14** and **CJL-1-80**.

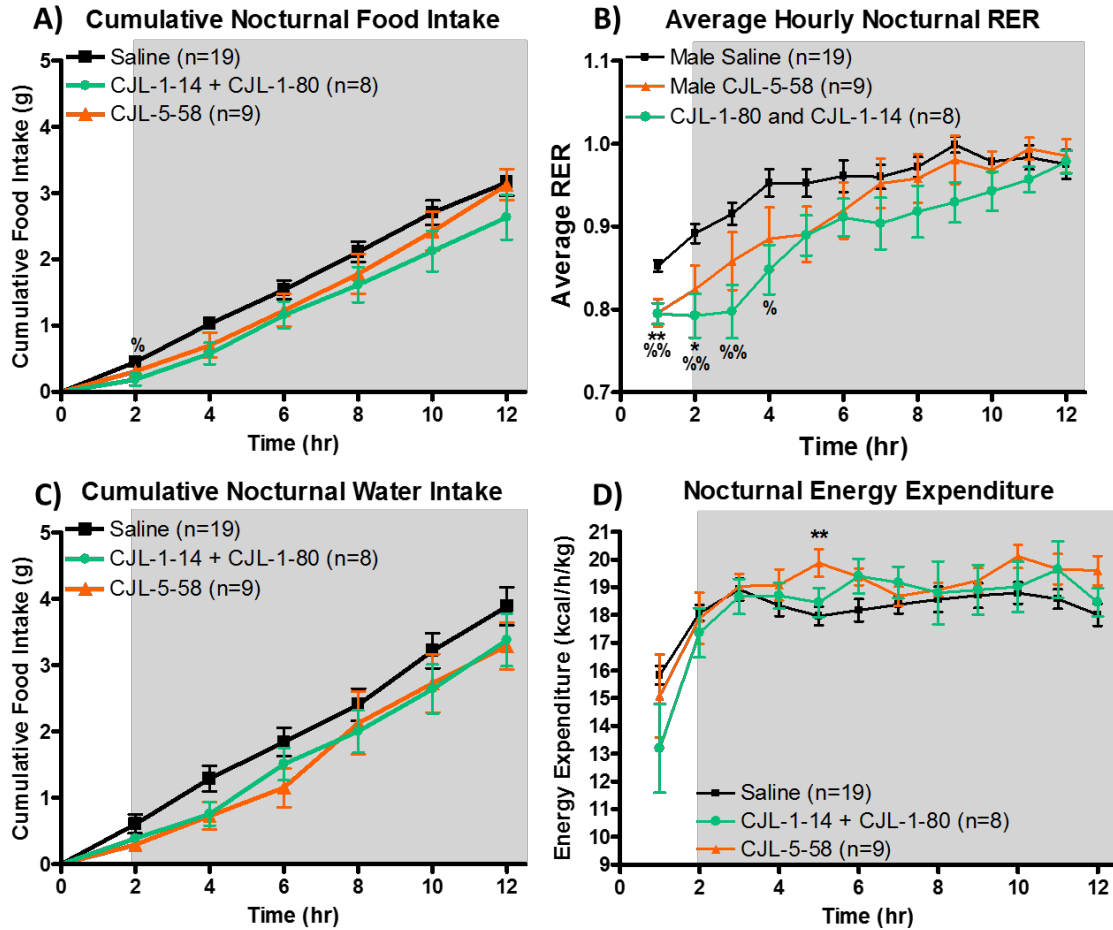


Figure 5.17. TSE metabolic cage parameters after ICV administration of 5 nmols of **CJL-5-58**, or a combination of **CJL-1-14** and **CJL-1-80** (10 nmols total peptide) to male wild type mice in a nocturnal feeding paradigm (no fasting). Satiated mice were treated 2 hours prior to lights out. Data is shown as mean \pm SEM. Data was analyzed using the SPSS (v23, IBM) using a multivariate general linear model followed by a Bonferroni's *post hoc* test. * $p < 0.05$, ** $p = 0.01$, *** $p < 0.001$ for **CJL-5-58** compared to saline. % $p < 0.05$, %% $p = 0.01$, %%% $p < 0.001$ for saline compared to co-administration of **CJL-1-14** and **CJL-1-80**. For all parameters from 0 to 24 hours, see **Figure 5.18**.

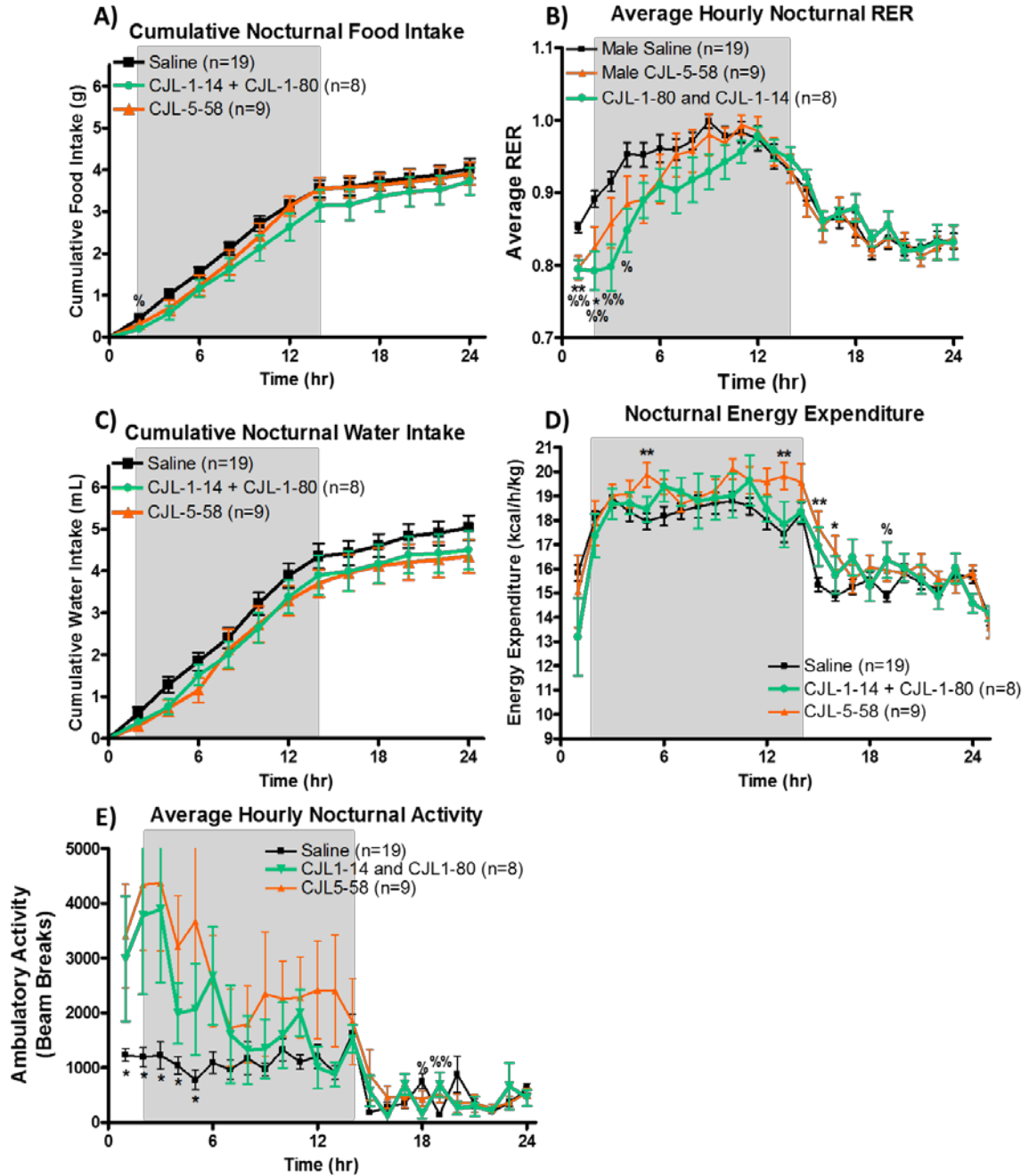


Figure 5.18: TSE metabolic cage parameters after ICV administration of 5 nmols of **CJL-5-58**, or a combination of **CJL-1-14** and **CJL-1-80** (10 nmols total peptide) to male wild type mice in a nocturnal feeding paradigm. Data is shown as mean \pm SEM. Data was

analyzed using the SPSS (v23, IBM). * $p < 0.05$, ** $p = 0.01$, *** $p < 0.001$ for **CJL-5-58** compared to saline. % $p < 0.05$, %% $p = 0.01$, %%% $p < 0.001$ for saline compared to co-administration of **CJL-1-14** and **CJL-1-80**. + $p < 0.05$, ++ $p = 0.01$, +++ $p < 0.001$ for **CJL-5-58** compared to co-administration of **CJL-1-14** and **CJL-1-80**.

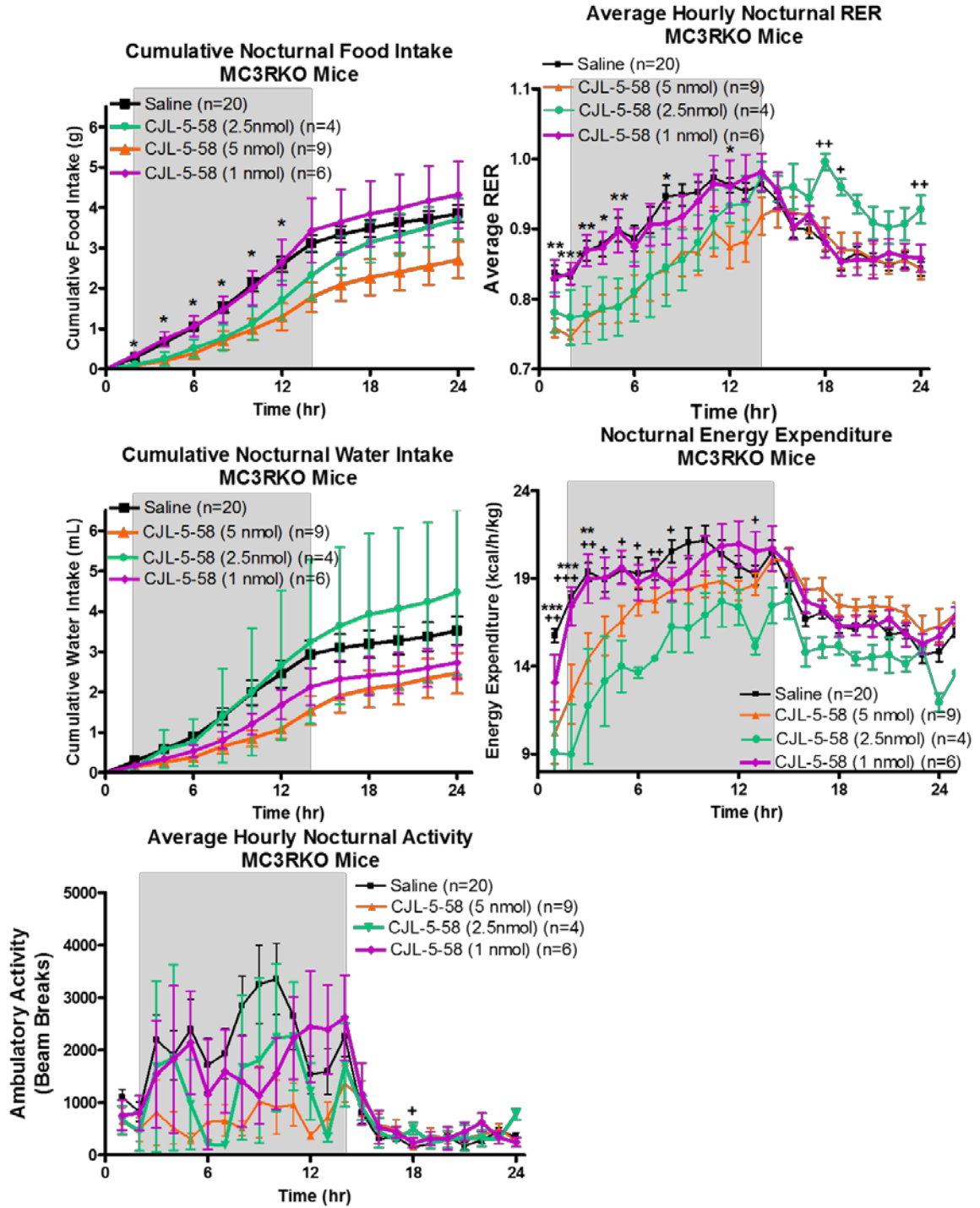


Figure 5.19. TSE metabolic cage parameters after ICV administration of 5.0, 2.5, or 1.0 nmols of **CJL-5-58** to male MC3RKO mice in a nocturnal feeding paradigm. Data is shown

as mean \pm SEM. Data was analyzed using the SPSS (v23, IBM). * $p < 0.05$, ** $p = 0.01$, *** $p < 0.001$ for saline compared to 5 nmols **CJL-5-58**. + $p < 0.05$, ++ $p = 0.01$, +++ $p < 0.001$ for saline compared 2.5 nmol **CJL-5-58**. Note: Some toxicity was observed that may confound these results. (See main text.)

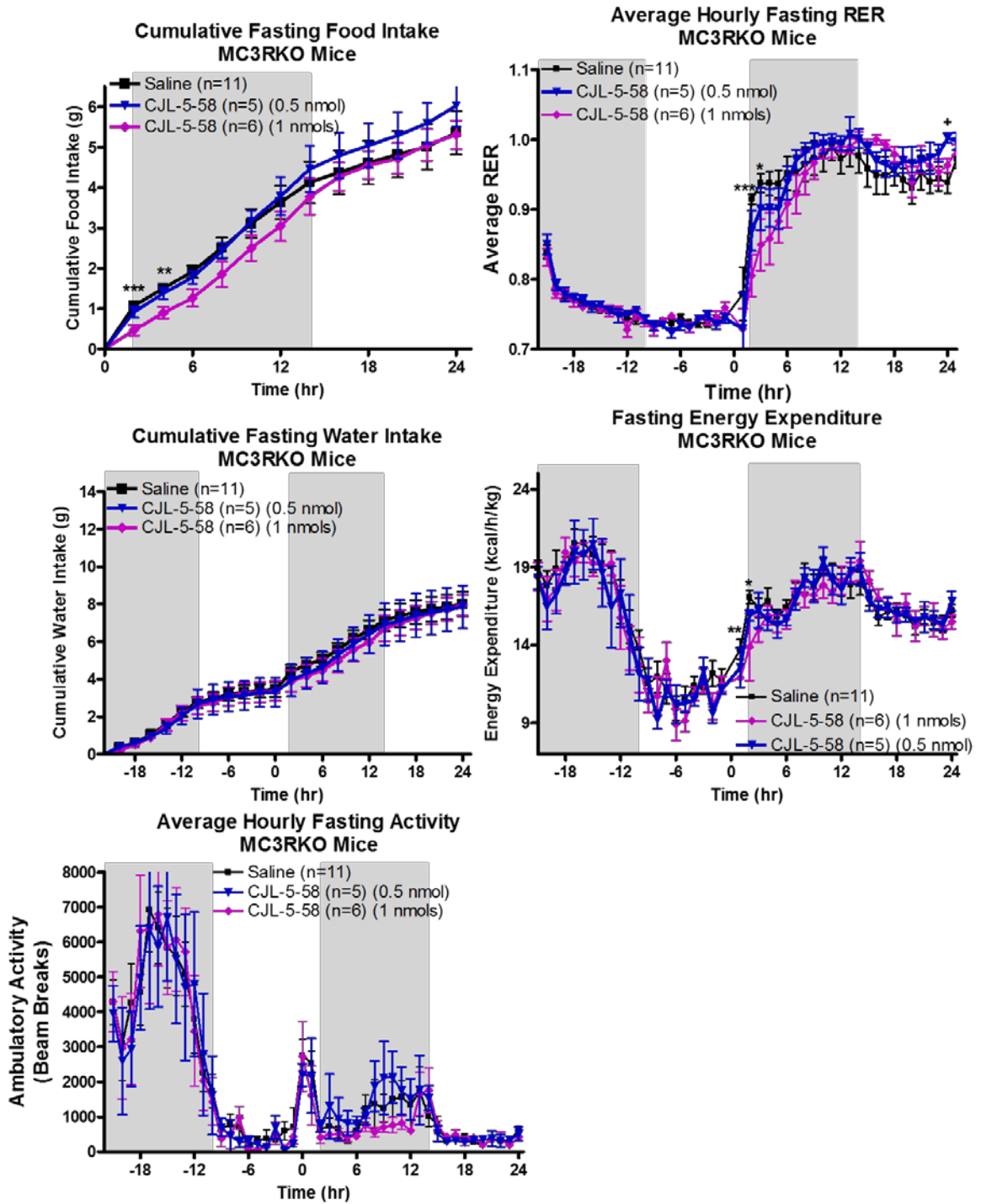


Figure 5.20. TSE metabolic cage parameters after ICV administration of 1.0 or 0.5 nmols of **CJL-5-58** to male MC3RKO mice in a fasting-refeeding paradigm. Data is shown as

mean \pm SEM. Data was analyzed using the SPSS (v23, IBM). * $p < 0.05$, ** $p = 0.01$, ***
 $p < 0.001$ for saline compared to 1.0 nmols **CJL-5-58**. + $p < 0.05$, ++ $p = 0.01$, +++ $p < 0.001$
for saline compared 0.5 nmol **CJL-5-58**. Note: Some toxicity was observed that may
confound these results. (See main text.)

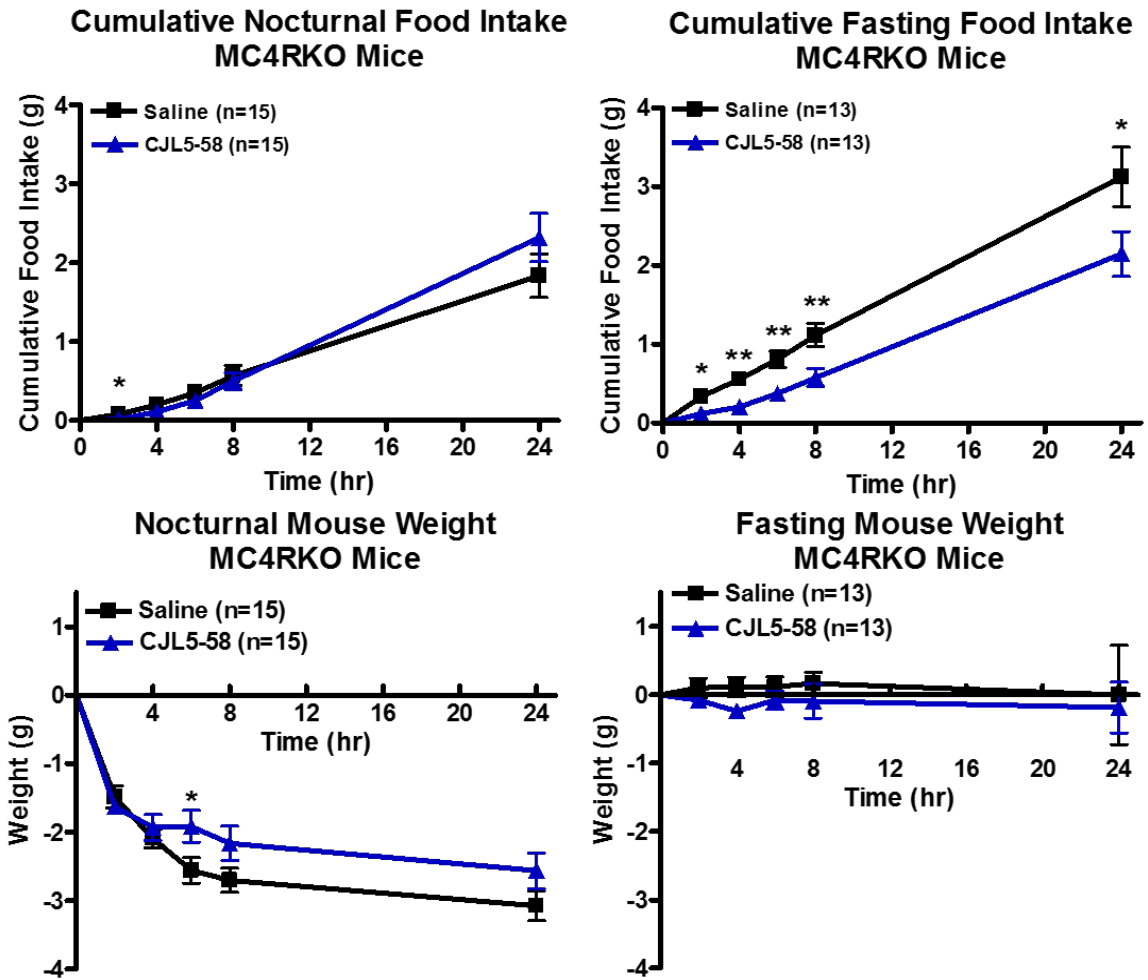


Figure 5.21. The effect of **CJL-5-58** (5 nmols) administered ICV on cumulative food intake and body weight in male MC4RKO mice utilizing nocturnal feeding and fasting-refeeding paradigm in conventional cages. Data is shown as mean \pm SEM. Data was analyzed using the SPSS (v23, IBM). * $p < 0.05$, ** $p = 0.01$, *** $p < 0.001$ for 5 nmol **CJL-5-58** compared to saline. Note: Some toxicity was observed that may confound these results. (See main text.)

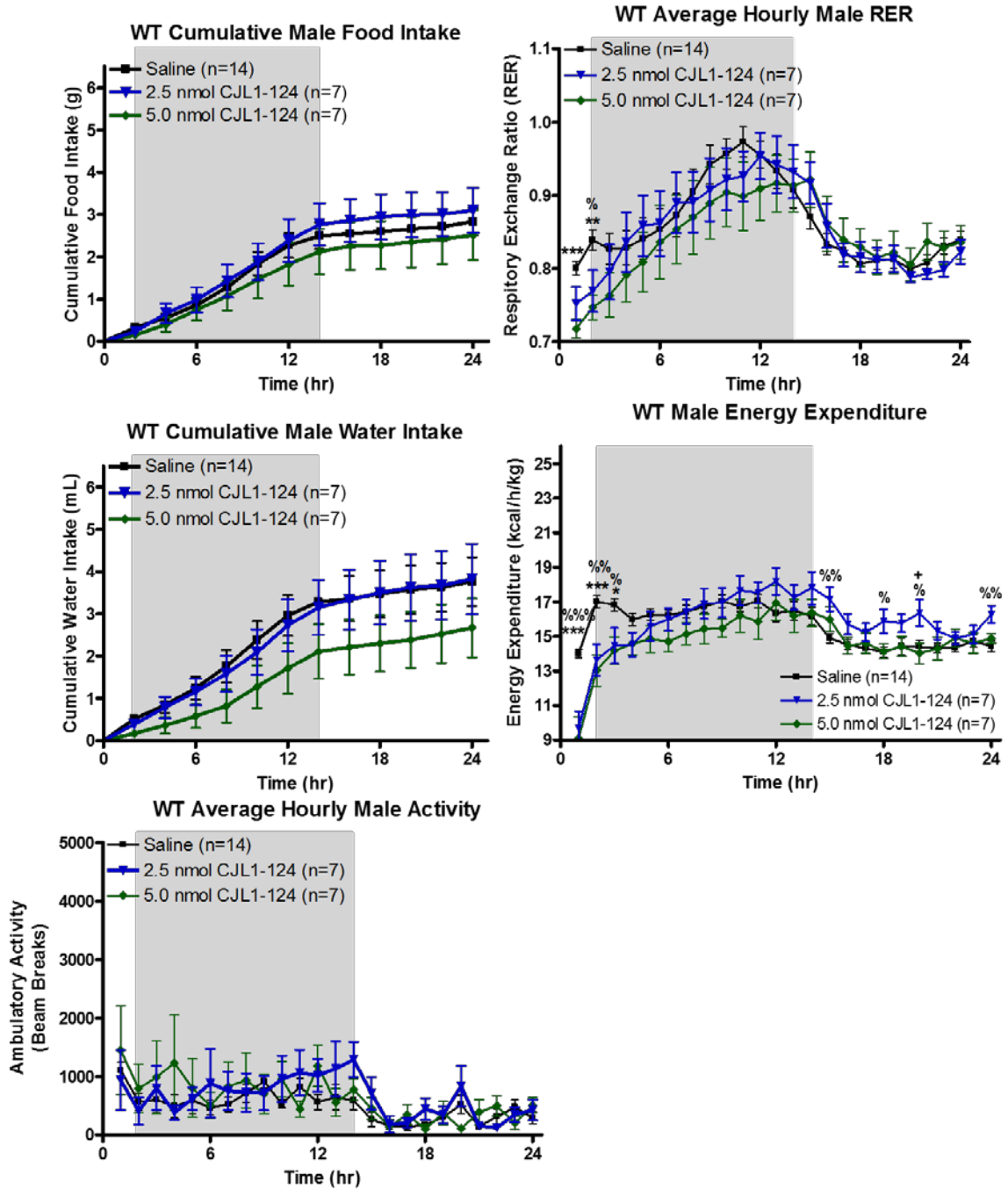


Figure 5.22. TSE metabolic cage parameters after ICV administration of 5.0 or 2.5 nmols of **CJL-1-124** to male wild type mice in a nocturnal feeding paradigm. Data is shown as

mean \pm SEM. Data was analyzed using the SPSS (v23, IBM). * $p < 0.05$, ** $p = 0.01$, ***
 $p < 0.001$ for saline compared to 5 nmols **CJL-5-58**. % $p < 0.05$, %% $p = 0.01$, %%% $p < 0.001$
for saline compared 2.5 nmol **CJL-5-58**. Note: Some toxicity was observed that may
confound these results. (See main text.)

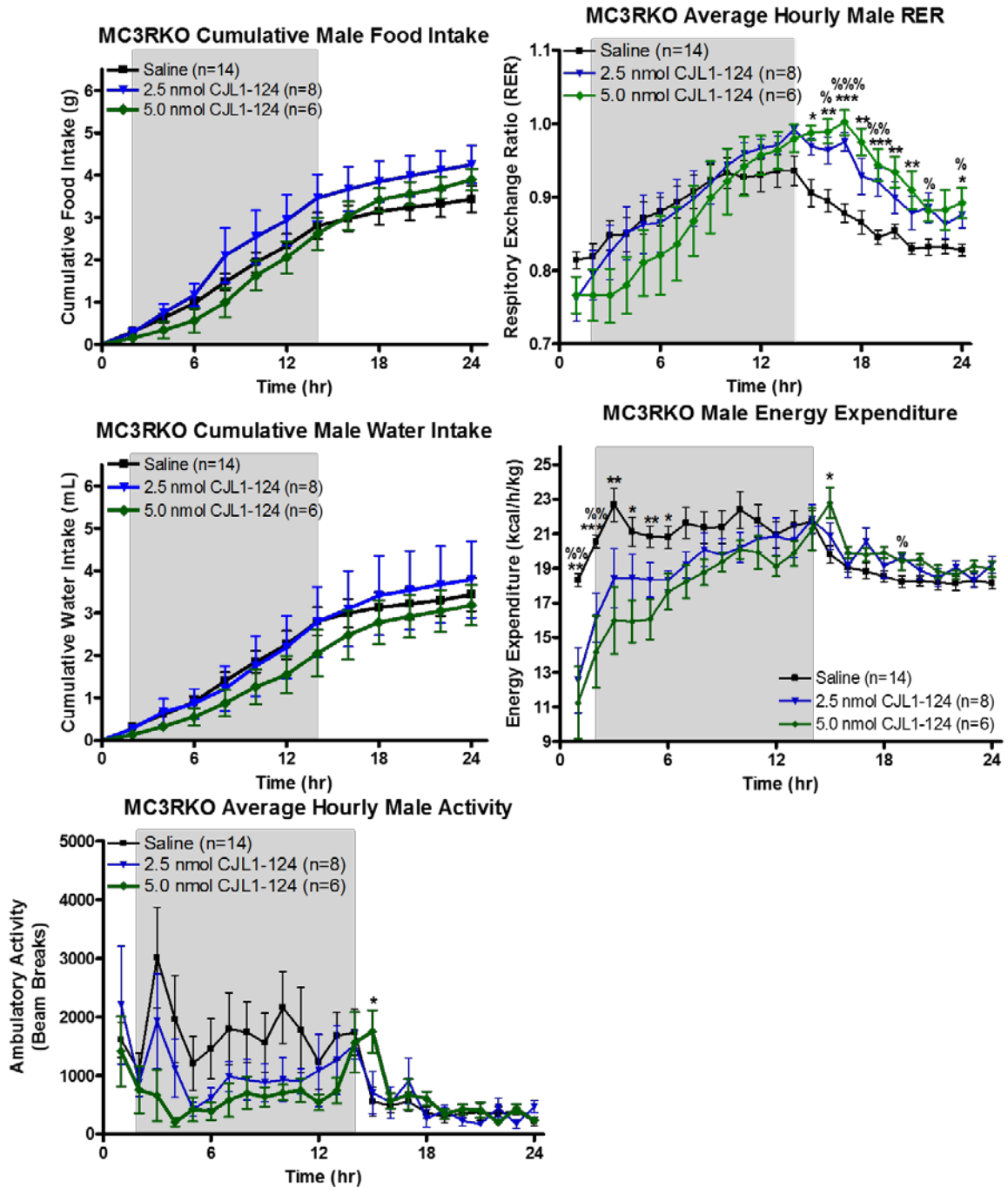


Figure 5.23. TSE metabolic cage parameters after ICV administration of 5.0 or 2.5 nmols of **CJL-1-124** to male MC3RKO mice in a nocturnal feeding paradigm. Data is shown as

mean \pm SEM. Data was analyzed using the SPSS (v23, IBM). * $p < 0.05$, ** $p = 0.01$, ***
 $p < 0.001$ for saline compared to 5 nmols **CJL-5-58**. % $p < 0.05$, %% $p = 0.01$, %%% $p < 0.001$
for saline compared 2.5 nmol **CJL-5-58**. Note: Some toxicity was observed that may
confound these results. (See main text.)

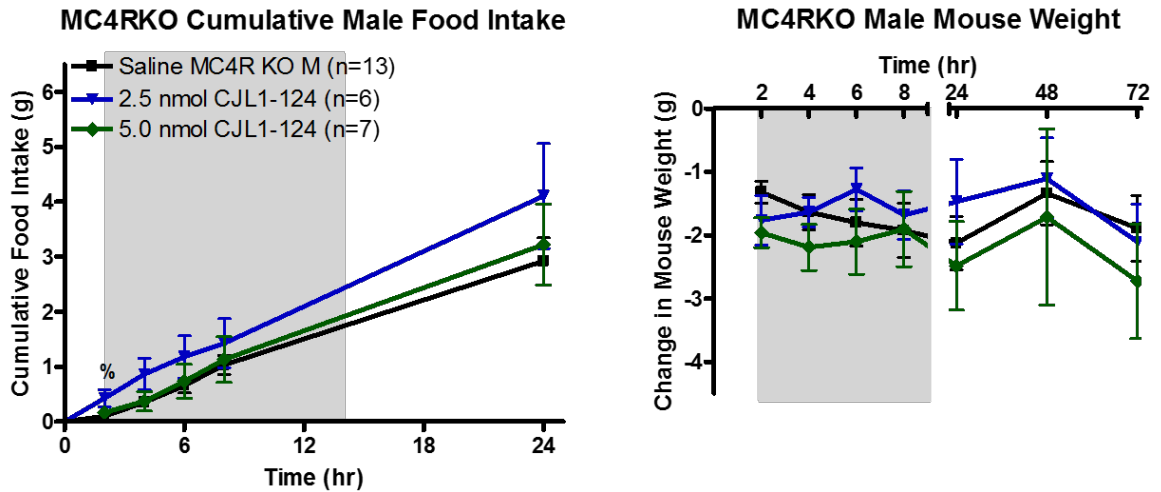


Figure 5.24. The effect of **CJL-1-124** (5.0 and 2.5 nmols) administered ICV on cumulative food intake and body weight in male MC4RKO mice utilizing nocturnal feeding paradigm in conventional cages. Data is shown as mean \pm SEM. Data was analyzed using the SPSS (v23, IBM). % $p < 0.05$ for 2.5 nmol **CJL-5-58** compared to saline. Note: Some toxicity was observed that may confound these results. (See main text.)

Compound	Structure	cAMP Signaling	β -Arrestin Recruitment
		EC ₅₀ (nM) Mean \pm SEM	EC ₅₀ (nM) Mean \pm SEM
NDP-MSH	Ac-Ser-Tyr-Ser-Nle-Glu- His-DPhe-Arg-Trp -Gly-Lys-Pro-Val-NH ₂	0.06 \pm 0.01	120 \pm 50
MTII	Ac-Nle-c[Asp- His-DPhe-Arg-Trp -Lys]-NH ₂	0.03 \pm 0.005	1.6 \pm 0.8
CJL-1-14	Ac- His-DPhe-Arg-Trp -NH ₂	1.8 \pm 0.2	290 \pm 150
CJL-5-35-4	Ac- His-DPhe-Arg-Trp -(PEDG20)-NH ₂	0.67 \pm 0.03	55 \pm 16
CJL-1-116	(PEDG20)- His-DPhe-Arg-Trp -NH ₂	2.0 \pm 0.3	140 \pm 70
CJL5-35-1	Ac- His-DPhe-Arg-Trp -(Pro-Gly) ₆ -NH ₂	5.5 \pm 0.7	1600 \pm 600
CJL-1-41	(Pro-Gly) ₆ - His-DPhe-Arg-Trp -NH ₂	1.1 \pm 0.07	1500 \pm 500
CJL-1-31	Ac- His-DPhe-Arg-Trp -(Pro-Gly) ₆ - His-DPhe-Arg-Trp -NH ₂	0.95 \pm 0.08	1900 \pm 600
CJL-1-87	Ac- His-DPhe-Arg-Trp -(PEDG20)- His-DPhe-Arg-Trp -NH ₂	0.57 \pm 0.05	130 \pm 30
CJL-5-72	Ac- His-DPhe-Arg-Trp -(PEDG20)-(PEDG20)- His-DPhe-Arg-Trp -NH ₂	1.2 \pm 0.3	280 \pm 40
CJL-1-80	Ac- His-DNal(2')-Arg-Trp -NH ₂	50% at 10 μ M	30% at 10 μ M
CJL5-35-5	Ac- His-DNal(2')-Arg-Trp -(PEDG20)-NH ₂	55% at 10 μ M	15% at 10 μ M
CJL-1-132	(PEDG20)- His-DNal(2')-Arg-Trp -NH ₂	50% at 10 μ M	20% at 10 μ M
CJL-5-35-2	Ac- His-DNal(2')-Arg-Trp -(Pro-Gly) ₆ -NH ₂	55% at 10 μ M	30% at 10 μ M
CJL-1-140	Ac- His-DNal(2')-Arg-Trp -(PEDG20)- His-DNal(2')-Arg-Trp -NH ₂	70% at 10 μ M	10% at 10 μ M
CJL-1-63	Ac- His-DNal(2')-Arg-Trp -(Pro-Gly) ₆ - His-DPhe-Arg-Trp -NH ₂	1.9 \pm 0.2	55% at 10 μ M
CJL-5-58	Ac- His-DPhe-Arg-Trp -(PEDG20)- His-DNal(2')-Arg-Trp -NH ₂	1.9 \pm 0.5	45% at 10 μ M
CJL-1-124	Ac- His-DNal(2')-Arg-Trp -(PEDG20)- His-DPhe-Arg-Trp -NH ₂	4.7 \pm 1.0	20% at 10 μ M
CJL-5-74	Ac- His-DNal(2')-Arg-Trp -(PEDG20)-(PEDG20)- His-DPhe-Arg-Trp -NH ₂	5.9 \pm 3.2	25% at 10 μ M
CJL-1-14+ CJL-1-80	Ac- His-DPhe-Arg-Trp -NH ₂ and Ac- His-DNal(2')-Arg-Trp -NH ₂	1.9 \pm 0.2	40% at 10 μ M

Table 5.1: Functional data at the hMC4R. The cAMP signaling potency was determined by AlphaScreen™ assays. The β -arrestin recruitment potency was determined by PRESTO-Tango assays.²⁰² The reported errors are the standard error of the mean (SEM)

determined from at least three independent experiments. Changes less than 3-fold were considered to be within the inherent experimental assay error. The % symbol represents amount of maximal signal observed at 10 μ M compared to control NDP-MSH maximal signal.

Comp.	Structure	HPLC k' (Syst. 1)	HPLC k' (Syst. 2)	Mass (calcd.)	Mass (obs.)	Purity %
CJL-5-35-2	Ac- His-DNal(2') -Arg-Trp-(Pro-Gly) ₆ -NH ₂	5.3	9.7	1660.9	1660.0	>96%
CJL-1-63	Ac- His-DNal(2') -Arg-Trp-(Pro-Gly) ₆ - His-DPhe-Arg-Trp -NH ₂	5.3	8.6	2287.6	2287.3	>95%
CJL-5-58	Ac- His-DPhe-Arg-Trp -(PEDG20)-His- DNal(2') -Arg-Trp-NH ₂	5.4	9.7	1680.9	1680.6	>95%
CJL-1-124	Ac- His-DNal(2') -Arg-Trp-(PEDG20)- His-DPhe-Arg-Trp -NH ₂	6.0	9.5	1680.9	1681.0	>97%
CJL-5-74	Ac- His-DNal(2') -Arg-Trp-(PEDG20)-(PEDG20)- His-DPhe-Arg-Trp -NH ₂	5.7	10.2	1999.3	1999.2	>95%

Table 5.2. The analytical data for peptides synthesized currently. HPLC $k' = (\text{peptide retention time} - \text{solvent retention time}) / \text{solvent retention time}$. System 1 is a 10% to 90% gradient of acetonitrile in water containing 0.1% trifluoroacetic acid over 35 minutes at a flow rate of 1.5 mL/min, and system 2 is the same but with methanol replacing acetonitrile. Product purity was determined by HPLC purity in the solvent system which showed the least purity and integrating the area under the curves of the chromatograms collected at 214 nm. Mass observed was calculated from the M+1 or (M+2)/2 peak.

Comp. ID	mMC1R		mMC3R		mMC4R		mMC5R
	cAMP EC ₅₀ (nM)	Binding IC ₅₀ (nM)	cAMP EC ₅₀ (nM)	Binding IC ₅₀ (nM)	cAMP EC ₅₀ (nM)	Binding IC ₅₀ (nM)	cAMP EC ₅₀ (nM)
	Mean± SEM	Mean± SEM	Mean± SEM	Mean± SEM	Mean± SEM	Mean± SEM	Mean± SEM
CJL-1-14^a	14.1±2.6	390±50	55.5±12.2	60% @100 μM	13.7±1.9	210±60	9.8±2.7
CJL-1-31^a	4.4±0.6	27.5±2.2	20.2±4.0	3300±800	9.2±1.0	33.3±5.1	3.8±0.9
CJL-1-87^a	6.4±1.5	68.6±5.3	10.1±2.5	3500±500	3.6±0.5	9.9±2.9	3.1±0.6
CJL-5-72^a	12.6±3.8	130±20	22.7±3.7	10200±1300	7.3±2.1	53.8±14.1	4.0±0.2
CJL-1-80^a	98.4±32.2	1630±120	15% at 10 μM	1400±200	15% at 10 μM	26.0±3.4	50% at 10 μM
CJL1-140^a	560±140	430±40	60% at 10 μM	350±80	45% at 10 μM	10.4±0.03	790±190
CJL-1-63	16.1±3.5	57.3±10.5	14.9±5.7	170±40	13.0±1.6	15.3±0.7	5.49±0.85
CJL-5-58	10.1±1.5	70.8±7.2	22.4±6.5	590±125	13.5±6.3	14.0±2.5	8.09±3.27
CJL-1-124	13.7±3.5	110±20	18.6±3.8	360±30	70% at 10 μM	7.3±1.5	11.7±3.1
CJL-5-74	44.2±13.6	93.0±9.6	30.4±3.3	570±110	55% at 10 μM	9.6±5.6	8.1±1.8
CJL-1-14+ CJL-1-80	12.7±1.9	ND	75% at 10 μM	6810±330	50% at 10 μM	18.4±5.6	4.7±1.3

Table 5.3: Summary of cAMP functional experiments and competitive binding experiments at the mMC1R, mMC3R, mMC4R, and mMC5R. The cAMP signaling potency was determined by AlphaScreen® assays in at least three independent experiments. In ALPHAScreen™ cAMP functional experiments, % represents amount of maximal signal observed at 10 μM compared to control NDP-MSH maximal signal. IC₅₀ values were determined by competitive binding in which experimental compounds were used to displace ¹²⁵I-NDP-MSH in a dose-response manner. In competitive experiments,

% symbol represent the amount of ^{125}I -NDP-MSH signal reduction at 10 μM . ND means the value was not determined. The reported errors are the standard error of the mean (SEM). Changes less than 3-fold were considered to be within the inherent experimental assay error. The ^a indicates that the synthesis and pharmacology was already reported in Lensing, C.J. *et al J. Med Chem.* 2016, and is included here for comparison. A full summary table of results can be found in the **Table 5.4 and 5.5**.

Comp.	mMC1R	mMC3R		mMC4R		mMC5R
	Agonist EC ₅₀ (nM)	Agonist EC ₅₀ (nM)	Antagonist (pA ₂)	Agonist EC ₅₀ (nM)	Antagonist (pA ₂)	Agonist EC ₅₀ (nM)
	Mean±SEM	Mean±SEM	Mean±SEM	Mean±SEM	Mean±SEM	Mean±SEM
NDP-MSH	0.03±0.01	0.24±0.01		0.46±0.04		0.31±0.03
α-MSH	0.15±0.05	0.76±0.05		4.0±0.9		0.59±0.03
γ-MSH	1090±300	34.6±4.0		869±66		35.1±18.7
CJL-1-14	14.1±2.6	55.5±12.2		13.7±1.9		9.8±2.7
CJL-5-35-4	26.2±9.9	47.4±12.7		5.7±2.9		2.1±0.3
CJL-1-116	24.9±5.9	30.9±7.5		18.5±2.9		3.9±1.3
CJL5-35-1	5.7±.7	107±66		74.1±14.1		52.4±10.3
CJL-1-41	16.4±4.7	27.2±5.2		14.5±2.7		4.9±1.2
CJL-1-31	4.4±0.6	20.2±4.0		9.2±1.0		3.8±0.9
CJL-1-87	6.4±1.5	10.1±2.5		3.6±0.5		3.1±0.6
CJL-5-72	12.6±3.8	22.7±3.7		7.3±2.1		4.0±0.2
CJL-1-80	98.4±32.2	15% at 10 μM	6.04±0.09	15% at 10 μM	8.09±0.04	50% at 10 μM
CJL5-35-5	112±19	25% at 10 μM	6.14±0.06	10% at 10 μM	8.39±0.08	PA, 70% at 10 μM
CJL-1-132	139±17	PA, 45% at 10 μM	6.07±0.18	15% at 10 μM	7.97±0.29	PA, 50% at 10 μM
CJL-5-35-2	153±73	10% at 10 μM	6.88±0.19	5% at 10 μM	7.20±0.9	60% at 10 μM
CJL-1-140	563±142	15% at 10 μM	6.08±0.11	45% at 10 μM	7.68±0.37	786±185
CJL-1-63	16.1±3.5	14.9±5.7		12.99±1.60		5.49±0.85
CJL-5-58	10.1±1.54	22.4±6.5		13.54±6.34		8.09±3.27
CJL-1-124	13.7±3.5	18.56±3.8		70% at 10 μM		11.71±3.13
CJL-5-74	44.2±13.6	30.4±3.3		55% at 10 μM		8.09±1.75
CJL-1-14+ CJL-1-80	12.71±1.9	75% at 10 μM		50% at 10 μM		4.66±1.28

Table 5.4: Functional data at the mMC1R, mMC3R, mMC4R, and mMC5R with data from Chapter 3 for comparison. The cAMP signaling potency was determined by AlphaScreen®

assays. The reported errors are the standard error of the mean (SEM) determined from at least three independent experiments. PA represents partial agonist. The % symbol represents amount of maximal signal observed at 10 μ M compared to control NDP-MSH maximal signal. Changes less than 3-fold were considered to be within the inherent experimental assay error. The synthesis and pharmacology was already reported in Lensing, CJ *et al J. Med Chem.* 2016, 59, 3112-3128 for some compounds.²⁵

Published	Compound Name	mMC1R		mMC3R		mMC4R	
		IC ₅₀ (nM) Mean± SEM	n	IC ₅₀ (nM) Mean±SEM	n	IC ₅₀ (nM) Mean±SEM	n
	NDP-MSH	0.31±0.08	6	4.18±0.61	14	1.09±0.12	19
Published	CJL-1-14	388±52	2	60% @100 μM	2	214±55	6
Published	CJL-5-35-4	178±4	2	13400±5100	2	83±14	4
Published	CJL-1-116	705±6	2	78% @100 μM	3	292±67	4
Published	CJL-5-35-1	225±63	2	85% @100 μM	2	841±290	2
Published	CJL-1-41	1090±110	3	8430±230	2	258±27	2
Published	CJL-1-31	27.5±2.2	2	3250±760	2	33±5.1	3
Published	CJL-1-87	68.6±5.3	3	3470±510	2	9.9±2.9	4
Published	CJL-5-72	131±18	2	10200±1300	2	54±10	2
Published	CJL-1-80	1630±120	2	1430±190	2	26.0±3.4	2
Published	CJL-5-35-5	997±190	2	1310±120	2	10.7±0.6	2
Published	CJL-1-132	1870±220	4	999±290	2	21.8±1.9	3
	CJL-5-35-2	633±128	2	350±60		39.2±1.0	2
Published	CJL-1-140	430±40	3	350±80	5	10.4±0.03	2
	CJL-1-63	57.3±10.5	2	167±36.1	2	15.3±0.7	2
	CJL-5-58	70.8±7.2	2	592.3±123.5	2	14.0±2.5	2
	CJL-1-124	106.69±20.8	2	364.5±28.6	2	7.3±1.5	4
	CJL5-74	93±9.6	2	566.1±110	2	9.6±5.6	2
	CJL-1-14+ CJL-1-80	ND		6810±330	2	18.4±5.6	2

Table 5.5: Summary of competitive binding experiments at the mMC1R, mMC3R, and mMC4R with data from Chapter 3 for comparison. IC₅₀ values were determined by competitive binding in which experimental compounds were used to displace ¹²⁵I-NDP-MSH in a dose-response manner. In competitive experiments, % represent the amount of

¹²⁵I-NDP-MSH signal reduction at 100 μM. The reported errors are the standard error of the mean (SEM). Changes less than 3-fold were considered to be within the inherent experimental assay error. The **Pub.** Indicates that the synthesis and pharmacology was already reported in Lensing, CJ *et al J. Med Chem.* 2016, 59, 3112-3128.²⁵

Paradigm	Housing	Wild-type	MC3RKO	MC4RKO
Fasting	TSE	Adverse; Sig. Effect	Adverse; Sig. Effect	N.D
Nocturnal	Conventional	No Adverse; Sig. Effect	N.D	Adverse; Sig. Effect
Fasting	TSE	Adverse; No Effect	Adverse; Sig. Effect	N.D.
Nocturnal	Conventional	No Adverse; No Effect	N.D	No Adverse; No Effect

Table 5.6. Table of adverse reactions observed in the current experiments with **CJL-5-58** in wild-type mice, MC3RKO mice, and MC4RKO mice. Adverse means that adverse reactions were observed in the experiments as described in the text. Sig. Effect means that a significant effect on food intake was observed. N.D. means not determined indicating that the experiment was not performed.

Chapter 6: Progressing the Structure Activity Relationship (SAR) of Bivalent Ligands: Evaluating the Effects of the Linker Length and Pursuing a Retro-Inverso Approach

All peptides were designed, synthesized, purified, and analytically characterized by Cody Lensing under the supervision of Carrie Haskell-Luevano. Katlyn Fleming helped with mass determination by MALDI-TOF. The *in vitro* pharmacology studies were performed by Cody Lensing, Katie Freeman, and Sathya Schnell, all members of the Haskell-Luevano lab group. Radiolabeled ^{125}I -NDP-MSH was prepared by Robert Speth. Serum stability studies were performed by Cody Lensing and Adam Zarth.

6.1 Chapter Overview

The previous chapters provide evidence that melanocortin bivalent ligands have unique effects that are distinct from their monovalent counterparts in both *in vitro* and *in vivo* assay paradigms. This work validates further pursuit of melanocortin bivalent ligand design as pharmacological probes for both *in vitro* and *in vivo* exploratory studies. However, there is much work to be done to further explore the medicinal chemistry space around melanocortin bivalent ligand design. In this chapter, we describe two different approaches that were pursued to further study melanocortin bivalent ligands' structure activity relationship (SAR). Homobivalent ligands were designed with 13, 16, 19, 20, and 22 atom linkers to explore the effects of linker length. Overall, these studies resulted in a "flat" SAR in which the compounds all have similar potencies and efficacies. Bivalent ligands were also designed to include the retro-inverso tetrapeptide scaffold DTrp-DArg-

Phe-DHis. Although this scaffold lacked high binding affinity and potency, it was very metabolically stable. The incorporation of this scaffold into bivalent ligands yielded ligands with varying potency and metabolic stabilities. The SAR trends observed from this design and their future implications are discussed in this chapter.

6.2 Introduction

Although the main focus of the current thesis was to establish the effects of bivalent ligands at multiple melanocortin receptors *in vitro* and to understand their effects *in vivo*, we did initiate preliminary medical chemistry campaigns to optimize the melanocortin bivalent ligand design. These medicinal chemistry design strategies were attempts to better understand the structure activity relationship (SAR) of the bivalent ligands as well as circumvent foreseeable problems. The two main strategies that will be discussed in this chapter include: 1) testing the effects of linker length using polyethylene glycol (PEG)-based linkers and 2) incorporating a retro-inverso scaffold into the bivalent ligands.

The current approach of testing the effects of linker length was based on work performed by Portoghese and coworkers. They have previously observed that bivalent ligands are quite sensitive to linker length.^{10, 11, 224, 225} Small extensions in the length of the linker can significantly change activity.^{10, 11, 224, 225} Single atom linker extensions previously resulted in noteworthy changes (>500-fold) in the *in vivo* potency in a series of bivalent ligands tested for antinociception.¹⁰ A two-atom linker extension in a bivalent ligand previously increased potency by 1100-fold.²²⁵ Therefore, based on the previous results presented in **Chapter 3** and **Chapter 4** that the PEDG20 linker when incorporated

into compound **CJL-1-87** resulted in increased binding affinity at the mMC4R and was metabolically stable,^{25, 132} we choose to explore the chemical space around this linker. Homobivalent ligands similar to **CJL-1-87** were designed that utilized the His-DPhe-Arg-Trp tetrapeptide scaffold. The ligands were designed to include PEG-based linkers that were 13, 16, 19, and 22 atoms long and connected two His-DPhe-Arg-Trp scaffolds (**Figure 6.1**). A MUmBLs series similar to **CJL-5-58** in **Chapter 5** was also designed with the 19 and 22 atom PEG-based linkers connecting a His-DPhe-Arg-Trp scaffold and a His-DNal(2')-Arg-Trp scaffold (**Figure 6.1**).

Another feature of the melanocortin bivalent ligands presented in **Chapter 3-5** is that all of these ligands, even the homobivalent ligands, are asymmetric.^{25, 132} This is due to the standard solid phase peptide synthesis convention utilized in which ligands are synthesized from the C-terminus to the N-terminus in a linear fashion. This results in a Trp residue connected to the linker on the N-terminus and a His residue connected to the linker on the C-terminus. Depending on how each receptor in a melanocortin dimer orientates itself, the asymmetry of the bivalent ligands could positively or negatively affect binding. The previous results of increased binding affinity and changes in pharmacology of the melanocortin bivalent ligands compared to their monovalent counterparts suggests that the asymmetric design utilized in **Chapter 3-5** does bridge melanocortin dimers.^{25, 132} However, to explore more thoroughly the effects of pharmacophore orientation on bivalent ligand design, we sought a design strategy that could be utilized to study this quickly and efficiently. Ideally, we wanted familiar and optimized chemistry that would give us access

to all four possible orientations rapidly. As these ligands were designed prior to the metabolic studies performed in **Chapter 4** and **Chapter 5**, we also had some concern at this point about metabolic stability of the peptidic ligands. We sought to optimize metabolic stability simultaneously with the design strategy. One known strategy that fit all these requirements was to incorporate a retro-inverso scaffold in the bivalent ligands.³¹²⁻³¹⁴

In a retro-inverso isomer, the direction of the sequence is reversed and the chirality of each sidechain are switched [*e.g.* levo (L) to dextro (D)]. In making both changes simultaneously the orientation of each side chain would be the same in theory, but with the directionality of the backbone reversed (**Figure 6.2A**). The retro-inverso strategy has previously been used to increase metabolic stability of peptides, while retaining or even increasing the activity of the original pharmacophore.^{312, 313} It should also be noted that although the paper chemistry appears to be a “golden goose” and is successful in some systems, the retro-inverso strategy has also been reported to have detrimental effects on activity.^{312, 313} Nonetheless, we persisted in hopes of both increasing the bivalent ligands’ metabolic stabilities and increasing their potencies. The retro-inverso tetrapeptide scaffold DTrp-DArg-Phe-DHis was incorporated into the bivalent ligand design by standard solid phase synthesis to create pseudo-symmetric bivalent ligands (**Figure 6.2B**). All the different orientations of the retro-inverso bivalent ligands with different linker lengths were designed and synthesized in parallel (**Table 6.1**).

6.3 Results and Discussion

6.3.1 Synthesis

The retro-inverso and linker length libraries were envisioned and synthesized at the same time in parallel. Resin was split at various points as described in **Chapter 2** and **Chapter 3 (Scheme 2.1)**. Specifically, the common C-terminal tetrapeptide scaffolds were synthesized in bulk for each ligand and the resin was split before adding the linker and N-terminus tetrapeptide scaffold. Compounds **CJL-5-119-1**, **CJL-5-119-2**, **CJL-5-119-3**, **CJL-5-119-4**, **CJL-5-119-6**, **CJL-9-22-1**, and **CJL-9-22-2** were synthesized from common resin that had the His-DPhe-Arg-Trp scaffold added. Compounds **CJL-5-127-1**, **CJL-5-127-2**, **CJL-5-127-3**, **CJL-5-127-4**, **CJL-5-127-5**, **CJL-5-127-6**, **CJL-5-127-7**, **CJL-5-127-8** were synthesized from common resin that had the DTrp-DArg-Phe-DHis scaffold added. Compounds **CJL-9-22-3**, **CJL-9-22-4**, and **CJL-9-22-5** were synthesized from common resin that had the His-DNal(2')-Arg-Trp scaffold added. All ligands were cleaved from resin and purified to >95% by RP-HPLC. Their masses were confirmed by MALDI-TOF (**Table 6.1**).

6.3.2 *In Vitro* Biological Characterization

As previously described in **Chapter 2-5**, the ability of compound to induce cAMP signaling was measured by the AlphaScreen[®] cAMP Assay Technology in live HEK293 cells stably expressing the mMC1R, mMC3R, mMC4R, and mMC5R. Competitive binding affinity studies with the experimental ligands were also performed utilizing ¹²⁵I-NDP-MSH as previously described in **Chapters 2-5**. Data from **CJL-1-14** was previously

reported in **Chapter 3**.²⁵ Compound **CJL-5-119-2** is the same structure as compound **CJL-1-87**, but was remade during parallel synthesis as a control. It was observed to be slightly more potent in the cAMP functional AlphaScreen assay than previous results in **Chapter 3** (*i.e.* 2-fold at the mMC1R, 4-fold at the mMC3R, 2-fold at the mMC4R, and 6-fold at the mMC5R).²⁵ This may have been due to changes that the manufacture PerkinElmer made to their AlphaScreen kit as control peptide NDP-MSH was also observed to be slightly more potent (*i.e.* 3-fold at the mMC1R, 4-fold at the mMC3R, even at the mMC4R, and 5-fold at the mMC5R) compared to those achieved previously in **Chapter 3**.²⁵ A PerkinElmer sales representative emailed us the following about the changes in the AlphaScreen kit: “There were two things that were changed in the kit. The antibody was changed, because our sole supplier discontinued that antibody and we also changed the tracer, which is the same as the AlphaLISA. You should see better signal with the new kit. Everything should be the same, but if you need help, please do not hesitate to let me know.”

It should be noted that the IC₅₀ values of **CJL-5-119-2** and **CJL-1-87** calculated from competition with ¹²⁵I-NDP-MSH were within experimental error at the mMC1R, mMC3R, and mMC4R. This suggests the compounds were indeed the same, and the changes in cAMP functional potency were due to the manufacture’s changes in the AlphaScreen Kit. Compound **CJL-9-22-4** is the same structure as **CJL-5-58** reported in **Chapter 5**, but was also remade during parallel synthesis as a control. Similar to **CJL-1-87** and NDP-MSH, it showed increased potency (*i.e.* 2-fold at mMC1R, 3-fold at the

mMC3R, 3-fold at the mMC4R, and 4-fold at the mMC5R). Because all control compounds had increased functional potency in the “new” AlphaScreen® cAMP Assay after PerkinElmer made changes (but binding affinity was unaffected), it seems likely that the changes in potency are due to the AlphaScreen assay components. Because all compounds appear more potent, comparison internally with the “new” AlphaScreen kit should not be affected. However, direct comparison to previous cAMP AlphaScreen results should be avoided. Therefore, only results from the current studies are included in this chapter for AlphaScreen data.

6.3.2.1 Linker Length Analogs

The homobivalent ligands based on the His-DPhe-Arg-Trp tetrapeptide with varying linker lengths showed a “flat” SAR in the AlphaScreen assay (**Table 6.2**). This suggests that the linker lengths tested did not measurably affect cAMP signaling at least in this particular assay paradigm. At the mMC1R, the EC₅₀ values ranged from 2.1 to 3.1 nM. At the mMC3R, the EC₅₀ values ranged from 1.3 to 2.7 nM. At the mMC4R, the EC₅₀ values ranged from 1.1 to 1.7 nM. At the mMC5R, the EC₅₀ values ranged from 0.39 to 0.63 nM. The linker length for MUmBL analogs **CJL-9-22-3**, **CJL-9-22-4**, and **CJL-9-22-5** also appeared to have a “flat” SAR (**Table 6.2**). The lack of SAR in the functional cAMP assays was not surprising considering that we and others have reported only small gains in functional signaling when measuring a single assay parameter with melanocortin bivalent ligands.^{25, 26, 132 28} In fact the results are very consistent with the hypothesis presented

in **Chapter 5** of asymmetrically signaling homodimers in which only one binding event of the melanocortin bivalent ligands results in cAMP signaling (**Figure 5.1**).

To further evaluate the homobivalent linker length analogs, competitive binding affinity experiments were performed (**Table 6.3**). The competitive binding experiments of the linker length analogs competing against ^{125}I -NDP-MSH also showed relatively flat SAR. At the mMC1R, the IC_{50} values ranged from 34 to 58 nM. At the mMC3R, the IC_{50} values ranged from 1170 to 2140 nM. At the mMC4R, the IC_{50} values ranged from 10 to 15 nM. The lack of SAR observed in the competitive binding assay paradigms following linker length extensions was surprising, but may be explained in several ways. First, detecting small disturbances in already highly potent ligands can be difficult. It has previously been observed that high potency (or affinity) pharmacophores incorporated into bivalent ligands can potentially mask multivalent interactions.^{27, 122, 223} This was discussed in detail in **Chapter 3** to rationalize the lack of increased binding affinity observed with compound **CJL-1-140** at the mMC4R.²⁵

A second possibility for the lack of improvement observed may be due the kinetics of the assay. In the current binding assay paradigm, a one-hour compound incubation was used. The purposed bivalent binding mode increases binding affinity by increasing the local concentration of the second pharmacophore and by lowering the dissociation of the bivalent ligand from the receptor (**Figure 3.4**). However, bivalent ligand design should not dramatically affect the entropic costs of the first binding event with the first pharmacophore. This means that the bivalent binding mode has a strong kinetic component

that may be affected by time. It could be hypothesized that our current one hour endpoint in the assay paradigm may not be optimal for measuring changes in the bivalent binding mode due to linker length, and therefore, no effects are observed currently. Also different melanocortin ligands have been reported to have different kinetics of binding, and different radiolabeled probes have been reported to give different IC_{50} or K_i values for the same experimental ligands in competitive binding assays.^{27, 132, 205, 219, 315} Therefore, ^{125}I -NDP-MSH may not be the optimal probe for detecting bivalent ligand effects due to its slow dissociation.^{205, 315} If NDP-MSH has a faster on-rate than the bivalent ligands and a slow dissociation, it may be difficult to detect small changes in binding affinity due to bivalent ligand design. However, more dramatic changes would be detectable such as the differences between the 20 atom PEDG20 linker in **CJL-1-87** and the 40 atom PEDG20-PEDG20 linker in **CJL-5-72** observed in **Chapter 3**.²⁵

A third possibility is that the currently used PEG-based linkers are too flexible to detect small changes in linker length. It may be that with small 3 atom changes in linker length segments, the flexible PEG-based linker can “bend” to the appropriate length to bridge the receptor dimers. It may be necessary to use a more rigid linker system. Or a wider range of linker lengths could be used. Again, evidence of this hypothesis may be observed in the results presented in **Chapter 3** in which the 20 atom PEDG20 was doubled to the 40-atom PEDG20-PEDG20 and resulted in observable changes in binding affinity (3-5 fold).²⁵

Finally, it must be mentioned that it is possible that the hypothesized bivalent binding mode has not been realized. This seems unlikely given the increased binding affinity observed with bivalent ligands compared to their monovalent counterparts that has been described in **Chapter 3-5**.^{25, 132} Also in strong support of the bivalent binding mode is the data that the linkers with bigger differences in length (*i.e.* 20-atom PEDG20, 36-atom (Pro-Gly)₆, and 40 atom PEDG20-PEDG20) did result in differential effects on binding affinity in **Chapter 3**.²⁵ Finally, if the bivalent ligands were binding in a monovalent fashion, it would be difficult to rationalize the unique *in vitro* and *in vivo* functional pharmacologies described in **Chapter 4** and **Chapter 5** with **CJL-1-87** and **CJL-5-58**.¹³² However, since no direct structural data of melanocortin bivalent ligand binding exists to date, it cannot be completely ruled out that some other mechanism is at play to explain the complex pharmacology that has been observed throughout current thesis work. Further work into characterizing the pharmacology and probing the SAR of bivalent ligands will provide further evidence to prove or disprove the hypothesized bivalent binding mode. But in order to gain confirmation of bivalent ligand binding, most likely a crystal structure of a bivalent ligand binding a melanocortin receptor dimer will be necessary.

6.3.2.2 Retro-Inverso Analogs

The first set-back while assessing the retro-inverso analogs was the discovery that both **CJL-5-127-7** (Ac-DTrp-DArg-Phe-DHis-NH₂) and **CJL-5-127-8** (DTrp-DArg-Phe-DHis-NH₂) showed minimal agonist cAMP functional activity (<35% at 100 μM at any receptor subtype) (**Table 6.2**). Furthermore, compound **CJL-5-127-7** showed little ability

to displace ^{125}I -NDP-MSH in competitive binding assays (**Table 6.3, Figure 6.3**). At a concentration of 100 μM , **CJL-5-127-7** reduced signal from ^{125}I -NDP-MSH binding by 30% at the mMC1R, 25% at the mMC4R, and showed no detectable result at the mMC3R. Although concerning, this lack of binding affinity may not be too problematic in the bivalent ligands that contain the His-DPhe-Arg-Trp scaffold considering the hypothesized bivalent binding mode. This is because the His-DPhe-Arg-Trp scaffold may act as a “targeting moiety” for the poorly-binding DTrp-DArg-Phe-DHis, tethering it in the precise location where it needs to be to bind the second receptor. Considering the greatly reduced entropic cost of binding for this second pharmacophore, it can still be hypothesized that the retro-inverso scaffold in a bivalent ligand will bind the second receptor in a dimer pair even with its poor binding affinity. Evidence of “targeting moiety” effect was presented in **Chapter 5** in which the MUmBLs’ binding affinities increased 130 to 480-fold compared to the weaker binding tetrapeptide scaffold. In fact, the weak binding affinity of the retro-inverso pharmacophore scaffold may aid in the detection of the synergistic effects of the purported bivalent binding mode.

All bivalent compounds that contained the His-DPhe-Arg-Trp scaffold had EC_{50} values less than 10 nM in the cAMP AlphaScreen assay at all receptor subtypes even when containing the DTrp-DArg-Phe-DHis scaffold (**Table 6.2**). This is consistent with the hypothesis of asymmetric signaling homodimers presented in **Chapter 5** in which only one pharmacophore in a bivalent ligand is responsible for the cAMP signaling. This means the lack of functional activity of the DTrp-DArg-Phe-DHis scaffold would not affect cAMP

signaling assay results. No discernable SAR was observed at the mMC1R, mMC3R, and mMC5R for these compounds. At the mMC4R, there was a trend that placement of the His-DPhe-Arg-Trp scaffold in the N-terminus and the DTrp-DArg-Phe-DHis on the C-terminus was slightly more potent than the opposite orientation. This can be observed with the 3-fold increased potency of **CJL-5-127-3** compared to **CJL-5-119-6** that both contain the 19 atom PEG-based linker. There is also a 3-fold increased cAMP potency of **CJL-5-127-2** compared **CJL-5-119-5** that both contain the PEDG20 linker (**Table 6.2**).

The ligands that contained only the DTrp-DArg-Phe-DHis (*i.e.* **CJL-5-127-4**, **CJL-5-127-5**, and **CJL-5-127-6**) had greatly reduced ability to induce cAMP signaling. Compound **CJL-5-127-5** was the most potent compound and was a full agonist at the mMC4R ($EC_{50} = 3200$ nM). This was as significant improvement in cAMP signaling potency at the mMC4R compared to its monovalent counterpart **CJL-5-127-7** that showed only 20% activity at 100,000 nM. This suggests that the bivalent ligand design can dramatically increase the functional potency of the retro-inverso monovalent tetrapeptide. The full agonism observed with **CJL-5-127-5** suggests that retro-inverso scaffold may still be useful for targeting the melanocortin receptors, but further optimization of the scaffold will be necessary. This also recapitulates the previous trend established in **Chapter 3** that the PEDG20 linker is an optimal linker for targeting the mMC4R.²⁵ Even more interestingly, it shows trends in the cAMP functional activity that are based on the length of the linker connecting the two tetrapeptide scaffolds (*i.e.* 20 atom PEDG20 > 22 atom PEG > 19 atom PEG). These trends were not observed above with the more potent linker

length analogs. This supports the hypothesis explained above that the high potency of His-DPhe-Arg-Trp is masking the subtler effects of linker length in the analogs above.

It was decided to focus on only the retro-inverso bivalent ligands that contained the PEDG20 linker for competitive binding experiments at the mMC1R, mMC3R, and mMC4R (**Figure 6.3, Table 6.3**). Bivalent ligand **CJL-5-127-5** that contains two DTrp-DArg-Phe-DHis pharmacophores had the lowest binding affinity of the retro-inverso bivalent analogs, but it did show improvement compared to the monovalent ligand **CJL-5-127-7** (Ac-DTrp-DArg-Phe-DHis-NH₂) at all three subtypes tested. Both the bivalent ligands that contained one DTrp-DArg-Phe-DHis scaffold and one His-DPhe-Arg-Trp scaffold had improved binding affinity compared to both their monovalent counterparts **CJL-1-14** (Ac-His-DPhe-Arg-Trp-NH₂) and **CJL-5-127-7** (Ac-DTrp-DArg-Phe-DHis-NH₂). At the mMC1R, **CJL-5-119-5** and **CJL-5-127-2** were both *c.a.* 3-fold more potent than the monovalent ligand **CJL-1-14**. At the mMC3R, **CJL-5-119-5** and **CJL-5-127-2** was estimated to have 12-fold and 21-fold increased binding affinities, respectively, compared to **CJL-1-14**. At the mMC4R, **CJL-5-127-2** had 7-fold increased binding affinity compared to **CJL-1-14**.

Two important trends were observed in the binding experiments with the retro-inverso analogs. First, the increased binding affinity of the retro-inverso scaffold containing bivalent ligands **CJL-5-119-5** and **CJL-5-127-2** compared to **CJL-1-14** (Ac-His-DPhe-Arg-Trp-NH₂) supports the hypothesized bivalent binding mode. It is unlikely that the addition of the very weakly binding DTrp-DArg-Phe-DHis would be able to

increase binding affinity beyond **CJL-1-14** alone without some sort of reduction in entropic cost, presumably through the bivalent binding mode. If monovalent binding of the His-DPhe-Arg-Trp pharmacophore was the only factor in binding, it would be expected that **CJL-5-119-5** and **CJL-5-127-2** would be the same as **CJL-1-14**. It can be proposed that the His-DPhe-Arg-Trp scaffold acts as a “targeting” region to bring the DTrp-DArg-Phe-DHis scaffold very close to the second binding pocket in a melanocortin dimer (**Figure 3.4**). This increases the local concentration of the DTrp-DArg-Phe-DHis scaffold dramatically, resulting in the increased binding affinity of the bivalent ligands. This also helps explain the high potency of these ligands in the cAMP functional assays. Second, based on the observation that **CJL-5-127-2** had greater fold enhancements than **CJL-5-119-5**, it can be hypothesized that the orientation having the Trp and DTrp residues connected to the linker, and therefore closer together, was favored at the mMC3R and mMC4R. This may have future design implications if completely symmetric bivalent ligands are synthesized.

6.3.3 *In Vitro* Mouse Serum Stability Assays

In order to assess the metabolic stability of both the linker length analogs and retro-inverso analogs, *in vitro* mouse serum stability assays were performed as described previously in **Chapter 2 (Figure 6.4)**.¹³² The linker length analogs **CJL-5-119-1**, **CJL-5-119-2**, and **CJL-5-119-3** all had similar metabolic stability in mouse serum (**Figure 6.4A**). Considering **CJL-1-87** (which is the same as **CJL-5-119-2**) has adequate metabolic

stability for *in vivo* studies as reported in **Chapter 4**,¹³² this suggests that all these linker systems may be used in future design strategies.

The retro-inverso tetrapeptide **CJL-5-127-7** was very metabolically stable in mouse serum. There was 90% of the parent peptide intact after 24 h. (**Figure 6.4B**) and 80% intact after 72 h (**Figure 6.4C**). It can be estimated that the half-life of **CJL-5-127-7** would be 210 h. The most stable bivalent ligand assayed was **CJL-5-127-5** that is comprised of two DTrp-DArg-Phe-DHis pharmacophores. The parent peptide was still 45% intact at 24 h. This was approximately the same stability reported in **Chapter 4** for compound **CJL-1-14**.¹³² The two bivalent ligands that contained both the His-DPhe-Arg-Trp and DTrp-DArg-Phe-DHis had slightly increased metabolic stability than **CJL-5-119-2** (that is the same as **CJL-1-87**). The half-life of **CJL-5-119-5** and **CJL-5-127-2** were 8.6 h and 7.5 h, respectively. The half-life of **CJL-5-119-2** was 6.0 h.

6.4 Conclusions

Although the current SAR campaigns described in this chapter were less than ideal, we hope it serves as a guide for future melanocortin bivalent ligand SAR campaigns. The studies focused on linker length analogs show that further confirmation of the bivalent binding mode will be necessary. Specifically, it can be hypothesized that the current binding assay paradigm utilized will need optimization to be sensitive enough to detect small changes in binding affinity that result from linker length adjustments. It may be necessary to do kinetic binding assays, or some other type of assay that allows real-time monitoring. It may also be necessary to utilize a more rigid linker so that the flexibility of

the linker cannot compensate for changes in linker length. This may allow for further optimization of melanocortin bivalent ligand design.

The retro-inverso design strategy currently presented was thought-provoking to develop and push forward, but the loss in affinity and efficacy with the retro-inverso tetrapeptide scaffold was undesirable. Interestingly, we did accomplish increased metabolic stability with this scaffold. It was almost inversely proportional that with decreased binding affinity and functional potency, there was increased metabolic stability. It still seems tempting to hypothesize that the retro-inverso tetrapeptide scaffold, given its dramatically increased metabolic stability, may be a valuable scaffold for future melanocortin ligand design. Starting with a metabolically stable tetrapeptide scaffold combined with the years of knowledge on how to create potent and high affinity melanocortin ligands may allow for the creation of a metabolically stable and high affinity peptidic melanocortin ligands.

While there are a variety of possibilities to explain the lack of SAR observed in the linker length analogs, it still may raise questions about the purported bivalent binding mode. Interestingly, the gain in binding affinity of retro-inverso containing bivalent analogs **CJL-5-119-5** and **CJL-5-127-5** beyond that of the monovalent ligand Ac-His-DPhe-Arg-Trp-NH₂ provides strong evidence of the presumed bivalent binding mode. It is almost paradoxical that these two libraries that were idealized, design, synthesized, and assayed in parallel provide a strong argument for and a strong argument against the bivalent binding mode. However, given all we have learned throughout this thesis work,^{25, 132} I

believe there is more evidence in support of the bivalent binding mode than against it. More exploration into bivalent ligand SAR will be necessary to understand more thoroughly the complex pharmacology that has been observed in the current thesis work.

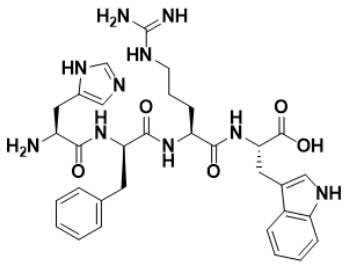
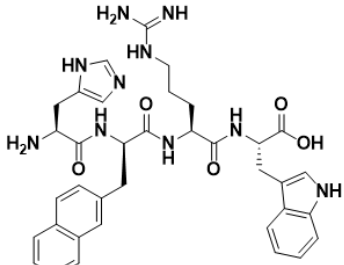
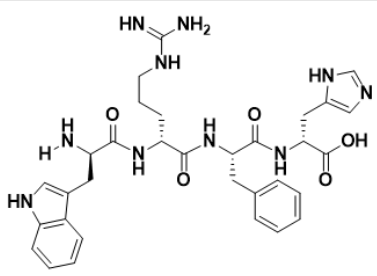
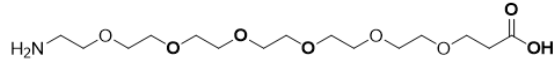
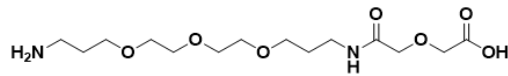
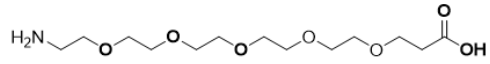
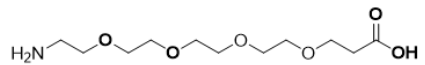
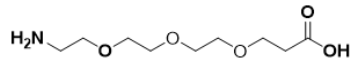
Selected Scaffolds	
His-DPhe-Arg-Trp	
His-DNal(2')-Arg-Trp	
DTrp-DArg-Phe-DHis	
Selected Linkers	
(PEG)(22 atoms)	
(PEDG20)	
(PEG)(19 atoms)	
(PEG)(16 atoms)	
(PEG)(13 atoms)	

Figure 6.1. The chemical structures of selected scaffolds and linkers used in **Chapter 6**.

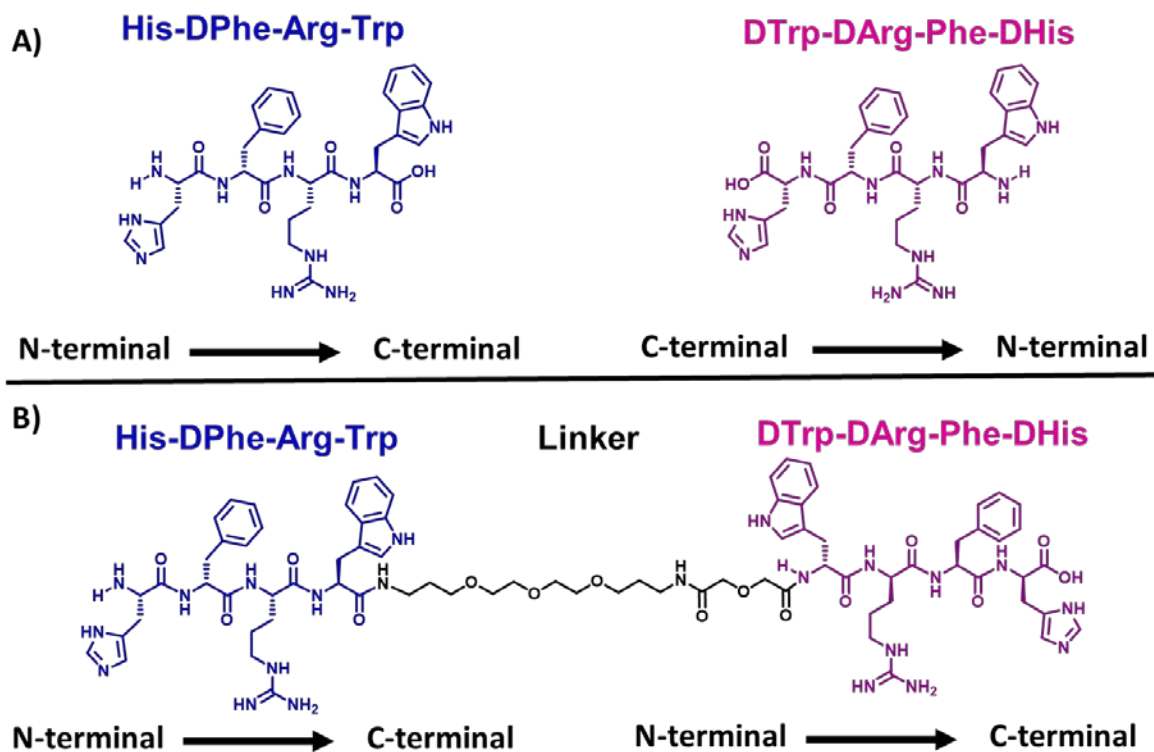


Figure 6.2. Design of melanocortin bivalent ligands containing retro-inverso scaffolds. **A)** By reversing the sequence and by switching the chirality of each side chains, a retro-inverso isomer has the same side chain orientations but with the directionality of the backbone reversed. **B)** Bivalent ligands can be synthesized with standard solid phase peptide synthesis that have pseudo-symmetry in their side chain orientation.

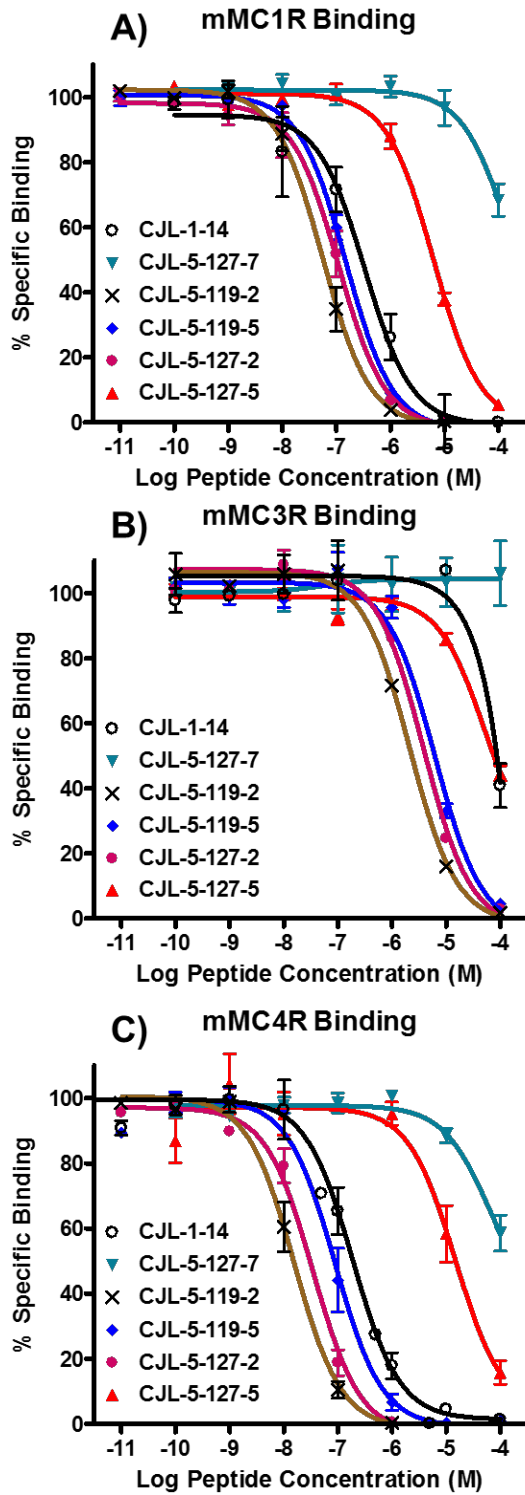


Figure 6.3. Illustrations of the competitive binding experiments at the mMC1R (A), mMC3R (B), and mMC4R (C) looking at the effects of the retro-inverso scaffold **DTrp-DArg-Phe-DHis** when it is incorporated in the bivalent ligands with the PEDG20 linker. **CJL-1-14** is from previously reported data from **Chapter 3**.²⁵

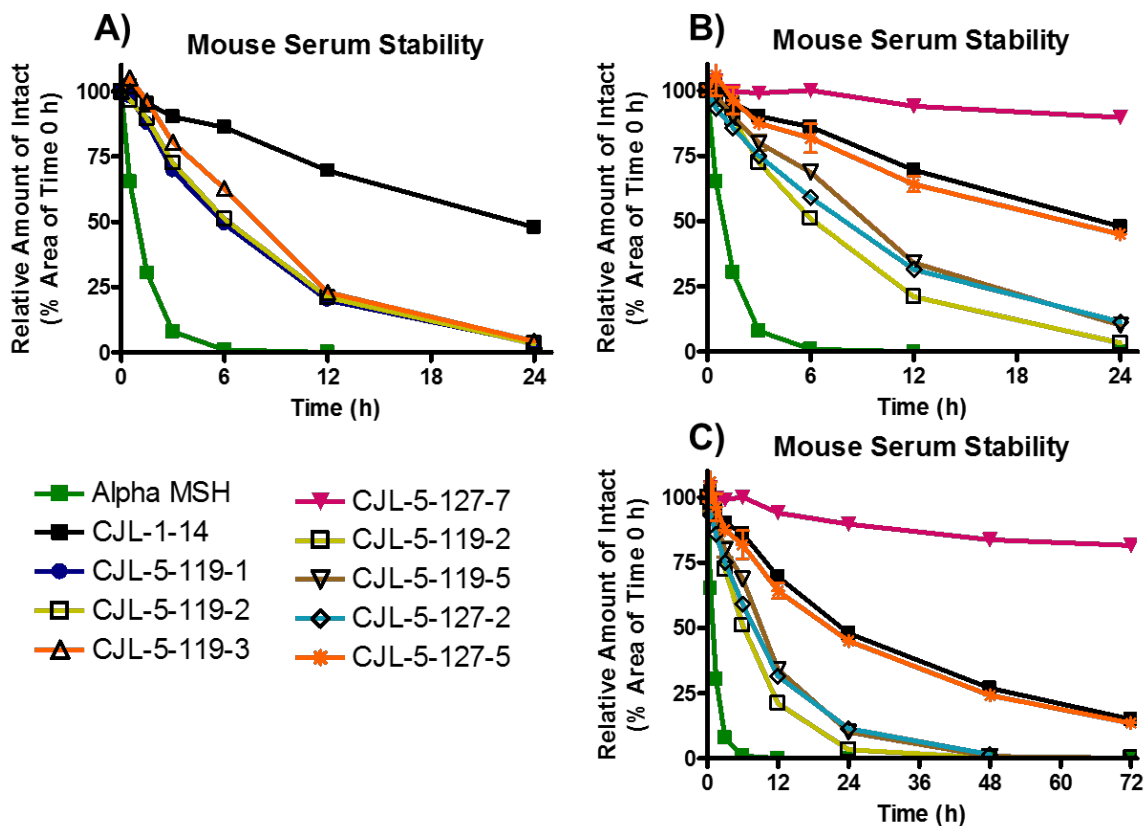


Figure 6.4. *In vitro* serum stability of linker length bivalent analogs at 24 h (A) and retro-inverso analogs at 24 h (B) and 72 h (C). Ligands (10 μ M) were incubated in mouse serum and monitored for degradation of the parent molecule by LC-ESI⁺-MS/MS as described in Chapter 2.

Compound	Structure	HPLC <i>k'</i> (Syst. 1)	HPLC <i>k'</i> (Syst. 2)	Mass (calcd.)	Mass (obs.)	Purity %
CJL-5-119-1	Ac-His-DPhe-Arg-Trp-(PEG)(22 atoms)-His-DPhe-Arg-Trp-NH ₂	5.26	10.08	1646.85	1646.9	>96%
CJL-5-119-2	Ac-His-DPhe-Arg-Trp-(PEDG20)-His-DPhe-Arg-Trp-NH ₂	5.35	9.20	1629.83	2629.9	>95%
CJL-5-119-3	Ac-His-DPhe-Arg-Trp-(PEG)(19 atoms)-His-DPhe-Arg-Trp-NH ₂	5.82	9.84	1602.82	1602.8	>97%
CJL-9-22-1	Ac-His-DPhe-Arg-Trp-(PEG)(16 atoms)-His-DPhe-Arg-Trp-NH ₂	5.35	9.12	1558.79	1559.03	>96%
CJL-9-22-2	Ac-His-DPhe-Arg-Trp-(PEG)(13 atoms)-His-DPhe-Arg-Trp-NH ₂	5.28	7.75	1514.77	1515.01	>98%
CJL-9-22-3	Ac-His-DPhe-Arg-Trp-(PEG) ₂ (22atoms)-His-DNal(2')-Arg-Trp-NH ₂	5.91	8.71	1696.86	1697.04	>98%
CJL-9-22-4	Ac-His-DPhe-Arg-Trp-(PEDG20)-His-DNal(2')-Arg-Trp-NH ₂	5.74	8.59	1679.85	1680.05	>96%
CJL-9-22-5	Ac-His-DPhe-Arg-Trp-(PEG)(19atoms)-His-DNal(2')-Arg-Trp-NH ₂	5.86	9.98	1652.84	1652.92	>98%
CJL-5-127-7	Ac-DTrp-DArg-Phe-DHis-NH ₂	4.57	6.43	685.34	685.28	>97%
CJL-5-127-8	DTrp-DArg-Phe-DHis-NH ₂	3.15	4.32	643.33	643.27	>98%
CJL-5-119-4	Ac-DTrp-DArg-Phe-DHis-(PEG)(22 atoms)-His-DPhe-Arg-Trp-NH ₂	5.92	9.89	1646.85	1646.9	97%
CJL-5-119-5	Ac-DTrp-DArg-Phe-DHis-(PEDG20)-His-DPhe-Arg-Trp-NH ₂	5.50	9.78	1629.83	1629.9	>95%
CJL-5-119-6	Ac-DTrp-DArg-Phe-DHis-(PEG)(19 atoms)-His-DPhe-Arg-Trp-NH ₂	5.65	9.60	1602.82	1602.8	>98%
CJL-5-127-1	Ac-His-DPhe-Arg-Trp-(PEG)(22 atoms)-DTrp-DArg-Phe-DHis-NH ₂	6.54	7.67	1646.85	1646.8	>95%
CJL-5-127-2	Ac-His-DPhe-Arg-Trp-(PEDG20)-DTrp-DArg-Phe-DHis-NH ₂	5.66	9.90	1629.83	1629.8	>95%
CJL-5-127-3	Ac-His-DPhe-Arg-Trp-(PEG)(19 atoms)-DTrp-DArg-Phe-DHis-NH ₂	5.94	10.11	1602.82	1603.04	>97%

CJL-5-127-4	Ac-DTrp-DArg-Phe-DHis-(PEG)(22 atoms)-DTrp-DArg-Phe-DHis-NH ₂	5.49	8.97	1646.85	1647.03	>98%
CJL-5-127-5	Ac-DTrp-DArg-Phe-DHis-(PEDG20)-DTrp-DArg-Phe-DHis-NH ₂	5.92	10.60	1629.83	1630.10	>98%
CJL-5-127-6	Ac-DTrp-DArg-Phe-DHis-(PEG)(19 atoms)-DTrp-DArg-Phe-DHis-NH ₂	5.48	9.03	1602.82	1602.87	>97%

Table 6.1. The analytical data for peptides synthesized currently. HPLC k' = (peptide retention time - solvent retention time) / solvent retention time. System 1 is a 10% to 90% gradient of acetonitrile in water containing 0.1% trifluoroacetic acid over 35 minutes at a flow rate of 1.5 mL/min, and system 2 is the same but with methanol replacing acetonitrile. Product purity was determined by HPLC purity in the solvent system which showed the least purity and integrating the area under the curves of the chromatograms collected at 214 nm. Mass observed was calculated from the M+1.

Compound	mMC1R	mMC3R	mMC4R	mMC5R
	Agonist EC ₅₀ (nM)	Agonist EC ₅₀ (nM)	Agonist EC ₅₀ (nM)	Agonist EC ₅₀ (nM)
	Mean±SEM	Mean±SEM	Mean±SEM	Mean±SEM
NDP-MSH	0.009±0.002	0.06±0.007	0.34±0.10	0.06±0.005
CJL-5-119-1	2.1±0.4	2.3±0.6	1.7±0.8	0.48±0.01
CJL-5-119-2	3.1±0.6	2.7±0.5	1.7±0.6	0.52±0.04
CJL-5-119-3	2.8±0.5	2.4±0.4	1.7±0.7	0.63±0.06
CJL-9-22-1	2.4±0.5	1.3±0.2	1.1±0.5	0.41±0.03
CJL-9-22-2	2.2±0.2	1.5±0.3	1.1±0.5	0.39±0.03
CJL-9-22-3	6.9±0.9	6.4±1.4	5.5±2.2	1.8±0.04
CJL-9-22-4	6.4±1.2	9.0±2.1	4.8±1.7	2.1±0.2
CJL-9-22-5	5.9±1.0	5.8±1.4	4.8±2.5	1.7±0.2
CJL-5-127-7	5% at 100 μM	15% at 100 μM	20% at 100 μM	35% at 100 μM
CJL-5-127-8	15% at 100 μM	15% at 100 μM	15% at 100 μM	1% at 100 μM
CJL-5-119-4	7.2±1.6	3.6±1.1	5.7±2.5	1.3±0.05
CJL-5-119-5	9.0±1.5	4.5±0.7	8.8±4.1	1.4±0.2
CJL-5-119-6	8.8±1.3	4.9±1.9	7.1±4.3	1.5±0.4
CJL-5-127-1	5.6±1.3	4.9±1.6	2.8±1.2	0.74±0.05
CJL-5-127-2	7.2±0.6	5.9±1.4	3.2±1.1	1.0±0.05
CJL-5-127-3	5.0±0.6	3.6±0.7	2.1±0.9	0.63±0.02
CJL-5-127-4	25% at 100 μM	45% at 100 μM	80% at 100 μM	60% at 100 μM
CJL-5-127-5	45% at 100 μM	55% at 100 μM	3200±1200	80% at 100 μM
CJL-5-127-6	25% at 100 μM	45% at 100 μM	65% at 100 μM	50% at 100 μM

Table 6.2: Functional cAMP signaling data at the mMC1R, mMC3R, mMC4R, and mMC5R. The cAMP signaling potency was determined by AlphaScreen® assays. The reported errors are the standard error of the mean (SEM) determined from at least three

independent experiments. Changes less than 3-fold were considered to be within the inherent experimental assay error.

Compound Name	mMC1R		mMC3R		mMC4R	
	IC ₅₀ (nM)		IC ₅₀ (nM)		IC ₅₀ (nM)	
	Mean ± SEM	n	Mean±SEM	n	Mean±SEM	n
NDP-MSH	0.39±0.07	2	5.9±0.7	2	1.9±0.3	3
CJL-1-14	388±52*	2	60% @100 μM*	2	214±55*	6
CJL-5-119-1	45±4	2	1680±240	2	15±5	3
CJL-5-119-2	58±16	2	2140±170	2	14±4	3
CJL-5-119-3	37±1	2	1700±180	2	14±3	3
CJL-9-22-1	37±8	2	1170±10	2	12±4	3
CJL-9-22-2	34±7	2	1310±220	2	10±4	3
CJL-5-127-7	30% @100 μM	2	NA	2	25% @100 μM	2
CJL-5-119-5	150±20	2	6220±270	2	93±40	2
CJL-5-127-2	110±34	2	3800±250	2	29±4	2
CJL-5-127-5	6300±1000	2	55% @100 μM	2	80% @100 μM	2

Table 6.3: Summary of competitive binding experiments at the mMC1R, mMC3R, and mMC4R. IC₅₀ values were determined by competitive binding in which experimental compounds were used to displace ¹²⁵I-NDP-MSH in a dose-response manner. In competitive experiments, % represents the amount of ¹²⁵I-NDP-MSH signal reduction at 100 μM. The reported errors are the standard error of the mean (SEM). Changes less than 3-fold were considered to be within the inherent experimental assay error. NA means no displacement was observed at 100 μM.

Chapter 7: Advancements Made, Lessons Learned, and Future Directions

The current thesis provides the field foundational work into the design of melanocortin bivalent ligands, characterization of their *in vitro* pharmacology, and evaluation of their *in vivo* effects. As proposed in the introductory chapter, it appears we have successfully utilized bivalent ligands to target GPCR oligomers to decrease the entropic cost of binding and elicit novel melanocortin signaling patterns. These bivalent ligands are lead probes that may help in the design of therapeutics to treat obesity and other metabolic disorders.

Lead ligand **CJL-1-87** showed promising effects as an anti-obesity probe as described in **Chapter 3** and **Chapter 4**.^{25, 132} Compared to its monovalent counterpart, it possessed increased binding affinity, increased *in vitro* functional potency, increased the duration of action in spite of decreased serum stability, decreased *in vivo* food intake, decreased mice's body fat percentage, and differentially affected mouse hormone levels.^{25, 132} The design principles learned along the way about receptor subtype preference patterns, paradigm-specific *in vivo* effects, and more will hopefully help guide future development of bivalent ligands targeting not only melanocortin receptors, but also targeting other GPCRs.

In **Chapter 5**, a design strategy to target asymmetric GPCR homodimers with unmatched bivalent ligands (UmBLs) is presented. Melanocortin bivalent ligands featuring one agonist pharmacophore and one antagonist pharmacophore for the same receptor are synthesized, characterized *in vitro*, and evaluated *in vivo*. Employing this design strategy,

we discovered first in class biased ligands at the hMC4R in which the cAMP signaling pathway was robustly activated at nanomolar concentrations ($EC_{50} \sim 2$ to 6 nM), but the β -arrestin pathway was only partially activated at a concentration of 10 μ M. We also provided competitive binding and BRET data that supported our proposed asymmetric homodimer targeting strategy. Administration of lead compound **CJL-5-58** to mice affected the measured metabolic endpoints, but also resulted in some signs of adverse reactions which may be paradigm specific. This design strategy may find applications for other melanocortin-dependent physiological effects or in other GPCR systems as well. To our knowledge, this is the first single compound design strategy to target asymmetric homodimers that is easily amendable for use in both *in vitro* and *in vivo* assay paradigms.

In **Chapter 6**, the structure activity relationship (SAR) of bivalent ligands is investigated in more depth. Bivalent ligands with various linker lengths were designed, synthesized, and evaluated *in vitro*. Also, bivalent ligands that contained the retro-inverso scaffold DTrp-DArg-Phe-DHis were studied. The ligands synthesized were not selected for further *in vivo* work, but they do highlight the need for further *in vitro* SAR studies.

Based on the foundational work provided in this thesis, there are many different design strategies that could be explored. More rigid linkers could be used to gauge more effectively the SAR of linker length. Truly symmetric bivalent ligands could be synthesized and evaluated. Heterobivalent ligands with selective pharmacophores for two different melanocortin subtypes could be designed. This may become even more relevant as MC3R-selective tetrapeptides are reported in the literature.¹¹⁹ Given the discovery in **Chapter 4**

of the mMC3R-mMC4R heterodimer,¹³² heterobivalent ligands that feature one selective mMC4R pharmacophore and one selective mMC3R pharmacophore may be interesting pharmacological probes to study this heterodimer. Heterobivalent ligands targeting the melanocortin receptors and a different receptor system may also be of interest. For example, heterobivalent ligands targeting known heterodimers such as the MC3R-GHSR (*i.e.* growth hormone secretagogue receptor) and MC4R-GPR7 (*i.e.* G protein-coupled receptor 7) could be synthesized and evaluated.³¹⁶ Another interesting design aspect would be bitopic ligands as allosteric modulators are discovered and reported. By tethering an allosteric modulator to a high affinity orthosteric ligand, it may provide unique and distinct pharmacologies. This would be especially useful if the allosteric modulators are low affinity, as the orthosteric agonist or antagonist can act as the targeting moiety and allow for high overall binding affinity (as discussed in **Chapter 5** and **Chapter 6**).

It was once stated by sociologist and economist Thorstein Veblen that: “The outcome of any serious research can only be to make two questions grow where only one grew before.” This thesis appears to have followed this maxim. Throughout this thesis many different pieces of data led to further questioning. For example: “Why is there an incongruity between the gains in binding affinity (*c.a.* 20- to 25-fold) and the gains in functional potency (*c.a.* 3- to 5-fold) with lead bivalent ligands?” “What is responsible for the physiological differences between administering bivalent ligands to fasted mice versus normal feeding mice?” “What is the equilibrium between melanocortin receptor

monomers, dimers, and higher-order oligomers?” and “Why was no distinct effect on SAR observed with the linker length library in **Chapter 6**?”

Although this thesis opens the door to many more questions and hypotheses, it is my hope that the discoveries herein provide a foundation of work for future studies of both melanocortin dimers and of bivalent ligands targeting them. This work provides novel applications of melanocortin bivalent ligands, and suggests physiological relevancy of melanocortin dimers. It also provides evidence of two novel drug targets (*i.e.* MC3R-MC4R heterodimer and asymmetric MC4R homodimer). It appears likely to me that as more is elucidated about the melanocortin dimers and GPCR dimers in general, the strategies and lessons learned in this thesis will become increasingly valuable. GPCRs remain one of the most highly successful drug targets, and additional ways to pharmacologically target them will hopefully garner new opportunities to improve human health. This dissertation will hopefully serve as a valuable resource for future researchers exploring “The Bivalent Advantage.”

Bibliography

1. Ericson, M. D., Lensing, C. J., Fleming, K. A., Schlasner, K. N., Doering, S. R., and Haskell-Luevano, C. (2017) Bench-top to clinical therapies: A review of melanocortin ligands from 1954 to 2016, *Biochim. Biophys. Acta*. In press.
2. Rask-Andersen, M., Almen, M. S., and Schiöth, H. B. (2011) Trends in the exploitation of novel drug targets, *Nature Reviews Drug Discovery* 10, 579-590.
3. Santos, R., Ursu, O., Gaulton, A., Bento, A. P., Donadi, R. S., Bologa, C. G., Karlsson, A., Al-Lazikani, B., Hersey, A., Oprea, T. I., and Overington, J. P. (2017) A comprehensive map of molecular drug targets, *Nature reviews. Drug discovery* 16, 19-34.
4. Ferre, S., Casado, V., Devi, L. A., Filizola, M., Jockers, R., Lohse, M. J., Milligan, G., Pin, J. P., and Guitart, X. (2014) G protein-coupled receptor oligomerization revisited: functional and pharmacological perspectives, *Pharmacol. Rev.* 66, 413-434.
5. Bhushan, R. G., Sharma, S. K., Xie, Z. H., Daniels, D. J., and Portoghese, P. S. (2004) A bivalent ligand (KDN-21) reveals spinal delta and kappa opioid receptors are organized as heterodimers that give rise to delta(1) and kappa(2) phenotypes. Selective targeting of delta-kappa heterodimers, *J. Med. Chem.* 47, 2969-2972.
6. Xu, L. P., Josan, J. S., Vagner, J., Caplan, M. R., Hraby, V. J., Mash, E. A., Lynch, R. M., Morse, D. L., and Gillies, R. J. (2012) Heterobivalent ligands target cell-surface receptor combinations in vivo, *Proc. Natl. Acad. Sci. U. S. A.* 109, 21295-21300.
7. Portoghese, P. S., Ronsisvalle, G., Larson, D. L., Yim, C. B., Sayre, L. M., and Takemori, A. E. (1982) Opioid agonist and antagonist bivalent ligands as receptor probes, *Life Sci.* 31, 1283-1286.
8. Portoghese, P. S., Larson, D. L., Sayre, L. M., Yim, C. B., Ronsisvalle, G., Tam, S. W., and Takemori, A. E. (1986) Opioid agonist and antagonist bivalent ligands: The relationship between spacer length and selectivity at multiple opioid receptors, *J. Med. Chem.* 29, 1855-1861.
9. Portoghese, P. S., Nagase, H., Lipkowski, A. W., Larson, D. L., and Takemori, A. E. (1988) Binaltorphimine-related bivalent ligands and their kappa-opioid receptor antagonist selectivity, *J. Med. Chem.* 31, 836-841.
10. Akgün, E., Javed, M. I., Lunzer, M. M., Powers, M. D., Sham, Y. Y., Watanabe, Y., and Portoghese, P. S. (2015) Inhibition of inflammatory and neuropathic pain by targeting a mu opioid receptor/chemokine receptor5 heteromer (MOR-CCR5), *J. Med. Chem.* 58, 8647-8657.
11. Daniels, D. J., Lenard, N. R., Etienne, C. L., Law, P. Y., Roerig, S. C., and Portoghese, P. S. (2005) Opioid-induced tolerance and dependence in mice is modulated by the distance between pharmacophores in a bivalent ligand series, *Proc. Natl. Acad. Sci. U. S. A.* 102, 19208-19213.

12. Erez, M., Takemori, A. E., and Portoghese, P. S. (1982) Narcotic antagonistic potency of bivalent ligands which contain beta-naltrexamine. Evidence for bridging between proximal recognition sites, *J. Med. Chem.* 25, 847-849.
13. Conn, P. M., Rogers, D. C., Stewart, J. M., Niedel, J., and Sheffield, T. (1982) Conversion of a gonadotropin-releasing hormone antagonist to an agonist, *Nature* 296, 653-655.
14. Blum, J. J., and Conn, P. M. (1982) Gonadotropin-releasing hormone stimulation of luteinizing hormone release: A ligand-receptor-effector model, *Proc. Natl. Acad. Sci. U. S. A.* 79, 7307-7311.
15. Karellas, P., McNaughton, M., Baker, S. P., and Scammells, P. J. (2008) Synthesis of bivalent beta(2)-adrenergic and adenosine A(1) receptor ligands, *J. Med. Chem.* 51, 6128-6137.
16. Huang, G., Pemp, D., Stadtmuller, P., Nimczick, M., Heilmann, J., and Decker, M. (2014) Design, synthesis and in vitro evaluation of novel uni- and bivalent ligands for the cannabinoid receptor type 1 with variation of spacer length and structure, *Bioorg. Med. Chem. Lett.* 24, 4209-4214.
17. Nimczick, M., Pemp, D., Darras, F. H., Chen, X., Heilmann, J., and Decker, M. (2014) Synthesis and biological evaluation of bivalent cannabinoid receptor ligands based on hCB(2)R selective benzimidazoles reveal unexpected intrinsic properties, *Bioorg. Med. Chem.* 22, 3938-3946.
18. Russo, O., Berthouze, M., Giner, M., Soulier, J. L., Rivail, L., Sicsic, S., Lezoualc'h, F., Jockers, R., and Berque-Bestel, I. (2007) Synthesis of specific bivalent probes that functionally interact with 5-HT(4) receptor dimers, *J. Med. Chem.* 50, 4482-4492.
19. Singh, N., Hazari, P. P., Prakash, S., Chuttani, K., Khurana, H., Chandra, H., and Mishra, A. K. (2012) A homodimeric bivalent radioligand derived from 1-(2-methoxyphenyl) piperazine with high affinity for in vivo 5-HT1A receptor imaging, *Medchemcomm* 3, 814-823.
20. Soulier, J. L., Russo, O., Giner, M., Rivail, L., Berthouze, M., Ongeri, S., Maigret, B., Fischmeister, R., Lezoualc'h, F., Sicsic, S., and Berque-Bestel, I. (2005) Design and synthesis of specific probes for human 5-HT4 receptor dimerization studies, *J. Med. Chem.* 48, 6220-6228.
21. Kuhhorn, J., Hubner, H., and Gmeiner, P. (2011) Bivalent dopamine D2 receptor ligands: Synthesis and binding properties, *J. Med. Chem.* 54, 4896-4903.
22. Kuhhorn, J., Gotz, A., Hubner, H., Thompson, D., Whistler, J., and Gmeiner, P. (2011) Development of a Bivalent Dopamine D-2 Receptor Agonist, *J. Med. Chem.* 54, 7911-7919.
23. Xu, Y., Duggineni, S., Espitia, S., Richman, D. D., An, J., and Huang, Z. (2013) A synthetic bivalent ligand of CXCR4 inhibits HIV infection, *Biochem. Biophys. Res. Commun.* 435, 646-650.
24. Busnelli, M., Kleinau, G., Muttenthaler, M., Stoev, S., Manning, M., Bibic, L., Howell, L. A., McCormick, P. J., Di Lascio, S., Braidia, D., Sala, M., Rovati, G. E.,

- Bellini, T., and Chini, B. (2016) Design and Characterization of Superpotent Bivalent Ligands Targeting Oxytocin Receptor Dimers via a Channel-Like Structure, *J. Med. Chem.* *59*, 7152-7166.
25. Lensing, C. J., Freeman, K. T., Schnell, S. M., Adank, D. N., Speth, R. C., and Haskell-Luevano, C. (2016) An in Vitro and in Vivo Investigation of Bivalent Ligands That Display Preferential Binding and Functional Activity for Different Melanocortin Receptor Homodimers, *J. Med. Chem.* *59*, 3112-3128.
 26. Carrithers, M. D., and Lerner, M. R. (1996) Synthesis and characterization of bivalent peptide ligands targeted to G-protein-coupled receptors, *Chem. Biol.* *3*, 537-542.
 27. Alletti, R., Vagner, J., Dehigaspitiya, D. C., Moberg, V. E., Elshan, N. G., Tafreshi, N. K., Brabez, N., Weber, C. S., Lynch, R. M., Hruby, V. J., Gillies, R. J., Morse, D. L., and Mash, E. A. (2013) Synthesis and characterization of time-resolved fluorescence probes for evaluation of competitive binding to melanocortin receptors, *Bioorg. Med. Chem.* *21*, 5029-5038.
 28. Brabez, N., Lynch, R. M., Xu, L. P., Gillies, R. J., Chassaing, G., Lavielle, S., and Hruby, V. J. (2011) Design, synthesis, and biological studies of efficient multivalent melanotropin ligands: Tools toward melanoma diagnosis and treatment, *J. Med. Chem.* *54*, 7375-7384.
 29. Elshan, N. G. R. D., Jayasundera, T., Anglin, B. L., Weber, C. S., Lynch, R. M., and Mash, E. A. (2015) Trigonal scaffolds for multivalent targeting of melanocortin receptors, *Org. Biomol. Chem.* *13*, 1778-1791.
 30. Fernandes, S. M., Lee, Y. S., Gillies, R. J., and Hruby, V. J. (2014) Synthesis and evaluation of bivalent ligands for binding to the human melanocortin-4 receptor, *Bioorg. Med. Chem.* *22*, 6360-6365.
 31. Handl, H. L., Sankaranarayanan, R., Josan, J. S., Vagner, J., Mash, E. A., Gillies, R. J., and Hruby, V. J. (2007) Synthesis and evaluation of bivalent NDP-alpha-MSH(7) peptide ligands for binding to the human melanocortin receptor 4 (hMC4R), *Bioconjugate Chem.* *18*, 1101-1109.
 32. Vagner, J., Handl, H. L., Monguchi, Y., Jana, U., Begay, L. J., Mash, E. A., Hruby, V. J., and Gillies, R. J. (2006) Rigid linkers for bioactive peptides, *Bioconjugate Chem.* *17*, 1545-1550.
 33. Vagner, J., Handl, H. L., Gillies, R. J., and Hruby, V. J. (2004) Novel targeting strategy based on multimeric ligands for drug delivery and molecular imaging: Homooligomers of alpha-MSH, *Bioorg. Med. Chem. Lett.* *14*, 211-215.
 34. Bowen, M. E., Monguchi, Y., Sankaranarayanan, R., Vagner, J., Begay, L. J., Xu, L., Jagadish, B., Hruby, V. J., Gillies, R. J., and Mash, E. A. (2007) Design, synthesis, and validation of a branched flexible linker for bioactive peptides, *J. Org. Chem.* *72*, 1675-1680.
 35. Jagadish, B., Sankaranarayanan, R., Xu, L., Richards, R., Vagner, J., Hruby, V. J., Gillies, R. J., and Mash, E. A. (2007) Squalene-derived flexible linkers for bioactive peptides, *Bioorg. Med. Chem. Lett.* *17*, 3310-3313.

36. Dehigaspitiya, D. C., Navath, S., Weber, C. S., Lynch, R. M., and Mash, E. A. (2015) Synthesis and bioactivity of MSH4 oligomers prepared by an A + B strategy, *Tetrahedron Lett.* *56*, 3060-3065.
37. Dehigaspitiya, D. C., Anglin, B. L., Smith, K. R., Weber, C. S., Lynch, R. M., and Mash, E. A. (2015) Linear scaffolds for multivalent targeting of melanocortin receptors, *Organic & biomolecular chemistry* *13*, 11507-11517.
38. Bapst, J. P., Froidevaux, S., Calame, M., Tanner, H., and Eberle, A. N. (2007) Dimeric DOTA-alpha-melanocyte-stimulating hormone analogs: synthesis and in vivo characteristics of radiopeptides with high in vitro activity, *J. Recept. Signal Transduction Res.* *27*, 383-409.
39. Bagutti, C., Stolz, B., Albert, R., Bruns, C., Pless, J., and Eberle, A. N. (1994) [¹¹¹In]-DTPA-labeled analogues of alpha-melanocyte-stimulating hormone for melanoma targeting: receptor binding in vitro and in vivo, *Int. J. Cancer* *58*, 749-755.
40. Morais, M., Raposinho, P. D., Oliveira, M. C., Correia, J. D. G., and Santos, I. (2012) Evaluation of novel Tc-99m(I)-labeled homobivalent alpha-melanocyte-stimulating hormone analogs for melanocortin-1 receptor targeting, *J. Biol. Inorg. Chem.* *17*, 491-505.
41. Jorg, M., May, L. T., Mak, F. S., Lee, K. C., Miller, N. D., Scammells, P. J., and Capuano, B. (2015) Synthesis and pharmacological evaluation of dual acting ligands targeting the adenosine A2A and dopamine D2 receptors for the potential treatment of Parkinson's disease, *J. Med. Chem.* *58*, 718-738.
42. Harikumar, K. G., Akgun, E., Portoghese, P. S., and Miller, L. J. (2010) Modulation of cell surface expression of nonactivated cholecystokinin receptors using bivalent ligand-induced internalization, *J. Med. Chem.* *53*, 2836-2842.
43. Yekkirala, A. S., Kalyuzhny, A. E., and Portoghese, P. S. (2013) An immunocytochemical-derived correlate for evaluating the bridging of heteromeric mu-delta opioid protomers by bivalent ligands, *ACS Chem. Biol.* *8*, 1412-1416.
44. Le Naour, M., Akgun, E., Yekkirala, A., Lunzer, M. M., Powers, M. D., Kalyuzhny, A. E., and Portoghese, P. S. (2013) Bivalent ligands that target mu opioid (MOP) and cannabinoid1 (CB1) receptors are potent analgesics devoid of tolerance, *J. Med. Chem.* *56*, 5505-5513.
45. Le Naour, M., Lunzer, M. M., Powers, M. D., Kalyuzhny, A. E., Benneyworth, M. A., Thomas, M. J., and Portoghese, P. S. (2014) Putative Kappa Opioid Heteromers As Targets for Developing Analgesics Free of Adverse Effects, *J. Med. Chem.* *57*, 6383-6392.
46. Smeester, B. A., Lunzer, M. M., Akgun, E., Beitz, A. J., and Portoghese, P. S. (2014) Targeting putative mu opioid/metabotropic glutamate receptor-5 heteromers produces potent antinociception in a chronic murine bone cancer model, *Eur. J. Pharmacol.* *743*, 48-52.
47. Hiller, C., Kuhhorn, J., and Gmeiner, P. (2013) Class A G-protein-coupled receptor (GPCR) dimers and bivalent ligands, *J. Med. Chem.* *56*, 6542-6559.

48. Portoghese, P. S., Akgun, E., and Lunzer, M. M. (2017) Heteromer Induction: An Approach to Unique Pharmacology?, *ACS Chem. Neurosci.* 8, 426-428.
49. Mountjoy, K. G., Robbins, L. S., Mortrud, M. T., and Cone, R. D. (1992) The cloning of a family of genes that encode the melanocortin receptors, *Science* 257, 1248-1251.
50. Lerner, A. B., and McGuire, J. S. (1961) Effect of alpha- and betamelanocyte stimulating hormones on the skin colour of man, *Nature* 189, 176-179.
51. Van der Ploeg, L. H., Martin, W. J., Howard, A. D., Nargund, R. P., Austin, C. P., Guan, X., Drisko, J., Cashen, D., Sebhat, I., Patchett, A. A., Figueroa, D. J., DiLella, A. G., Connolly, B. M., Weinberg, D. H., Tan, C. P., Palyha, O. C., Pong, S. S., MacNeil, T., Rosenblum, C., Vongs, A., Tang, R., Yu, H., Sailer, A. W., Fong, T. M., Huang, C., Tota, M. R., Chang, R. S., Stearns, R., Tamvakopoulos, C., Christ, G., Drazen, D. L., Spar, B. D., Nelson, R. J., and MacIntyre, D. E. (2002) A role for the melanocortin 4 receptor in sexual function, *Proc. Natl. Acad. Sci. U. S. A.* 99, 11381-11386.
52. Greenfield, J. R., Miller, J. W., Keogh, J. M., Henning, E., Satterwhite, J. H., Cameron, G. S., Astruc, B., Mayer, J. P., Brage, S., See, T. C., Lomas, D. J., O'Rahilly, S., and Farooqi, I. S. (2009) Modulation of blood pressure by central melanocortineric pathways, *N. Engl. J. Med.* 360, 44-52.
53. Gonzalez, P. V., Schioth, H. B., Lasaga, M., and Scimonelli, T. N. (2009) Memory impairment induced by IL-1beta is reversed by alpha-MSH through central melanocortin-4 receptors, *Brain. Behav. Immun.* 23, 817-822.
54. Beckwith, B. E., Sandman, C. A., Hothersall, D., and Kastin, A. J. (1977) Influence of neonatal injections of Alpha-MSH on learning, memory and attention in rats, *Physiol. Behav.* 18, 63-71.
55. Sandman, C. A., George, J. M., Nolan, J. D., Vanriezen, H., and Kastin, A. J. (1975) Enhancement of attention in man with ACTH-MSH 4-10, *Physiol. Behav.* 15, 427-431.
56. Fan, W., Boston, B. A., Kesterson, R. A., Hruby, V. J., and Cone, R. D. (1997) Role of melanocortineric neurons in feeding and the agouti obesity syndrome, *Nature* 385, 165-168.
57. Huszar, D., Lynch, C. A., Fairchild-Huntress, V., Dunmore, J. H., Fang, Q., Berkemeier, L. R., Gu, W., Kesterson, R. A., Boston, B. A., Cone, R. D., Smith, F. J., Campfield, L. A., Burn, P., and Lee, F. (1997) Targeted disruption of the melanocortin-4 receptor results in obesity in mice, *Cell* 88, 131-141.
58. Chen, A. S., Marsh, D. J., Trumbauer, M. E., Frazier, E. G., Guan, X. M., Yu, H., Rosenblum, C. I., Vongs, A., Feng, Y., Cao, L., Metzger, J. M., Strack, A. M., Camacho, R. E., Mellin, T. N., Nunes, C. N., Min, W., Fisher, J., Gopal-Truter, S., MacIntyre, D. E., Chen, H. Y., and Van der Ploeg, L. H. (2000) Inactivation of the mouse melanocortin-3 receptor results in increased fat mass and reduced lean body mass, *Nat. Genet.* 26, 97-102.

59. Haskell-Luevano, C., Schaub, J. W., Andreasen, A., Haskell, K. R., Moore, M. C., Koerper, L. M., Rouzaud, F., Baker, H. V., Millard, W. J., Walter, G., Litherland, S. A., and Xiang, Z. (2009) Voluntary exercise prevents the obese and diabetic metabolic syndrome of the melanocortin-4 receptor knockout mouse, *FASEB J.* 23, 642-655.
60. Giuliani, D., Galantucci, M., Neri, L., Canalini, F., Calevro, A., Bitto, A., Ottani, A., Vandini, E., Sena, P., Sandrini, M., Squadrito, F., Zaffe, D., and Guarini, S. (2014) Melanocortins protect against brain damage and counteract cognitive decline in a transgenic mouse model of moderate Alzheimers disease, *Eur. J. Pharmacol.* 740, 144-150.
61. Giuliani, D., Bitto, A., Galantucci, M., Zaffe, D., Ottani, A., Irrera, N., Neri, L., Cavallini, G. M., Altavilla, D., Botticelli, A. R., Squadrito, F., and Guarini, S. (2014) Melanocortins protect against progression of Alzheimer's disease in triple-transgenic mice by targeting multiple pathophysiological pathways, *Neurobiol. Aging* 35, 537-547.
62. Giuliani, D., Neri, L., Canalini, F., Calevro, A., Ottani, A., Vandini, E., Sena, P., Zaffe, D., and Guarini, S. (2015) NDP-alpha-MSH induces intense neurogenesis and cognitive recovery in Alzheimer transgenic mice through activation of melanocortin MC4 receptors, *Mol. Cell. Neurosci.* 67, 13-21.
63. Josan, J. S., Handl, H. L., Sankaranarayanan, R., Xu, L., Lynch, R. M., Vagner, J., Mash, E. A., Hruby, V. J., and Gillies, R. J. (2011) Cell-specific targeting by heterobivalent ligands, *Bioconjugate Chem.* 22, 1270-1278.
64. Barkey, N. M., Tafreshi, N. K., Josan, J. S., De Silva, C. R., Sill, K. N., Hruby, V. J., Gillies, R. J., Morse, D. L., and Vagner, J. (2011) Development of Melanoma-Targeted Polymer Micelles by Conjugation of a Melanocortin 1 Receptor (MC1R) Specific Ligand, *Journal of Medicinal Chemistry* 54, 8078-8084.
65. Barkey, N. M., Preihs, C., Cornell, H. H., Martinez, G., Carie, A., Vagner, J., Xu, L. P., Lloyd, M. C., Lynch, V. M., Hruby, V. J., Sessler, J. L., Sill, K. N., Gillies, R. J., and Morse, D. L. (2013) Development and in vivo quantitative magnetic resonance imaging of polymer micelles targeted to the melanocortin 1 receptor, *J. Med. Chem.* 56, 6330-6338.
66. Uckert, S., Bannowsky, A., Albrecht, K., and Kuczyk, M. A. (2014) Melanocortin receptor agonists in the treatment of male and female sexual dysfunctions: results from basic research and clinical studies, *Expert Opin. Invest. Drugs* 23, 1477-1483.
67. Penagarikano, O., Lazaro, M. T., Lu, X. H., Gordon, A., Dong, H. M., Lam, H. A., Peles, E., Maidment, N. T., Murphy, N. P., Yang, X. W., Golshani, P., and Geschwind, D. H. (2015) Exogenous and evoked oxytocin restores social behavior in the Cntnap2 mouse model of autism, *Sci. Transl. Med.* 7.
68. Barrett, C. E., Modi, M. E., Zhang, B. C., Walum, H., Inoue, K., and Young, L. J. (2014) Neonatal melanocortin receptor agonist treatment reduces play fighting and promotes adult attachment in prairie voles in a sex-dependent manner, *Neuropharmacology* 85, 357-366.

69. Joppa, M. A., Ling, N., Chen, C., Gogas, K. R., Foster, A. C., and Markison, S. (2005) Central administration of peptide and small molecule MC4 receptor antagonists induce hyperphagia in mice and attenuate cytokine-induced anorexia, *Peptides* 26, 2294-2301.
70. DeBoer, M. D., and Marks, D. L. (2006) Cachexia: lessons from melanocortin antagonism, *Trends Endocrinol. Metab.* 17, 199-204.
71. DeBoer, M. D., and Marks, D. L. (2006) Therapy insight: Use of melanocortin antagonists in the treatment of cachexia in chronic disease, *Nat. Clin. Pract. Endocrinol. Metab.* 2, 459-466.
72. Doering, S. R., Todorovic, A., and Haskell-Luevano, C. (2015) Melanocortin antagonist tetrapeptides with minimal agonist activity at the mouse melanocortin-3 receptor, *ACS Med. Chem. Lett.* 6, 123-127.
73. Ericson, M. D., Wilczynski, A., Sorensen, N. B., Xiang, Z., and Haskell-Luevano, C. (2015) Discovery of a beta-Hairpin Octapeptide, c[Pro-Arg-Phe-Phe-Dap-Ala-Phe-DPro], Mimetic of Agouti-Related Protein(87-132) [AGRP(87-132)] with Equipotent Mouse Melanocortin-4 Receptor (mMC4R) Antagonist Pharmacology, *J. Med. Chem.* 58, 4638-4647.
74. Singh, A., Dirain, M. L., Wilczynski, A., Chen, C., Gosnell, B. A., Levine, A. S., Edison, A. S., and Haskell-Luevano, C. (2014) Synthesis, biophysical, and pharmacological evaluation of the melanocortin agonist AST3-88: modifications of peptide backbone at Trp 7 position lead to a potent, selective, and stable ligand of the melanocortin 4 receptor (MC4R), *ACS Chem. Neurosci.* 5, 1020-1031.
75. Haslach, E. M., Huang, H., Dirain, M., Debevec, G., Geer, P., Santos, R. G., Giulianotti, M. A., Pinilla, C., Appel, J. R., Doering, S. R., Walters, M. A., Houghten, R. A., and Haskell-Luevano, C. (2014) Identification of tetrapeptides from a mixture based positional scanning library that can restore nM full agonist function of the L106P, I69T, I102S, A219V, C271Y, and C271R human melanocortin-4 polymorphic receptors (hMC4Rs), *J. Med. Chem.* 57, 4615-4628.
76. Irani, B. G., Xiang, Z., Yarandi, H. N., Holder, J. R., Moore, M. C., Bauzo, R. M., Proneth, B., Shaw, A. M., Millard, W. J., Chambers, J. B., Benoit, S. C., Clegg, D. J., and Haskell-Luevano, C. (2011) Implication of the melanocortin-3 receptor in the regulation of food intake, *Eur. J. Pharmacol.* 660, 80-87.
77. Chhajlani, V., and Wikberg, J. E. S. (1992) Molecular cloning and expression of the human melanocyte stimulating hormone receptor cDNA, *FEBS Lett.* 309, 417-420.
78. Gantz, I., Konda, Y., Tashiro, T., Shimoto, Y., Miwa, H., Munzert, G., Watson, S. J., Delvalle, J., and Yamada, T. (1993) Molecular cloning of a novel melanocortin receptor, *J. Biol. Chem.* 268, 8246-8250.
79. Gantz, I., Miwa, H., Konda, Y., Shimoto, Y., Tashiro, T., Watson, S. J., Delvalle, J., and Yamada, T. (1993) Molecular cloning, expression, and gene localization of a 4th melanocortin receptor, *J. Biol. Chem.* 268, 15174-15179.

80. Gantz, I., Tashiro, T., Barcroft, C., Konda, Y., Shimoto, Y., Miwa, H., Glover, T., Munzert, G., and Yamada, T. (1993) Localization of the genes encoding the melanocortin-2 (adrenocorticotrophic hormone) and melanocortin-3 receptors to chromosomes 18p11.2 and 20q13.2-Q13.3 by fluorescence in-situ hybridization, *Genomics* 18, 166-167.
81. Mountjoy, K. G., Mortrud, M. T., Low, M. J., Simerly, R. B., and Cone, R. D. (1994) Localization of the melanocortin-4 receptor (MC4-R) in neuroendocrine and autonomic control circuits in the brain, *Mol. Endocrinol.* 8, 1298-1308.
82. Roselli-Rehfuss, L., Mountjoy, K. G., Robbins, L. S., Mortrud, M. T., Low, M. J., Tatro, J. B., Entwistle, M. L., Simerly, R. B., and Cone, R. D. (1993) Identification of a receptor for gamma melanotropin and other proopiomelanocortin peptides in the hypothalamus and limbic system, *Proc. Natl. Acad. Sci. U. S. A.* 90, 8856-8860.
83. Butler, A. A., Kesterson, R. A., Khong, K., Cullen, M. J., Pellemounter, M. A., Dekoning, J., Baetscher, M., and Cone, R. D. (2000) A unique metabolic syndrome causes obesity in the melanocortin-3 receptor-deficient mouse, *Endocrinology* 141, 3518-3521.
84. Chen, A. S., Marsh, D. J., Trumbauer, M. E., Frazier, E. G., Guan, X. M., Yu, H., Rosenblum, C. I., Vongs, A., Feng, Y., Cao, L. H., Metzger, J. M., Strack, A. M., Camacho, R. E., Mellin, T. N., Nunes, C. N., Min, W., Fisher, J., Gopal-Truter, S., MacIntyre, D. E., Chen, H. Y., and Van der Ploeg, L. H. T. (2000) Inactivation of the mouse melanocortin-3 receptor results in increased fat mass and reduced lean body mass, *Nat Genet* 26, 97-102.
85. Gantz, I., Konda, Y., Tashiro, T., Shimoto, Y., Miwa, H., Munzert, G., Watson, S. J., DelValle, J., and Yamada, T. (1993) Molecular cloning of a novel melanocortin receptor, *The Journal of biological chemistry* 268, 8246-8250.
86. Gantz, I., Miwa, H., Konda, Y., Shimoto, Y., Tashiro, T., Watson, S. J., DelValle, J., and Yamada, T. (1993) Molecular cloning, expression, and gene localization of a fourth melanocortin receptor, *The Journal of biological chemistry* 268, 15174-15179.
87. Roselli-Rehfuss, L., Mountjoy, K. G., Robbins, L. S., Mortrud, M. T., Low, M. J., Tatro, J. B., Entwistle, M. L., Simerly, R. B., and Cone, R. D. (1993) Identification of a receptor for gamma melanotropin and other proopiomelanocortin peptides in the hypothalamus and limbic system, *Proceedings of the National Academy of Sciences of the United States of America* 90, 8856-8860.
88. Dorr, R. T., Lines, R., Levine, N., Brooks, C., Xiang, L., Hruby, V. J., and Hadley, M. E. (1996) Evaluation of Melanotan-II, a superpotent cyclic melanotropic peptide in a pilot phase-I clinical study, *Life Sciences* 58, 1777-1784.
89. Van der Ploeg, L. H. T., Martin, W. J., Howard, A. D., Nargund, R. P., Austin, C. P., Guan, X. M., Drisko, J., Cashen, D., Sebat, I., Patchett, A. A., Figueroa, D. J., DiLella, A. G., Connolly, B. M., Weinberg, D. H., Tan, C. P., Palyha, O. C., Pong, S. S., MacNeil, T., Rosenblum, C., Vongs, A., Tang, R., Yu, H., Sailer, A. W., Fong, T. M., Huang, C., Tota, M. R., Chang, R. S., Stearns, R., Tamvakopoulos,

- C., Christ, G., Drazen, D. L., Spar, B. D., Nelson, R. J., and MacIntyre, D. E. (2002) A role for the melanocortin 4 receptor in sexual function, *Proceedings of the National Academy of Sciences of the United States of America* 99, 11381-11386.
90. Gantz, I., Shimoto, Y., Konda, Y., Miwa, H., Dickinson, C. J., and Yamada, T. (1994) Molecular cloning, expression, and characterization of a fifth melanocortin receptor, *Biochemical and Biophysical Research Communications* 200, 1214-1220.
 91. Griffon, N., Mignon, V., Facchinetti, P., Diaz, J., Schwartz, J. C., and Sokoloff, P. (1994) Molecular cloning and characterization of the rat fifth melanocortin receptor, *Biochemical and Biophysical Research Communications* 200, 1007-1014.
 92. Chen, W., Kelly, M. A., Opitz-Araya, X., Thomas, R. E., Low, M. J., and Cone, R. D. (1997) Exocrine gland dysfunction in MC5-R-deficient mice: evidence for coordinated regulation of exocrine gland function by melanocortin peptides, *Cell* 91, 789-798.
 93. Nakanishi, S., Inoue, A., Kita, T., Nakamura, M., Chang, A. C., Cohen, S. N., and Numa, S. (1979) Nucleotide sequence of cloned cDNA for bovine corticotropin-beta-lipotropin precursor, *Nature* 278, 423-427.
 94. Sawyer, T. K., Sanfilippo, P. J., Hruby, V. J., Engel, M. H., Heward, C. B., Burnett, J. B., and Hadley, M. E. (1980) 4-Norleucine, 7-D-Phenylalanine-Alpha-Melanocyte-Stimulating Hormone - a Highly Potent Alpha-Melanotropin with Ultralong Biological-Activity, *P Natl Acad Sci-Biol* 77, 5754-5758.
 95. Hruby, V. J., Lu, D. S., Sharma, S. D., Castrucci, A. D., Kesterson, R. A., Alobeidi, F. A., Hadley, M. E., and Cone, R. D. (1995) Cyclic Lactam Alpha-Melanotropin Analogs of Ac-Nle(4)-Cyclo[Asp(5),D-Phe(7),Lys(10)] Alpha-Melanocyte-Stimulating Hormone-(4-10)-NH₂ with Bulky Aromatic-Amino-Acids at Position-7 Show High Antagonist Potency and Selectivity at Specific Melanocortin Receptors, *J. Med. Chem.* 38, 3454-3461.
 96. Haskell-Luevano, C., Holder, J. R., Monck, E. K., and Bauzo, R. M. (2001) Characterization of melanocortin NDP-MSH agonist peptide fragments at the mouse central and peripheral melanocortin receptors, *J. Med. Chem.* 44, 2247-2252.
 97. Holder, J. R., Bauzo, R. M., Xiang, Z., and Haskell-Luevano, C. (2002) Structure-activity relationships of the melanocortin tetrapeptide Ac-His-DPhe-Arg-Trp-NH₂ at the mouse melanocortin receptors: Part 2 modifications at the Phe position, *J. Med. Chem.* 45, 3073-3081.
 98. Haskell-Luevano, C., Hendrata, S., North, C., Sawyer, T. K., Hadley, M. E., Hruby, V. J., Dickinson, C., and Gantz, I. (1997) Discovery of prototype peptidomimetic agonists at the human melanocortin receptors MC1R and MC4R, *J. Med. Chem.* 40, 2133-2139.
 99. Castrucci, A. M., Hadley, M. E., Sawyer, T. K., Wilkes, B. C., al-Obeidi, F., Staples, D. J., de Vaux, A. E., Dym, O., Hintz, M. F., Riehm, J. P., and et al. (1989) Alpha-melanotropin: the minimal active sequence in the lizard skin bioassay, *Gen. Comp. Endocrinol.* 73, 157-163.

100. Blanchard, S. G., Harris, C. O., Ittoop, O. R., Nichols, J. S., Parks, D. J., Truesdale, A. T., and Wilkison, W. O. (1995) Agouti antagonism of melanocortin binding and action in the B16F10 murine melanoma cell line, *Biochemistry* 34, 10406-10411.
101. Fong, T. M., Mao, C., MacNeil, T., Kalyani, R., Smith, T., Weinberg, D., Tota, M. R., and Van der Ploeg, L. H. T. (1997) ART (Protein Product of Agouti-Related Transcript) as an Antagonist of MC-3 and MC-4 Receptors, *Biochemical and Biophysical Research Communications* 237, 629-631.
102. Ollmann, M. M., Wilson, B. D., Yang, Y. K., Kerns, J. A., Chen, Y. R., Gantz, I., and Barsh, G. S. (1997) Antagonism of central melanocortin receptors in vitro and in vivo by Agouti-related protein, *Science* 278, 135-138.
103. Haskell-Luevano, C., and Monck, E. K. (2001) Agouti-related protein functions as an inverse agonist at a constitutively active brain melanocortin-4 receptor, *Regul. Pept.* 99, 1-7.
104. Nijenhuis, W. A. J., Oosterom, J., and Adan, R. A. H. (2001) AgRP(83-132) acts as an inverse agonist on the human-melanocortin-4 receptor, *Mol. Endocrinol.* 15, 164-171.
105. Ogden, C. L., Carroll, M. D., Kit, B. K., and Flegal, K. M. (2014) Prevalence of childhood and adult obesity in the United States, 2011-2012, *JAMA* 311, 806-814.
106. Cawley, J., and Meyerhoefer, C. (2012) The medical care costs of obesity: An instrumental variables approach, *J. Health Econ.* 31, 219-230.
107. Marsh, D. J., Hollopeter, G., Huszar, D., Laufer, R., Yagaloff, K. A., Fisher, S. L., Burn, P., and Palmiter, R. D. (1999) Response of melanocortin-4 receptor-deficient mice to anorectic and orexigenic peptides, *Nat. Genet.* 21, 119-122.
108. Dempfle, A., Hinney, A., Heinzl-Gutenbrunner, M., Raab, M., Geller, F., Gudermann, T., Schafer, H., and Hebebrand, J. (2004) Large quantitative effect of melanocortin-4 receptor gene mutations on body mass index, *J. Med. Genet.* 41, 795-800.
109. Stutzmann, F., Tan, K., Vatin, V., Dina, C., Jouret, B., Tichet, J., Balkau, B., Potoczna, N., Horber, F., O'Rahilly, S., Farooqi, I. S., Froguel, P., and Meyre, D. (2008) Prevalence of melanocortin-4 receptor deficiency in Europeans and their age-dependent penetrance in multigenerational pedigrees, *Diabetes* 57, 2511-2518.
110. Farooqi, I. S., Keogh, J. M., Yeo, G. S., Lank, E. J., Cheetham, T., and O'Rahilly, S. (2003) Clinical spectrum of obesity and mutations in the melanocortin 4 receptor gene, *N. Engl. J. Med.* 348, 1085-1095.
111. Rowland, N. E., Schaub, J. W., Robertson, K. L., Andreasen, A., and Haskell-Luevano, C. (2010) Effect of MTII on food intake and brain c-Fos in melanocortin-3, melanocortin-4, and double MC3 and MC4 receptor knockout mice, *Peptides* 31, 2314-2317.
112. Clemmensen, C., Finan, B., Fischer, K., Tom, R. Z., Legutko, B., Seherer, L., Heine, D., Grassl, N., Meyer, C. W., Henderson, B., Hofmann, S. M., Tschop, M. H., Van der Ploeg, L. H., and Muller, T. D. (2015) Dual melanocortin-4 receptor and GLP-

- 1 receptor agonism amplifies metabolic benefits in diet-induced obese mice, *EMBO Mol. Med.* 7, 288-298.
113. Marsh, D. J., Miura, G. I., Yagaloff, K. A., Schwartz, M. W., Barsh, G. S., and Palmiter, R. D. (1999) Effects of neuropeptide Y deficiency on hypothalamic agouti-related protein expression and responsiveness to melanocortin analogues, *Brain Res.* 848, 66-77.
114. Clayton, A. H., Althof, S. E., Kingsberg, S., DeRogatis, L. R., Kroll, R., Goldstein, I., Kaminetsky, J., Spana, C., Lucas, J., Jordan, R., and Portman, D. J. (2016) Bremelanotide for female sexual dysfunctions in premenopausal women: a randomized, placebo-controlled dose-finding trial, *Womens Health (Lond Engl)*.
115. Portman, D., Clayton, A., Jordan, R., Edelson, J., Greenberg, S., DeRogatis, L., Kingsberg, S., Rosen, R., Althof, S., and Krychman, M. (2014) Efficacy of Subcutaneous Bremelanotide Self-Administered at Home by Premenopausal Women with Female Sexual Dysfunction: A Placebo-Controlled Dose-Ranging Study, *Reprod. Sci.* 21, 119a-120a.
116. Kingsberg, S., Jordan, R., Clayton, A., and Krychman, M. (2015) Bremelanotide for Hypoactive Sexual Desire Disorder: Analyses from a Phase 2b Dose-Ranging Study, *J. Sex. Med.* 12, 389-389.
117. Langendonk, J. G., Balwani, M., Anderson, K. E., Bonkovsky, H. L., Anstey, A. V., Bissell, D. M., Bloomer, J., Edwards, C., Neumann, N. J., Parker, C., Phillips, J. D., Lim, H. W., Hamzavi, I., Deybach, J. C., Kauppinen, R., Rhodes, L. E., Frank, J., Murphy, G. M., Karstens, F. P. J., Sijbrands, E. J. G., de Rooij, F. W. M., Lebwohl, M., Naik, H., Goding, C. R., Wilson, J. H. P., and Desnick, R. J. (2015) Afamelanotide for Erythropoietic Protoporphyrria, *N. Engl. J. Med.* 373, 48-59.
118. Maranon, R. O., Lima, R., Mathbout, M., do Carmo, J. M., Hall, J. E., Roman, R. J., and Reckelhoff, J. F. (2014) Postmenopausal hypertension: role of the sympathetic nervous system in an animal model, *Am J Physiol-Reg I* 306, R248-R256.
119. Carotenuto, A., Merlino, F., Cai, M., Brancaccio, D., Yousif, A. M., Novellino, E., Hruby, V. J., and Grieco, P. (2015) Discovery of Novel Potent and Selective Agonists at the Melanocortin3 Receptor, *J. Med. Chem.*
120. Jagadish, B., Sankaranarayanan, R., Xu, L., Richards, R., Vagner, J., Hruby, V. J., Gillies, R. J., and Mash, E. A. (2007) Squalene-derived flexible linkers for bioactive peptides, *Bioorganic & Medicinal Chemistry Letters* 17, 3310-3313.
121. Kiessling, L. L., Gestwicki, J. E., and Strong, L. E. (2000) Synthetic multivalent ligands in the exploration of cell-surface interactions, *Current Opinion in Chemical Biology* 4, 696-703.
122. Carlson, C. B., Mowery, P., Owen, R. M., Dykhuizen, E. C., and Kiessling, L. L. (2007) Selective tumor cell targeting using low-affinity, multivalent interactions, *ACS Chem. Biol.* 2, 119-127.
123. Alletti, R., Vagner, J., Dehigaspitiya, D. C., Moberg, V. E., Elshan, N., Tafreshi, N. K., Brabez, N., Weber, C. S., Lynch, R. M., Hruby, V. J., Gillies, R. J., Morse, D.

- L., and Mash, E. A. (2013) Synthesis and Characterization of Time-resolved Fluorescence Probes for Evaluation of Competitive Binding to Melanocortin Receptors, *Bioorganic & Medicinal Chemistry* 21, 5029-5038.
124. Kiessling, L. L., and Lamanna, A. C. (2003) *Multivalency in biological systems*, Vol. 129.
 125. Zanna, P. T., Sanchez-Laorden, B. L., Perez-Oliva, A. B., Turpin, M. C., Herraiz, C., Jimenez-Cervantes, C., and Garcia-Borron, J. C. (2008) Mechanism of dimerization of the human melanocortin 1 receptor, *Biochem. Biophys. Res. Commun.* 368, 211-216.
 126. Mandrika, I., Petrovska, R., and Wikberg, J. (2005) Melanocortin receptors form constitutive homo- and heterodimers, *Biochemical and Biophysical Research Communications* 326, 349-354.
 127. Sebag, J. A., and Hinkle, P. M. (2009) Opposite effects of the melanocortin-2 (MC2) receptor accessory protein MRAP on MC2 and MC5 receptor dimerization and trafficking, *J. Biol. Chem.* 284, 22641-22648.
 128. Piechowski, C. L., Rediger, A., Lagemann, C., Muhlhaus, J., Muller, A., Pratzka, J., Tarnow, P., Gruters, A., Krude, H., Kleinau, G., and Biebermann, H. (2013) Inhibition of melanocortin-4 receptor dimerization by substitutions in intracellular loop 2, *J Mol Endocrinol* 51, 109-118.
 129. Rediger, A., Piechowski, C. L., Habegger, K., Gruters, A., Krude, H., Tschop, M. H., Kleinau, G., and Biebermann, H. (2012) MC4R dimerization in the paraventricular nucleus and GHSR/MC3R heterodimerization in the arcuate nucleus: Is there relevance for body weight regulation?, *Neuroendocrinology* 95, 277-288.
 130. Nickolls, S. A., and Maki, R. A. (2006) Dimerization of the melanocortin 4 receptor: A study using bioluminescence resonance energy transfer, *Peptides* 27, 380-387.
 131. Biebermann, H., Krude, H., Elsner, A., Chubanov, V., Gudermann, T., and Gruters, A. (2003) Autosomal-dominant mode of inheritance of a melanocortin-4 receptor mutation in a patient with severe early-onset obesity is due to a dominant-negative effect caused by receptor dimerization, *Diabetes* 52, 2984-2988.
 132. Lensing, C. J., Adank, D. N., Wilber, S. L., Freeman, K. T., Schnell, S. M., Speth, R. C., Zarth, A. T., and Haskell-Luevano, C. (2017) A Direct in Vivo Comparison of the Melanocortin Monovalent Agonist Ac-His-DPhe-Arg-Trp-NH₂ versus the Bivalent Agonist Ac-His-DPhe-Arg-Trp-PEDG20-His-DPhe-Arg-Trp-NH₂: A Bivalent Advantage, *ACS Chem. Neurosci.* In press.
 133. Kopanchuk, S., Veiksina, S., Petrovska, R., Mutule, I., Szardenings, M., Rinken, A., and Wikberg, J. E. S. (2005) Co-operative regulation of ligand binding to melanocortin receptor subtypes: Evidence for interacting binding sites, *European Journal of Pharmacology* 512, 85-95.
 134. Kopanchuk, S., Veiksina, S., Mutulis, F., Mutule, I., Yahorava, S., Mandrika, I., Petrovska, R., Rinken, A., and Wikberg, J. E. S. (2006) Kinetic evidence for

- tandemly arranged ligand binding sites in melanocortin 4 receptor complexes, *Neurochemistry International* 49, 533-542.
135. Eberle, A. N., and Froidevaux, S. (2003) Radiolabeled alpha-melanocyte-stimulating hormone analogs for receptor-mediated targeting of melanoma: from tritium to indium, *J. Mol. Recognit.* 16, 248-254.
 136. Eberle, A. N., Bapst, J. P., Calame, M., Tanner, H., and Froidevaux, S. (2010) MSH Radiopeptides for Targeting Melanoma Metastases, In *Melanocortins: Multiple Actions and Therapeutic Potential* (Catania, A., Ed.), pp 133-142.
 137. Ren, G., Pan, Y., and Cheng, Z. (2010) Molecular Probes for Malignant Melanoma Imaging, *Current Pharmaceutical Biotechnology* 11, 590-602.
 138. Rosenkranz, A. A., Slastnikova, T. A., Durymanov, M. O., and Sobolev, A. S. (2013) Malignant melanoma and melanocortin 1 receptor, *Biochemistry-Moscow* 78, 1228-1237.
 139. Miao, Y. B., and Quinn, T. P. (2007) Alpha-melanocyte stimulating hormone peptide-targeted melanoma imaging, *Front. Biosci.* 12, 4514-4524.
 140. Suzuki, I., Cone, R. D., Im, S., Nordlund, J., and Abdel-Malek, Z. A. (1996) Binding of melanotropic hormones to the melanocortin receptor MC1R on human melanocytes stimulates proliferation and melanogenesis, *Endocrinology* 137, 1627-1633.
 141. Rosenkranz, A. A., Slastnikova, T. A., Durymanov, M. O., and Sobolev, A. S. (2013) Malignant melanoma and melanocortin 1 receptor, *Biochemistry (Mosc.)* 78, 1228-1237.
 142. Eberle, A., Hubscher, W., and Schwyzer, R. (1977) Synthesis of Radioactive Alpha-Melanotropin Derivatives Containing a Bromoacetyl or Diazoacetyl Group for Studies of Covalent Hormone-Macromolecule Complexes, *Helv. Chim. Acta* 60, 2895-2910.
 143. Eberle, A., Kriwaczek, V. M., and Schwyzer, R. (1977) Hormone-Receptor Interactions - Melanotropic Activities of Covalent Serum-Albumin Complexes with Alpha-Melanotropin, Alpha-Melanotropin Fragments, and Enkephalin, *FEBS Lett.* 80, 246-250.
 144. Kriwaczek, V. M., Eberle, A. N., Muller, M., and Schwyzer, R. (1978) Tobacco Mosaic-Virus as a Carrier for Small Molecules .1. Preparation and Characterization of a Tmv-Alpha-Melanotropin Conjugate, *Helv. Chim. Acta* 61, 1232-1240.
 145. Schwyzer, R., and Kriwaczek, V. M. (1981) Tobacco Mosaic-Virus as a Carrier for Small Molecules - Artificial Receptor Antibodies and Super-Hormones, *Biopolymers* 20, 2011-2020.
 146. Wunderlin, R., Minakakis, P., Tunkyi, A., Sharma, S. D., and Schwyzer, R. (1985) Melanotropin Receptors .1. Synthesis and Biological-Activity of N-Alpha-(5-Bromovaleryl)-N-Alpha-Deacetyl-Alpha-Melanotropin, *Helv. Chim. Acta* 68, 1-11.
 147. Wunderlin, R., Sharma, S. D., Minakakis, P., and Schwyzer, R. (1985) Melanotropin Receptors .2. Synthesis and Biological-Activity of Alpha-

- Melanotropin Tobacco Mosaic-Virus Disulfide Conjugates, *Helv. Chim. Acta* 68, 12-22.
148. Schwyzer, R., Kriwaczek, V. M., and Wunderlin, R. (1981) A Method for Mapping Peptide Receptors, *Naturwissenschaften* 68, 95-96.
 149. Kriwaczek, V. M., Bristow, A. F., Eberle, A. N., Gleed, C., Schulster, D., and Schwyzer, R. (1981) Super-Potency and Super-Affinity Phenomena in the Stimulation of Steroidogenesis in Adrenocortical-Cells by Adrenocorticotropin-Tobacco Mosaic-Virus Conjugates, *Mol. Cell. Biochem.* 40, 49-59.
 150. Sharma, S. D., Granberry, M. E., Jiang, J. W., Leong, S. P. L., Hadley, M. E., and Hruby, V. J. (1994) Multivalent Melanotropic Peptide And Fluorescent Macromolecular Conjugates - New Reagents For Characterization Of Melanotropin Receptors, *Bioconjugate Chemistry* 5, 591-601.
 151. Sharma, S. D., Hruby, V., Hadley, M. E., Granberry, M. E., and Leong, S. P. L. (1992) Multivalent ligands for diagnosis and therapeutics, *Peptides: Chemistry and Biology, Proceedings of the Twelfth American Peptide Symposium*, 599-600.
 152. Sharma, S. D., Jiang, J. W., Hadley, M. E., Bentley, D. L., and Hruby, V. J. (1996) Melanotropic peptide-conjugated beads for microscopic visualization and characterization of melanoma melanotropin receptors, *Proceedings of the National Academy of Sciences of the United States of America* 93, 13715-13720.
 153. Jiang, J. W., Sharma, S. D., Hruby, V. J., Bentley, D. L., Fink, J. L., and Hadley, M. E. (1996) Human epidermal melanocyte and keratinocyte melanocortin receptors: Visualization by melanotropic peptide conjugated microspheres (latex beads), *Pigment Cell Res.* 9, 240-247.
 154. Jiang, J., Sharma, S. D., Hruby, V. J., Fink, J. L., and Hadley, M. E. (1997) Human epidermal melanocyte and keratinocyte melanotropin receptors: Visualization by melanotropic peptide conjugated macrospheres (polyamide beads), *Exp. Dermatol.* 6, 6-12.
 155. Newton, J. R., Miao, Y. B., Deutscher, S. L., and Quinn, T. P. (2007) Melanoma imaging with pretargeted bivalent bacteriophage, *Journal of Nuclear Medicine* 48, 429-436.
 156. Barkey, N. M., Tafreshi, N. K., Josan, J. S., De Silva, C. R., Sill, K. N., Hruby, V. J., Gillies, R. J., Morse, D. L., and Vagner, J. (2011) Development of melanoma-targeted polymer micelles by conjugation of a melanocortin 1 receptor (MC1R) specific ligand, *J. Med. Chem.* 54, 8078-8084.
 157. Vagner, J., Handl, H. L., Gillies, R. J., and Hruby, V. J. (2004) Novel targeting strategy based on multimeric ligands for drug delivery and molecular imaging: homooligomers of alpha-MSH, *Bioorganic & Medicinal Chemistry Letters* 14, 211-215.
 158. Brabez, N., Saunders, K., Nguyen, K. L., Jayasundera, T., Weber, C., Lynch, R. M., Chassaing, G., Lavielle, S., and Hruby, V. J. (2013) Multivalent Interactions: Synthesis and Evaluation of Melanotropin Multimers-Tools for Melanoma Targeting, *ACS Med. Chem. Lett.* 4, 98-102.

159. Alleti, R., Rao, V., Xu, L. P., Gillies, R. J., and Mash, E. A. (2010) A Solanesol-Derived Scaffold for Multimerization of Bioactive Peptides, *Journal of Organic Chemistry* 75, 5895-5903.
160. Rao, V., Alleti, R., Xu, L. P., Tafreshi, N. K., Morse, D. L., Gillies, R. J., and Mash, E. A. (2011) A sucrose-derived scaffold for multimerization of bioactive peptides, *Bioorganic & Medicinal Chemistry* 19, 6474-6482.
161. Dehigaspitiya, D. C., Navath, S., Weber, C. S., Lynch, R. M., and Mash, E. A. (2015) Synthesis and bioactivity of MSH4 oligomers prepared by an A(2) + B-2 strategy, *Tetrahedron Letters* 56, 3060-3065.
162. Elshan, N., Jayasundera, T., Anglin, B. L., Weber, C. S., Lynch, R. M., and Mash, E. A. (2015) Trigonal scaffolds for multivalent targeting of melanocortin receptors, *Organic & Biomolecular Chemistry* 13, 1778-1791.
163. Dehigaspitiya, D. C., Anglin, B. L., Smith, K. R., Weber, C. S., Lynch, R. M., and Mash, E. A. (2015) Linear scaffolds for multivalent targeting of melanocortin receptors, *Organic & Biomolecular Chemistry* 13, 11507-11517.
164. Bard, D. R., Knight, C. G., and Pagethomas, D. P. (1990) A Chelating Derivative Of Alpha-Melanocyte Stimulating Hormone As A Potential Imaging Agent For Malignant-Melanoma, *British Journal of Cancer* 62, 919-922.
165. Wraight, E. P., Bard, D. R., Maughan, T. S., Knight, C. G., and Pagethomas, D. P. (1992) The Use Of A Chelating Derivative Of Alpha Melanocyte Stimulating Hormone For The Clinical Imaging Of Malignant-Melanoma, *British Journal of Radiology* 65, 112-118.
166. Bard, D. R., Wraight, E. P., and Knight, C. G. (1993) Bismsh-Dtpa - A Potential Imaging Agent For Malignant-Melanoma, *Annals of the New York Academy of Sciences* 680, 451-453.
167. Bard, D. R. (1995) An Improved Imaging Agent For Malignant-Melanoma, Based On Nle(4), D-Phe(7) Alpha-Melanocyte Stimulating Hormone, *Nuclear Medicine Communications* 16, 860-866.
168. Josan, J. S., Vagner, J., Handl, H. L., Sankaranarayanan, R., Gillies, R. J., and Hruby, V. J. (2008) Solid-phase synthesis of heterobivalent ligands targeted to melanocortin and cholecystokinin receptors, *Int. J. Pept. Res. Ther.* 14, 293-300.
169. Hruby, V., Josan, J., Vagner, J., Fernandes, S., Handl, H., Xu, L. P., Lynch, R., Mash, E., and Gillies, R. (2008) New approaches to the design, synthesis and biochemical and biophysical evaluation of heteromultivalent Ligands for detection and treatment of cancer, *J. Pept. Sci.* 14, 23-23.
170. Vagner, J., Xu, L. P., Handl, H. L., Josan, J. S., Morse, D. L., Mash, E. A., Gillies, R. J., and Hruby, V. J. (2008) Heterobivalent ligands crosslink multiple cell-surface receptors: The human melanocortin-4 and delta-opioid receptors, *Angew Chem Int Edit* 47, 1685-1688.
171. Xu, L. P., Vagner, J., Josan, J., Lynch, R. M., Morse, D. L., Baggett, B., Han, H. Y., Mash, E. A., Hruby, V. J., and Gillies, R. J. (2009) Enhanced targeting with heterobivalent ligands, *Mol. Cancer Ther.* 8, 2356-2365.

172. Josan, J. S., Handl, H. L., Sankaranarayanan, R., Xu, L. P., Lynch, R. M., Vagner, J., Mash, E. A., Hruby, V. J., and Gillies, R. J. (2011) Cell-Specific Targeting by Heterobivalent Ligands, *Bioconjugate Chemistry* 22, 1270-1278.
173. Yang, J. Q., Guo, H. X., Gallazzi, F., Berwick, M., Padilla, R. S., and Miao, Y. B. (2009) Evaluation of a Novel Arg-Gly-Asp-Conjugated alpha-Melanocyte Stimulating Hormone Hybrid Peptide for Potential Melanoma Therapy, *Bioconjugate Chemistry* 20, 1634-1642.
174. Jayawickreme, C. K., Quillan, J. M., Graminski, G. F., and Lerner, M. R. (1994) Discovery and structure-function analysis of alpha-melanocyte-stimulating hormone antagonists, *J. Biol. Chem.* 269, 29846-29854.
175. Carrithers, M. D., and Lerner, M. R. (1996) Synthesis and characterization of bivalent peptide ligands targeted to G-protein-coupled receptors, *Chemistry & Biology* 3, 537-542.
176. Vagner, J., Handl, H. L., Monguchi, Y., Jana, U., Begay, L. J., Mash, E. A., Hruby, V. J., and Gillies, R. J. (2006) Rigid linkers for bioactive peptides, *Bioconjugate Chemistry* 17, 1545-1550.
177. Handl, H. L., Sankaranarayanan, R., Josan, J. S., Vagner, J., Mash, E. A., Gillies, R. J., and Hruby, V. J. (2007) Synthesis and evaluation of bivalent NDP-alpha-MSH(7) peptide ligands for binding to the human melanocortin receptor 4 (hMC4R), *Bioconjugate Chemistry* 18, 1101-1109.
178. Bowen, M. E., Monguchi, Y., Sankaranarayanan, R., Vagner, J., Begay, L. J., Xu, L. P., Jagadish, B., Hruby, V. J., Gillies, R. J., and Mash, E. A. (2007) Design, synthesis, and validation of a branched flexible linker for bioactive peptides, *Journal of Organic Chemistry* 72, 1675-1680.
179. Fernandes, S. M., Lee, Y. S., Gillies, R. J., and Hruby, V. J. (2014) Synthesis and evaluation of bivalent ligands for binding to the human melanocortin-4 receptor, *Bioorganic & Medicinal Chemistry* 22, 6360-6365.
180. Lensing, C. J., Freeman, K. T., Schnell, S. M., Adank, D. N., Speth, R. C., and Haskell-Luevano, C. (2016) An in vitro and in vivo investigation of bivalent ligands that display preferential binding and functional activity for different melanocortin receptor homodimers, *J. Med. Chem.* 59, 3112-3128.
181. Bapst, J. P., Froidevaux, S., Calame, M., Tanner, H., and Eberle, A. N. (2007) Dimeric DOTA-alpha-melanocyte-stimulating hormone analogs: Synthesis and in vivo characteristics of radiopeptides with high in vitro activity, *Journal of Receptors and Signal Transduction* 27, 383-409.
182. Bagutti, C., Stolz, B., Albert, R., Bruns, C., Pless, J., and Eberle, A. N. (1994) In-111 -Dtpa-Labeled Analogs Of Alpha-Melanocyte-Stimulating Hormone For Melanoma Targeting - Receptor-Binding In-Vitro And In-Vivo, *International Journal of Cancer* 58, 749-755.
183. Erez, M., Takemori, A. E., and Portoghese, P. S. (1982) Narcotic Antagonistic Potency Of Bivalent Ligands Which Contain Beta-Naltrexamine - Evidence For

- Bridging Between Proximal Recognition Sites, *Journal of Medicinal Chemistry* 25, 847-849.
184. Portoghese, P. S., Larson, D. L., Sayre, L. M., Yim, C. B., Ronsisvalle, G., Tam, S. W., and Takemori, A. E. (1986) Opioid Agonist and Antagonist Bivalent Ligands - the Relationship between Spacer Length and Selectivity at Multiple Opioid Receptors, *Journal of Medicinal Chemistry* 29, 1855-1861.
 185. Kuhhorn, J., Hubner, H., and Gmeiner, P. (2011) Bivalent Dopamine D-2 Receptor Ligands: Synthesis and Binding Properties, *Journal of Medicinal Chemistry* 54, 4896-4903.
 186. Irani, B. G., Xiang, Z. M., Yarandi, H. N., Holder, J. R., Moore, M. C., Bauzo, R. M., Proneth, B., Shaw, A. M., Millard, W. J., Chambers, J. B., Benoit, S. C., Clegg, D. J., and Haskell-Luevano, C. (2011) Implication of the melanocortin-3 receptor in the regulation of food intake, *European Journal of Pharmacology* 660, 80-87.
 187. Busnelli, M., Kleinau, G., Muttenthaler, M., Stoev, S., Manning, M., Bibic, L., Howell, L. A., McCormick, P. J., Di Lascio, S., Braidia, D., Sala, M., Rovati, G. E., Bellini, T., and Chini, B. (2016) Design and Characterization of Superpotent Bivalent Ligands Targeting Oxytocin Receptor Dimers via a Channel-Like Structure, *Journal of Medicinal Chemistry* 59, 7152-7166.
 188. Akgun, E., Javed, M. I., Lunzer, M. M., Powers, M. D., Sham, Y. Y., Watanabe, Y., and Portoghese, P. S. (2015) Inhibition of Inflammatory and Neuropathic Pain by Targeting a Mu Opioid Receptor/Chemokine Receptor5 Heteromer (MOR-CCR5), *Journal of Medicinal Chemistry* 58, 8647-8657.
 189. Lensing, C. J., Adank, D. N., Doering, S. R., Wilber, S. L., Andreasen, A., Schaub, J. W., Xiang, Z., and Haskell-Luevano, C. (2016) Ac-Trp-DPhe(p-I)-Arg-Trp-NH₂, a 250-Fold Selective Melanocortin-4 Receptor (MC4R) Antagonist over the Melanocortin-3 Receptor (MC3R), Affects Energy Homeostasis in Male and Female Mice Differently, *ACS Chem. Neurosci.* 7, 1283-1291.
 190. Carpino, L. A., and Han, G. Y. (1972) 9-Fluorenylmethoxycarbonyl amino-protecting group, *J. Org. Chem.* 37, 3404-3409.
 191. Stewart, J. M., and Young, J. D. (1984) *Solid Phase Peptide Synthesis*, 2nd ed., Pierce Chemical Co., Rockford, Il. .
 192. Kaiser, E., Colescott, R. L., Bossinger, C. D., and Cook, P. I. (1970) Color test for detection of free terminal amino groups in the solid-phase synthesis of peptides, *Anal. Biochem.* 34, 595-598.
 193. Christensen, T. (1979) Qualitative test for monitoring coupling completeness in solid-phase peptide-synthesis using chloranil, *Acta Chem. Scand.* 33, 763-766.
 194. Chen, C. A., and Okayama, H. (1988) Calcium phosphate-mediated gene transfer: a highly efficient transfection system for stably transforming cells with plasmid DNA, *Biotechniques* 6, 632-638.
 195. Hunter, W. M., and Greenwood, F. C. (1962) Preparation of iodine-131 labelled human growth hormone of high specific activity, *Nature* 194, 495-496.

196. Chen, W., Shields, T. S., Stork, P. J., and Cone, R. D. (1995) A colorimetric assay for measuring activation of Gs- and Gq-coupled signaling pathways, *Anal. Biochem.* 226, 349-354.
197. Singh, A., Tala, S. R., Flores, V., Freeman, K., and Haskell-Luevano, C. (2015) Synthesis and Pharmacology of alpha/beta(3)-Peptides Based on the Melanocortin Agonist Ac-His-DPhe-Arg-Trp-NH₂ Sequence, *ACS Med. Chem. Lett.* 6, 568-572.
198. Schild, H. O. (1947) pA, a new scale for the measurement of drug antagonism, *Br. J. Pharmacol. Chemother.* 2, 189-206.
199. Shinyama, H., Masuzaki, H., Fang, H., and Flier, J. S. (2003) Regulation of melanocortin-4 receptor signaling: Agonist-mediated desensitization and internalization, *Endocrinology* 144, 1301-1314.
200. Cai, M. Y., Varga, E. V., Stankova, M., Mayorov, A., Perry, J. W., Yamamura, H. I., Trivedi, D., and Hruby, V. J. (2006) Cell signaling and trafficking of human melanocortin receptors in real time using two-photon fluorescence and confocal laser microscopy: Differentiation of agonists and antagonists, *Chem. Biol. Drug Des.* 68, 183-193.
201. Gao, Z. H., Lei, D. C., Welch, J., Le, K., Lin, J., Leng, S., and Duhl, D. (2003) Agonist-dependent internalization of the human melanocortin-4 receptors in human embryonic kidney 293 cells, *J. Pharmacol. Exp. Ther.* 307, 870-877.
202. Kroeze, W. K., Sassano, M. F., Huang, X. P., Lansu, K., McCorvy, J. D., Giguere, P. M., Sciaky, N., and Roth, B. L. (2015) PRESTO-Tango as an open-source resource for interrogation of the druggable human GPCRome, *Nat. Struct. Mol. Biol.* 22, 362-U328.
203. Barnea, G., Strapps, W., Herrada, G., Berman, Y., Ong, J., Kloss, B., Axel, R., and Lee, K. J. (2008) The genetic design of signaling cascades to record receptor activation, *Proc. Natl. Acad. Sci. U. S. A.* 105, 64-69.
204. Mandrika, I., Petrovska, R., and Wikberg, J. (2005) Melanocortin receptors form constitutive homo- and heterodimers, *Biochem. Biophys. Res. Commun.* 326, 349-354.
205. Kopanchuk, S., Veiksina, S., Mutulis, F., Mutule, I., Yahorava, S., Mandrika, I., Petrovska, R., Rinken, A., and Wikberg, J. E. (2006) Kinetic evidence for tandemly arranged ligand binding sites in melanocortin 4 receptor complexes, *Neurochem. Int.* 49, 533-542.
206. Piechowski, C. L., Rediger, A., Lagemann, C., Muhlhaus, J., Muller, A., Pratzka, J., Tarnow, P., Gruters, A., Krude, H., Kleinau, G., and Biebermann, H. (2013) Inhibition of melanocortin-4 receptor dimerization by substitutions in intracellular loop 2, *J. Mol. Endocrinol.* 51, 109-118.
207. Chapman, K. L., and Findlay, J. B. (2013) The melanocortin 4 receptor: oligomer formation, interaction sites and functional significance, *Biochim. Biophys. Acta* 1828, 535-542.

208. Elsner, A., Tarnow, P., Schaefer, M., Ambrugger, P., Krude, H., Gruters, A., and Biebermann, H. (2006) MC4R oligomerizes independently of extracellular cysteine residues, *Peptides* 27, 372-379.
209. Kobayashi, Y., Hamamoto, A., Takahashi, A., and Saito, Y. (2016) Dimerization of melanocortin receptor 1 (MC1R) and MC5R creates a ligand-dependent signal modulation: Potential participation in physiological color change in the flounder, *Gen. Comp. Endocrinol.* 230-231, 103-109.
210. Atalayer, D., Robertson, K. L., Haskell-Luevano, C., Andreasen, A., and Rowland, N. E. (2010) Food demand and meal size in mice with single or combined disruption of melanocortin type 3 and 4 receptors, *Am. J. Physiol. Regul. Integr. Comp. Physiol.* 298, R1667-1674.
211. Wachira, S. J., Hughes-Darden, C. A., Nicholas, H. B., Jr., Taylor, C. V., and Robinson, T. J. (2004) Neural melanocortin receptors are differentially expressed and regulated by stress in rat hypothalamic-pituitary-adrenal axis, *Cell. Mol. Biol. (Noisy-le-grand)* 50, 703-713.
212. Mountjoy, K. G. (2010) Distribution and Function of Melanocortin Receptors within the Brain, *Melanocortins: Multiple Actions and Therapeutic Potential* 681, 29-48.
213. Zheng, Y., Akgun, E., Harikumar, K. G., Hopson, J., Powers, M. D., Lunzer, M. M., Miller, L. J., and Portoghese, P. S. (2009) Induced association of mu opioid (MOP) and type 2 cholecystokinin (CCK2) receptors by novel bivalent ligands, *J. Med. Chem.* 52, 247-258.
214. Tabor, A., Weisenburger, S., Banerjee, A., Purkayastha, N., Kaindl, J. M., Hubner, H., Wei, L. X., Gromer, T. W., Kornhuber, J., Tschammer, N., Birdsall, N. J. M., Mashanov, G. I., Sandoghdar, V., and Gmeiner, P. (2016) Visualization and ligand-induced modulation of dopamine receptor dimerization at the single molecule level, *Sci. Rep.* 6.
215. Lensing, C. J., Doering, S. R., Danielle, N. A., and Haskell-Luevano, C. (2015) Investigating Metabolic Gender Differences with Melanocortin Antagonist SKY 2-23-7, *Proceedings of the 24th American Peptide Symposium* 24, 162-164.
216. Lensing, C. J., Adank, D. N., Doering, S. R., Wilber, S. L., Andreasen, A., Schaub, J. W., Xiang, Z., and Haskell-Luevano, C. (2016) The Ac-Trp-DPhe(p-I)-Arg-Trp-NH₂ 250-Fold Selective Melanocortin-4 Receptor (MC4R) Antagonist over the Melanocortin-3 Receptor (MC3R) Affects Energy Homeostasis in Male and Female Mice Differently, *ACS Chem. Neurosci.*
217. Franklin, K. B. J., and Paxinos, G. (1997) *The Mouse Brain in Stereotaxic Coordinates*, Academic Press, San Diego.
218. Ellacott, K. L., Morton, G. J., Woods, S. C., Tso, P., and Schwartz, M. W. (2010) Assessment of feeding behavior in laboratory mice, *Cell Metab.* 12, 10-17.
219. Kopanchuk, S., Veiksina, S., Petrovska, R., Mutule, I., Szardenings, M., Rinken, A., and Wikberg, J. E. (2005) Co-operative regulation of ligand binding to

- melanocortin receptor subtypes: Evidence for interacting binding sites, *Eur. J. Pharmacol.* *512*, 85-95.
220. Proneth, B., Pogozheva, I. D., Portillo, F. P., Mosberg, H. I., and Haskell-Luevano, C. (2008) Melanocortin tetrapeptide Ac-His-DPhe-Arg-Trp-NH₂ modified at the para position of the benzyl side chain (DPhe): importance for mouse melanocortin-3 receptor agonist versus antagonist activity, *J. Med. Chem.* *51*, 5585-5593.
221. Haskell-Luevano, C., Sawyer, T. K., Hendrata, S., North, C., Panahinia, L., Stum, M., Staples, D. J., Castrucci, A. M., Hadley, M. F., and Hruby, V. J. (1996) Truncation studies of alpha-melanotropin peptides identify tripeptide analogues exhibiting prolonged agonist bioactivity, *Peptides* *17*, 995-1002.
222. Hruby, V. J., Wilkes, B. C., Hadley, M. E., Alobeidi, F., Sawyer, T. K., Staples, D. J., Devaux, A. E., Dym, O., Castrucci, A. M. D., Hintz, M. F., Riehm, J. P., and Rao, K. R. (1987) Alpha-melanotropin: The minimal active sequence in the frog-skin bioassay, *J. Med. Chem.* *30*, 2126-2130.
223. Kiessling, L. L., and Lamanna, A. C. (2003) Multivalency in biological systems, *Nato Sci Ser Ii Math* *129*, 345-357.
224. Zhang, S. J., Yekkirala, A., Tang, Y., and Portoghese, P. S. (2009) A bivalent ligand (KMN-21) antagonist for mu/kappa heterodimeric opioid receptors, *Bioorg. Med. Chem. Lett.* *19*, 6978-6980.
225. Akgun, E., Javed, M. I., Lunzer, M. M., Smeester, B. A., Beitz, A. J., and Portoghese, P. S. (2013) Ligands that interact with putative MOR-mGluR5 heteromer in mice with inflammatory pain produce potent antinociception, *Proc. Natl. Acad. Sci. U. S. A.* *110*, 11595-11599.
226. Kostelnik, K. B., Els-Heindl, S., Kloting, N., Baumann, S., von Bergen, M., and Beck-Sickinger, A. G. (2015) High metabolic in vivo stability and bioavailability of a palmitoylated ghrelin receptor ligand assessed by mass spectrometry, *Bioorg. Med. Chem.* *23*, 3925-3932.
227. Veronese, F. M., and Pasut, G. (2005) PEGylation, successful approach to drug delivery, *Drug Discovery Today* *10*, 1451-1458.
228. Carpino, L. A., and Han, G. Y. (1970) 9-Fluorenylmethoxycarbonyl function, a new base-sensitive amino-protecting group, *J. Am. Chem. Soc.* *92*, 5748-5749.
229. Trokowski, R., Akine, S., and Nabeshima, T. (2011) Remarkably Selective Recognition of Iodobenzene Derivatives by a Macrocyclic Bis-Pt-II Metallohost, *Chem-Eur J* *17*, 14420-14428.
230. Kiessling, L. L., Gestwicki, J. E., and Strong, L. E. (2000) Synthetic multivalent ligands in the exploration of cell-surface interactions, *Curr. Opin. Chem. Biol.* *4*, 696-703.
231. Han, Y., Moreira, I. S., Urizar, E., Weinstein, H., and Javitch, J. A. (2009) Allosteric communication between protomers of dopamine class A GPCR dimers modulates activation, *Nat. Chem. Biol.* *5*, 688-695.
232. Batterham, R. L., Cowley, M. A., Small, C. J., Herzog, H., Cohen, M. A., Dakin, C. L., Wren, A. M., Brynes, A. E., Low, M. J., Ghatei, M. A., Cone, R. D., and

- Bloom, S. R. (2002) Gut hormone PYY3-36 physiologically inhibits food intake, *Nature* 418, 650-654.
233. Batterham, R. L., Cowley, M. A., Small, C. J., Herzog, H., Cohen, M. A., Dakin, C. L., Wren, A. M., Brynes, A. E., Low, M. J., Ghatei, M. A., Cone, R. D., and Bloom, S. R. (2004) Does gut hormone PYY3-36 decrease food intake in rodents? Reply, *Nature* 430.
234. Tschop, M., Castaneda, T. R., Joost, H. G., Thone-Reineke, C., Ortmann, S., Klaus, S., Hagan, M. M., Chandler, P. C., Oswald, K. D., Benoit, S. C., Seeley, R. J., Kinzig, K. P., Moran, T. H., Beck-Sickinger, A. G., Koglin, N., Rodgers, R. J., Blundell, J. E., Ishii, Y., Beattie, A. H., Holch, P., Allison, D. B., Raun, K., Madsen, K., Wulff, B. S., Stidsen, C. E., Birringer, M., Kreuzer, O. J., Schindler, M., Arndt, K., Rudolf, K., Mark, M., Deng, X. Y., Withcomb, D. C., Halem, H., Taylor, J., Dong, J., Datta, R., Culler, M., Craney, S., Flora, D., Smiley, D., and Heiman, M. L. (2004) Physiology: Does gut hormone PYY3-36 decrease food intake in rodents?, *Nature* 430.
235. Sorge, R. E., Martin, L. J., Isbester, K. A., Sotocinal, S. G., Rosen, S., Tuttle, A. H., Wieskopf, J. S., Acland, E. L., Dokova, A., Kadoura, B., Leger, P., Mapplebeck, J. C., McPhail, M., Delaney, A., Wigerblad, G., Schumann, A. P., Quinn, T., Frasnelli, J., Svensson, C. I., Sternberg, W. F., and Mogil, J. S. (2014) Olfactory exposure to males, including men, causes stress and related analgesia in rodents, *Nature methods* 11, 629-632.
236. Perez, M., Pauwels, P. J., Fourrier, C., Chopin, P., Valentin, J. P., John, G. W., Marien, M., and Halazy, S. (1998) Dimerization of sumatriptan as an efficient way to design a potent, centrally and orally active 5-HT_{1B} agonist, *Bioorg. Med. Chem. Lett.* 8, 675-680.
237. Zhang, Y. N., Gilliam, A., Maitra, R., Damaj, M. I., Tajuba, J. M., Seltzman, H. H., and Thomas, B. F. (2010) Synthesis and Biological Evaluation of Bivalent Ligands for the Cannabinoid 1 Receptor, *J. Med. Chem.* 53, 7048-7060.
238. Castrucci, A. M. D., Hadley, M. E., Sawyer, T. K., and Hruby, V. J. (1984) Enzymological Studies of Melanotropins, *Comp Biochem Phys B* 78, 519-524.
239. Haskell-Luevano, C., Chen, P. L., Li, C., Chang, K., Smith, M. S., Cameron, J. L., and Cone, R. D. (1999) Characterization of the neuroanatomical distribution of agouti-related protein immunoreactivity in the rhesus monkey and the rat, *Endocrinology* 140, 1408-1415.
240. Renquist, B. J., Murphy, J. G., Larson, E. A., Olsen, D., Klein, R. F., Ellacott, K. L., and Cone, R. D. (2012) Melanocortin-3 receptor regulates the normal fasting response, *Proc. Natl. Acad. Sci. U. S. A.* 109, E1489-1498.
241. Hahn, T. M., Breininger, J. F., Baskin, D. G., and Schwartz, M. W. (1998) Coexpression of *Agrp* and *NPY* in fasting-activated hypothalamic neurons, *Nat. Neurosci.* 1, 271-272.

242. Goodin, S. Z., Keichler, A. R., Smith, M., Wendt, D., and Strader, A. D. (2008) Effect of gonadectomy on AgRP-induced weight gain in rats, *Am J Physiol-Reg I* 295, R1747-R1753.
243. Jensen, T. L., Kiersgaard, M. K., Sorensen, D. B., and Mikkelsen, L. F. (2013) Fasting of mice: a review, *Lab. Anim.* 47, 225-240.
244. Speakman, J. R. (2013) Measuring energy metabolism in the mouse - theoretical, practical, and analytical considerations, *Front. Physiol.* 4, 34.
245. Meyer, C. W., Reitmeir, P., and Tschop, M. H. (2015) Exploration of Energy Metabolism in the Mouse Using Indirect Calorimetry: Measurement of Daily Energy Expenditure (DEE) and Basal Metabolic Rate (BMR), *Curr. Protoc. Mouse Biol.* 5, 205-222.
246. Tanner, J. M., Kearns, D. T., Kim, B. J., Sloan, C., Jia, Z., Yang, T., Abel, E. D., and Symons, J. D. (2010) Fasting-induced reductions in cardiovascular and metabolic variables occur sooner in obese versus lean mice, *Exp. Biol. Med. (Maywood)* 235, 1489-1497.
247. Marvyn, P. M., Bradley, R. M., Mardian, E. B., Marks, K. A., and Duncan, R. E. (2016) Data on oxygen consumption rate, respiratory exchange ratio, and movement in C57BL/6J female mice on the third day of consuming a high-fat diet, *Data in brief* 7, 472-475.
248. Pardridge, W. M. (1997) Drug delivery to the brain, *J. Cereb. Blood Flow Metab.* 17, 713-731.
249. Maness, L. M., Kastin, A. J., Farrell, C. L., and Banks, W. A. (1998) Fate of leptin after intracerebroventricular injection into the mouse brain, *Endocrinology* 139, 4556-4562.
250. Pardridge, W. M. (2011) Drug transport in brain via the cerebrospinal fluid, *Fluids and barriers of the CNS* 8, 7.
251. Fan, W., Dinulescu, D. M., Butler, A. A., Zhou, J., Marks, D. L., and Cone, R. D. (2000) The central melanocortin system can directly regulate serum insulin levels, *Endocrinology* 141, 3072-3079.
252. Obici, S., Feng, Z. H., Tan, J. Z., Liu, L. S., Karkanias, G., and Rossetti, L. (2001) Central melanocortin receptors regulate insulin action, *J. Clin. Invest.* 108, 1079-1085.
253. Pierroz, D. D., Ziotopoulou, M., Ungsuan, L., Moschos, S., Flier, J. S., and Mantzoros, C. S. (2002) Effects of acute and chronic administration of the melanocortin agonist MTII in mice with diet-induced obesity, *Diabetes* 51, 1337-1345.
254. Steiner, D. F., Cunningham, D., Spigelman, L., and Aten, B. (1967) Insulin biosynthesis: evidence for a precursor, *Science* 157, 697-700.
255. Rubenstein, A. H., Clark, J. L., Melani, F., and Steiner, D. F. (1969) Secretion of Proinsulin C-Peptide by Pancreatic [beta] Cells and its Circulation in Blood, *Nature* 224, 697-699.

256. Panaro, B. L., Tough, I. R., Engelstoft, M. S., Matthews, R. T., Digby, G. J., Moller, C. L., Svendsen, B., Gribble, F., Reimann, F., Holst, J. J., Holst, B., Schwartz, T. W., Cox, H. M., and Cone, R. D. (2014) The Melanocortin-4 Receptor Is Expressed in Enteroendocrine L Cells and Regulates the Release of Peptide YY and Glucagon-like Peptide 1 In Vivo, *Cell metabolism* 20, 1018-1029.
257. Lee, J. H., Bullen, J. W., Jr., Stoyneva, V. L., and Mantzoros, C. S. (2005) Circulating resistin in lean, obese, and insulin-resistant mouse models: lack of association with insulinemia and glycemia, *Am. J. Physiol. Endocrinol. Metab.* 288, E625-632.
258. Lin, J., Choi, Y. H., Hartzell, D. L., Li, C. L., Della-Fera, M. A., and Baile, C. A. (2003) CNS melanocortin and leptin effects on stearoyl-CoA desaturase-1 and resistin expression, *Biochem. Biophys. Res. Commun.* 311, 324-328.
259. Huang, Q. H., Hruby, V. J., and Tatro, J. B. (1998) Systemic alpha-MSH suppresses LPS fever via central melanocortin receptors independently of its suppression of corticosterone and IL-6 release, *Am J Physiol-Reg I* 275, R524-R530.
260. Ottani, A., Neri, L., Canalini, F., Calevro, A., Rossi, R., Cappelli, G., Ballestri, M., Giuliani, D., and Guarini, S. (2014) Protective effects of the melanocortin analog NDP-alpha-MSH in rats undergoing cardiac arrest, *Eur. J. Pharmacol.* 745, 108-116.
261. Bohm, M., Apel, M., Sugawara, K., Brehler, R., Jurk, K., Luger, T. A., Haas, H., Paus, R., Eiz-Vesper, B., Walls, A. F., Ponimaskin, E., Gehring, M., Kapp, A., and Raap, U. (2012) Modulation of basophil activity: A novel function of the neuropeptide alpha-melanocyte-stimulating hormone, *J. Allergy Clin. Immunol.* 129, 1085-1093.
262. Jun, D. J., Na, K. Y., Kim, W., Kwak, D., Kwon, E. J., Yoon, J. H., Yea, K., Lee, H., Kim, J., Suh, P. G., Ryu, S. H., and Kim, K. T. (2010) Melanocortins induce interleukin 6 gene expression and secretion through melanocortin receptors 2 and 5 in 3T3-L1 adipocytes, *J. Mol. Endocrinol.* 44, 225-236.
263. Engelstoft, M. S., Park, W. M., Sakata, I., Kristensen, L. V., Husted, A. S., Osborne-Lawrence, S., Piper, P. K., Walker, A. K., Pedersen, M. H., Nohr, M. K., Pan, J., Sinz, C. J., Carrington, P. E., Akiyama, T. E., Jones, R. M., Tang, C., Ahmed, K., Offermanns, S., Egerod, K. L., Zigman, J. M., and Schwartz, T. W. (2013) Seven transmembrane G protein-coupled receptor repertoire of gastric ghrelin cells, *Molecular metabolism* 2, 376-392.
264. Steppan, C. M., Bailey, S. T., Bhat, S., Brown, E. J., Banerjee, R. R., Wright, C. M., Patel, H. R., Ahima, R. S., and Lazar, M. A. (2001) The hormone resistin links obesity to diabetes, *Nature* 409, 307-312.
265. Champy, M. F., Selloum, M., Piard, L., Zeitler, V., Caradec, C., Chambon, P., and Auwerx, J. (2004) Mouse functional genomics requires standardization of mouse handling and housing conditions, *Mamm. Genome* 15, 768-783.
266. Elliott, R. M., Morgan, L. M., Tredger, J. A., Deacon, S., Wright, J., and Marks, V. (1993) Glucagon-like peptide-1 (7-36)amide and glucose-dependent insulinotropic

- polypeptide secretion in response to nutrient ingestion in man: acute post-prandial and 24-h secretion patterns, *J. Endocrinol.* 138, 159-166.
267. Asakawa, A., Inui, A., Kaga, T., Yuzuriha, H., Nagata, T., Ueno, N., Makino, S., Fujimiya, M., Niijima, A., Fujino, M. A., and Kasuga, M. (2001) Ghrelin is an appetite-stimulatory signal from stomach with structural resemblance to motilin, *Gastroenterology* 120, 337-345.
268. Lavin, D. N., Joesting, J. J., Chiu, G. S., Moon, M. L., Meng, J., Dilger, R. N., and Freund, G. G. (2011) Fasting induces an anti-inflammatory effect on the neuroimmune system which a high-fat diet prevents, *Obesity* 19, 1586-1594.
269. Ericson, M. D., Schnell, S. M., Freeman, K. T., and Haskell-Luevano, C. (2015) A fragment of the Escherichia coli ClpB heat-shock protein is a micromolar melanocortin 1 receptor agonist, *Bioorg. Med. Chem. Lett.* 25, 5306-5308.
270. Tala, S. R., Schnell, S. M., and Haskell-Luevano, C. (2015) Microwave-assisted solid-phase synthesis of side-chain to side-chain lactam-bridge cyclic peptides, *Bioorg. Med. Chem. Lett.* 25, 5708-5711.
271. Santos, R. G., Giulianotti, M. A., Dooley, C. T., Pinilla, C., Appel, J. R., and Houghten, R. A. (2011) Use and Implications of the Harmonic Mean Model on Mixtures for Basic Research and Drug Discovery, *Acs Comb Sci* 13, 337-344.
272. Ferre, S. (2015) The GPCR heterotetramer: challenging classical pharmacology, *Trends Pharmacol. Sci.* 36, 145-152.
273. Pellissier, L. P., Barthet, G., Gaven, F., Cassier, E., Trinquet, E., Pin, J. P., Marin, P., Dumuis, A., Bockaert, J., Baneres, J. L., and Claeysen, S. (2011) G protein activation by serotonin type 4 receptor dimers: evidence that turning on two protomers is more efficient, *J. Biol. Chem.* 286, 9985-9997.
274. Teitler, M., and Klein, M. T. (2012) A new approach for studying GPCR dimers: Drug-induced inactivation and reactivation to reveal GPCR dimer function in vitro, in primary culture, and in vivo, *Pharmacol. Ther.* 133, 205-217.
275. Comps-Agrar, L., Kniazeff, J., Norskov-Lauritsen, L., Maurel, D., Gassmann, M., Gregor, N., Prezeau, L., Bettler, B., Durroux, T., Trinquet, E., and Pin, J. P. (2011) The oligomeric state sets GABA(B) receptor signalling efficacy, *EMBO J.* 30, 2336-2349.
276. Pin, J. P., Kniazeff, J., Liu, J., Binet, V., Goudet, C., Rondard, P., and Prezeau, L. (2005) Allosteric functioning of dimeric class C G-protein-coupled receptors, *Febs J* 272, 2947-2955.
277. Hlavackova, V., Goudet, C., Kniazeff, J., Zikova, A., Maurel, D., Vol, C., Trojanova, J., Prezeau, L., Pin, J. P., and Blahos, J. (2005) Evidence for a single heptahelical domain being turned on upon activation of a dimeric GPCR, *EMBO J.* 24, 499-509.
278. Prezeau, L., Goudet, C., Kniazeff, J., Hlavackova, V., Malhaire, F., Maurel, D., Acher, F., Blahos, J., and Pin, J. P. (2005) Binding of a single positive allosteric modulator per dimer is sufficient for full enhancement of metabotropic glutamate receptor activity, *Neuropharmacology* 49, 267-267.

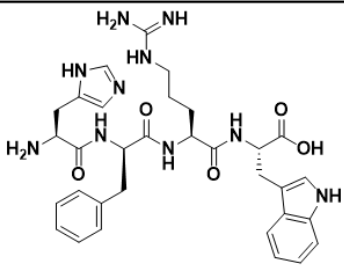
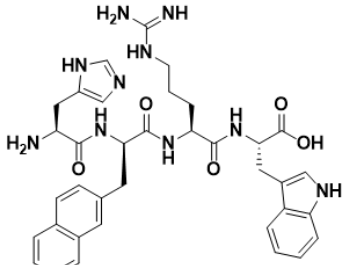
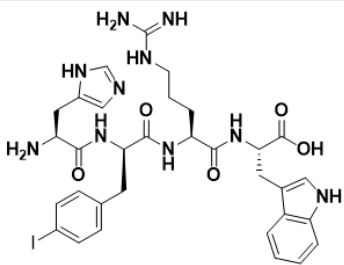
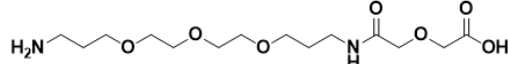
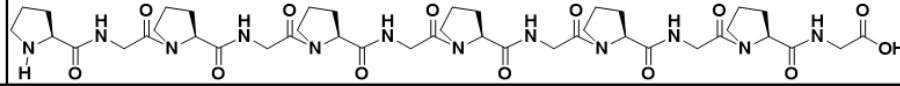
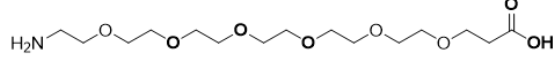
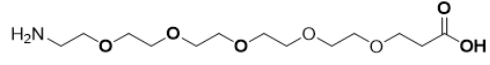
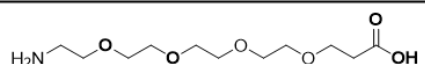
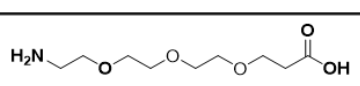
279. Kniazeff, J., Bessis, A. S., Maurel, D., Ansanay, H., Prezeau, L., and Pin, J. P. (2004) Closed state of both binding domains of homodimeric mGlu receptors is required for full activity, *Nat. Struct. Mol. Biol.* *11*, 706-713.
280. Kniazeff, J., Saintot, P. P., Goudet, C., Liu, J., Charnet, A., Guillon, G., and Pin, J. P. (2004) Locking the dimeric GABA(B) G-protein-coupled receptor in its active state, *J. Neurosci.* *24*, 370-377.
281. Zylbergold, P., and Hebert, T. E. (2009) A division of labor: asymmetric roles for GPCR subunits in receptor dimers, *Nat. Chem. Biol.* *5*, 608-609.
282. Szalai, B., Barkai, L., Turu, G., Szidonya, L., Varnai, P., and Hunyady, L. (2012) Allosteric interactions within the AT(1) angiotensin receptor homodimer: Role of the conserved DRY motif, *Biochem. Pharmacol.* *84*, 477-485.
283. Damian, M., Martin, A., Mesnier, D., Pin, J. P., and Baneres, J. L. (2006) Asymmetric conformational changes in a GPCR dimer controlled by G-proteins, *EMBO J.* *25*, 5693-5702.
284. Brock, C., Oueslati, N., Soler, S., Boudier, L., Rondard, P., and Pin, J. P. (2007) Activation of a dimeric metabotropic glutamate receptor by intersubunit rearrangement, *J. Biol. Chem.* *282*, 33000-33008.
285. Sartania, N., Appelbe, S., Padiani, J. D., and Milligan, G. (2007) Agonist occupancy of a single monomeric element is sufficient to cause internalization of the dimeric beta2-adrenoceptor, *Cell. Signal.* *19*, 1928-1938.
286. Gracia, E., Moreno, E., Cortes, A., Lluís, C., Mallol, J., McCormick, P. J., Canela, E. I., and Casado, V. (2013) Homodimerization of adenosine A(1) receptors in brain cortex explains the biphasic effects of caffeine, *Neuropharmacology* *71*, 56-69.
287. Orcel, H., Albizu, L., Perkovska, S., Durroux, T., Mendre, C., Ansanay, H., Mouillac, B., and Rabie, A. (2009) Differential coupling of the vasopressin V1b receptor through compartmentalization within the plasma membrane, *Mol. Pharmacol.* *75*, 637-647.
288. Smith, N. J., and Milligan, G. (2010) Allosterism at G Protein-Coupled Receptor Homo- and Heteromers: Uncharted Pharmacological Landscapes, *Pharmacol. Rev.* *62*, 701-725.
289. Chen, M., Georgeson, K. E., Harmon, C. M., Haskell-Luevano, C., and Yang, Y. K. (2006) Functional characterization of the modified melanocortin peptides responsible for ligand selectivity at the human melanocortin receptors, *Peptides* *27*, 2836-2845.
290. Fernandes, S. M., Sankaranarayanan, R., Handl, H. L., Josan, J., Vagner, J., Xu, L., Mash, E., Gillies, R. J., and Hruby, V. J. (2007) Synthesis and evaluation of bivalent ligands with NDP-alpha-MSH and SHU9119 for melanocortin 4 receptor, *Biopolymers* *88*, 619-619.
291. Merrifield, R. B. (1963) Solid Phase Peptide Synthesis. I. The Synthesis of a Tetrapeptide, *J. Am. Chem. Soc.* *85*, 2149-2154.
292. Xiang, Z., Proneth, B., Dirain, M. L., Litherland, S. A., and Haskell-Luevano, C. (2010) Pharmacological characterization of 30 human melanocortin-4 receptor

- polymorphisms with the endogenous proopiomelanocortin-derived agonists, synthetic agonists, and the endogenous agouti-related protein antagonist, *Biochemistry* 49, 4583-4600.
293. Xiang, Z., Litherland, S. A., Sorensen, N. B., Proneth, B., Wood, M. S., Shaw, A. M., Millard, W. J., and Haskell-Luevano, C. (2006) Pharmacological characterization of 40 human melanocortin-4 receptor polymorphisms with the endogenous proopiomelanocortin-derived agonists and the agouti-related protein (AGRP) antagonist, *Biochemistry* 45, 7277-7288.
 294. Stephenson, R. P. (1956) A modification of receptor theory, *Br. J. Pharmacol. Chemother.* 11, 379-393.
 295. Takeyasu, K., Uchida, S., Wada, A., Maruno, M., Lai, R. T., Hata, F., and Yoshida, H. (1979) Experimental evidence and dynamic aspects of spare receptor, *Life Sci.* 25, 1761-1771.
 296. Nickolls, S. A., Fleck, B., Hoare, S. R. J., and Maki, R. A. (2005) Functional selectivity of melanocortin 4 receptor peptide and nonpeptide agonists: Evidence for ligand-specific conformational states, *J. Pharmacol. Exp. Ther.* 313, 1281-1288.
 297. Breit, A., Buch, T. R. H., Boekhoff, I., Solinski, H. J., Damm, E., and Gudermann, T. (2011) Alternative G protein coupling and biased agonism: New insights into melanocortin-4 receptor signalling, *Mol. Cell. Endocrinol.* 331, 232-240.
 298. Yang, Z., and Tao, Y. X. (2016) Biased signaling initiated by agouti-related peptide through human melanocortin-3 and -4 receptors, *Biochim. Biophys. Acta.*
 299. Violin, J. D., Crombie, A. L., Soergel, D. G., and Lark, M. W. (2014) Biased ligands at G-protein-coupled receptors: promise and progress, *Trends Pharmacol. Sci.* 35, 308-316.
 300. Marti-Solano, M., Schmidt, D., Kolb, P., and Selent, J. (2016) Drugging specific conformational states of GPCRs: challenges and opportunities for computational chemistry, *Drug Discovery Today* 21, 625-631.
 301. Durroux, T. (2005) Principles: A model for the allosteric interactions between ligand binding sites within a dimeric GPCR, *Trends Pharmacol. Sci.* 26, 376-384.
 302. Casado, V., Cortes, A., Ciruela, F., Mallol, J., Ferre, S., Lluís, C., Canela, E. I., and Franco, R. (2007) Old and new ways to calculate the affinity of agonists and antagonists interacting with G-protein-coupled monomeric and dimeric receptors: the receptor-dimer cooperativity index, *Pharmacol. Ther.* 116, 343-354.
 303. Zhu, B. T. (2005) Mechanistic explanation for the unique pharmacologic properties of receptor partial agonists, *Biomed. Pharmacother.* 59, 76-89.
 304. Pflieger, K. D., Seeber, R. M., and Eidne, K. A. (2006) Bioluminescence resonance energy transfer (BRET) for the real-time detection of protein-protein interactions, *Nat. Protoc.* 1, 337-345.
 305. Cottet, M., Faklaris, O., Maurel, D., Scholler, P., Doumazane, E., Trinquet, E., Pin, J. P., and Durroux, T. (2012) BRET and Time-resolved FRET strategy to study

- GPCR oligomerization: from cell lines toward native tissues, *Front. Endocrinol. (Lausanne)* 3, 92.
306. Grant, M., Collier, B., and Kumar, U. (2004) Agonist-dependent dissociation of human somatostatin receptor 2 dimers: a role in receptor trafficking, *J. Biol. Chem.* 279, 36179-36183.
307. Albizu, L., Cottet, M., Kralikova, M., Stoev, S., Seyer, R., Brabet, I., Roux, T., Bazin, H., Bourrier, E., Lamarque, L., Breton, C., Rives, M. L., Newman, A., Javitch, J., Trinquet, E., Manning, M., Pin, J. P., Mouillac, B., and Durroux, T. (2010) Time-resolved FRET between GPCR ligands reveals oligomers in native tissues, *Nat. Chem. Biol.* 6, 587-594.
308. Journe, A. S., Habib, S. A. M., Dodda, B. R., Morcos, M. N. F., Sadek, M. S., Tadros, S. A. A., Witt-Enderby, P. A., Jockers, R., and Zlotos, D. P. (2014) N1-linked melatonin dimers as bivalent ligands targeting dimeric melatonin receptors, *Medchemcomm* 5, 792-796.
309. Broussard, J. A., Rappaz, B., Webb, D. J., and Brown, C. M. (2013) Fluorescence resonance energy transfer microscopy as demonstrated by measuring the activation of the serine/threonine kinase Akt, *Nat. Protoc.* 8, 265-281.
310. Kooijman, S., Boon, M. R., Parlevliet, E. T., Geerling, J. J., van de Pol, V., Romijn, J. A., Havekes, L. M., Meurs, I., and Rensen, P. C. N. (2014) Inhibition of the central melanocortin system decreases brown adipose tissue activity, *J. Lipid Res.* 55, 2022-2032.
311. Ni, X. P., Butler, A. A., Cone, R. D., and Humphreys, M. H. (2006) Central receptors mediating the cardiovascular actions of melanocyte stimulating hormones, *J. Hypertens.* 24, 2239-2246.
312. Weeden, T., Stefano, J., Duan, S., Edling, A., Hou, L. H., Chuang, W. L., Perricone, M. A., Pan, C., and Dzuris, J. L. (2011) A retro-inverso alpha-melanocyte stimulating hormone analog with MC1R-binding selectivity, *J. Pept. Sci.* 17, 47-55.
313. Chorev, M., and Goodman, M. (1993) A dozen years of retro-inverso peptidomimetics, *Acc. Chem. Res.* 26, 266-273.
314. Hano, K., Koida, M., Kubo, K., and Yajima, H. (1964) Evaluation of the Physiological Properties of D-Histidyl-D-Phenylalanyl-D-Arginyl-D-Tryptophyl-Glycine in Frog Melanocyte, *Biochim. Biophys. Acta* 90, 201-204.
315. Link, R., Veiksina, S., Rinken, A., and Kopanchuk, S. (2017) Characterization of ligand binding to melanocortin 4 receptors using fluorescent peptides with improved kinetic properties, *Eur. J. Pharmacol.*
316. Rediger, A., Tarnow, P., Bickenbach, A., Schaefer, M., Krude, H., Gruters, A., and Biebermann, H. (2009) Heterodimerization of hypothalamic G-protein-coupled receptors involved in weight regulation, *Obes Facts* 2, 80-86.

Appendix: Summary of Analytical Information and Pharmacology of Compounds

Figure A-1 presents the chemical structures of bivalent ligands synthesized throughout the current thesis. Table A-1 presents the analytical information of each peptide synthesized. Table A-2 presents the functional cAMP AlphaScreen® Assay results at the mMC1R, mMC3R, mMC4R, and mMC5R. Table A-3 presents the summary of competitive binding experiments with ¹²⁵I-NDP-MSH at the mMC1R, mMC3R, and mMC4R.

Selected Scaffolds	
His-DPhe-Arg-Trp	 <p>The structure shows a central Arginine residue (with a guanidino group) linked to a D-Phenylalanine residue (with a benzyl group) and a Tryptophan residue (with an indol-3-ylmethyl group).</p>
His-DNal(2')-Arg-Trp	 <p>The structure is similar to His-DPhe-Arg-Trp, but the D-Phenylalanine residue is replaced by D-Nal(2'), which has a naphthalen-2-ylmethyl group.</p>
His-DPhe(pI)-Arg-Trp	 <p>The structure is similar to His-DPhe-Arg-Trp, but the D-Phenylalanine residue is replaced by D-Phenylalanine(pI), which has a 4-iodophenylmethyl group.</p>
Selected Linkers	
(PEDG20)	 <p>A linear poly(ethylene glycol) chain with a terminal primary amine group and a terminal carboxylic acid group.</p>
(Pro-Gly) ₆	 <p>A cyclic peptide linker consisting of six repeating Proline-Glycine units.</p>
(PEG)(22 atoms)	 <p>A linear poly(ethylene glycol) chain with 22 oxygen atoms, terminal amine and carboxylic acid groups.</p>
(PEG)(19 atoms)	 <p>A linear poly(ethylene glycol) chain with 19 oxygen atoms, terminal amine and carboxylic acid groups.</p>
(PEG)(16 atoms)	 <p>A linear poly(ethylene glycol) chain with 16 oxygen atoms, terminal amine and carboxylic acid groups.</p>
(PEG)(13 atoms)	 <p>A linear poly(ethylene glycol) chain with 13 oxygen atoms, terminal amine and carboxylic acid groups.</p>

Appendix Figure A-1. The chemical structures of selected scaffolds and linkers used.

Publ?	Comp	Structure	HPLC <i>k'</i> (Syst. 1)	HPLC <i>k'</i> (Syst. 2)	Mass (calcd.)	Mass (obs.)	Purity %
Pub	CJL-1-14	Ac-His-DPhe-Arg-Trp-NH ₂	3.2	5.5	685.34	685.39	>99%
Pub	CJL-5-35-4	Ac-His-DPhe-Arg-Trp-(PEDG20)-NH ₂	4.6	8.3	1003.52	1003.70	>95%
Pub	CJL-1-116	(PEDG20)-His-DPhe-Arg-Trp-NH ₂	4.0	6.4	961.51	961.57	>96%
Pub	CJL-5-35-1	Ac-His-DPhe-Arg-Trp-(Pro-Gly) ₆ -NH ₂	4.3	8.5	1609.79	1610.00	>97%
Pub	CJL-1-41	(Pro-Gly) ₆ -His-DPhe-Arg-Trp-NH ₂	3.6	6.2	1567.78	1568.28	>95%
Pub	CJL-1-31	Ac-His-DPhe-Arg-Trp-(Pro-Gly) ₆ -His-DPhe-Arg-Trp-NH ₂	4.9	7.4	2237.10	2237.18	>99%
Pub	CJL-1-87	Ac-His-DPhe-Arg-Trp-(PEDG20)-His-DPhe-Arg-Trp-NH ₂	4.0	7.9	1629.83	1629.80	>99%
Pub	CJL-5-72	Ac-His-DPhe-Arg-Trp-(PEDG20)-(PEDG20)-His-DPhe-Arg-Trp-NH ₂	5.2	9.5	1949.01	1949.00	>95%
Pub	CJL-1-80	Ac-His-DNal(2')-Arg-Trp-NH ₂	4.3	7.5	735.36	735.30	>98%
Pub	CJL-5-35-5	Ac-His-DNal(2')-Arg-Trp-(PEDG20)-NH ₂	4.7	8.6	1053.54	1053.70	>95%
Pub	CJL-1-132	(PEDG20)-His-DNal(2')-Arg-Trp-NH ₂	5.2	8.3	1011.53	1011.59	>98%
	CJL-5-35-2	Ac-His-DNal(2')-Arg-Trp-(Pro-Gly) ₆ -NH ₂	5.3	9.7	1660.9	1660.0	>96%
Pub	CJL-1-140	Ac-His-DNal(2')-Arg-Trp-(PEDG20)-His-DNal(2')-Arg-Trp-NH ₂	6.4	10.9	1729.86	1730.03	>95%
Pub	CJL-1-20	Ac-His-DPhe(p-I)-Arg-Trp-NH ₂	3.4	6.1	811.2	811.4	>99%
	CJL-5-35-6	Ac-His-DPhe(p-I)-Arg-Trp-(PEDG20)-NH ₂	4.7	8.7	1129.4	1129.6	>96%

	CJL-5-009	(PEDG20)-His-DPhe(p-I)-Arg-Trp-NH ₂	4.5	8.0	1087.4	1087.3	>98%
	CJL-5-35-3	Ac-His-DPhe(p-I)-Arg-Trp-(Pro-Gly) ₆ -NH ₂	5.23	9.67	1735.7	1735.8	>97%
	CJL-5-64	Ac-His-DPhe(p-I)-Arg-Trp-(PEDG20)-His-DPhe(p-I)-Arg-Trp-NH ₂	6.0	10.5	1881.6	1881.6	>97%
	CJL-1-63	Ac-His-DNal(2')-Arg-Trp-(Pro-Gly) ₆ -His-DPhe-Arg-Trp-NH ₂	5.3	8.6	2287.6	2287.3	>95%
	CJL-5-58	Ac-His-DPhe-Arg-Trp-(PEDG20)-His-DNal(2')-Arg-Trp-NH ₂	5.4	9.7	1680.9	1680.6	>95%
	CJL-1-124	Ac-His-DNal(2')-Arg-Trp-(PEDG20)-His-DPhe-Arg-Trp-NH ₂	6.0	9.5	1680.9	1681.0	>97%
	CJL-5-74	Ac-His-DNal(2')-Arg-Trp-(PEDG20)-(PEDG20)-His-DPhe-Arg-Trp-NH ₂	5.7	10.2	1999.3	1999.2	>95%
	CJL-1-53	Ac-His-(p-I)DPhe-Arg-Trp-(Pro-Gly) ₆ -His-DPhe-Arg-Trp-NH ₂	5.50	9.75	2363.4	2363.4	>98%
	CJL-1-108	Ac-His-DPhe(p-I)-Arg-Trp-(PEDG20)-His-DPhe-Arg-Trp-NH ₂	6.29	9.33	1755.7	1755.8	>96%
	CJL-5-12	Ac-His-DPhe-Arg-Trp-(PEDG20)-His-DPhe(p-I)-Arg-Trp-NH ₂	5.47	9.63	1755.7	1755.8	>96%
	CJL-5-15	Ac-His-DNal(2')-Arg-Trp-(PEDG20)-His-DPhe(p-I)-Arg-Trp-NH ₂	5.95	10.40	1806.8	1806.6	>95%
	CJL-5-61	Ac-His-DPhe(p-I)-Arg-Trp-(PEDG20)-His-DNal(2')-Arg-Trp-NH ₂	5.95	10.71	1806.8	1806.6	>96%
	CJL-5-119-1	Ac-His-DPhe-Arg-Trp-(PEG)(22 atoms)-His-DPhe-Arg-Trp-NH ₂	5.26	10.08	1646.85	1646.9	>96%
Pub	CJL-5-119-2	Ac-His-DPhe-Arg-Trp-(PEDG20)-His-DPhe-Arg-Trp-NH ₂	5.35	9.20	1629.83	2629.9	>95%
	CJL-5-119-3	Ac-His-DPhe-Arg-Trp-(PEG)(19 atoms)-His-DPhe-Arg-Trp-NH ₂	5.82	9.84	1602.82	1602.8	>97%
	CJL-9-22-1	Ac-His-DPhe-Arg-Trp-(PEG)(16 atoms)-His-DPhe-Arg-Trp-NH ₂	5.35	9.12	1558.79	1559.03	>96%
	CJL-9-22-2	Ac-His-DPhe-Arg-Trp-(PEG)(13 atoms)-His-DPhe-Arg-Trp-NH ₂	5.28	7.75	1514.77	1515.01	>98%

CJL-9-22-3	Ac-His-DPhe-Arg-Trp-(PEG) ₂ (22atoms)-His-DNal(2')-Arg-Trp-NH ₂	5.91	8.71	1696.86	1697.04	>98%
CJL-9-22-4	Ac-His-DPhe-Arg-Trp-(PEDG20)-His-DNal(2')-Arg-Trp-NH ₂	5.74	8.59	1679.85	1680.05	>96%
CJL-9-22-5	Ac-His-DPhe-Arg-Trp-(PEG)(19atoms)-His-DNal(2')-Arg-Trp-NH ₂	5.86	9.98	1652.84	1652.92	>98%
CJL-5-127-7	Ac-DTrp-DArg-Phe-DHis-NH ₂	4.57	6.43	685.34	685.28	>97%
CJL-5-127-8	DTrp-DArg-Phe-DHis-NH ₂	3.15	4.32	643.33	643.27	>98%
CJL-5-119-4	Ac-DTrp-DArg-Phe-DHis-(PEG)(22 atoms)-His-DPhe-Arg-Trp-NH ₂	5.92	9.89	1646.85	1646.9	>97%
CJL-5-119-5	Ac-DTrp-DArg-Phe-DHis--(PEDG20)-His-DPhe-Arg-Trp-NH ₂	5.50	9.78	1629.83	1629.9	>95%
CJL-5-119-6	Ac-DTrp-DArg-Phe-DHis-(PEG)(19 atoms)-His-DPhe-Arg-Trp-NH ₂	5.65	9.60	1602.82	1602.8	>98%
CJL-5-127-1	Ac-His-DPhe-Arg-Trp-(PEG)(22 atoms)-DTrp-DArg-Phe-DHis-NH ₂	6.54	7.67	1646.85	1646.8	>95%
CJL-5-127-2	Ac-His-DPhe-Arg-Trp-(PEDG20)-DTrp-DArg-Phe-DHis-NH ₂	5.66	9.90	1629.83	1629.8	>95%
CJL-5-127-3	Ac-His-DPhe-Arg-Trp-(PEG)(19 atoms)-DTrp-DArg-Phe-DHis-NH ₂	5.94	10.11	1602.82	1603.04	>97%
CJL-5-127-4	Ac-DTrp-DArg-Phe-DHis-(PEG)(22 atoms)-DTrp-DArg-Phe-DHis-NH ₂	5.49	8.97	1646.85	1647.03	>98%
CJL-5-127-5	Ac-DTrp-DArg-Phe-DHis-(PEDG20)-DTrp-DArg-Phe-DHis-NH ₂	5.92	10.60	1629.83	1630.10	>98%
CJL-5-127-6	Ac-DTrp-DArg-Phe-DHis-(PEG)(19 atoms)-DTrp-DArg-Phe-DHis-NH ₂	5.48	9.03	1602.82	1602.87	>97%

Appendix Table A-1. The analytical data for peptides synthesized in this thesis. HPLC k' = (peptide retention time - solvent retention time) / solvent retention time. System 1 is a 10% to 90% gradient of acetonitrile in water containing 0.1% trifluoroacetic acid over 35 minutes at a flow rate of 1.5 mL/min, and system 2 is the same but with methanol replacing acetonitrile. Product purity was determined by HPLC purity in the solvent system which showed the least purity and integrating the area under the curves of the chromatograms collected at 214 nm. Mass observed was calculated from the M+1 or (M+2)/2 peak. The **Pub.** Indicates that the synthesis and pharmacology was reported in Lensing, CJ *et al J. Med Chem.* 2016.^{25, 132}

Compound	mMC1R	mMC3R		mMC4R		mMC5R
	Agonist EC ₅₀ (nM)	Agonist EC ₅₀ (nM)	Antagonist (pA ₂)	Agonist EC ₅₀ (nM)	Antagonist (pA ₂)	Agonist EC ₅₀ (nM)
	Mean± SEM	Mean±SEM	Mean± SEM	Mean±SEM	Mean± SEM	Mean± SEM
NDP-MSH	0.03±0.01	0.24±0.01		0.46±0.04		0.31±0.03
α-MSH	0.15±0.05	0.76±0.05		4.0±0.9		0.59±0.03
γ-MSH	1090±300	34.6±4.0		869±66		35.1±18.7
CJL-1-14	14.1±2.6	55.5±12.2		13.7±1.9		9.8±2.7
CJL-5-35-4	26.2±9.9	47.4±12.7		5.7±2.9		2.1±0.3
CJL-1-116	24.9±5.9	30.9±7.5		18.5±2.9		3.9±1.3
CJL5-35-1	5.7±.7	107±66		74.1±14.1		52.4±10.3
CJL-1-41	16.4±4.7	27.2±5.2		14.5±2.7		4.9±1.2
CJL-1-31	4.4±0.6	20.2±4.0		9.2±1.0		3.8±0.9
CJL-1-87	6.4±1.5	10.1±2.5		3.6±0.5		3.1±0.6
CJL-5-72	12.6±3.8	22.7±3.7		7.3±2.1		4.0±0.2
CJL-1-80	98.4±32.2	15% at 10 μM	6.04±0.09	15% at 10 μM	8.09±0.04	50% at 10 μM
CJL5-35-5	112±19	25% at 10 μM	6.14±0.06	10% at 10 μM	8.39±0.08	PA, 70% at 10 μM
CJL-1-132	139±17	PA, 45% at 10 μM	6.07±0.18	15% at 10 μM	7.97±0.29	PA, 50% at 10 μM
CJL-5-35-2	153±73	10% at 10 μM	6.88±0.19	5% at 10 μM	7.20±0.9	60% at 10 μM
CJL-1-140	563±142	15% at 10 μM	6.08±0.11	45% at 10 μM	7.68±0.37	786±185
CJL-1-20	12±2	55% at 100 μM	6.79±0.08	50% at 100 μM	8.57±0.08	2.75±1.15
CJL-5-35-6	9.5±1.7	PA, 60% at 100 μM	7.30±0.07	PA, 45% at 100 μM	8.67±0.05	28±12
CJL-5-009	30±6	PA, 60% at 100 μM	7.01±0.22	PA, 45% at 100 μM	8.49±0.24	4.5±1.6
CJL-5-35-3	7.1±1.7	25% at 10 μM	7.05±0.13	30% at 10 μM	7.82±0.12	27.6±12
CJL-5-64	NS	NS	NS	NS	NS	NS
CJL-1-63	16.1±3.5	14.9±5.7		12.99±1.60		5.49±0.85
CJL-5-58	10.1±1.54	22.4±6.5		13.54±6.34		8.09±3.27
CJL-1-124	13.7±3.5	18.56±3.8		70% at 10 μM		11.71±3.13
CJL-5-74	44.2±13.6	30.4±3.3		55% at 10 μM		8.09±1.75
CJL-1-14+ CJL-1-80	12.71±1.9	75% at 10 μM		50% at 10 μM		4.66±1.28
CJL-1-53	26.6±14	PA, 70% at 100 μM	6.54±0.16	PA, 80% at 100 μM	6.95±0.23	35±4.0

CJL-1-108	5.8±1.06	29.1±5.8		PA, 65% at 10 μM		12.8±2.3
CJL-5-12	14.1±2.3	56.5±11.8		9.6±3.5		14.9±1.8
CJL-5-15	130±40	70% at 10 μM	6.63±0.12	60% at 10 μM	7.67±0.17	64.0±11.9
CJL-5-61	88.7±21.8	60% at 10 μM	6.60±0.10	55% at 10 μM	7.65±0.32	120±40
NDP-MSH	0.009±0.002	0.06±0.007		0.34±0.095		0.06±0.005
CJL-5-119-1	2.1±0.4	2.3±0.6		1.7±0.8		0.48±0.01
CJL-5-119-2	3.1±0.62	2.7±0.5		1.7±0.6		0.52±0.04
CJL-5-119-3	2.8±0.46	2.4±0.41		1.7±0.71		0.63±0.055
CJL-9-22-1	2.4±0.50	1.3±0.22		1.1±0.46		0.41±0.034
CJL-9-22-2	2.2±0.20	1.5±0.33		1.1±0.45		0.39±0.026
CJL-9-22-3	6.9±0.88	6.4±1.4		5.5±2.2		1.8±0.04
CJL-9-22-4	6.4±1.2	9.0±2.1		4.8±1.7		2.1±0.2
CJL-9-22-5	5.9±0.97	5.8±1.41		4.8±2.5		1.7±0.15
CJL-5-127-7	5% at 100 μM	15% at 100 μM		20% at 100 μM		35% at 100 μM
CJL-5-127-8	15% at 100 μM	15% at 100 μM		15% at 100 μM		1% at 100 μM
CJL-5-119-4	7.2±1.6	3.6±1.1		5.7±2.5		1.3±0.05
CJL-5-119-5	9.0±1.5	4.5±0.69		8.8±4.1		1.4±0.16
CJL-5-119-6	8.8±1.3	4.9±1.9		7.1±4.3		1.5±0.38
CJL-5-127-1	5.6±1.3	4.9±1.6		2.8±1.2		0.74±0.045
CJL-5-127-2	7.2±0.59	5.9±1.4		3.2±1.1		1.0±0.052
CJL-5-127-3	5.0±0.61	3.6±0.71		2.1±0.91		0.63±0.017
CJL-5-127-4	25% at 100 μM	45% at 100 μM		80% at 100 μM		60% at 100 μM
CJL-5-127-5	45% at 100 μM	55% at 100 μM		3213±1147		80% at 100 μM
CJL-5-127-6	25% at 100 μM	45% at 100 μM		65% at 100 μM		50% at 100 μM

Appendix Table A-2: Functional data at the mMC1R, mMC3R, mMC4R, and mMC5R. The cAMP signaling potency was determined by AlphaScreen® assays. The reported errors are the standard error of the mean (SEM) determined from at least three independent experiments. Changes less than 3-fold were considered to be within the inherent experimental assay error. NS means compound was not soluble in bioassay compatible solvent. PA means partial agonism was observed. The **Pub.** Indicates that the synthesis and pharmacology was already reported in Lensing, *CJ et al J. Med Chem.* 2016.^{25, 132}

Published?	Compound Name	mMC1R		mMC3R		mMC4R	
		IC ₅₀ (nM)	n	IC ₅₀ (nM)	n	IC ₅₀ (nM)	n
Pub	NDP-MSH	0.31±0.08	6	4.18±0.61	14	1.09±0.12	19
Pub	CJL-1-14	388±52	2	60% @100 μM	2	214±55	6
Pub	CJL-5-35-4	178±4	2	13400±5100	2	83±14	4
Pub	CJL-1-116	705±6	2	78% @100 μM	3	292±67	4
Pub	CJL-5-35-1	225±63	2	85% @100 μM	2	841±290	2
Pub	CJL-1-41	1090±110	3	8430±230	2	258±27	2
Pub	CJL-1-31	27.5±2.2	2	3250±760	2	33±5.1	3
Pub	CJL-1-87	68.6±5.3	3	3470±510	2	9.9±2.9	4
Pub	CJL-5-72	131±18	2	10200±1300	2	54±10	2
Pub	CJL-1-80	1630±120	2	1430±190	2	26.0±3.4	2
Pub	CJL-5-35-5	997±190	2	1310±120	2	10.7±0.6	2
Pub	CJL-1-132	1870±220	4	999±290	2	21.8±1.9	3
Pub	CJL-5-35-2	633±128	2	350±60		39.2±1.0	2
Pub	CJL-1-140	430±40	3	350±80	5	10.4±0.03	2
Pub	CJL-1-20	190±10	2	780±90	2	6.0±1.2	2
	CJL-5-35-6	130±10	2	550±10	2	2.7±0.4	2
	CJL-5-009	460±170	3	230±70	2	13.5±5.0	3
	CJL-5-35-3	63.5±12	2	175±17	2	9.8±1.9	2
	CJL-5-64	NS		NS		NS	
	CJL-1-63	57.3±10.5	2	167±36.1	2	15.3±0.7	2
	CJL-5-58	70.8±7.2	2	592.3±123.5	2	14.0±2.5	2
	CJL-1-124	106.69±20.8	2	364.5±28.6	2	7.3±1.5	4
	CJL5-74	93±9.6	2	566.1±110	2	9.6±5.6	2
	CJL-1-14+ CJL-1-80	ND		6810±330	2	18.4±5.6	2
	CJL-1-53	140±50	3	220±60	2	36±10	2
	CJL-1-108	19.5±0.5	2	69±14	3	3.0±0.2	3
	CJL-5-12	29.3±3.2	2	115±24	3	7.2±0.02	2
	CJL-5-15	96±3.8	2	64±16	2	7.1±0.9	2

	CJL-5-61	194±12	2	145±51	2	8.9±0.3	2
Pub	NDP-MSH	0.39±0.07	2	5.9±0.7	2	1.9±0.3	3
	CJL-5-119-1	45.2±3.6	2	1680±240	2	15±4.5	3
Pub	CJL-5-119-2	58±16	2	2140±170	2	14±3.7	3
	CJL-5-119-3	36.6±1.2	2	1700±180	2	14±3.1	3
	CJL-9-22-1	36.5±8.3	2	1170±10	2	12±3.5	3
	CJL-9-22-2	33.7±7.4	2	1310±220	2	10±3.9	3
	CJL-5-127-5	6300±1000	2	55% @100 μM	2	80% @100 μM	2
	CJL-5-127-7	30% @100 μM	2	NA	2	25% @100 μM	2
	CJL-5-119-5	150±20	2	6220±270	2	93±40	2
	CJL-5-127-2	110±34	2	3800±250	2	29±5.4	2

Appendix Table A-3: Summary of competitive binding experiments with ¹²⁵I-NDP-MSH at the mMC1R, mMC3R, and mMC4R. IC₅₀ values were determined by competitive binding in which experimental compounds were used to displace ¹²⁵I-NDP-MSH in a dose-response manner. In competitive experiments, % represent the amount of ¹²⁵I-NDP-MSH signal reduction at 100 μM. The reported errors are the standard error of the mean (SEM). Changes less than 3-fold were considered to be within the inherent experimental assay error. NA means no activity observed up to 100 μM. NA means no displacement was observed at 100 μM. NS means compound was not soluble in bioassay compatible solvent. The **Pub**. Indicates that the synthesis and pharmacology was already reported in Lensing, CJ *et al J. Med Chem.* 2016.^{25, 132}